Numerical investigation of anisotropic and time-dependent behaviours of foliated rock mass

by

Pranay Yadav

A thesis submitted in partial fulfilment of the requirements for the degree of
Master of Applied Science (MASc) in Natural Resource Engineering

The Faculty of Graduate Studies
Laurentian University
Sudbury, Ontario, Canada

THESIS DEFENCE COMMITTEE/COMITÉ DE SOUTENANCE DE THÈSE
Laurentian Université/Université Laurentienne
Faculty of Graduate Studies/Faculté des études supérieures

Title of Thesis Titre de la thèse	Numerical investigation of the anisotropic and time-dependent behaviour of the foliated rock mass
Name of Candidate Nom du candidat	Yadav, Pranay
Degree Diplôme	Master of Science
Department/Program Département/Programme	Engineering
Date of Defence Date de la soutenance	September 07, 2018

APPROVED/APPROUVÉ

Thesis Examiners/Examinateurs de thèse:

Dr. Shailendra Sharan
(Supervisor/Directeur de thèse)

Dr. Ming Cai
(Committee member/Membre du comité)

Dr. Marty Hudyma
(Committee member/Membre du comité)

Dr. Yuhang Xu
(External Examiner/Examinateur externe)

Approved for the Faculty of Graduate Studies
Approuvé pour la Faculté des études supérieures
Dr. David Lesbarrères
Monsieur David Lesbarrères
Dean, Faculty of Graduate Studies
Doyen, Faculté des études supérieures

ACCESSIBILITY CLAUSE AND PERMISSION TO USE

Abstract

Squeezing ground conditions have become a major challenge faced by underground hard rock mines exploiting reserves at greater depth and in a high-stress environment. This thesis investigates the influence of various parameters on the severity of squeezing ground conditions in foliated rock mass utilizing continuum numerical modelling in FLAC3D finite difference code. A series of numerical simulations were carried out for selected cases of two mines subject to squeezing ground conditions to investigate the rock mass failure mechanisms, the influence of various geological, mining and stress parameters, time dependence and the role of rock reinforcements. The numerical models were calibrated using field data and underground observations.

The numerical models were successful in capturing the observed failure mechanisms at the two mines. The calibrated numerical models were used to investigate the influence of varying interception angle, excavation shape, excavation over-break, mining depth and parallel excavations on the severity of squeezing ground conditions utilizing ubiquitous joint model. The time dependence in the numerical models was simulated by using the power ubiquitous model and the role of various rock reinforcement elements was simulated by using structural elements. The results of the numerical simulations were found to be in good agreement with the underground convergence data and observations. The modelling methodology used in the thesis can be used to improve the understanding of the anisotropic and time-dependent behaviour of the foliated rock mass to various mining conditions. The methodology can also be used to evaluate performance of various rock reinforcement strategies and elements that are used in squeezing ground conditions.

Keywords: Squeezing ground, foliation, anisotropic rock mass, time-dependent behaviour, FLAC3D.

Acknowledgements

I would like to thank my supervisor Dr. Shailendra Sharan for his support and mentorship throughout my research at Laurentian University. Without his support and guidance this research would not have been possible. I would also like to thank my thesis advisor committee members Dr. Marty Hudyma and Dr. Ming Cai.

The access to FLAC3D software used for the research was provided by Itasca Consulting Group, under Itasca Education Partnership program. I would like to thank Dr. Tatyana Kastaga for her mentorship during my research. I would also like to thank Laurentian University for providing the financial support in the form of scholarships during the research. The support and valuable feedback from senior management and the geotechnical team at Rampura Agucha mine are acknowledged. Finally, I would like to thank Dr. Alexander Vyazmensky for setting me on the path of rock mechanics that lead me to this research.

Table of contents

List of Tables

List of Figures

Nomenclature

CMS	Cavity monitoring scan
CRF	Cemented rock fill
DEM	Distinct element method
DFN	Discrete fracture network
E	Young's modulus
FDM	Finite difference method
FEM	Finite element method
FLAC3D	Fast Lagrangian Analysis of Continua in 3 dimensions
FRS	Friction rock stabilizer
G	Shear modulus
GBSG	Garnet biotite sillimanite gneiss
GBSS	Garnet biotite sillimanite schist
GMS	Graphite mica schist
H	Overburden
ISRM	International Society of Rock Mechanics
MPBX	Multi-point borehole extensometer
OSRO	Surface support straps
OSZ	Ore shear zone
PFC	Particle flow code

Q	Tunnelling index
RA-UG	Rampura Agucha Underground Mine
RCF	Rock condition factor
SRF	Stress reduction factor
UCS	Uniaxial compressive strength
β	Angle between loading direction and anisotropy plane
γ	Overburden density
δ_{total}	Total convergence
ε_{total}	Total strain
v	Poisson's ratio
σ_1	Major principal stress
σ_2	Intermediate principal stress
σ_3	Minor principal stress
σ_c	Uniaxial compressive strength of the intact rock
σ_{cm}	Uniaxial compressive strength of the rock mass

Chapter 1

1 Introduction

As the mining industry exploits the ore reserves at greater depth, the industry will face several challenges associated with deep and high-stress mining. Squeezing ground condition is one of the major challenges faced by several mining operations around the globe. Squeezing ground conditions in underground hard rock mines are characterized by large deformations around the underground excavations resulting in significant reduction in the cross-sectional area of the excavation and results in severe to extreme damage to the surrounding rock mass. The aim of ground control in squeezing ground conditions is not to restrict the resulting displacements but to safely manage the deformations over the working life of the excavations allowing successful extraction of the ore reserves (Potvin and Hadjigeorgiou, 2008). Significant efforts and considerable investments in ground support and rehabilitation are required to keep the excavations undergoing squeezing operational over the required time. Often multiple passes of ground support are required, and rehabilitation works are difficult and frequently require hazardous scaling operations (Mercier-Langevin and Hadjigeorgiou, 2011). A significant cost in ground support and rehabilitation may be incurred to keep these excavations operational, and often the rehabilitation works may extend up to several weeks leading to significant delays in mine production and development. The deformations associated with the squeezing of foliated rock mass in underground hard rock mines can result in higher loads on the ground support systems and this may result in significant failure of the support elements. This results in increase in ground control hazards in such ground. A better understanding of the various aspects of the squeezing ground conditions in the foliated rock mass is required help form better ground support and mine design strategies that would increase the serviceability of these excavations while reducing the associated ground control hazards and costs.

The most accepted definition of the squeezing ground conditions was provided by Barla (1995) who defined the squeezing as large, time-dependent deformations that occur around underground excavations and these deformations are essentially associated with creep caused by exceeding limiting shear stress. The deformations may terminate during the development of the excavations or may continue over the life of excavation. In underground hard rock mines, often the squeezing is structurally controlled such as in the case of foliated rock mass, and this adds another factor to the mechanical behaviour of the foliated rock mass in squeezing conditions. The squeezing of foliated rock mass can be better defined as large, time-dependent anisotropic deformations around underground excavations that result in significant drive closure or rock mass damage. Several analytical, numerical and empirical methods have been used over the years to study squeezing ground conditions in civil engineering tunnels, and various authors have attempted to use these methods in mining environments. These methods, however, assume that the rock mass deforms and fails in a uniform manner and this is not true for squeezing of the foliated rock mass (Karampinos, 2016).

To better understand the response of foliated rock mass to mining in underground hard rock mines, use of sophisticated numerical methods capable of simulating the large time-dependent and anisotropic deformation around excavations needs to be evaluated. The objective of this thesis is to investigate various parameters and aspects of the squeezing ground conditions associated with deep and high-stress mining of foliated rock mass utilizing continuum numerical modelling in the finite difference code FLAC3D. For the purpose of this thesis two case studies with reported cases of squeezing in foliated rock mass were selected, LaRonde mine in Quebec, Canada and Rampura Agucha underground (RA-UG) mine in Rajasthan, India.

1.1 Research Scope

This thesis aims at investigating the failure mechanisms around underground excavations in foliated rock mass and influence of various geological, mine design and stress parameters on the severity of squeezing conditions at the two selected case studies. As mentioned earlier, the numerical modelling for the thesis was carried out by utilizing the finite difference code FLAC3D. The thesis also investigates the time-dependent deformations associated with squeezing in foliated rock mass and role of various rock reinforcements on the displacements around underground excavations undergoing squeezing. The primary objective of the thesis is to provide a methodology to conduct numerical investigations to improve the understanding of the response of foliated rock mass to mining and study the time-dependent behaviour of the foliated rock mass. The secondary objective of the thesis is to evaluate the applicability of available constitutive models in FLAC3D to capture the anisotropic and time-dependent response of anisotropic rocks such as foliated rock mass. The thesis also evaluates the applicability of various structural elements present in FLAC3D to simulate the role of rock reinforcement elements in numerical models.

1.2 Research approach

This research is primarily a numerical modelling study utilizing continuum modelling in FLAC3D. A comprehensive literature review was undertaken focusing on the cases reported on squeezing ground conditions in the foliated rock mass in underground hard rock mines. As mentioned earlier, two case studies were selected for the research carried out in this thesis, LaRonde mine in Canada and RA-UG mine in India. LaRonde mine has reported some of the highest deformations in underground hard rock mines and provides a wide spectrum of squeezing ground conditions. RA-UG mine has experienced several challenges associated with squeezing of the foliated rock mass, several cases of ground support failure and

extensive rehabilitation have been reported at the mine. The drive closures at RA-UG mine are significantly less than those reported at LaRonde mine, and this can better evaluate the applicability of the modelling methodology to capture a wide range of squeezing conditions.

A series of 3D numerical models were generated to reproduce the observed failure mechanisms in the foliated rock mass for the two selected case studies. The anisotropic response of the foliated rock mass was captured by utilizing Ubiquitous-Joint model in FLAC3D. Influence of various parameters such as varying interception angle between the foliation planes and excavation walls, the shape of excavations, excavation over-break, excavation mining depth and parallel excavations on the severity of squeezing ground conditions was investigated. The numerical modelling results were calibrated using the excavation convergence values recorded underground. The research also investigates the time-dependent response of foliated rock mass to mining and the role of various rock reinforcement elements on displacements around underground excavations in squeezing ground conditions. The time-dependent anisotropic response was captured in the numerical models by utilizing Power-Ubiquitous joint model in FLAC3D. The progression of deformation over time in the numerical models was calibrated to reproduce the displacements recorded over time at the two mines. The role of various reinforcement elements was investigated by utilizing the structural elements in FLAC3D to simulate rebar, friction rock stabilizers, hybrid and cable bolts used at the two mines. Structural elements simulating various rock reinforcement elements were introduced in the numerical models at different stages and influence on the displacements was studied. Effect of delayed installation of rock reinforcements was also investigated. The modelling results from all simulated cases were compared to available observations from underground excavations at the two mines.

1.3 Thesis structure

The thesis comprises of eight chapters. Chapter 1 of the thesis introduces the thesis and the problem statement and briefly describes the adopted methodology for this research.

Chapter 2 provides a review of the relevant literature carried out during this research. The chapter provides an overview of the squeezing ground conditions encountered by various underground hard rock mines across the globe. Various empirical, analytical and numerical techniques used are discussed. The chapter also provides a description of rock mass failure mechanisms and ground support systems used in squeezing ground conditions.

Chapter 3 provides a theoretical background of the anisotropic and time-dependent behaviour of rocks. Anisotropy of rock strength and deformability are discussed, and failure criteria used for anisotropic rocks are provided. The chapter also provides a description of creep in intact rock and rock mass and provides mathematical formulation and rheological models used to simulate the time-dependent behaviour of rocks.

Chapter 4 provides an overview of geotechnical conditions at RA-UG and LaRonde mines. For both mines a description of geological setting, mining method used, and in-situ stress conditions are provided. The chapter also provides a description of squeezing ground conditions, geotechnical monitoring and data collection procedure and ground support schemes used at the two mines.

Chapter 5 provides a detailed description of numerical modelling methodology adopted for the research. The chapter also provides results of the numerical simulations carried out to investigate the strength anisotropy of intact rock specimen at RA-UG mine. The results of numerical models investigating the rock mass failure mechanisms at the two mines are presented and a discussion on modelling results is provided.

Chapter 6 provides the results of numerical simulations carried out to investigate the influence of various parameters on the severity of squeezing of the foliated rock mass. The chapter provides the squeezing classification schemes used at the two mines. Modelling results and discussion on the effect of varying interception angle between foliation planes and excavation walls, different excavation shapes, excavation over break, excavation mining depth and parallel excavations are also provided.

Chapter 7 provides the details of numerical simulations conducted to investigate the time-dependent response of foliated rock mass to mining. Results of numerical simulation and discussion on modelling results for the two mines are provided. The chapter also provides the results and discussion on the numerical models investigating the role of various rock reinforcement elements on the severity of squeezing ground conditions.

Chapter 8 provides a conclusion of the research carried out in this thesis. The chapter outlines the key contributions of this thesis and recommendations for further work are provided.

Chapter 2

2 Literature review

This chapter of the thesis provides essential definitions of terminologies used in the thesis and background information on squeezing ground conditions in underground hard rock mines. It also provides an overview of experience in squeezing ground at various underground mines. A brief discussion on rock mass failure modes and a review of various tools available to identify the squeezing potential of the rock mass is presented. Ground support strategies adopted by underground mines dealing with squeezing ground conditions is provided, and applicability of various rock reinforcement and surface support elements is discussed. Other strategies that can be utilized to address the squeezing problem is also presented.

2.1 Definitions

Terminologies used in the thesis are defined in the following sections. The definitions are based on a review of literature from various authors that have conducted research in the field of squeezing ground conditions around underground excavations.

2.1.1 Squeezing

Terzaghi (1946) described squeezing rock as merely the rock, which contains a considerable amount of clay that may have been present originally, as in some shales, or it may be an alteration product. Squeezing rock slowly advances into the tunnel without perceptible volume increase. Criteria for squeezing is a high percentage of microscopic and submicroscopic particles of micaceous minerals or of clay with a low swelling capacity. Barton et al. (1974) defined squeezing rock as the plastic flow of incompetent rock under the influence of high pressure. Squeezing rock conditions are part of the Stress Reduction Factor (SRF) in Barton's Q system in which mild squeezing pressure results in an SRF rating between 5 and 10 and heavy squeezing rock pressure is given a value ranging from 10 – 20. It

follows that the presence of squeezing conditions results in a reduction on the Q rating of a rock mass.

O'Rourke (1984) described squeezing ground as ground that undergoes substantial time-dependent deformation around the tunnel as the result of load intensities exceeding its strength. This loading is a result of redistribution of stresses adjacent to the excavated opening. Jethwa et al. (1984) suggested squeezing rock conditions as a failure of soft rock mass under high primitive stress that results in the formation of a plastic or broken zone around tunnel opening and the failed rock mass undergoes plastic deformations that continues for months. Tunnel wall displacements under such conditions are predominantly time dependent.

In tunnels, rock mass failure associated with volumetric expansion due to overstressing is termed as squeezing and this is associated with movement of the failed rock mass into the opening (Singh et al. 1992). Aydan et al. (1993) defined squeezing as large inward closure of tunnels and provided three possible forms of failure during the closing of the surrounding medium, i.e. complete shear failure, buckling failure and shearing and sliding failure. Squeezing phenomenon may be treated as having an elastic-viscous-plastic behaviour, and it can only occur when the rock is yielded by the redistributed state of stress following the extraction of the tunnel. It can be defined as a physical process and involves the irrecoverable dilatant behaviour of the rock.

International Society of Rock Mechanics (ISRM), Barla (1995) defined squeezing in rock as the large time-dependent deformations that occur around underground excavations and is essentially associated with creep caused by exceeding limiting shear stress. Deformations may terminate during construction or continue over a long-time period. Einstein (1996) defined squeezing as the inward movement of the tunnel periphery over time. The intensity of

the movement rate and the magnitude of the displacement often vary over the tunnel surface depending on the geology, on the original stress state and on the shape of the tunnel. The author also described squeezing as the time-dependent shear displacement of the ground, which causes the tunnel periphery to move inward. It is associated with creep caused by exceeding shear stress, and in dilatant rocks, it is associated with volume increase. Gioda and Cividini (1996) defined the squeezing as time-dependent deformations produced by the concentration of shear stress in the zone surrounding the excavation. Both deviatoric and volumetric deformations may be present, the volumetric deformation is generally associated with the possible dilatant geotechnical medium. Kovári (1998) defined squeezing rock as large ground deformation causing reduction of cross section possibly even in the floor. These deformations go on during a long-time period. If these deformations are hindered, great pressure may arise sometimes resulting in the failure of the tunnel support.

2.1.2 Foliation

Foliation is a general term used to describe any planar feature that penetrates a body of rock. It may refer to thin rhythmic bedding in sedimentary rock, compositional layering in igneous rocks or cleavage, schistosity or other planar structures in metamorphic rocks. Joints are generally not considered, as they are not sufficiently penetrative. Foliation may be defined by a spatial variation in mineral composition or grain size, by preferred orientation of elongate or platy grains or aggregate of grains by planar discontinuity such as microfractures or by any combination of these elements. In three dimensions, many foliations show an associated linear element, i.e. the fabric elements defining the foliation may appear stronger in some sections (normal to the foliation) than in others (Passchier and Trouw 2005).

Foliation belongs to the group of geological structures called pervasive. These structures do not occur as individual features (like fractures or bedding planes) but rather affect the whole

of the rock usually as a preferred shape and / or crystallographic orientation of mineral grains and / or aggregates of mineral grains. Foliation planes are often referred to as S-planes from (original German nomenclature) (Milnes et al. 2006).

Presence of foliation influences the physical, dynamic, thermal, mechanical and hydraulic properties of rocks and these properties vary with direction. These rocks are inherently anisotropic. Anisotropy is a characteristic of foliated metamorphic rocks (slates, gneiss, phyllites and schist). In such rocks, the fabric can be expressed in different ways. Closely spaced fractures called cleavages are found, for instance, in slates and phyllites. These rocks tend to split into planes due to parallel orientation of microscopic grains of mica, chlorite or other platy minerals. In schist, the fabric is created by the parallel to the sub-parallel arrangement of large platy minerals such as mica, chlorite and talc. Foliation can also be expressed by alternating layers of the different mineral composition such as in gneisses.

Milnes et al. (2006) reported that the planar fabric of the foliation planes represents incipient weakness planes in the rock microstructure. The intact rock will be weaker when loading in one direction, and stronger when loading in another direction. A typical result of compressive strength test on the rock specimen was given by Milnes et al. (2006). The ‘U’ portion represents the failure induced by the foliation and the base of ‘U’ represents the orientation of foliation that has the greatest effect on the compressive strength.

Wanne (2002) utilized Particle Flow Code (PFC) to study the effect of anisotropy of the rock on the strength and deformation properties by simulating the unconfined compressive tests and reported four phases of damage formation due to the presence of schistosity in the foliated rocks. Influence of foliation on the rock matrix microstructural failure during loading simulated using PFC by (Wanne, 2002) show that the development of microcracking induced by the foliation is represented by the dark spots and failure plane along the foliation

orientation was observed.

2.1.3 Creep

Creep can be defined as slow deformation of solids under small loads acting over time. Some rocks, such as clay and shales, are observed to creep under relatively low loads acting over a few years, but other rocks exhibit creep when subjected to high differential stresses under high confining pressures. When a solid is subjected to constant differential stress, it may creep to deform continuously. This deformation is termed as “elastic viscous flow” and may be analyzed as an aggregate effect of “pseudo-viscous flow” and “elastic flow” (Griggs 1939).

Creep can be defined as a type of behaviours in which the strain continues to evolve under the imposition of constant stress, or vice versa. At any given value of the compressive stress, the strain continues to increase with time, as the stress is held constant. The rate of creep increases with increasing compressive stress. Generally, there is an initial period, during which the strain increases rapidly but at a decreasing rate, (i.e. the curve is concave down). This is followed by a period in which the strain increases at a constant rate (i.e. linear curve). After a certain time, the strain begins to increase at an ever-increasing rate (i.e. concave-upward curve), eventually causing a complete collapse of the sample (Jaeger et al. 2007). An example of idealized creep curve for primary, secondary and tertiary stages of creep was given by Pellet (2016).

Creep is a time-dependent process, which leads to deformations that are strongly related to rock’s physical properties. In mechanics, creep is related to the slow time-dependent deformations of a given body subjected to a constant state of stress over time. The deformations process can lead to large delayed strains and, eventually to the rupture of the studied body. A perfect example would be extreme strains developed in squeezing rocks,

which can produce a large convergence in underground openings (Pellet, 2016).

2.1.4 Anisotropy

Anisotropy is defined as variations of properties with respect to the directions concerned in design and analysis of rock structures (Noorian and Jing 2014). Barla (2001) provided a general classification of anisotropic rocks that consisted of two classes, A and B.

i) Class A – Rocks that would be expected to behave as isotropic media and however exhibit anisotropy.

ii) Class B – Rock which is clearly anisotropic in nature and shows directions of symmetry for their strength and deformation characteristics.

Anisotropy is a characteristic of intact laminated, stratified or bedded sedimentary rocks such as shales, sandstones, siltstones, siltstone, limestone, coal etc. Anisotropy results from complex physical and chemical process associated with transformation, deposition, compaction and cementation. Rocks that undergo several formation processes may present more than one direction of planar anisotropy such as foliation and bedding planes. Rock masses intersected by one or several regularly spaced joints sets are anisotropic in addition to being discontinuous. The rock between joints can be isotropic or anisotropic. If the joints develop parallel to the foliation or bedding, they are called foliation joints or bedding joints respectively (Amadei 1996).

Most sedimentary and metamorphic rocks are anisotropic, and the simplest form is planar anisotropy in which a rock mass has a set of parallel planes of weakness. Such rocks have different elastic properties along and perpendicular to the bedding plane in sedimentary rock or cleavage or foliation plane in metamorphic rocks (Jaeger et al. 2007).

2.2 Squeezing in the foliated rock mass

Squeezing ground conditions are encountered in underground hard rock mines while developing through foliated rock masses. These conditions result in considerable failure of ground support and require significant efforts in rehabilitation. Large-scale deformations associated with squeezing ground causes a delay of development and often has serious economic consequences. Squeezing ground conditions are often driven by the presence of inherent foliation and the orientation of excavation walls with respect to the foliation planes (Karampinos et al. 2015b). These deformations are typically characterized by a reduction in cross-sectional area of excavation due to a combination of induced stresses and relatively week rock mass properties. Several underground hard rock mines have faced the challenges associated with squeezing ground, for these mines, maintaining excavations open and operational is often difficult and requires extensive investment in rock reinforcement and surface support. Also, the process is time-consuming and requires hazardous scaling and rehabilitation operations (Mercier-Langevin and Hadjigeorgiou, 2011).

Frequently, underground mines are exposed to low strength rock types. The consequences of poor sequencing in these weaker materials may be severe, such as progressive degradation of development conditions associated with large deformation that can lead to premature loss of access and reserves. In extreme cases, development closure of 30 – 50 % has been experienced. This high-deformation ground behaviour has been observed in several underground mines, and the problem often manifests itself in drives parallel to the foliation, particularly where the major principal stress is orthogonal to the drive. In such conditions, several phases of ground support and rehabilitation may be required during development and to extended service life. Cases where deformations have been monitored over an extended period, it is evident that there is significant time-dependent behaviour in weaker rocks once the high stresses are attained that can induce fracturing.

2.2.1 Experience in squeezing ground

Over the past two decades, several authors have documented case studies of squeezing ground conditions in the high-stress environment and are summarized in the following sub-sections. High stress in mines is generally considered relative to the strength or load-bearing capacity of the rock mass. In cases where the induced stresses approach the rock mass strength, the conditions experienced are comparable to deep and high-stress mining irrelevant to the mining depth or the absolute magnitude of stress. Depending on the stiffness of rock mass such conditions generally exhibit rock bursting (seismicity) or high deformation behaviour (squeezing) (Potvin and Slade, 2006).

2.2.1.1 LaRonde Mine, Canada

Karampinos (2016) reported that the LaRonde mine had experienced a wide range of squeezing ground conditions. Haulage drives were subjected to the most difficult conditions as these drives ran parallel to the foliation planes and were sensitive to wall buckling and overall squeezing. In a few cases, the total wall convergence exceeded 1 m and a depth of failure of between 6 to 7 m was observed. The walls often required a second round of bolting within a few months of the initial development. In cases where wall convergence was high, and clearance for some equipment became too narrow, the broken material needed to be purged.

Rock mass failure mode in walls was found to be a complex buckling phenomenon. Stress concentration around excavations caused the wall to buckle and resulted in horizontal displacements of more than 1 m. Massive shearing forces were induced on the foliation planes as the buckling movement took place and the internal wall shearing associated with direct shear resulted in breaking of the ground support elements. Shearing led to locking of the reinforcement elements such as resin rebar and split sets and prevented these elements

from yielding.

LaRonde mine utilizes two-pass ground support system to manage the squeezing ground conditions. The first pass comprises of 20 mm diameter, 1.9 m long resin grouted rebar installed in the back and 39 mm diameter, 2.0 m long friction bolts installed in the walls on a 1.2 m x 0.6 m staggered pattern. The bolts are installed over a six-gauge, galvanized welded wire mesh. For the second pass, the mine utilizes hybrid bolts installed on a 1.2 m x 1.2 m square pattern in conjunction with horizontal, zero-gauge mesh straps. The secondary ground support was installed after an advance of 12 m. In addition to strategic ground support schemes, the mine planed the level layout and ore access strategically to restrict the high deformations in localized areas and away from the critical infrastructure.

2.2.1.2 Lapa Mine, Canada

Mercier-Langevin and Wilson (2013) provided an overview of squeezing ground conditions and ground control practices at Lapa mine. The mine utilizes a combination of longitudinal open stoping with cemented backfill and primary-secondary transverse stoping. The deposit is hosted in deformed and silicified volcanic and sedimentary rocks and has three distinct geotechnical domains, i.e. very weak schist (ultramafics) and two significantly more competent units. Deformation in the relatively competent sediments or volcanics are easily managed; however, the ultramafics display massive deformations and require time-consuming and hazardous rehabilitation operations that often interfere with the production targets.

Mercier-Langevin and Wilson (2013) reported that only the drifts developed at a shallow angle to the foliation exhibit a significant degree of convergence. Failure mechanism in all cases was identified to be buckling of foliation. In addition, wall convergence was exacerbated by back and floor failure and vice-versa. Most of the deformations started in the

wall and slowed down later in the process while the deformation accelerated in the back and floor. The mine utilized ‘Hard Rock Squeezing Ground Index’ for a preliminary indication of the squeezing potential of the rock mass and as a guide for ground support practices.

The Lapa mine followed a systematic support selection strategy. The ground support was chosen based on the interception angle between foliation and drive walls. For drives, parallel or subparallel (up to 45 degrees) to the foliation were considered susceptible to squeezing and required the use of longer reinforcement and hybrid bolts. In addition, the screen surface support was brought within 0.6 m from the floor. It was observed that the use of shotcrete in squeezing ground could present a short-term gain by preventing unravelling of the rock mass while the bolting operations were carried out. All bolts were installed on a staggered pattern, in spans exceeding 6.5 m such as at drive intersections longer bolts were used for primary support. In cases where the drive height was more than 5 m, the length of the wall support was increased. Cable bolting was also used as secondary support. Cable bolts were targeted to the walls and backs that exhibited conditions prone to squeezing and were installed in combination with high capacity mesh straps. The installation of cable bolts was delayed in time to allow the drives to deform. It was found that installing stiffer cable bolt later in the deformation process was more successful as the cable bolts installed too early were susceptible to premature failure. Typical squeezing examples observed at LaRonde and Lapa mines are presented in Figure 2.1.

Figure 2.1: Squeezing ground conditions at LaRonde and Lapa mine (Hadjigeorgiou et al., 2013)

2.2.1.3 Wattle Dam Gold Mine, Australia

Squeezing ground conditions at Wattle Dam Goldmine was reported by Marlow and Mikula (2013). The deposit consists of a sequence of steep dipping metamorphosed ultramafic, sedimentary and basaltic units. The mine access and infrastructures were placed in the

competent hanging wall rocks. Foliation planes were parallel to the strike of the orebody. Bulk open stoping mining methods with post-extraction backfill were used to achieve 100% extraction of the very high-grade ore. Squeezing ground conditions were observed as the mining depth increased to 360 m below the surface. The damage usually appeared a few hours after blasting and gradually exacerbated with time. Cracking was observed in the backs of various ore drives, essentially a skin of ore, usually 1 – 2 m thick fractured, bulked in volume and pushed down onto the shotcrete skin, causing cracks in the shotcrete. Walls and pillar noses experienced vertical squeezing which led to the fracturing of the week rock causing buckling.

Damage in walls developed gradually over time and was worse where sub-vertical wall structures were present. Survey prisms and borehole cameras were utilized at the mine to track the movements of walls and back during development and to identify the depth of failure. It was observed that rock mass was significantly fractured to a depth of 0.2 to 0.8 m into the wall as soon as it was developed. Further localized damages were seen up to 1.5 m. Closures of between 33 – 113 mm (0.6 – 2% wall closure strain) were observed in monitored cases. Worse ground conditions were observed where groundwater was encountered.

The mine utilized ‘Hard Rock Squeezing Index’ proposed by (Mercier-Langevin and Hadjigeorgiou, 2011) to quantify the degree of squeezing at the mine. To manage the squeezing ground conditions, the mine adopted primary and secondary ground control strategy. For primary ground support, in-cycle fibre reinforced shotcrete was used, followed by installation of bolts and welded mesh. This provided confining stress, which opposed buckling and reduced the eventual final movement. After enough time and face advance, fibercrete ribs were installed, rehabilitation was carried out where necessary by spraying additional 100 mm fibercrete, and in some cases, cable bolts between shotcrete ribs were

installed. The mine also trialled the use of shotcrete pillars to support the squeezing ground and had some success in controlling squeezing ground conditions, but the pillars were difficult to fabricate, and the installation was time-consuming.

2.2.1.4 Mount Isa, Yilgarn Star and Black Swan Nickel, Australia

Australian Center for Geomechanics and Xstrata Copper undertook a review of mines in squeezing ground conditions in Australia. The observations from four Australian mines including Mount Isa, Yilgarn Star and Black Swan Nickel reported by Potvin and Slade (2006) are summarized below.

At Mount Isa Copper operations, poor ground conditions were observed in areas where the number of bedding planes per metre was high, and the planes were associated with either graphite or talc coating. Practically all drives in such conditions exhibited high damage potential. The failure mechanics was largely controlled by the geometry of inclined bedding submitted to high horizontal stress ahead of the stoping front. The ground support system in the poorest areas included primary support utilizing split sets, welded mesh and 50 mm fibre reinforced shotcrete sprayed floor to floor to cover the mesh. As the ground continued to deform, cable bolts and 100 mm fibre reinforced shotcrete were used as secondary supports over existing support.

Mica Schist at Yilgarn Star mine exhibited high deformation behaviour. The deformation process started with first signs of floor heaving, followed by buckling of the bottom part of the hanging wall and evidence of hanging wall convergence. In some cases, footwall started to converge at a later stage. Back collapse was observed when hanging wall failed and undercut the backs. The hanging wall convergence increased when stoping started. The most successful ground support strategy at the mine included 3 m long cable bolts grouted inside

over drilled split sets and a single row of mesh strap installed over the mesh to increase its stiffness and provide an improved connection between reinforcement elements. In addition, profiling the drive in a shanty shape was used.

High deformation behaviour was observed in the ultramafic rock containing talc carbonate in the hanging wall at Black Swan Nickel. The squeezing ground conditions were observed in ore drives, which exhibited high convergence of the walls, on the footwall side. Despite the installation of heavy ground support, convergence in order of 1.5 m over a few months was observed. The depth of failure was estimated to be between 1.5 to 2 m. Ground control problems in the backs were caused by the convergence of the walls. The rapid deterioration of drives was observed in areas where the lower section of the wall was undercut or not adequately supported. In cases where the convergence was severe, ground support costs were generally very high and required rehabilitation works. The mine utilized in-cycle 75 mm thick fibre reinforced shotcrete sprayed floor to floor. Mesh was installed floor to floor over the shotcrete using split sets. In areas where high convergence was anticipated, single strand yielding Garford cable bolts were installed. The timing of installation of cable bolts was critical, and it was observed that once the wall movement reached a certain limit, the cable bolts became less effective in controlling the convergence. The cable bolts were installed at a three-cut lag to the development face.

2.2.1.5 Argyle Diamond Mine, Australia

Fernandez et al. (2012) reported squeezing ground conditions at Argyle Diamond mine. The mine utilized block caving to exploit the ore reserve and during undercutting stage, the mine experienced significant convergence in the zones of weak rock mass due to abutment stress. In several undercut drives, wall to wall convergence as high as 1.2 m was observed. Very high damage areas were mainly located in the area between the ore-body and Gap fault

system. In this area, severe and localized damage with associated failure of ground support was observed close to the brow location. High and moderate convergence was observed in the proximity of the undercut brows and near geological features. Recorded convergence and damage at various locations are presented in Figure 2.2. The mine utilized tape extensometers and damage mapping to monitor the squeezing ground conditions.

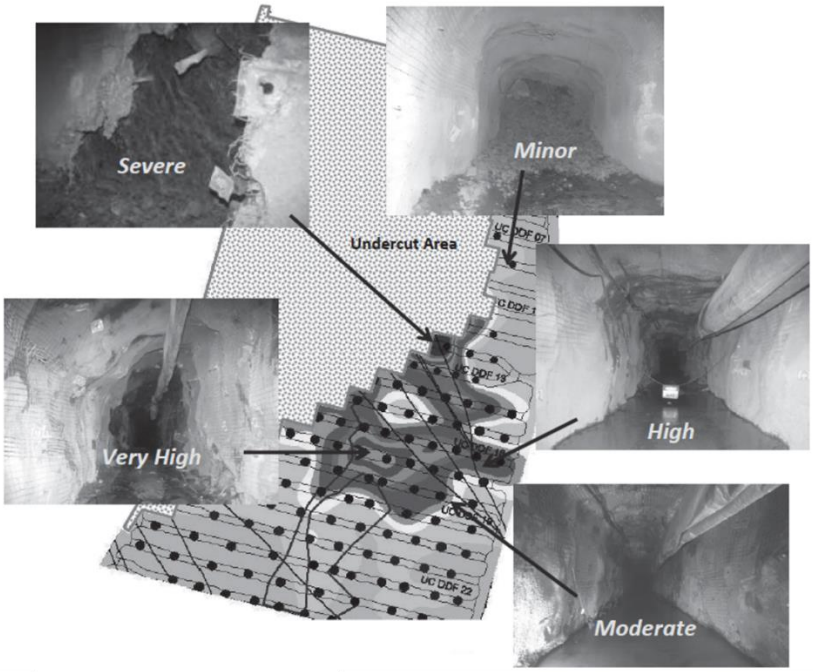

Figure 2.2: Convergence and damage at the undercut level in early January 2011, after Fernandez et al. (2012)

The mine utilized three ground support regimes – regular, medium and heavy to manage squeezing ground conditions. The regular ground support regime included 50 mm fibre reinforced shotcrete sprayed floor to floor with a combination of Posimix resin bolts and split sets. For medium ground support regime, the mine utilized 50 mm fibre reinforced shotcrete sprayed floor to floor, mesh installed shoulder to shoulder utilizing a combination of Posimix resin bolt and split sets. The heavy ground support regime consisted of 50 mm fibre reinforced shotcrete sprayed in the first pass with mesh installed floor to floor utilizing a combination of Posimix resin bolts and split sets. For the second pass, 50 mm fibre reinforced

shotcrete was sprayed on the walls to cover the mesh. In addition, the mines also used cable bolts at the intersection backs and OSRO straps on the pillar corners.

2.2.1.6 Rampura Agucha Underground Mine, India

Yadav et al. (2016) reported squeezing ground at Rampura Agucha Underground mine. The mine experienced squeezing in footwall drives and declines at a shallow angle to the foliation planes. At mining depth of between 500 to 600 m from the surface, minor to significant squeezing was observed at various locations. Two distinct failure mechanisms around the underground excavations were observed, i.e. Sliding and Toppling. Sliding failure was observed at the bottom portion of the western wall. The sliding failure was the result of shear deformation caused due to stress and foliation planes dipping into the wall. At shoulders of the wall, toppling failure was observed which was the result of deformation of rock mass under compression leading to buckling of the foliation planes. The mine utilized tape extensometer, damage mapping and cavity monitoring scans to monitor the squeezing ground conditions.

For primary ground support, 50 mm fibre reinforced shotcrete sprayed floor to floor with galvanized wire mesh at the height of 0.7 m from the floor, and resin rebars were used. Additional 50 mm fibre reinforced shotcrete was sprayed over the mesh. In cases where ground deterioration was observed following the primary ground support installation, cable bolts in conjunction with OSRO straps were utilized. For drives perpendicular to the foliation planes 50 mm fibre reinforced shotcrete and resin, rebar was used at 1.2 x 1.2 m square pattern. OSRO straps were also utilized at pillar corners of the intersections.

2.2.2 Failure modes in squeezing ground conditions

The first step in examining the potential of squeezing ground conditions in underground hard rock mines is to identify the likely driving mechanism (Hadjigeorgiou and Karampinos

2017). For civil engineering tunnelling projects, a phenomenological description of three possible forms of failure in squeezing ground provided by Aydan et al. (1993) is presented in Figure 2.3.

i) Complete shear failure – This type of failure involves complete shearing of the rock mass medium. It is generally observed in ductile rock masses or in the rock masses that have widely spaced discontinuities.

ii) Buckling failure – Metamorphic rocks such as phyllite and mica schists or thinly bedded ductile sedimentary rocks such as mudstone, shale, siltstone, sandstone and evaporitic rocks are susceptible to this mode of failure.

iii) Shearing and sliding failure – This type of failure is observed in relatively thickly bedded sedimentary rocks and involves sliding along bedding planes and shearing of intact rock.

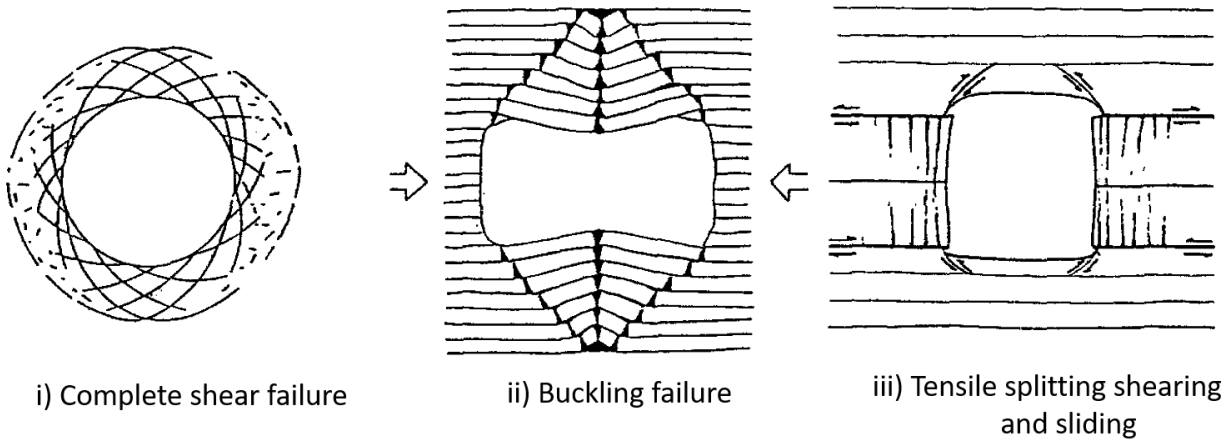

Figure 2.3: Classification of forms of failure in squeezing rock mass, after Aydan et al. (1993)

Hadjigeorgiou and Karampinos (2017) reported that these main mechanisms could be used in a mining context. The complete shear failure of the medium was observed in salt or coal mines. Malan (2002) reported shearing and sliding failure in South African mines. Potvin and

Hadjigeorgiou (2008) analyzed squeezing ground conditions at several mines in Australia and Canada and reported that high deformation in deep and high-stress mines are generally related to the presence of prominent structural features such as dominant fracture set, intense foliation or a shear zone and high stress that results in a buckling failure.

Beck and Sandy (2003) reported observations of failure mechanics from several Western Australian mining projects involving some exposure to low strength rock types, ultramafics (talc-chlorite schists) and micaceous metasediments or metavolcanic. The typical observations are summarized as follows, and failure mechanisms are presented in Figure 2.4.

i) Shearing of foliation on the drive footwall and hanging wall led to offsetting and 'guillotining' of support elements.

ii) Stress-induced fractures subparallel to the drive backs (and floors) led to significant 'bulking' as the fractures sheared and dilated. This, in turn, resulted in deformations and closure between the floors and backs of the drives and resulted in shearing of the walls.

iii) The initial indication of significant bulking above the backs was usually the development of an open crack along the contacts of the backs and the hanging wall.

iv) Buckling of the drive walls may occur if shearing is prevented.

In cases where deformations have been monitored over an extended period, it was found that there is a significant time-dependent behaviour of these weaker rocks once the stress conditions have been attained that is sufficient to cause induced fracturing. In some mines, this has been exploited by deferring the development in the weaker rocks as long as possible without affecting the production plan.

In high-stress mine, ground conditions around excavations changes in response to the

changing stress conditions due to mining activities. The exact nature of the stress path varies, but the variations can be understood in most cases utilizing a simple comparison of the stress component that limits the failure and the stress component that drive the failure.

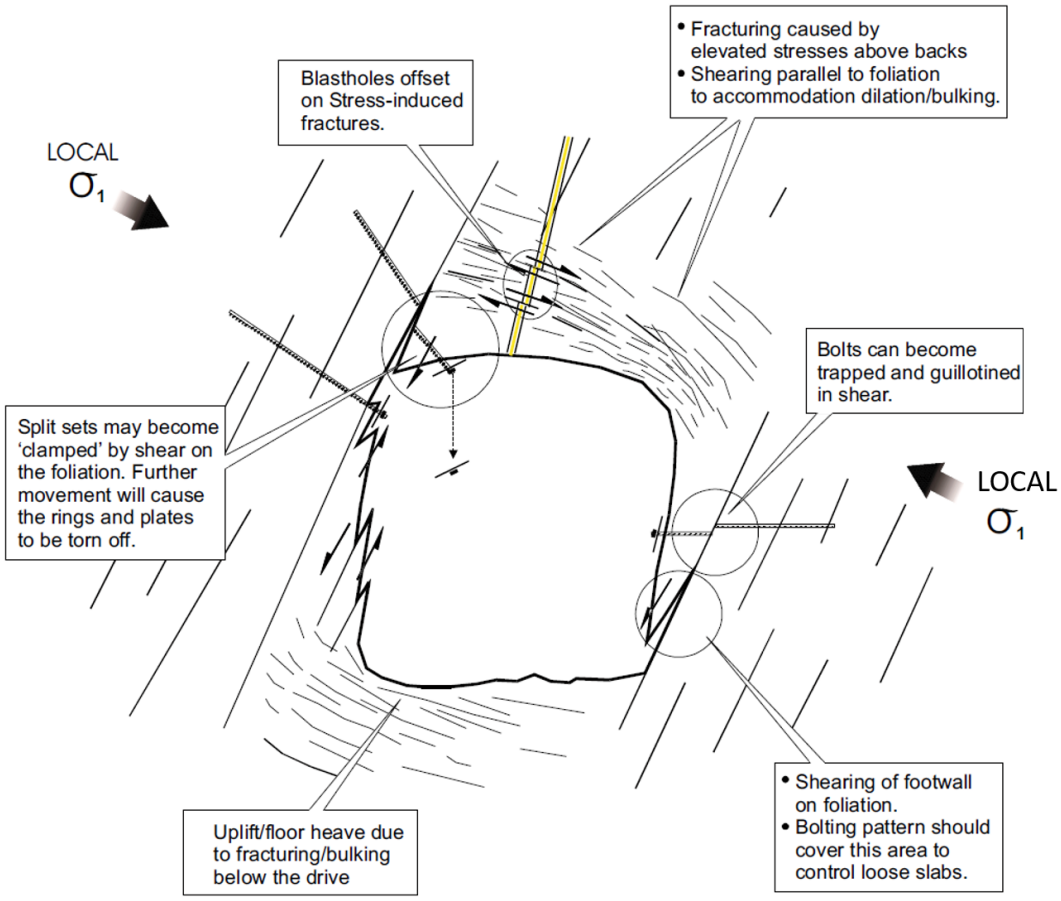

Figure 2.4: Failure modes in high deformation ground, after Beck and Sandy (2003)

2.2.3 Tools used to analyze squeezing ground

Several tools are available to analyze squeezing ground conditions in civil engineering tunnels. Over the last few decades, several of these tools have been adopted by the mining industry to analyze squeezing potential in underground hard rock mines. In addition, several new tools have been developed by the researchers. A brief description of the tools available to analyze squeezing ground conditions is provided as follows.

2.2.3.1 Observational method

Observation and monitoring method has been regularly used for establishing safe and adequate excavation design in the mining industry. Observation and monitoring of underground excavations can provide useful information to evaluate excavation stability, evaluate the adequacy of design and ground support and evaluate the influence of stoping activities and other excavations. The observational procedure has been successfully adopted in civil engineering tunnelling projects and in the mining industry. Peck (1969) provided the necessary steps of using the observational method as follows

i) Establish general nature, pattern and properties of the rock mass.

ii) Assess the most probable conditions and most unfavourable deviations from these conditions.

iii) Establish the design based on a working hypothesis of anticipated behaviour.

iv) Select the quantities to be observed as the development takes place and calculate their anticipated values based on the working hypothesis.

v) Calculate the values of the same quantities under the most unfavourable conditions compatible with the available subsurface data.

vi) Select in advance course of action or modification of design for every significant deviation from the observational findings.

vii) Measure quantities to be observed and evaluate actual conditions

viii) Modify the design to suit actual conditions

In addition to observations, systematic geological mapping and initial support are critical. Squeezing ground conditions are time-dependent, and amount of deformation may vary along the length of excavation due to mining conditions. It is important to measure the rock mass

response to mining. Instruments such as stress cells, strain gauges and extensometers can be used to measure various parameters that can potentially be utilized in the observational method. The observational method is a reliable and useful tool for the design of excavations in squeezing ground; it is however very critical that procedures are planned and executed in a scientific manner, and measurement of the quantities during the observational procedure, instrumentation and interpretation of the gathered results and observations are done analytically.

2.2.3.2 Analytical tools

Based on experiences with tunnels in Japan, Aydan et al. (1993) related the strength of the intact rock to the overburden pressure to estimate the squeezing potential along tunnels. The method was based on the analogy between the axial stress-strain response of rock in laboratory testing and tangential stress-strain response around tunnels. Two possible methods were proposed to recognize squeezing and measure its degree as follows.

i) Setting the level of deformation of tunnels in relation to the tunnel dimension, i.e. if the strain of the tunnel wall is more than 1% it is recognized as squeezing.

ii) Utilizing competency factor and mechanical behaviour of surrounding medium to set the squeezing potential and its degree.

The competency factor α is defined as the ratio of the uniaxial strength σ_c to the overburden pressure γH. Experiments showed that hypothetically five distinct states of specimens during a complete testing procedure could be distinguished. The following relations were established between normalised strain levels η_p, η_s and η_f obtained from normalising the strain levels, ε_p, ε_s and ε_f by elastic strain limit ε_e. The ratio of peak tangential strain at the circumference of the tunnel (ε_θ^a) to elastic strain (ε_θ^e) was used to define various degrees of

squeezing.

$$\eta_p = \frac{\varepsilon_p}{\varepsilon_e} = 2{\sigma_c}^{-0.17} \tag{2.1}$$

$$\eta_s = \frac{\varepsilon_s}{\varepsilon_e} = 3{\sigma_c}^{-0.25} \tag{2.2}$$

$$\eta_f = \frac{\varepsilon_f}{\varepsilon_e} = 5{\sigma_c}^{-0.32} \tag{2.3}$$

Five states were observed in the tests of the rock to make a proposal to predict and to define the squeezing potential of the rocks and its degree as shown in Figure 2.5. Considering the state of stress around the openings, the tangential stress is most likely to be the maximum stress components. Five states of uniaxial and triaxial tests of rock in laboratory or in-situ test were used to relate the squeezing potential of surrounding rock. Based on ratio ε_θ^a / ε_θ^e where ε_θ^a and ε_θ^e are the strain level around a circular tunnel in a hydrostatic stress field and the elastic strain limit for the rock mass, five different degrees of squeezing were defined. The parameters were derived from the following equations.

$$\varepsilon_\theta^a = \frac{u}{r} \tag{2.4}$$

$$\varepsilon_\theta^e = \frac{1+v}{E}\frac{\sigma_{cm}}{2} \tag{2.5}$$

where u is the radial displacement of the tunnel wall, r is the tunnel radius, v is the Poisson's ratio and E is Young's modulus.

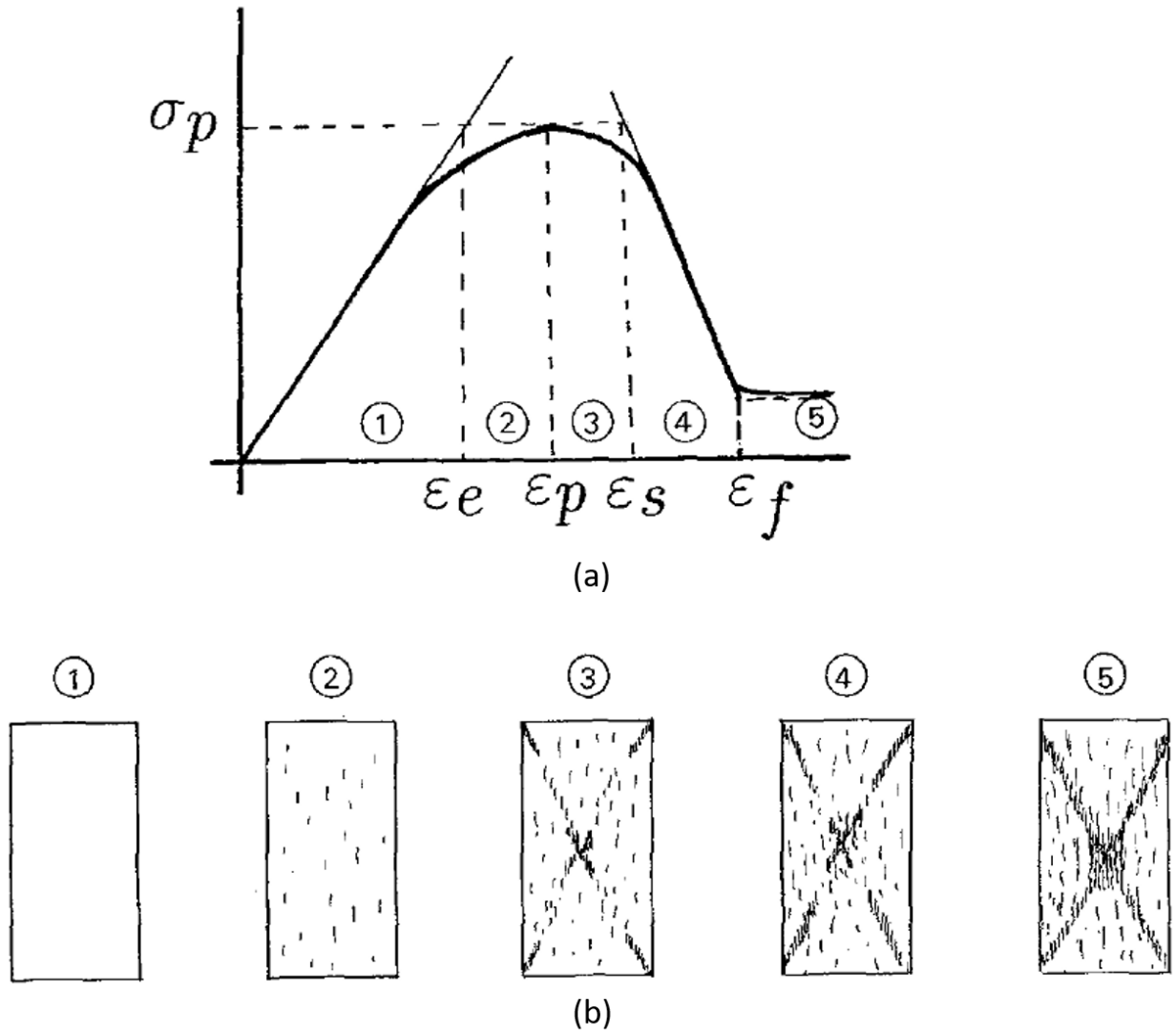

Figure 2.5: Idealizes stress-strain curves and associated states for squeezing rock, after Aydan et al. (1993)

Hoek and Marinos (2000) reported that the uniaxial compressive strength of the rock mass σ_{cm} can be used to evaluate potential tunnel squeezing problems. To estimate the deformation of a tunnel subjected to squeezing, an estimate of the deformation modulus of the rock mass is required. The ratio of the uniaxial compressive strength σ_{cm} of the rock mass to the in-situ stress p_0 can be used as an indicator of potential tunnel squeezing problems. Analysis was carried out to determine the relationship between σ_{cm}/p_0 and the percentage strain of the tunnel. The percentage strain ε is defined as 100 x the ratio of tunnel

closure to tunnel diameter. Kazakidis (2002) investigated an eccentric loading approach applied to quantify the confinement effects and examine the energy balance in a slab under buckling load around the underground opening by utilizing Euler's formula to examine the buckling failure around underground openings in highly stressed and jointed rock masses. Hadjigeorgiou and Karampinos (2017) reported that the ground reaction curve can provide an excellent 2D tool to illustrate the rock support interaction in tunnels. The method was originally proposed for circular tunnels in homogeneous and isotropic rock masses. The method, however, was extended for anisotropic rock masses by Brown et al. (1983). The method can potentially be used as a practical design tool for squeezing ground conditions, however, the method assumes uniform support pressure acting on the tunnel, and this is rarely the case in mining excavations.

2.2.3.3 Empirical tools

Empirical guidelines and design tools use experience from various sites for preliminary assessment. However, their applicability is dependent on identifying the driving failure mechanism that is linked to the specific guidelines. Once a potential failure mechanism is identifying, empirical tools can be used to assess the anticipated level of squeezing. The quality of predictions is restricted by the similarity of the ground conditions to cases in the database (Hadjigeorgiou and Karampinos 2017).

The Q-system includes a wide spectrum of rock mass qualities including heavy squeezing ground. Squeezing ground conditions are incorporated into the system in the stress reduction factor (SRF) (Barton et al. 1974). However, the system does not take into account the anisotropy, and the orientation of the structures and the Q-system is based on limited case studies of tunnel reporting squeezing problems (Hadjigeorgiou and Karampinos 2017). Singh et al. (1992) utilized Q-system to suggest squeezing in civil engineering tunnelling project

and provided the following relation to indicate the onset of squeezing conditions.

$$H = 350\ Q^{1/3} \tag{2.6}$$

where, H is the overburden in metres and Q is the Barton's rock mass quality index.

For buckling failure in the thinly layered rock mass, Mercier-Langevin and Hadjigeorgiou (2011) presented a 'hard rock squeezing index' for underground mines based on the case studies from several Australian and Canadian mines. The index has been used successfully by Wattle Dam mine in Western Australia (Marlow and Mikula, 2013), the Waroonga underground complex (Woolley and Andrews, 2015) and the Westwood mine in Canada (Armatys, 2012) to provide indication for the potential of squeezing and long-term strain levels based on ranges for the foliation spacing and the stress to strength ratios (Hadjigeorgiou and Karampinos, 2017). The index can be used to predict strain in a variety of conditions from no squeezing to extreme squeezing and considers the orientation of structures by using interception angle.

One such example was demonstrated by Mercier-Langevin and Wilson (2013) for Lapa mine. The influence of drift orientation with respect to the foliations was the most important factor affecting the severity of squeezing. It was also observed that as the angle of interception increases, squeezing becomes almost purely stress-driven and the foliation spacing had a negligible effect on the squeezing potential of the rock. Based on these observations a series of prediction matrices were developed at Lapa mines for varying interception angle to identify the potential of squeezing.

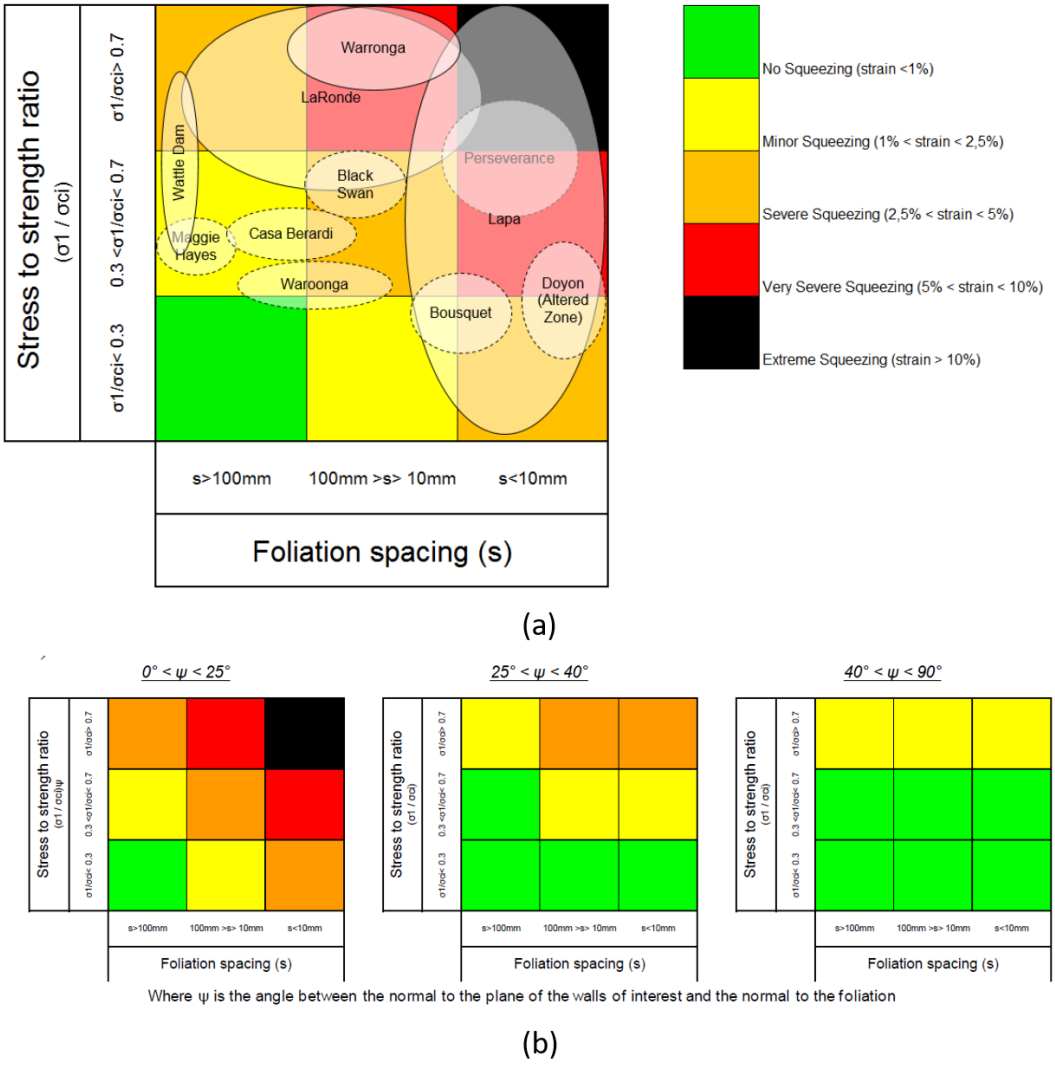

Figure 2.6: Hard rock squeezing index (a) foliation spacing – stress matrix (b) different squeezing matrices for varying interception angle, after Mercier-Langevin and Hadjigeorgiou, (2011)

2.2.3.4 Numerical tools

Numerical modelling tools can be utilized to simulate the behaviour of the in-situ rock mass under various mining conditions. Continuum or discontinuum models can be utilized to represent the rock mass, however, selecting the suitable modelling technique and constitutive models depends on the governing rock mass failure mechanism (Hadjigeorgiou and Karampinos, 2017).

Malan (2002) utilized an elastic viscous plastic approach to simulate the time-dependent deformations in underground hard rock mines in South Africa. The model was used to simulate the experimental closure profile and long-term development of fracture zones around excavations. The model was based on visco-plasticity, with time-dependent cohesion wakening rule to simulate the time-dependent failure of the rock. This model was successful in simulating the time-dependent closure behaviour of tabular excavations, giving both instantaneous response and the primary and steady-state closure phases.

Watson et al. (2015) utilized 3D finite difference code FLAC3D (Itasca Consulting Group Inc 2012) and Improved Unified Constitutive Model (IUCM) (Vakili et al., 2012) to simulate rock mass response of a shaft in high stress and anisotropic conditions. Bewick and Kaiser (2009) utilized Phase2 (Rocscience Inc., 2006) to assess the influence of structural features on excavation stability. Based on the modelling conducted an Orientation Reduction Factor, a modification to the Stress Reduction Factor (SRF) (Barton et al. 1974) was developed to assist in the design of tunnels in anisotropic rocks.

Mellies (2009) utilized 2D finite element code Phase2 (Rocscience Inc., 2008) to analyze the observed drift convergence and to reproduce the failure mechanism resulting from deformation at LaRonde underground mine. The in-situ foliation was simulated explicitly by introducing joints into the numerical models. An approximate reproduction of the observed conditions at LaRonde mine was achieved utilizing Phase2 in terms of deformation profile and deformation size. Influence of ground support and the time-dependent behaviour of the squeezing rock was not considered in these models. As a general limitation, the applied 2D analysis could not account for the dependency of drift and the strike direction of the foliation planes.

Hoek (2001) utilized 2D finite element models in Phase^2 to simulate the squeezing ground

conditions in tunnels. Bewick and Kaiser (2009) and Mercier-Langevin and Turcotte (2007) used 2D finite element models in Phase^2 with explicit representation of foliations to investigate the behaviour of anisotropic rocks. Sandy et al. (2007) utilized FEM in Phase^2 to predict failure along the foliation planes that can be indicated by joint separation.

Beck et al. (2010) utilized a multi-scale approach to mine deformation modelling to improve the simulation of capacity and demand for ground support. Case studies were used to demonstrate the behaviour of several heavy support system using this approach. Proposed designs were tested for a deep cave subjected to high stress and expected significant drive closures. In the models, Discrete Fracture Networks (DFNs) were used to represent drive scale structures that were based on a simple statistical representation of the discontinuity spatial distribution. 3D Finite Element Method with DFNs (FE DFN) was used to simulate the extreme closure of drives. Several different modelling concepts were utilized to simulate the support capacity and demand. The models intended to capture the mechanisms of discontinuous deformation around complex geometries. The magnitudes and extent of the deformation were calibrated using field data.

Vakili et al. (2012) used FLAC3D (Itasca Consulting Group, 2012) to investigate the impact of the time of installation of cable bolting and fibrecrete, as secondary support, on the effectiveness of a ground support system. Yadav et al. (2016) utilized FLAC3D (Itasca Consulting Group, 2012) and ubiquitous joint constitutive numerical model to investigate the influence of foliations on excavation stability. Sandy et al. (2007) utilized simple elastic models in FLAC3D to predict the location and extent of fracture zones.

Karampinos et al. (2015a) utilized a 3D distinct element method (DEM) 3DEC version 5 (Itasca Consulting Group, 2013) to simulate the buckling mechanism at LaRonde and Lapa mines in Canada. The DEM was used to capture the buckling mechanism in the foliated

ground under high-stress conditions. The numerical models focused on reproducing the mechanism in hard rock mining while explicitly considering the influence of structures, see Figure 2.7. The employed 3D DEM model simulated the buckling mechanism allowing for block rotation, fracture opening or detachment of a rock block from its original domain. The method was successful in simulating the progressive deformation during the development of drift with the progressive reduction of the forces acting at the boundaries of the excavation. The method was also used to investigate the suitable ground support strategy in squeezing ground conditions.

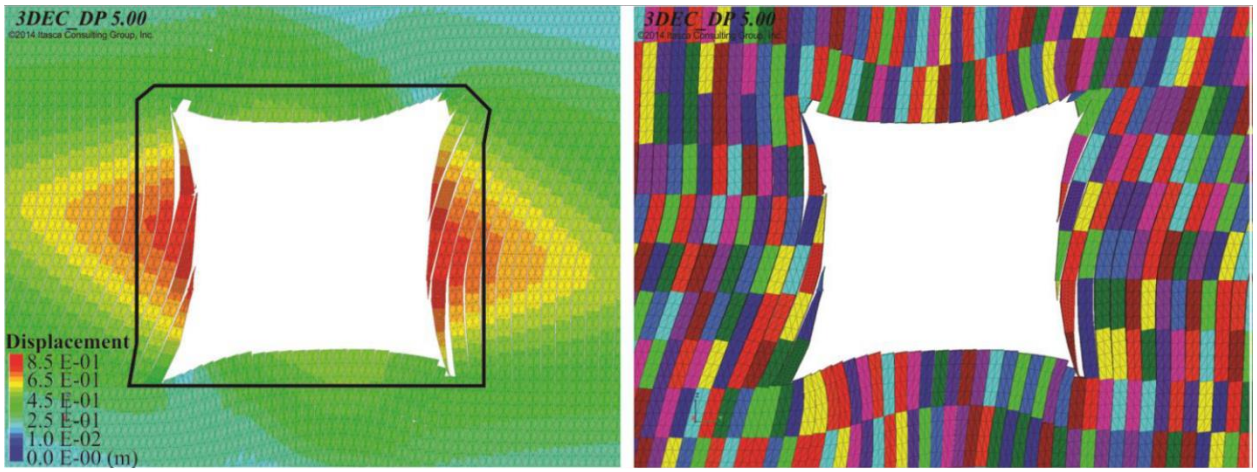

Figure 2.7: Modelled displacement in squeezing ground at LaRonde mine, after Karampinos et al. (2015a)

2.2.4 Ground support strategies in squeezing ground

Potvin and Hadjigeorgiou (2008) indicated that completely arresting the deformations associated with squeezing ground conditions is not realistic and such an approach results in frequent rehabilitation and high ground support costs. An effective ground support system for squeezing ground aims to control these deformations by utilizing both rock reinforcement and surface support units. Differences of ground support strategies in Australian and Canadian underground hard rock mines in squeezing ground were discussed. Australian mines favour

the use of soft reinforcement and surface support such as split sets and fibre reinforced shotcrete, and the Canadian mines use high-density bolts with yielding capabilities such as hybrid and rebar bolts in conjunction with welded wire mesh and mesh straps.

Potvin and Hadjigeorgiou (2008) reported that the tendon reinforcement in squeezing ground is required to maintain the self-supporting capacity of the rock mass and usually reaches a depth of between 1.8 to 2.5 m inside the excavation walls, depending upon the bolt length. The surface support elements are used to contain the immediate rock mass surrounding the excavation and should deform to accommodate the resulting high deformations while maintaining the integrity of the reinforced rock mass. Various rock reinforcement and surface support elements used in underground hard rock mines to control the deformations associated with squeezing ground conditions are discussed in the following sections.

2.2.4.1 Rock reinforcement

Failure zone in squeezing ground generally extends up to several metres behind the wall of excavations, and often the installed reinforcement unit may be entirely contained within the failed rock mass. In such conditions, the reinforcement units are used to provide some degree of confinement within the broken rock mass to create a reinforced shell. Mines experiencing stress driven failure as in squeezing ground conditions require careful consideration of the implication to select the appropriate ground support for development as squeezing ground presents a challenge for maintaining safe access during the development and subsequent stoping operations. Appropriate surface support needs to be combined with suitable rock reinforcement that can withstand the large displacements. Sandy et al. (2007) reported the observation of ground support practices from various Australian and Canadian underground metal mines. It was observed that shearing of foliation in the drive footwall and hanging wall lead to the offsetting of drill holes and guillotining or truncation of the support element in

Australian mines.

Stiff bolts such as fully grouted resin rebar, cannot accommodate large deformations, they tend to snap and break. This has led to the use of reinforcement elements that can yield under squeezing ground conditions. De-bonded or yielding reinforcement elements are required to maintain serviceability of underground excavations in high deformation conditions. Reinforcement elements in such conditions face the additional challenge of shearing, which may trap or cut the elements. Most reinforcement units do not perform well when subjected to heavy shearing. This phenomenon has been observed in-situ for split sets and cone bolts. Shearing of ground can also lead to guillotining of wall bolts such as split set and Swellex. Solid rock bolts provide greater resistance to shearing; however, shearing can limit the capacity of solid bolts to deform, slide and yield. Cone bolts locked up due to shearing in the walls and were very rigid like rebar which led to breaking of the face plates or the snapping of bolts at threaded portions.

Mercier and Turcotte (2007) reported the success of hybrid bolts in high deformation ground. A hybrid bolt comprises of resin-encapsulated rebar installed inside a 39 mm friction bolts. Significantly better performance of these bolts was observed as compared to other systems at LaRonde mine. The bolts provided increased resistance to shear and the friction resistance and provided a stiff early reaction at low displacement and almost plastic behaviour at high loads.

Most mines utilize cable bolts as secondary reinforcement elements. Generally the installation of cable bolts is deferred to a later stage in the deformation process, it was observed that installing cable bolts too early led to premature failure of cable bolts. Various types of cable bolts including double strand, yielding cables have been utilized by the operations dealing with squeezing ground conditions. Cement grouted cable bolts were found

to be too stiff to yield under load. Yielding cable bolts had limited success due to failure during loading or they sunk in the wall losing contact with the surface support elements.

In most operations, the increase in deformation has led to an increase in the intensity of the reinforcement elements in terms of bolt density and bolt length. Several mines in Australia and Canada have adopted the approach of intensively reinforcing the lower sidewalls, to prevent unravelling of the broken ground from behind the surface support shell.

2.2.4.2 Surface Support

A ground support system is as effective as the weakest link in the system. Reinforcement elements should work in agreement with surface support elements. It is critical to maintain the connection between the two. Welded mesh and mesh strap are very efficient to improve the connection between the reinforcement and surface support elements. As the excavation surface deforms, the surface pulls on the straps, and the load is distributed along the whole strap and transferred to all the bolts connected to the straps. It also effectively creates a shell of a reinforced shell of broken rock mass and reinforcement can then provide extra resistance to surface deformations and inhibit the rate of convergence.

Mercier-Langevin and Wilson (2013) reported that the use of shotcrete in squeezing ground conditions could provide a short-term gain by preventing unravelling of the rock mass while bolting operation is carried out. However, as deformation starts, the stiff shotcrete quickly degrades and spalls, to the point of becoming an additional hazard that requires scaling or screening to fix.

Welded mesh is used as a passive support system, it does not prevent or reduce rock mass degradation, but it can provide confinement to the broken rock and can deform considerably before failing. Generally, mesh failure occurs along the overlap area between two mesh

sheets. This problem can be managed by utilizing zero-gauge mesh straps installed along the contacts. Canadian and Australian mines install zero-gauge weld mesh straps along the overlaps between the mesh sheets with additional bolts to improve the durability of the connections. South African mines utilize OSRO strap in such conditions.

Several mines have explored the use of mesh embedded in between two layers of shotcrete resulting in a stiffer system that provides support at relatively small-scale deformations. However, this system often results in failure of the outer layer of shotcrete in the form of slabs and becomes difficult to rehabilitate.

2.3 Chapter summary

Squeezing is a time-dependent phenomenon resulting in large-scale deformations around underground excavations. In foliated rock mass, the squeezing results in anisotropic deformations. Several underground metal mines around the world have reported challenges associated with squeezing ground conditions in the foliated rock mass. This thesis focuses on investigating time-dependent and anisotropic deformations that occur around underground excavation in the foliated rock mass.

Review of cases in underground hard rock mines suggests that squeezing ground results in significant damage and large-scale deformations that poses a significant challenge to maintain the stability and keep the excavations operational for its service life. Squeezing ground conditions are encountered in a high-stress environment. However, the high-stress environment is independent of the depth of mining. Several mines have encountered squeezing at shallow depth due to a combination of pre-mining stress, past mining, mining method and layout. Three main failure mechanisms are associated with squeezing: complete shear failure of the medium, buckling failure and sliding and shearing failure. The review suggests that buckling failure is the most common failure mechanism as reported by several

authors for Australian and Canadian mines.

Several tools are available to assess the squeezing ground conditions in underground hard rock mines. However, each tool has its own limitations and applicability. The observational method cannot be used to predict the squeezing ground conditions, and it works on the 'design as you go' principle. Empirical tools are limited to the case studies in the database and majority of these tools were developed for civil engineering projects, and hence, their applicability to mining excavations requires caution. Sophisticated numerical tools can be utilized to predict the squeezing ground conditions and investigate the failure mechanism and influence of various parameters, this increases the model complexity and requires greater efforts for calibration.

A variety of ground support strategies have been adopted to control the deformations of squeezing ground. Rock reinforcement and surface support elements need to work in agreement to arrest the deforming ground. The combination of reinforcement and surface support elements vary from mine to mine depending upon the severity of squeezing. There is a distinct difference between ground support practices of Australian and Canadian mines in high deformation environment. In squeezing ground, rehabilitation is a common process and mines have developed strategies to identify the need for rehabilitation and systematically execute rehabilitation plans that agree with the production targets of the mine.

Chapter 3

3 Anisotropic and time-dependent behaviours of rocks

This chapter of the thesis provides a theoretical background of anisotropic and time-dependent behaviours of rocks. Anisotropy of deformability and strength of rocks is discussed. Theory of plasticity and associated failure criteria used in rock mechanics for anisotropic rocks are presented. The chapter also provides an overview of time-dependent behaviour of rocks. Creep in intact rocks and rock masses are discussed, and mathematical formulations for various stages of creep are presented. Basic rheological models used to simulate the visco-elastic and elasto-visco-plastic behaviours of rocks are discussed.

3.1 Anisotropy in rocks

For underground excavations, monitoring the ground response with respect to the mining activities is a very common procedure. It is carried out to collect the data for displacements and strains that can assist in developing the fundamental understanding of rock mass behaviour and predict or evaluate the rock mass failure mode. The measured strains or displacements are then related to the stresses to understand the redistribution and influence of mining through the assumption of material behaviour. A common procedure is to assume that the rock mass is linearly elastic, isotropic, continuous and homogeneous. However, any rock mass is to a certain extent anisotropic and/or heterogeneous and/or discontinuous and somewhat non-linearly elastic.

A medium is anisotropic if its properties vary with direction, it is heterogeneous if they vary from point to point and it is discontinuous if there are separations or gaps in the stress field. These definitions are in general scale dependent, and they depend on the relative size of the smallest structural feature of the problem of interest with respect to the largest structural feature of the medium. The medium is said to be elastic if the deformations associated with

its loading are fully recovered during unloading. If the stress and strain are linearly related the material is termed as linearly-elastic. The applicability of the theory of elasticity is a function of the duration of loading. Elasticity assumes an immediate response upon the application or removal of loads (Amadei, 1983).

Rocks composed of parallel arrangements of flat minerals like mica, chlorite and clay, or long minerals like hornblende show strong anisotropic characteristics. Metamorphic rocks, especially schist and slate, are often directional in their behaviour. Anisotropy can also occur in regularly interlayered mixtures of different components, as in banded gneiss, sandstone/shale alternation, or Chet/shale alternations (Goodman, 1989). Generally, two forms of anisotropy are found in rock materials – intact rock anisotropy and rock mass anisotropy. Intact rock anisotropy is a result of natural fabrics such as schistosity, foliation and bedding, constituting the rock which can cause directional dependency even in a homogeneous intact anisotropic rock. Rock mass anisotropy, on the other hand, is large scale and is often due to the presence of well-defined and persistent joint sets in the rock mass (Vakili et al., 2014). Foliated rocks are strongly anisotropic, and their properties vary along and perpendicular to the direction of the foliation planes

3.1.1 Deformability of anisotropic rocks

Deformability can be defined as the capacity of a rock to strain under the applied load or in response to unloading on an excavation. Deformability of anisotropic rocks varies with spatial orientation. Foliated rocks such as schist, gneiss or slates are commonly associated with transverse anisotropy or orthotropy. Amadei (1996) reported that the directional character of the deformability properties of anisotropic rocks and rock masses is usually assessed by field and laboratory testing. Deformability test results on anisotropic rocks are commonly analyzed in terms of the theory of elasticity for anisotropic media by assuming

Hooke's law. In contrast to the isotropic rocks, the generalized Hooke's law for an anisotropic rock has more than two-independent elastic coefficients and hence it is more difficult to characterize the elastic properties of an anisotropic rock experimentally. An anisotropic version of Hooke's law has been used on rock mechanics for the analysis of in situ subsurface stress measurement by Amadei (1996) and for analyzing seismic wave propagation by Helbig (1996) and Schoenberg and Sayers (1995).

Hooke's law for isotropic rocks considers both stress and strain to be second-order tensors, with nine components each, the most generalized linear relationship between the stresses and strains could be expressed using a fourth-order tensor, see Equation (3.1) and has 9 x 9 = 81 components.

$$\boldsymbol{\tau} = \boldsymbol{C}\,\boldsymbol{\varepsilon} \tag{3.1}$$

where, $\boldsymbol{C}$ is a fourth-order tensor whose elastic components are known as elastic stiffness.

However, due to the symmetry of stress and strain tensors, there are 36 distinct components. The number of components is further reduced to 21 if the existence of a strain energy density function is assumed. Generalized Hooke's law can be written in the Voigt notation as follows

$$\begin{bmatrix}\tau_{xx}\\ \tau_{yy}\\ \tau_{zz}\\ \tau_{yz}\\ \tau_{xz}\\ \tau_{xy}\end{bmatrix} = \begin{bmatrix}c_{11} & c_{12} & c_{13} & c_{14} & c_{15} & c_{16}\\ c_{12} & c_{22} & c_{23} & c_{24} & c_{25} & c_{26}\\ c_{13} & c_{23} & c_{33} & c_{34} & c_{35} & c_{36}\\ c_{14} & c_{24} & c_{34} & c_{44} & c_{45} & c_{46}\\ c_{15} & c_{25} & c_{35} & c_{45} & c_{55} & c_{56}\\ c_{16} & c_{26} & c_{36} & c_{46} & c_{56} & c_{66}\end{bmatrix}\begin{bmatrix}\varepsilon_{xx}\\ \varepsilon_{yy}\\ \varepsilon_{zz}\\ 2\varepsilon_{yz}\\ 2\varepsilon_{xz}\\ 2\varepsilon_{xy}\end{bmatrix} \tag{3.2}$$

For the most practical cases, anisotropic rocks are often modelled as orthotropic or transversely isotropic media in a coordinate system attached to their apparent structure of directions of symmetry. Orthotropic medium is characterized by three mutually orthogonal planes of symmetry. If the axes of a Cartesian reference coordinate system are aligned within

the symmetry planes, the stiffness matrix of the orthotropic medium has nine independent elastic constants. Transverse isotropy is the simplest anisotropy model and is characterized by the existence of a single plane of isotropy and only one single axis of symmetry, the normal to the isotropy plane. Any plane containing the axis of symmetry represents a plane of mirror symmetry. Five independent elastic constants are needed to describe the deformability of the transversely isotropic rocks.

Amadei (1996) indicated that the transverse isotropy formulations have been used to characterize the deformability of rocks such as schists, gneisses, phyllites, siltstones, mudstones, sandstones, shales and basalts. For such rocks, the plane of transverse isotropy is assumed to be parallel to the foliation, schistosity or bedding planes. For transverse isotropic media, five independent elastic constants E, E', ν, ν' and G' can be defined as follows.

i. E and E' are the Young's moduli in the plane of transverse isotropy and in direction normal to it, respectively

ii. ν and ν' are the Poisson's ratios characterizing the lateral strain response in the plane of transverse isotropy to a stress acting parallel and normal to it respectively and

iii. G' is the shear modulus in planes normal to the plane of transverse isotropy

For transversely isotropic rocks, the shear modulus G' is often expressed in terms of E, E', ν and ν' through the following empirical equation.

$$\frac{1}{G'} = \frac{1}{E} + \frac{1}{E'} + 2\frac{\nu'}{E'} \tag{3.3}$$

For transverse isotropy, the five elastic constants must satisfy the following thermodynamic constraints that imply that the rock strain energy must remain positive

$$E, E', G' > 0 \tag{3.4}$$

$$-1 < \nu < 1 \tag{3.5}$$

$$-\sqrt{\frac{E'}{E}\frac{(1-\nu)}{2}} < \nu' < \sqrt{\frac{E'}{E}\frac{(1-\nu)}{2}} \tag{3.6}$$

Anisotropic rocks should be carefully analyzed keeping in mind that the plane of schistosity and the directions normal to the planes can be assumed, respectively, to be the plane of isotropy and axis of rotational symmetry. Anisotropic rocks show non-linear elastic behaviour even at low stresses. When using numerical methods, the influence of anisotropy and non-linearity should be included in the constitutive equations for anisotropic media.

3.1.2 The strength of anisotropic rocks

Strength anisotropy is defined as the variation of compressive strength according to the direction of the principal stresses. Strength varies continuously with directions and is minimum when the planes of anisotropy are parallel to the major principal stress. The magnitude of strength anisotropy of intact rock can be described by testing the intact rock at different orientations of inherent anisotropy relative to the direction of applied load. The difference in directional strength is often controlled by the amount of flaky and elongated minerals present such as mica, chlorite or amphibolite. The variation of uniaxial compressive strength may also occur due to the presence of foliation planes in cases of schist, gneiss or marbles.

Vakili et al. (2014) reported that compressive strength of anisotropic rocks can vary significantly with respect to plane of weakness depending on the loading direction and the lowest strength value occurs when the orientation of the plane of anisotropy (bedding or

foliation) is between 35° and 45° to the specimens loading axis (β angle). The highest strength is achieved when the orientation is either 0° and 90°. Theoretical variation of uniaxial compressive strength depending on the orientation of anisotropy planes in presented in Figure 3.1. The theoretical model is an over-simplified representation of the variation of strength in anisotropic rocks.

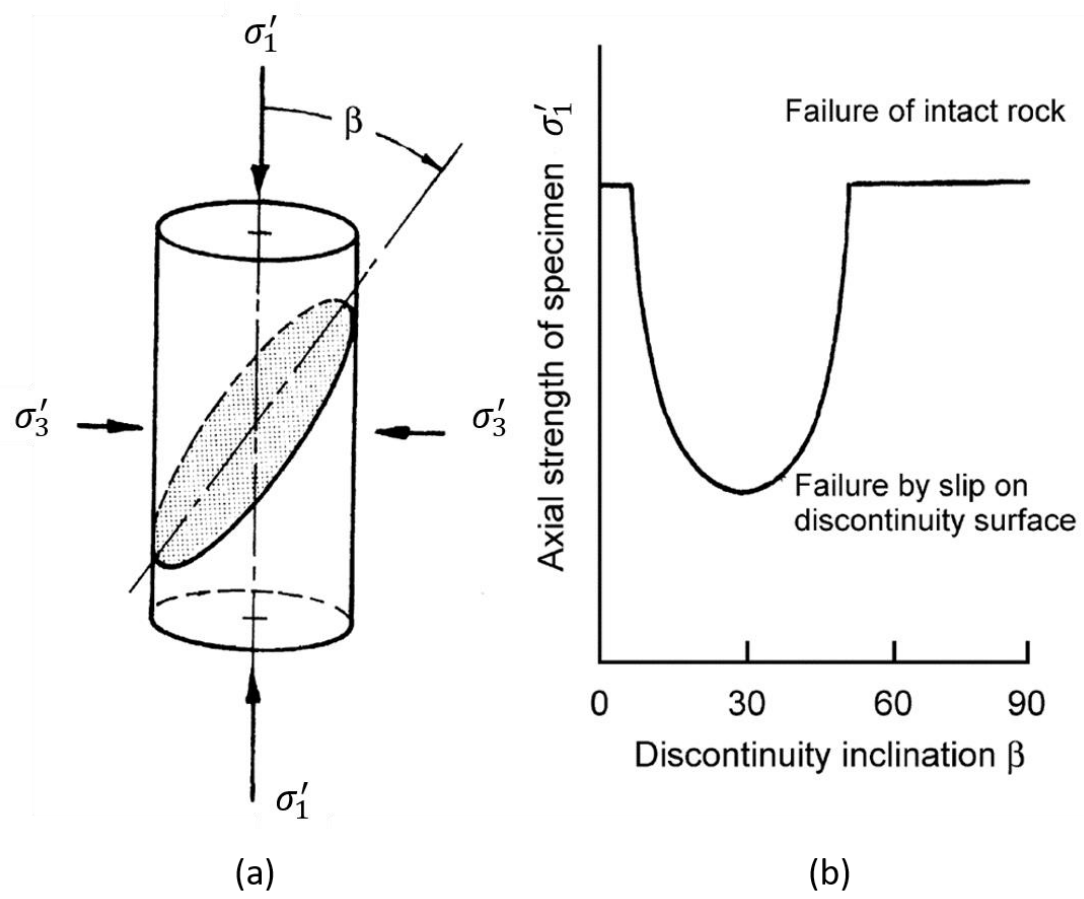

Figure 3.1: Anisotropic rock failure (a) definition of anisotropy plane (b) variation of peak strength with the angle of weakness plane, after Hoek and Brown (1980a)

The ratio of maximum to minimum compressive strength provides an indication of anisotropy intensity for various rock types. The ratio is often referred to as the anisotropy factor or anisotropy ratio. Most uniaxial compressive tests on anisotropic rocks fail in shear. A classification of anisotropy and associated factors extracted from several literatures by Vakili et al. (2014), is provided in Table 3.1.

Table 3.1: Classification of anisotropy intensity in various rocks, after Vakili et al. (2014)

Anisotropy classification	**Example rock types**	**Anisotropy factor**
Isotropic	Quartzite, hornfels, granulite	1 – 1.1
Low anisotropy	Quartzofeltspatic gneiss, mylonite, migmatite, shales	1.1 – 2.0
Medium anisotropy	Schistose gneiss, quartz schist	2.0 – 4.0
High anisotropy	Mica schist, hornblende schist	4.0 – 6.0
Very high anisotropy	Slate, phyllite	> 6.0

Milnes et al. (2006) reported that when an excavation is created in rock, the pre-mining stress state is altered so that the maximum principal stress is oriented tangentially around the opening. In case of foliated rocks, the strength varies with the orientation of foliation and hence with respect to the direction of the excavations peripheral stress component. This interaction between stress state and foliation induced anisotropy results in asymmetrical failure patterns around underground excavations. The location of failure depends on the orientation of foliation planes, interception angle, direction of major and minor principal stress and excavation geometry.

3.1.3 Plasticity of anisotropic rocks

The theory of plasticity is based on replacing the actual material with an idealized material that behaves elastically up to some limiting state of stress at which failure occurs. Essential elements of the theory are equations of equilibrium, the geometry of strain, a stress-strain relationship and a yield condition or criteria. Equations of equilibrium and strain geometry are independent of the material. The stress-strain relation for the anisotropic rocks can be obtained by considering the rocks to be transversely isotropic in case of foliated rocks or orthotropic in case of jointed rocks with three mutually perpendicular set of joints. To extend the plasticity theory for anisotropic rocks an appropriate yield condition or failure criteria is

required (Pariseau, 1968)

3.1.3.1 The single plane of weakness theory

Jaeger (1960) proposed the single plane of weakness theory for anisotropic rocks that considered the anisotropic material as an isotropic body containing a single set of weakness plane. The theory postulated that there are two independent failure modes, slip on the discontinuity and shear fracture of the intact rock material, depending on the orientation of the discontinuity to the principal stress directions. This behaviour can be well represented in specimens containing a single open joint or an artificially induced discontinuity.

The failure of rock matrix and the failure along the discontinuity planes was described by the Mohr-Coulomb criterion using different values of cohesion and friction for the rock matrix and the weakness plane. The failure criteria can be expressed as follows.

For rock matrix failure

$$\tau = c + \sigma tan\phi \tag{3.7}$$

For weakness plane failure

$$\tau_\theta = c' + \sigma_\theta tan\phi' \tag{3.8}$$

where, ϕ and c are the friction angle and cohesion of the intact rock or rock matrix, τ and σ are the shear and, normal stresses, ϕ' and c' are the friction angle and cohesion of the weakness plane oriented at θ degrees to the horizontal plane, τ_θ and σ_θ are the shear and normal stresses on the weakness plane.

The criterion provides an accurate simulation of the experimental data for transversely isotropic materials, but it requires a wide range of tests and a considerable amount of curve fitting and overestimates the strength when the orientation of the weakness plane is between

60° and 90°.

3.1.3.2 Hoek-Brown failure criterion for anisotropic rocks

Hoek and Brown (1980a) developed an empirical mathematical relationship between principal stresses to predict the failure propagation in rocks. In developing the empirical criterion, it was attempted to satisfy the following conditions.

i. The failure criterion should be in good agreement with the experimentally determined rock strength values.

ii. The criterion should be expressed using simple mathematical equations based on dimensionless parameters.

iii. The failure criterion should have the possibility of extension to deal with the failure of anisotropic and jointed rock masses.

A process based on trial and error using the experimental data was adopted. The proposed criterion was based on major and minor principal stresses. The empirical relationship between these stresses is given by the following equation.

$$\sigma_1 = \sigma_3 + (m\sigma_c\sigma_3 + s{\sigma_c}^2)^{1/2} \qquad \text{with } \sigma_1 > \sigma_2 > \sigma_3 \qquad (3.9)$$

where, σ_1 is the major principal effective stress at failure, σ_3 is the minor principal effective stress or, in case of a triaxial test, the confining pressure, σ_c is the uniaxial compressive strength of the intact rock material from which the rock mass is made up, and m and s are empirical constants

The original Hoek-Brown criterion assumed that the rock was isotropic and its strength was the same in all directions. Hoek and Brown (1980a) indicated that the empirical parameters m and s cannot be constant for anisotropic rocks and they must vary with the orientation of the

plane of weakness as defined by the angle β in Figure 3.1 (a). By a process of trial and error, it was found that a good fit to experimental data can be obtained by using the following values of empirical constants.

$$m = m_i[1 - N_1 \exp(-\theta)^4] \tag{3.10}$$

$$s = 1 - P_1 \exp(-\zeta)^4 \tag{3.11}$$

In which, m_i is the value of m for intact rock determined for β equal to 90°

$$\theta = \frac{\beta - \beta_m}{N_2 + N_3\beta} \tag{3.12}$$

$$\zeta = \frac{\beta - \beta_s}{P_2 + P_3\beta} \tag{3.13}$$

where, $\beta_m$is the value of β at which m is minimum, β_s is the value of β at which s is minimum; N_1, N_2, N_3, P_1, P_2 and $P_3$are constants.

The general criterion was modified to account for the anisotropic strength behaviour. However, the reasonable fit to the data was obtained given a large number of parameters and constants. Hoek (1983) proposed the anisotropic criterion for the strength of the schistose rock. The criterion assumes that the shear strength of the discontinuity surfaces in schist rocks can be defined by an instantaneous friction angle ϕ_i' and an instantaneous cohesion c_i'. The axial strength σ_1' of a triaxial specimen containing inclined discontinuities is given by the following equation.

$$\sigma_1' = \sigma_3' + \frac{2(c_i' + \sigma_3' Tan\phi_i')}{(1 - Tan\phi_i' Tan\beta)Sin2\beta} \tag{3.14}$$

where, σ_3' is the minimum principal stress or confining pressure, β is the inclination of the

discontinuity surface to the direction of major principal stress σ_1.

Equation (3.14) can only be solved for values of β within 25° of the friction angle. Very small values of β will give very high values of σ_1', while values of β close to 90° will give negative values of σ_1'. The physical significance of these results is that slip on the discontinuity surface is not possible, and failure will occur through the intact material. A typical plot of the axial strength σ_1' and β is given in Figure 3.1 (b). The criterion depends on the pre-determined values of the instantaneous friction angle ϕ_i' and the instantaneous cohesion c_i' of the weakness planes and these values can be derived from following equations.

The instantaneous cohesive strength ϕ_i' is given by

$$\phi_i' = Arctan(4hCos^2\left(30 + \frac{1}{3}Arcsin\, h^{-\frac{3}{2}}\right) - 1)^{-1/2} \tag{3.15}$$

where

$$h = 1 + \frac{16(m\sigma' + s\sigma_c)}{3m^2\sigma_c} \tag{3.16}$$

and σ' is the effective normal stress given by

$$\sigma' = \frac{1}{2}(\sigma_1' + \sigma_3') - \frac{1}{2}(\sigma_1' - \sigma_3')Cos2\beta \tag{3.17}$$

The instantaneous cohesive strength c_i' is given by

$$c_i' = \tau - \sigma' Tan\phi_i' \tag{3.18}$$

where, τ is the shear stress at failure and is given by:

$$\tau = (Cot\phi_i' - Cos\phi_i')\frac{m\sigma_c}{8} \tag{3.19}$$

Experimental data was used to assess the quality of the anisotropic Hoek-Brown criterion. Prediction of strength variation with schistosity angle was found to be accurate where the weakness planes orientation was between 20° to 60° to the principal stress.

Several modifications to the Hoek-Brown failure criterion have been proposed over the last few decades for anisotropic rocks. Colak and Unlu (2004) investigated the effects of anisotropy on the Hoek-Brown strength parameter m_i and reported that the m_i value can be used to quantify the anisotropic effect. Saroglou and Tsiambaos (2008) modified the Hoek-Brown failure criterion by introducing a new parameter to account for the effect of strength anisotropy. The modified criterion was used to determine the strength of intact anisotropic rock under loading for different orientations of the plane of anisotropy. The proposed modification can be used to predict the strength of the intact metamorphic rocks and potentially, the criterion can be extended to rock masses. The criterion proposed by Saroglou and Tsiambaos (2008) is given by the following relation.

$$\sigma_1 = \sigma_3 + \sigma_{c\beta}\left(k_\beta m_i \frac{\sigma_3}{\sigma_{c\beta}} + 1\right)^{0.5} \tag{3.20}$$

where $\sigma_{c\beta}$ is the uniaxial compressive strength at an angle of loading β, and k_β is the parameter describing the anisotropy effect.

Shi et al. (2016) developed a modified Hoek-Brown failure criterion to describe the triaxial strength behaviour of rocks by utilizing an anisotropic index. The proposed criterion considered the variation of the uniaxial compressive strength of the intact anisotropic rocks and the parameter α_β was introduced in the modified failure criterion to represent the effect of strength anisotropy. The modified criterion proposed by Shi et al. (2016) is given by the following equation.

$$\sigma_1 = \sigma_3 + \sigma_{c\beta}\left(m_i \frac{\sigma_3}{\sigma_{ci}} + 1\right)^{\alpha_\beta} \quad (3.21)$$

3.1.3.3 Ubiquitous joint model

The ubiquitous joint model accounts for the presence of weakness planes, such as weathering, joints, bedding planes or foliation planes in the Mohr-Coulomb failure criterion. The criterion for failure in the weakness planes of known orientation consists of a composite Mohr-Coulomb envelop with tension cut-off. Yielding may occur either in the solid or along the weakness planes, depending on the stress state, the orientation of the weakness planes and material properties of the solid and weakness planes (Itasca Consulting Group, 2017a).

The Mohr-Coulomb failure criterion is a set of linear equations in principal stress space describing the conditions for which an isotropic material will fail, with any effect from the intermediate principal stress σ_2 neglected. Jaeger et al. (2007) reported that based on an extensive experimental investigation into friction, Coulomb assumed that failure in a rock or soil takes place along a plane due to the shear stress τ acting along that plane. The Coulomb failure criteria can be written as follows.

$$|\tau| = S_0 + \sigma \, tan\phi \quad (3.22)$$

where τ is the shear stress acting on the plane, S_0 is the inherent shear strength, also known as cohesion c, σ is the normal stress acting on the plane and ϕ is the angle of internal friction.

The Coulomb criterion contains two material constants, cohesion c and angle of internal friction ϕ and can be represented in the Mohr dagram by a straight line inclined to the σ-axis by the angle ϕ as shown in Figure 3.2. Coulomb's theory postulated that the failure will occur on a plane when the normal and shear stresses acting on that plane satisfy the condition in Equation (3.22). Experimentally it was observed that for some negative values of σ_3,

failure occurs by extensional fractures in planes perpendicular to the tensile stress. Coulomb's theory also predicts that the compressive stress required to cause failure, σ_1, will increase linearly with the confining stress σ_3. However, experiments typically show shat that σ_1 at failure increases at a less than a linear rate with σ_3.

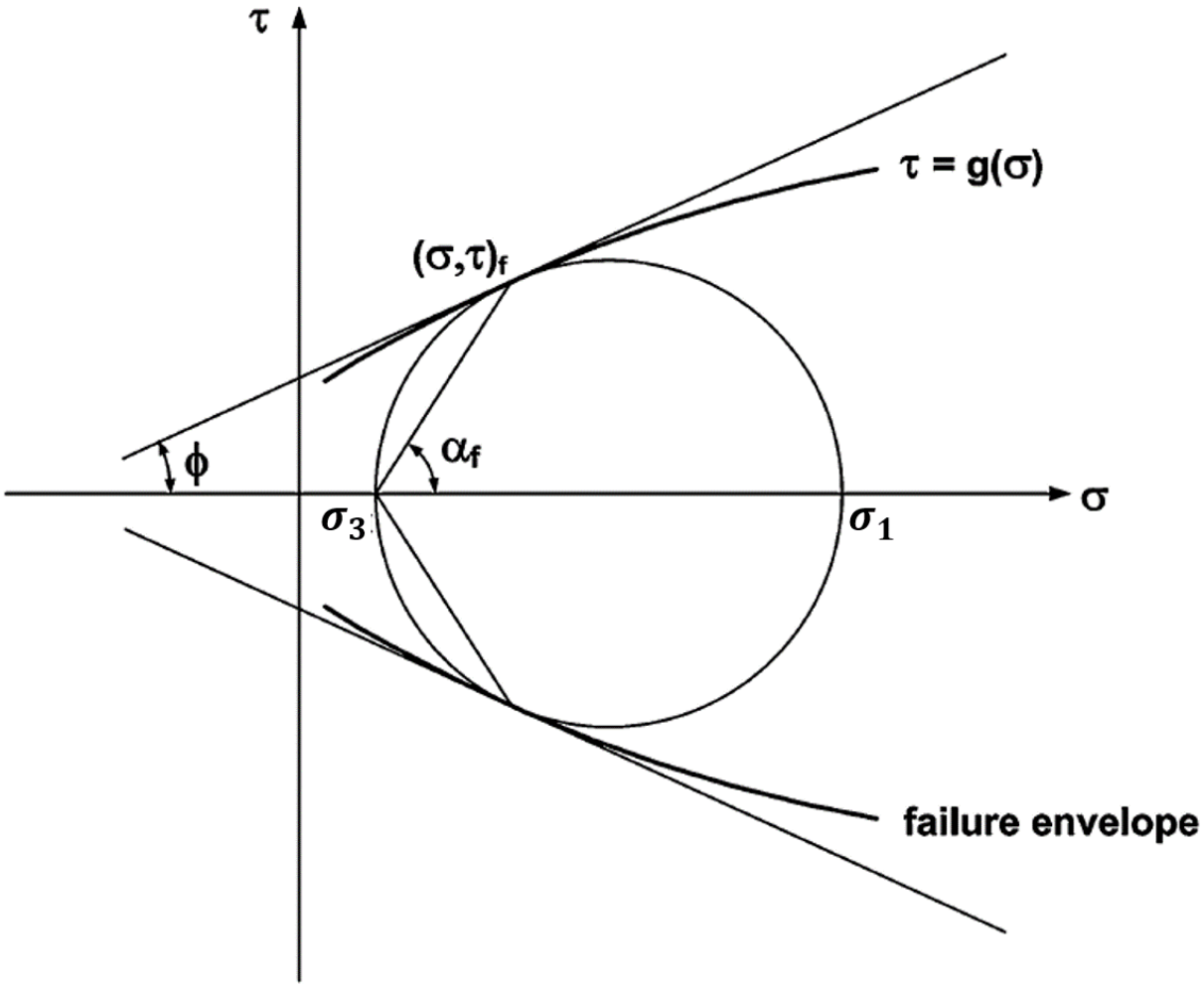

Figure 3.2: Mohr diagram and failure envelopes, after Ulusay (2015)

To correct the deficiencies in Coulomb's theory, Mohr provided a hypothesis that assumed that when a shear failure occurs across a plane, the normal stress and shear stress can be related by a function and the equation can be represented by a more general, possibly non-linear, relation of the form as follows.

$$|\tau| = f(\sigma) \tag{3.23}$$

The failure is assumed when in any plane the shear stress τ reaches the failure shear stress τ_{max} which is given by a functional relation of the form as follows.

$$\tau_{max} = c + \sigma_n \, tan\phi \tag{3.24}$$

where, c is the cohesion of the material, ϕ is the angle of internal friction of the material and σ_n is the normal stress acting on the respective failure plane.

The Mohr-Coulomb criterion can be expressed in terms of the principal stresses as follows.

$$\sigma_1 = \frac{1 + \sin\phi}{1 - \sin\phi}\sigma_3 + 2c \, \frac{\cos\phi}{1 - \sin\phi} \tag{3.25}$$

where, σ_1 and σ_3 are major and minor principal stresses.

The unconfined compressive strength σ_{ci} postulated by the Mohr-Coulomb criterion is obtained by setting $\sigma_3 = 0$ and is given by the following relation.

$$\sigma_{ci} = 2c \, tan\left(\frac{\pi}{4} + \frac{\phi}{2}\right) \tag{3.26}$$

The curve shown in Figure 3.3 can be determined experimentally as the envelope of all the Mohr's circles that corresponds to states of stress that cause failure. The failure will occur if one of the Mohr's circles touches the curve defined by Equation 3.24, see Figure 3.3.

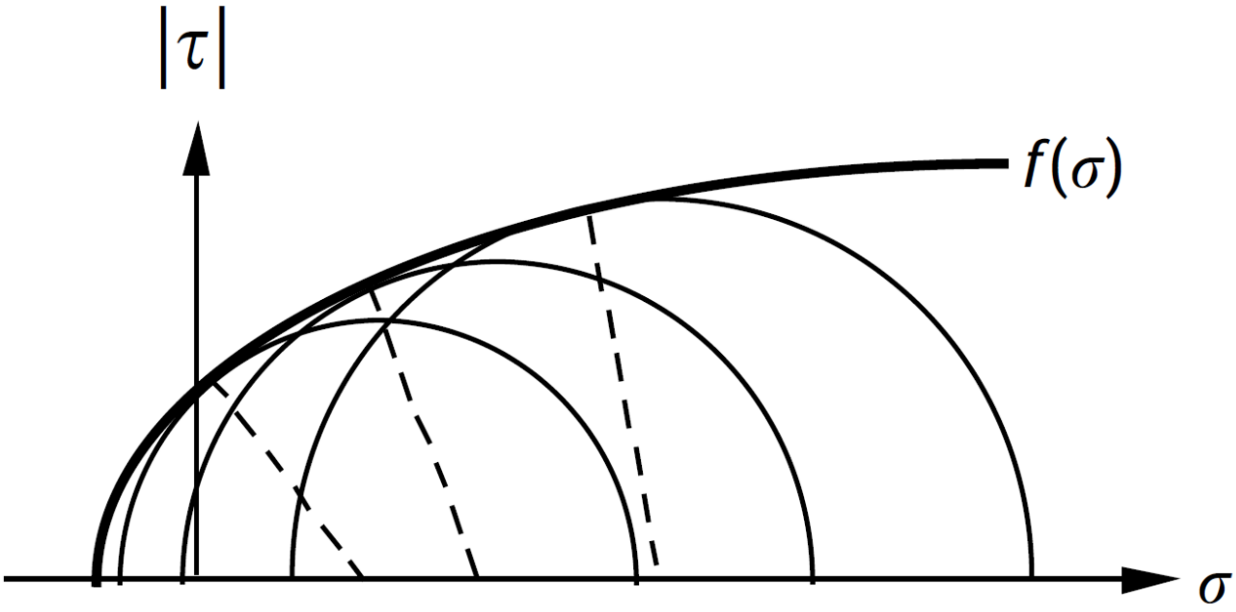

Figure 3.3: Non-linear failure curve, after Jaeger et al. (2007)

The two envelopes coincide when the Mohr criterion is a linear function which is commonly known as Mohr-Coulomb failure theory. A representation of the Mohr-Coulomb failure envelope on a Mohr diagram is provided in Figure 3.4.

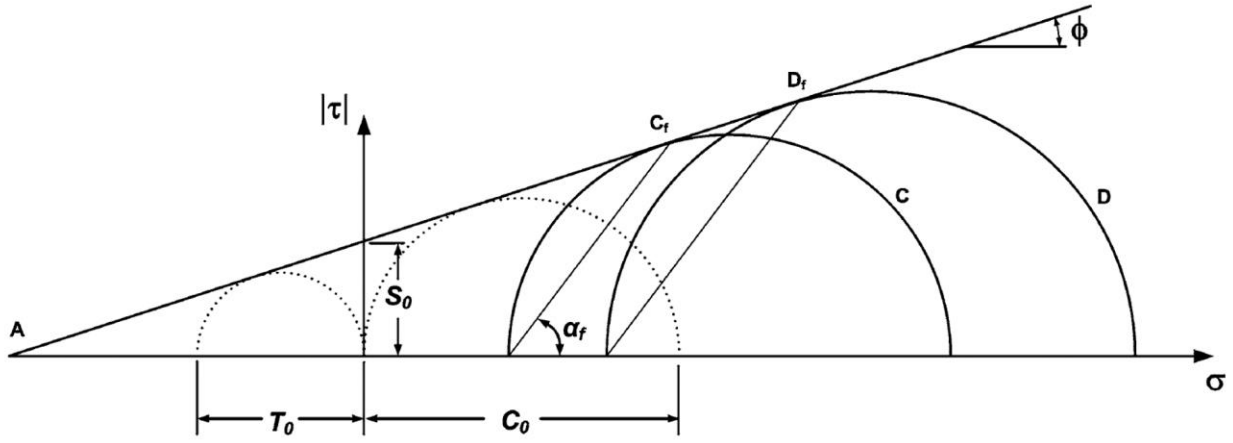

Figure 3.4: Linear envelope in Mohr diagram showing Mohr-Coulomb failure criterion, after Ulusay (2015)

The dashed circle with a diameter C_0 represents the state of stress during the uniaxial compressive test, with C_0 being the uniaxial compressive strength. The dashed circle with a

diameter T_0 represents the tensile strength predicted from Mohr-Coulomb criterion. The shape of failure surface in principal stress space is dependent on the form of the failure criterion, linear functions map as planes and non-linear functions as curvilinear surfaces. The Mohr-Coulomb criterion can be represented by six planes in that intersect one another along six edges, defining a hexagonal pyramid in the principal stress space. It can also be described as an irregular hexagon with sides of equal length on the equi-pressure or π-plane as shown in Figure 3.5 (Ulusay, 2015).

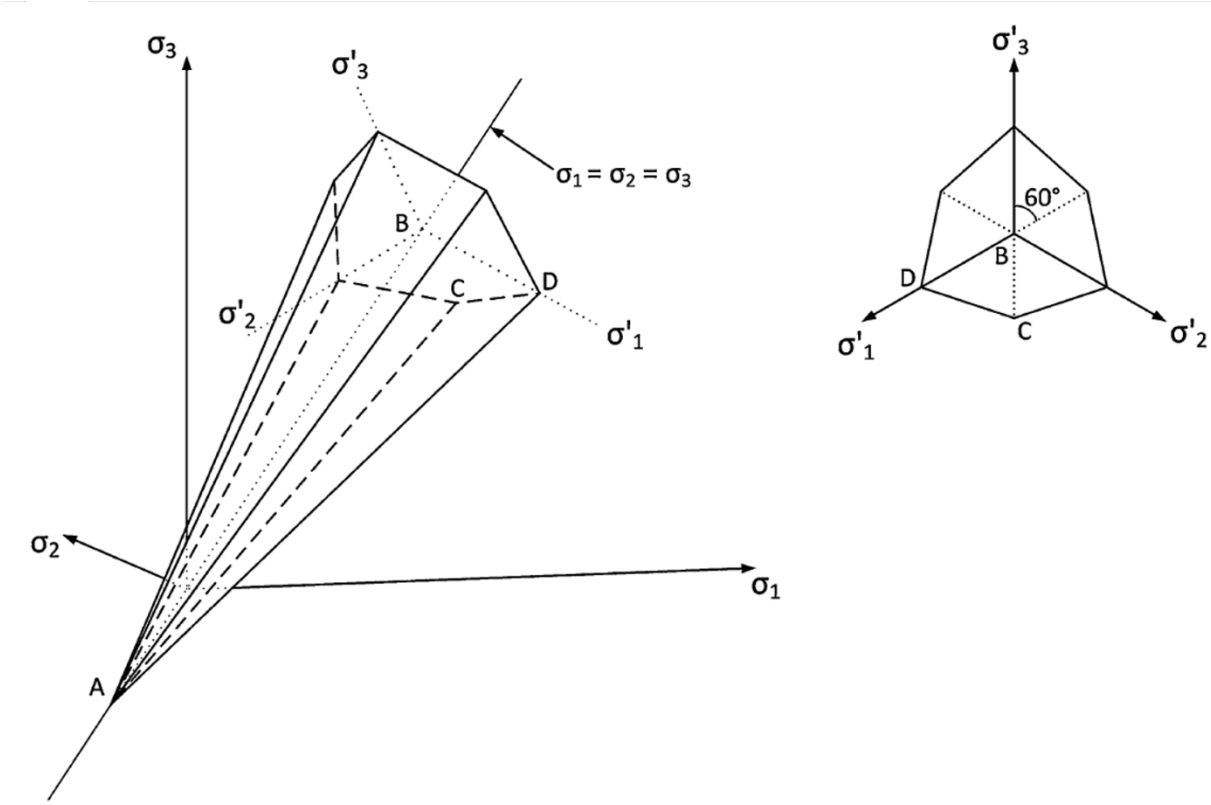

Figure 3.5: Pyramidal surface in principal stress space and cross-section in the equi-pressure plane, after Ulusay (2015)

For negative values (tensile) of the minor principal stress, experiments show that the failure plane is perpendicular to $\sigma_3 = -T$. The tensile failure mode is completely different from the shear failure mode that occurs with compressive normal stresses. To account for the tensile failure Paul (1961) introduced the concept of tension cut-offs and modified the Mohr-

Coulomb failure criterion that required three material constants the modified criterion can be written as follows

For $\sigma_1 > (C_0 - mT)$

$$|\tau| = f(\sigma) \tag{3.27}$$

and for $\sigma_1 < (C_0 - mT)$

$$\sigma_3 = -T \tag{3.28}$$

where, $m = \frac{1+\sin\phi}{1-\sin\phi}$

The representation of tension cut-offs on the Mohr diagram is provided in Figure 3.6. In principal stress space, the modified MC criterion with tension cut-offs involves the MC pyramid intercepted by the second pyramid with three planes perpendicular stress axes. Stress state depicted by the broken circle in Figure 3.6, is defined by $\sigma_1 = \sigma_1^* = (C_0 - mT)$. $\sigma_3^* = -T$ is not a part of the failure envelope and all the Mohr circles with $\sigma_1 < \sigma_1^*$ are tangent to the envelope at the point $\sigma_3^* = -T$.

Mohr-Coulomb failure criterion is mathematically simple and has a clear physical meaning of the material parameters, and general level of acceptance in rock mechanics.

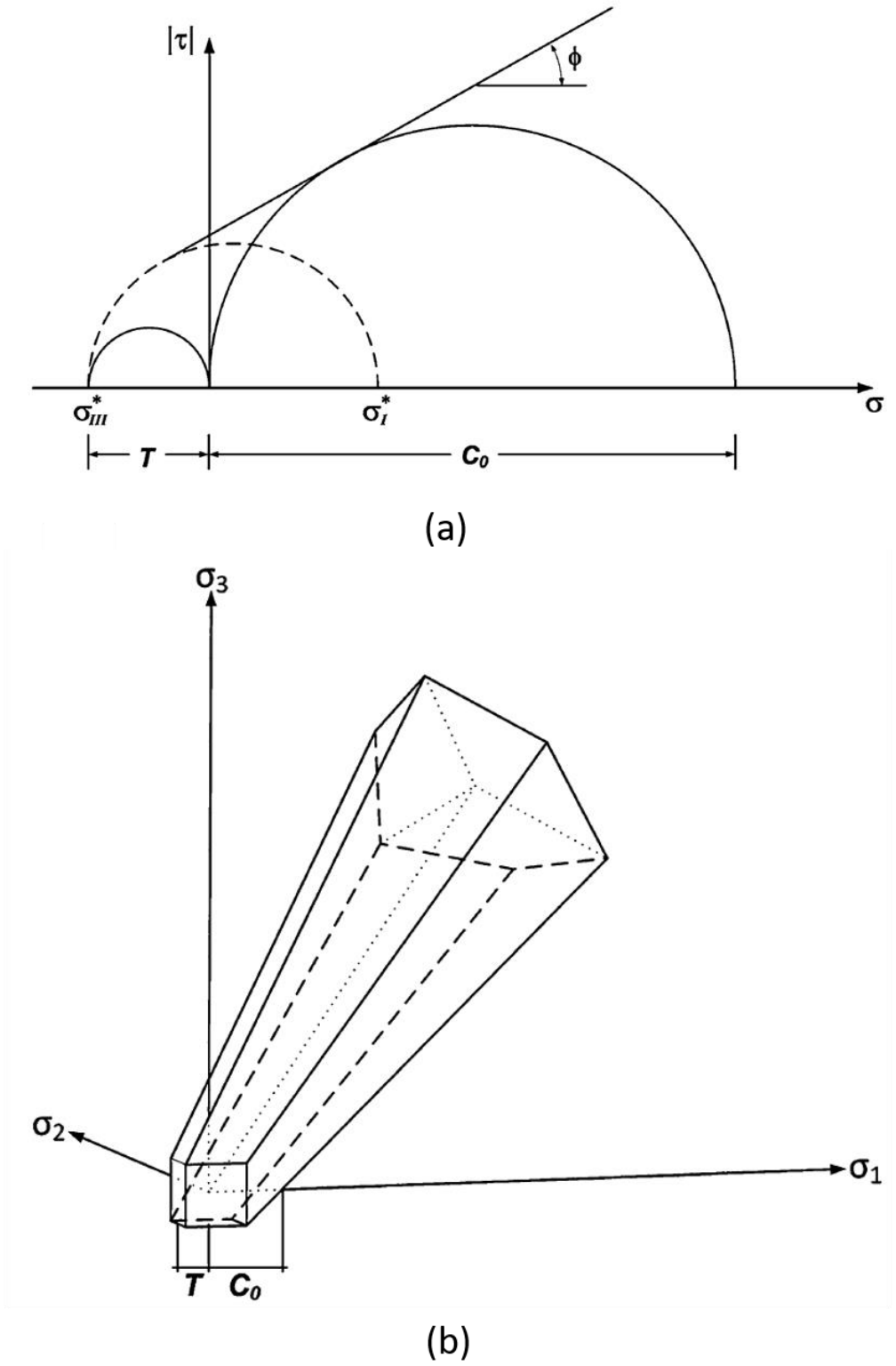

Figure 3.6: Modified Mohr-Coulomb criterion with tension cut-off a) failure envelope in Mohr diagram b) representation in principal stress space, after Ulusay (2015)

3.2 Time-dependent behaviour of rocks

Malan and Basson (1998) provided distinct definitions of creep and time-dependency. Creep is defined as the continued deformation due to constant applied stress and is generally used in relation to intact laboratory-sized specimens containing no large-scale discontinuities. Time dependency is a more general term that includes concept like the creep of intact rock, creep of large-scale discontinuities, delayed failure and long-term strength. Time dependency can also refer to the deformations that are not related to geometric changes in the dimensions of excavations and occur on a time scale of days to years.

3.2.1 Creep in rocks

Jaeger et al. (2007) reported strains measured by Griggs (1939) during uniaxial compression of alabaster samples immersed in water. When stress is applied instantaneously to a sample, the immediate elastic strain is observed, and the strain continues to increase at an ever-decreasing rate, and this is termed as the primary or transient creep. This stage is followed by a steady state creep in which the strain increases linearly with time, finally followed by tertiary creep, in which the strain increases at an increasing rate until failure occurs. These three stages have different characteristics. If the applied stress is suddenly reduced to zero during primary creep, the strain will relax to zero. However, if the stress is removed during steady-state creep, the strain will relax to a nonzero value. A typical strain-time graph showing primary, secondary and tertiary creep phases was provided by Lama and Vutukuri (1978). The schematic curve provided by the authors illustrates a case where the applied load is sufficiently high to take the rock samples through all stages of creep and is constant over time.

Griggs (1939) used empirical strain time laws to describe creep curves of rock specimens under uniaxial compression as follows.

$$\varepsilon(t) = \mathrm{A} + \mathrm{B}\log t + \mathrm{C}t \tag{3.29}$$

where A is the instantaneous elastic strain, $B \log t$ represents the primary or transient creep, Ct is the secondary or steady state creep and A, B and C are constants

In the most general form, the creep function can be expressed as follows.

$$\varepsilon = \varepsilon_e + \varepsilon_1(t) + Vt + \varepsilon_3(t) \tag{3.30}$$

where ε_e is the instantaneous elastic strain, $\varepsilon_1(t)$ is the transient creep, Vt is the steady-state creep and $\varepsilon_3(t)$ is the tertiary or accelerating creep.

During the primary or transient creep, the creep velocity decreases at a steady rate, in the secondary or steady-state creep the creep velocity is constant with time and in the tertiary or accelerating creep stage, the creep velocity increases with time. These stages of creep can dominate the deformation process, depending on the material and conditions. Creep movements around underground excavations in an underground mine do not take place under constant load conditions. The effect of creep movements is to reduce the stress anisotropy so that the rock dilates.

Jaeger et al. (2007) reported that various expressions have been proposed to represent the primary or transient state creep term and the expressions can generally fit strain data over certain limited periods of time but do not have appropriate behaviour at either small or large values of time. Also, these expressions fail to provide a smooth transition from transient to steady-state creep. The steady-state creep rate (V) depends on the specific experimental conditions, temperature and the stress.

In rock masses, the creep can manifest as creep of intact rock material and / or creep along the discontinuities. In intact rock, creep is primarily caused due to the time-dependent micro-

fracturing of the rock which produces shear and volumetric strains if the rock is dilatant. Creep rates of intact rock are principally controlled by applied deviatoric stress, effective confining pressure and moisture content. Increase in deviatoric stress results in an increase of creep rate. Several rocks do not show significant creep unless the deviatoric stress is above some threshold value. Confining pressure is inversely related to the creep rates, increase in confining pressure results in an increase of compressive strength of the rock samples and hence the creep rate will decrease with increase in confining pressure.

The creep displacement in a discontinuity is a function of the normal stress and shear stress of the fracture. Under constant normal stress, the creep deformation is expected to increase as the shear stress is increased and, for constant shear stress, decrease if the normal stress increases (Amadei, 1979). Bowden and Curran (1984) reported that the creep movement in a discontinuity varies depending upon the planarity, roughness and filling of the discontinuities. In planar joints, creep is presumed to be controlled by an adhesion-frictional mechanism.

3.2.2 Rock rheology

Goodman (1989) indicated that solids are viewed as bodies that retain shape indefinitely. However, an apparent solid material distorts slowly and continuously in response to shearing stresses and hence can be viewed as an at least partially viscous liquid. Jaeger et al. (2007) defined rheology as the study of time-dependent stress-strain behaviour. The simplest rheological stress-strain relation that reflects the time dependence of rocks can be constructed using springs and dashpots and the non-linear rheological models are created by using Saint Venant's element. Various elements used in rheological models are provided in Figure 3.7. The spring element represents an elastic Hookean material in which the stress and strain are related according to the Hooke's law as shown in Equation (3.31). When a force is applied,

the length of the spring increases by a certain amount, and when the force is removed the spring returns to its original length.

$$\sigma = k\varepsilon \tag{3.31}$$

where, σ is stress, ε is strain and k is constant of proportionality.

In these models, an analogy is made between variables of force and displacement for the spring and stress and strain in the solid material. The elastic Hookean element is used to simulate the instantaneous strains and is governed by a constant stiffness modulus for non-linear elastic materials. These materials follow the Hooke's law and are linear and independent of time (Paraskevopoulou, 2016).

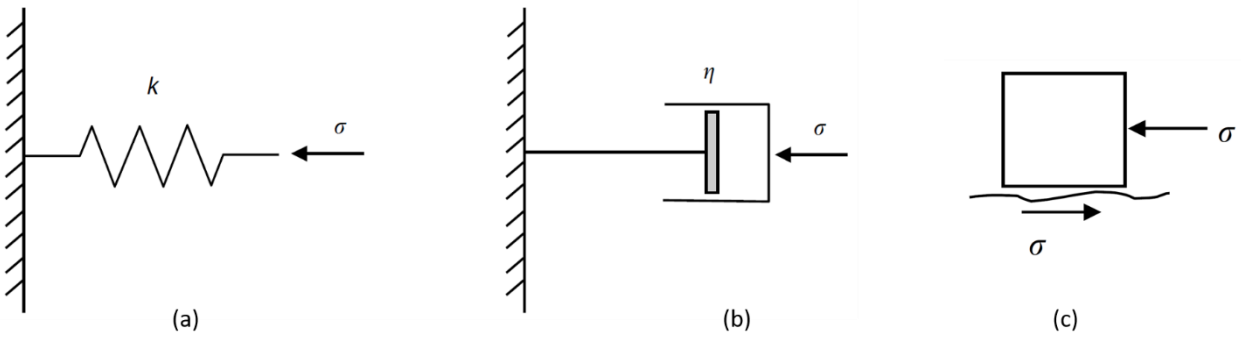

Figure 3.7:Elements used in rheological models a) Hookean elastic element b) Newtonian viscous element c) Saint Venant substance, after Jaeger et al. (2007)

Dashpot is the second basic element used for constructing rheological models. Dashpot can be considered as a piston moving in a cylinder with a perforated bottom so that no air is trapped inside and between the cylinder and the piston wall there is a viscous lubricant, so a force is needed to displace the piston. The stronger this force is, the faster the piston will move. Dashpot represents a Newtonian viscous substance which follows the following stress-strain relationship.

$$\sigma = \eta \frac{d\varepsilon}{dt} \equiv \eta \dot{\varepsilon} \tag{3.32}$$

where η is a constant and over dot indicates the derivative with respect to time.

The viscous body considers the time component of rock behaviour, however, it cannot adequately represent the complete behaviour of rocks, as it fails to account for the instantaneous elastic response of the rock when the initial load is applied and a plastic component of the rock behaviour. The viscous element has no memory and cannot sustain the accumulated strains once the load is removed.

Non-linear rheological models are mathematically more difficult to treat. These models can be formulated by utilizing Saint Venant's element. The element can be represented by a block of mass m placed on a rough, frictional surface. If the friction coefficient between the mass and the surface is μ and the contact area is A, the block will not move until the applied stress σ reaches the value of $mg\mu/A$, which can be denoted by σ^*. Hence the strain will be zero for $\sigma < \sigma^*$ and will be indeterminate if $\sigma > \sigma^*$. The St. Venant element is commonly used to simulate the failure state and three-dimensional theory of plasticity

The rheological models are constitutive stress and strain relationship. Complicated behaviour such as the time-dependent behaviour of rocks can be simulated by utilizing the three mechanical analogues, i.e. Hookean element, Newtonian element and St. Venant element together in various parallel and series combination. These combinations can be used to describe a wide range of rock behaviour including elasticity, plasticity, visco-elasticity and visco-plasticity.

3.2.2.1 Visco-elastic models

Fahimifar et al. (2015) reported that various constitutive equations have been developed to

simulate the behaviour of rocks based on various assumptions and principles. The most general assumption is that of elastic behaviour or reversible deformations. The classic visco-elastic models can be represented by a series of spring and dashpots connected in series or parallel combinations. Constitutive models in these elastic models attempt to relate the current strain rate and the current stress rate to define creep deformation in rocks through analytical formulation. To enhance the visco-elastic models, several rheological models have been proposed to simulate time-dependent behaviour.

Visco-elastic rheological models are constructed using springs and dashpots to simulate the elastic and viscous behaviour, and these models do not account for plastic behaviour as plastic slider elements are not used. Most common visco-elastic models used include the Kelvin model, the Maxwell model and the Burgers model.

The Kelvin-Voigt model is constructed by combining the elastic Hookean and viscous Newtonian element in parallel. In this model, the two elements experience identical strain and the total stress applied to the model equals the sum of stress on each element. When stress is applied, the elastic element shows the initial deformation, but the viscous element resists the applied stress. Over time, the dashpot deforms, and a part of applied stress on the dashpot is transmitted to the elastic element, and this results in a decrease of applied stress and strain-rate on the viscous element. This behaviour is termed as delayed elasticity. The model does not show any instantaneous deformations as the elastic and viscous element can only be deformed simultaneously. Mechanical analogue and typical strain time relationship for Kelvin model are shown in Figure 3.8.

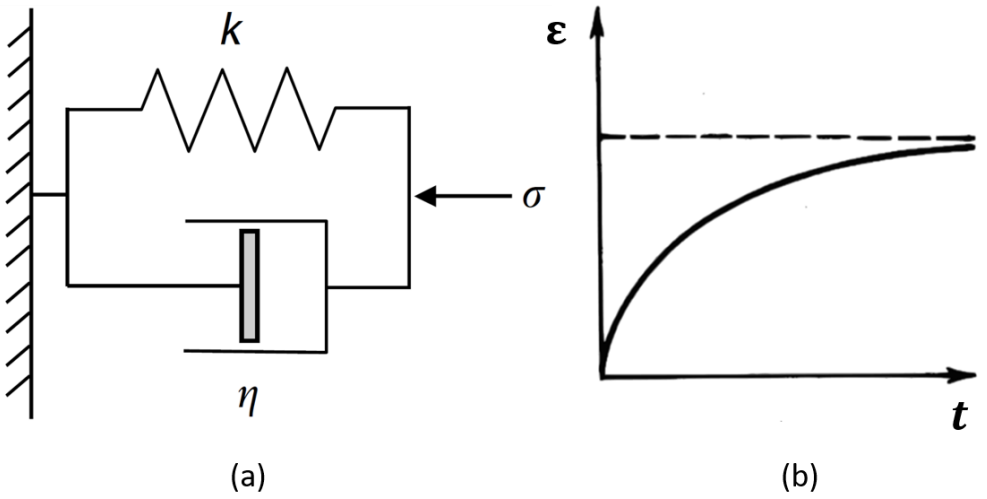

Figure 3.8: a) Kelvin-Voight model, after Jaeger et al. (2007) b) strain-time relationship, after Goodman, (1989)

The Maxwell model is constructed by connecting an elastic spring element and viscous dashpot element in series. In this model, the two elements experience identical stress, and the resulting total strain is the sum of the strains in spring and dashpot elements. When constant stress is applied to the model, elastic spring element shows instantaneous strain, and for constant stress over time the total strain of model increases with a constant rate due to the viscous dashpot element. If the applied stress is removed, the elastic strain in spring is recovered while the viscous strain in the dashpot remains. The viscous strain can only be recovered over time with a complete reversal of the boundary conditions. Paraskevopoulou (2016) reported that the Maxwell model could be approximately used to simulate the visco-elastic behaviour of rocks. However, the model has some limitations as the model has a linear strain-time relationship, but the actual strain-time behaviour commonly observed from rock testing is non-linear. Mechanical analogue and strain-time relationship for Maxwell model is provided in Figure 3.9.

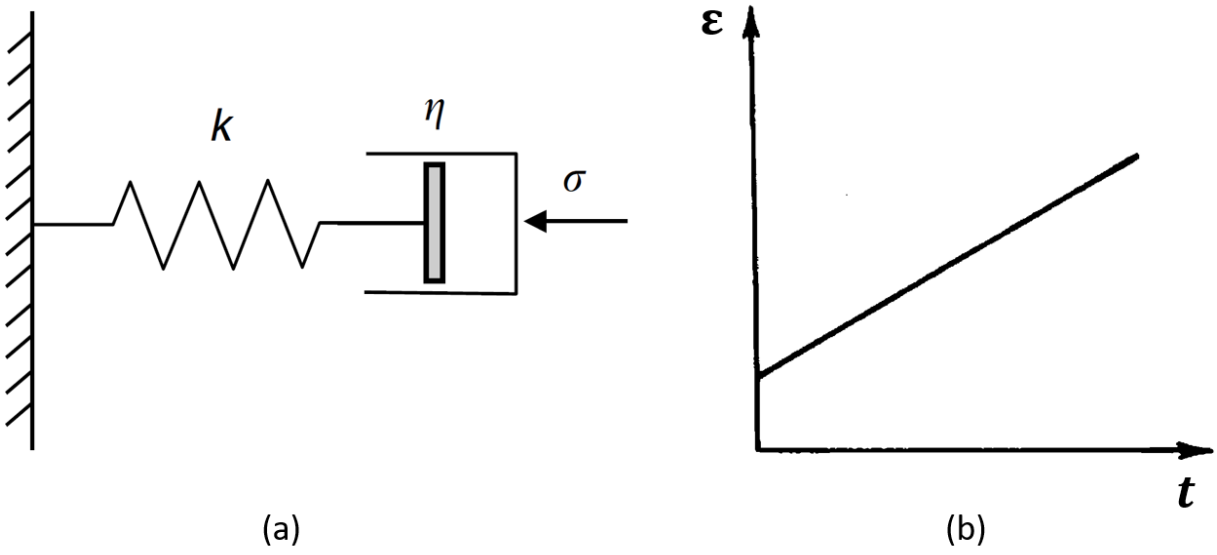

Figure 3.9: a) Maxwell model, after Jaeger et al. (2007) b) strain-time relationship, after (Goodman, 1989)

The Burgers model is constructed by placing the Kelvin model in series with a Maxwell model, see Figure 3.10. The model exhibits instantaneous strain, transient creep and steady-state creep. The governing equations for this model can be found by utilizing the equations for Kelvin and Maxwell model. In this model, the stress in each model is the same, and the total strain will be the sum of individual strains from the two models.

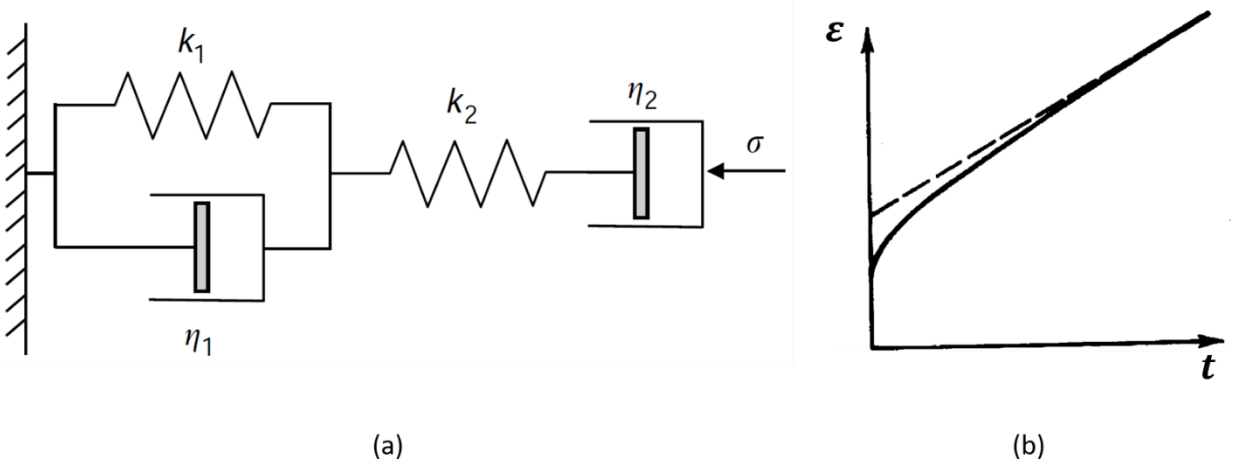

Figure 3.10: a) Burgers model, after Jaeger et al. (2007) b) strain-time relationship, after (Goodman, 1989)

3.2.2.2 Visco-plastic models

The visco-plastic behaviour of rocks plays a relevant role in deep underground excavations subjected to initial stresses (Sterpi and Gioda, 2009). The creep behaviour of geological materials can be approximated through rheological models that are represented as the assemblage of a simple element such as Hookean spring element, Newtonian viscous element and St. Venant frictional cohesive element (Cristescu and Gioda, 1994). These elements can be combined in series or parallel to depict visco-plastic response of soils and rocks. The rheological model for rocks should account for the three creep stages previously mentioned and even in the simple isotropic case, the model should separately consider the volumetric and the deviatoric behaviour.

The Bingham model is constructed by placing a spring, dashpot and St. Venant element in series. For St. Venant element the block will not move until the applied stress reaches the value of $\sigma^* = mg\mu/A$. In Bingham model, for applied stress less than σ^*, the block will not move, and the displacement will be confined to the elastic spring. The strain in the elastic spring will be σ/k. If a stress greater than σ^* is instantaneously applied, the block will move, and this motion will be resisted by the frictional stress $\sigma_o > \sigma^*$ applied to the block by the rough surface. A force balance on the block shows that the stress transmitted to the dashpot will be $\sigma_o - \sigma^*$ and the strain in the dashpot will be $(\sigma_o - \sigma^*)t/\eta$. The dashpot and the block are assumed to be coupled rigidly, hence the total strain of the system will be the sum of the strain in the spring and in the dashpot. The response of a Bingham model to an instantaneous stress is given by

For $\sigma_o < \sigma^*$

$$\varepsilon = \frac{\sigma_o}{k} \tag{3.33}$$

And for $\sigma_o > \sigma^*$

$$\varepsilon = \frac{\sigma_o}{k} + \frac{(\sigma_o - \sigma^*)t}{\eta} \tag{3.34}$$

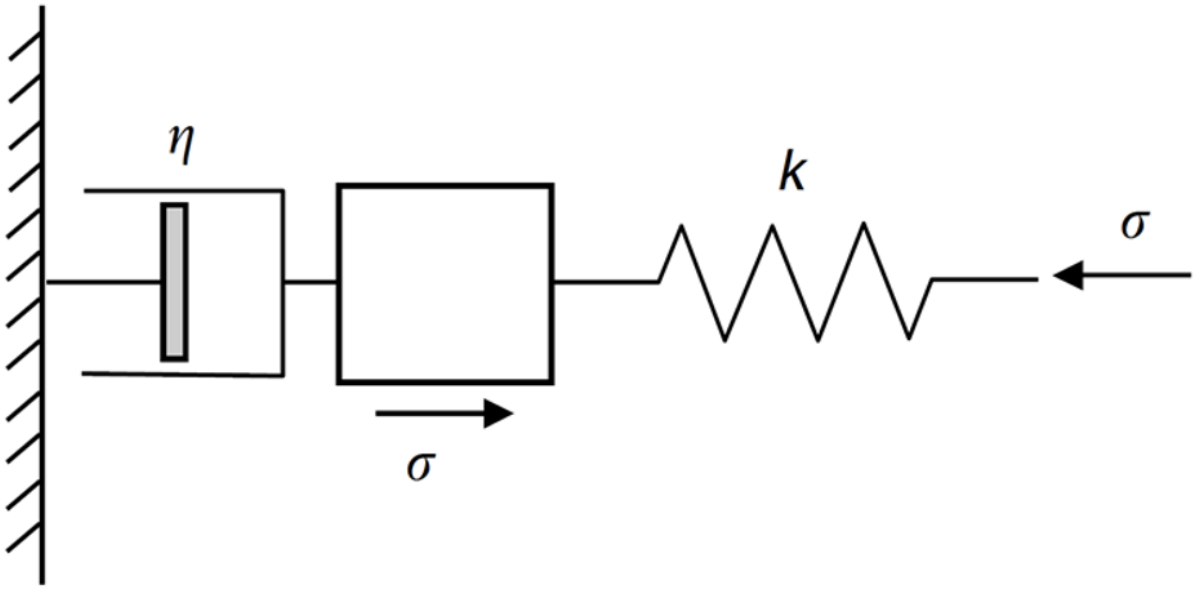

Figure 3.11: Bingham model mechanical analogue, after Jaeger et al. (2007)

3.2.2.3 Application to simulate creep behaviour

The visco-elastic and visco-plastic rheological models described above have been used by several authors to investigate the creep mechanisms in intact rock and rock masses. Zhang et al. (2015) investigated the creep behaviour of clastic rocks by conducting triaxial creep tests on an intact rock sample using a rock servo-controlling rheological testing machine. The authors investigated the relationship between axial strain and time under varying confining pressures and Burgers creep model was utilized to fit the creep curves. Sterpi and Gioda (2009) developed a rheological model to simulate the visco-plastic behaviour around advancing tunnel in squeezing rock. The model accounts for the primary (visco-elastic), and secondary (visco-plastic) contributions to the rock creep. The models consisted of a visco-elastic Kelvin-Voigt and a visco-plastic softening unit connected in series, and the model assumed that the volumetric response of the rock is independent of time. Fahimifar et al.

(2015) modified the rheological model proposed by Sterpi and Gioda (2009) to simulate the creep behaviour of soft rocks under different stress levels at loading, unloading and reloading phases. The modification enhanced the modelling of the secondary creep at low-stress levels and allowed to calculate the unloading and reloading deformations.

Paraskevopoulou and Diederichs (2018) analyzed the total displacements around a circular tunnel in a visco-elastic medium by performing an isotropic axisymmetric finite difference modelling. The rock mass was assumed to behave as an elasto-visco-elastic material and Burgers-creep viscous model was used to simulate creep. To investigate the time-dependent component of the total radial displacements, two different analyses were performed. The first analysis aimed at examining the contribution of the primary creep by using the Kelvin-Voigt model and the Maxwell body was deactivated. In the second analysis, the contribution of the Burgers model was investigated to capture both primary and secondary stages of creep. Tran Manh et al. (2015) proposed an anisotropic time-dependent constitutive model to account for the time-dependent and anisotropic response of the rock mass in squeezing ground conditions at the Saint-Martin-la-Porte access gallery excavated within the Lyon-Turin railway project. The proposed model included ubiquitous joints of specific orientation embedded in an isotropic visco-plastic medium. The model was implemented in FLAC3D and numerical simulations were performed to back-analyze the anisotropic closure. The creep behaviour of the rock mass was simulated by using Burgers-creep visco-plastic model that allows for the computation of both instantaneous and delayed deviatoric strains, and the anisotropic behaviour was simulated by the ubiquitous joint model.

3.3 Chapter summary

Numerical simulations of rock mass behaviour around underground excavations often assume that the rock mass is linearly elastic, isotropic, continuous and homogeneous. However, in

reality, the rock exhibits anisotropic, heterogeneous, viscous and non-linear behaviour. This chapter presented a review of the theoretical background and provided methods to address the anisotropic and time-dependent behaviour of the rock mass during numerical simulations. These methods can be used to provide a better understanding of these behaviours.

Several metamorphic rocks exhibit anisotropic behaviours depending upon the compositions and arrangement of minerals. These rocks exhibit both intact rock anisotropy and rock mass anisotropy. The anisotropic nature results in variation of strength and deformability of such rocks according to the direction of anisotropic planes such as schistose or bedding planes. Anisotropy of deformability can be addressed by considering the rock to be orthotropic or transversely isotropic materials. Strength anisotropy indicates that the compressive strength of anisotropic rocks can vary significantly with respect to the plane of weakness depending upon the loading directions. Various failure criteria have been proposed for anisotropic rocks. The single plane of weakness theory proposed by Jaeger (1960) considers the failure of rock matrix and the weakness planes. Hoek-Brown failure criterion was modified to account for the anisotropic nature of the rock. Ubiquitous joint model is a modification of Mohr-Coulomb failure criterion that considers composite Mohr-Coulomb envelope with tension cut-off. The ubiquitous joint model has been used by several researchers to simulate the anisotropic damage and failure around underground excavations in foliated or stratified rock masses.

Time-dependent behaviour of rocks is a more general term that includes concepts such as the creep of the intact rock, creep of large discontinuities, delayed fracture and long-term strength. Creep of rock can be categorized into three distinct stages; primary, secondary and tertiary. These stages of creep can dominate the deformation process and needs to be accounted for during numerical simulations. Time-dependent response of rock mass can be simulated by utilizing various rheological models. Rheology strides the time-dependent

stress-strain behaviour of rocks. Visco-elastic models such as Kelvin model, Maxwell model and Burgers model can be used to simulate the elastic and time-dependent behaviour. However, these models do not consider the plastic deformations and the failure process and have various limitations. To simulate the plastic behaviour in additions to elastic and viscous behaviour, visco-plastic models such as Bingham model can be used.

Chapter 4

4 Overview of geotechnical conditions at Rampura Agucha and LaRonde mines

This chapter of the thesis provides an overview of geotechnical conditions and characteristics of the squeezing ground conditions at Rampura Agucha underground (RA-UG) and LaRonde mines. Information on geological settings, mining methods and pre-mining stresses are provided. The geotechnical conditions at these mines are discussed and experience in squeezing ground conditions is provided. The chapter also provides information on the various geotechnical monitoring systems and data collection methodology utilized at the two mines to monitor the squeezing ground conditions. Ground support methodologies adopted at mines to manage the squeezing ground conditions are also discussed.

4.1 Rampura Agucha underground mine

The Rampura Agucha mine is located in the state of Rajasthan, India, north of the district Bhilwara. The mine has a world-class Zn-Pb deposit and is being exploited by open pit mining operations since 1988. The mine is currently under transition from open pit to underground mining operations to mine the reserves beyond the ultimate pit limit. At present, both underground and open pit operations are working concurrently, and it is proposed to cease the open pit mining operations by the end of the year 2018.

4.1.1 Geological setting

The geological setting of Rampura Agucha deposit is within the pre-Cambrian banded gneiss complex group of rocks which occupies a large area of central Rajasthan. The principal geological units at the mine consist of gneisses and schists and their variants of the banded gneissic complex. The lithological units show NE-SW strike with steep dips in hanging wall between 75 - 80° and moderate dips in footwalls between 60 - 65° towards the South-East

and plunge towards North-Northeast. Majority of the country rock at RA-UG mine is composed of GBSG/GBSS (garnet biotite sillimanite gneiss/schist) domain. This domain is associated with well-defined foliation planes that occur parallel to the ore body with dip varying between 65 - 80°. In addition to foliation, GBSG/GBSS domain is also associated with intrusions of amphibolites, pegmatites, and mylonitic rocks. GBSG/GBSS exhibits strong anisotropic behaviour due to the presence of foliation and is highly susceptible to squeezing particularly in drives parallel or sub-parallel to the foliation planes. Majority of the mining infrastructures such as substations, crusher chamber and shaft are planned to be developed in GBSG/GBSS domain which makes proper understanding of squeezing ground conditions and associated rock mass response critical for effective ground control strategies throughout the life of mine.

The mineralization at RA-UG mine occurs in GMS (graphite mica schist), and the mineralized zone comprises an ore shear zone (OSZ) existing within the ore zone. The shear zone is also mineralized and is of low strength. The shear zone is continuous throughout the ore body and constitutes to about 30% of the ore body. The ore shear zone is non-uniform with varying degrees of shearing and presents significant challenges during the development of ore access crosscuts, in several cases chimney type cave-in failures have been observed. Transverse geological section showing various lithological units from hanging wall to footwall at RA-UG mine is provided in Figure 4.1.

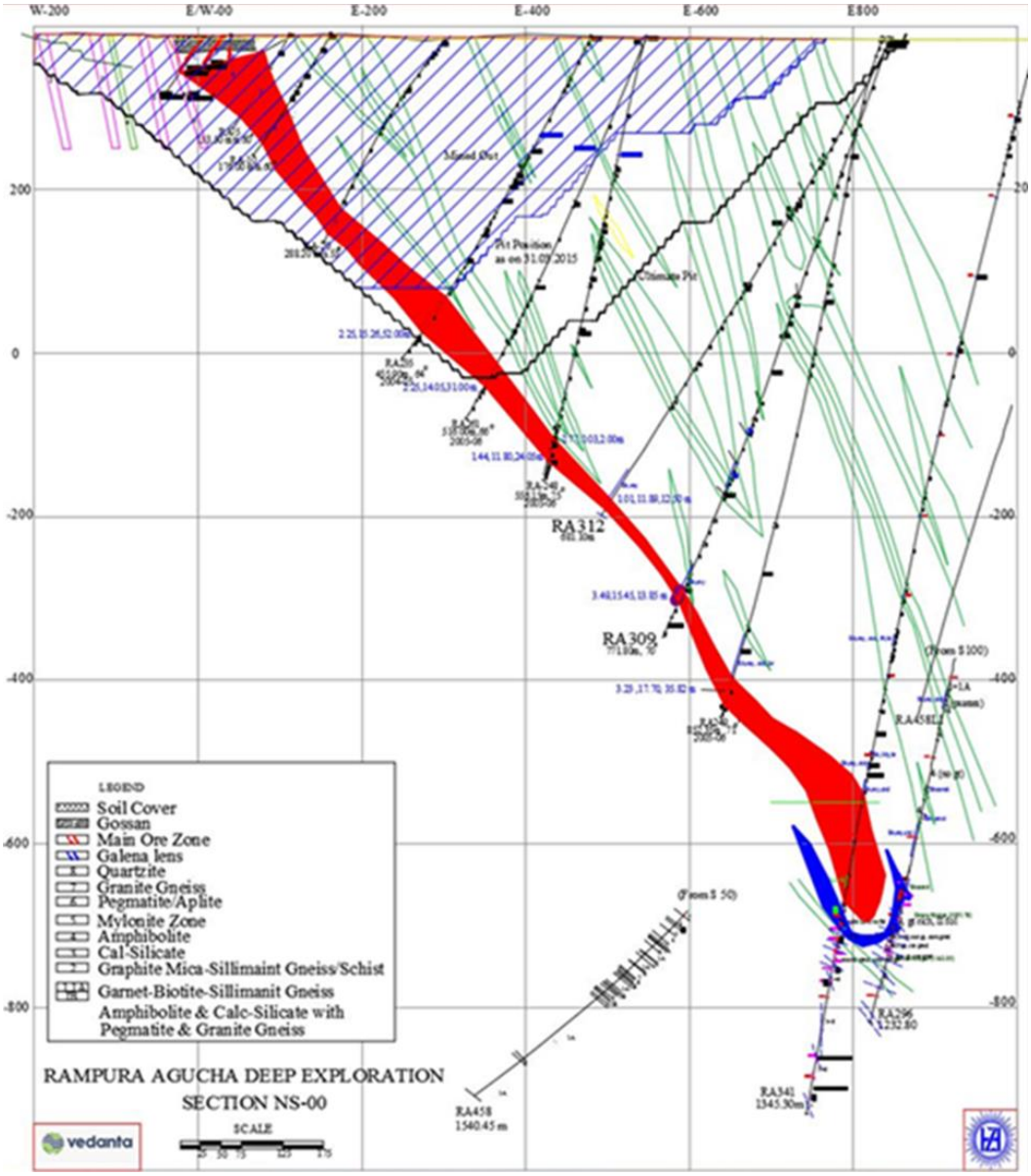

Figure 4.1: RA-UG mine geological section

4.1.2 Mining Method

RA-UG mine primarily uses transverse open stoping with primary and secondary stopes. In extreme northern and southern parts of the ore body, the mine has planned to use longitudinal stopes to mine the narrower portions of the ore body. Generally, the mine uses single lift stopes, however, in few areas feasibility of double lift stopes has been evaluated. Typically, the stopes are 25 m high (floor to floor), both primary and secondary stopes are 15 m wide. Due to the presence of ore shear zone within the ore body, frequently the stopes are extracted

in two or three panels between the footwall and hanging wall depending upon the extent of ore shear zone and strength characteristics. The mine has planned to adopt a combination of underhand and overhand sublevel open stoping to exploit the ore body. Primary and secondary stopes are backfilled with paste fill, cemented rock fill and rock fill. The mine is still in the process of finalizing the global mining sequence, several scientific studies have been carried out to analyze the global stability of the mine for various proposed mining sequences. A generic mining sequence proposed for top-down mining during one of the scientific studies is provided in Figure 4.2.

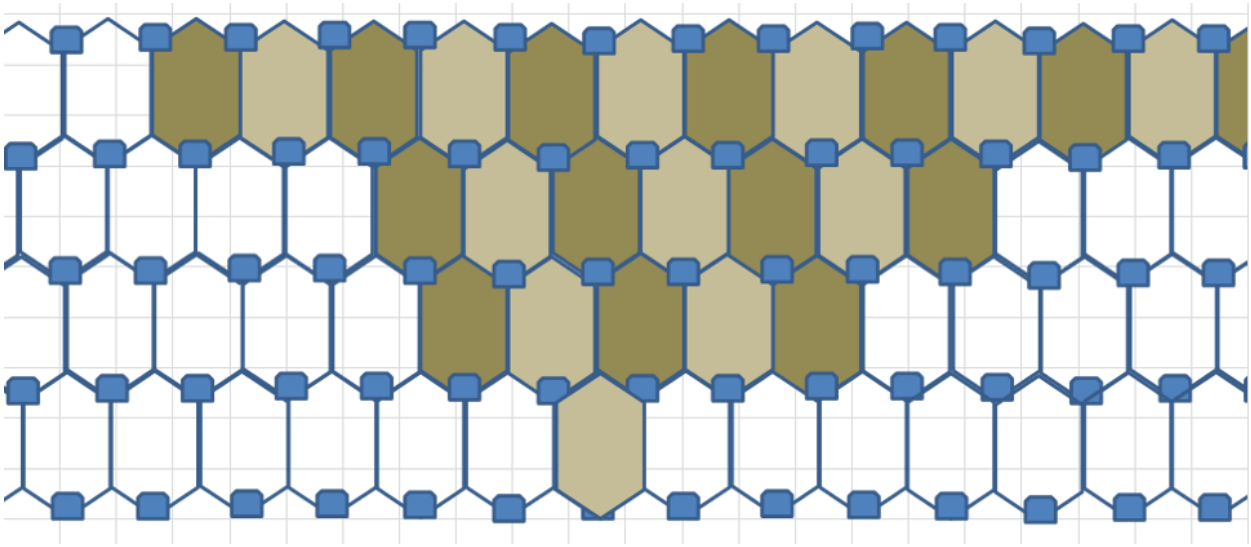

Figure 4.2: Example of RA-UG mine stope extraction sequence

4.1.3 In-situ stress conditions

In-situ stress measurements at RA-UG mine were carried out by Mesy (2011) at various depth using hydraulic fracturing technique in three vertical boreholes at three different locations. The interpreted stress results were averaged across the three drill holes, giving the equations for estimating the maximum horizontal (σ_H), minimum horizontal (σ_h) and vertical stress (σ_v) for a given depth (z) below the surface, the equations are provided in Table 4.1.

Table 4.1: Interpreted in-situ stress results for Rampura Agucha underground mine, after Mesy (2011)

Stress component	**Equations**	**Plunge (°)**	**Trend (°)**	**Value at -105 Level (~ 500 m depth) (MPa)**
σ_H	6.56 + 0.034z	0	162	24
σ_h	1.73 + 0.017z	0	072	10
σ_v	0.0282z	90	302	14

4.1.4 Ground Conditions

Vyazmensky and Yadav (2015) reported that the presence of foliation in nearly 70% of country rock makes most of the excavations that are parallel or sub-parallel to foliation susceptible to squeezing ground conditions. Footwall drives parallel to the foliation are subjected to minor to moderate squeezing ground conditions at current mining levels. As the depth of mining at RA-UG mine increases more severe squeezing ground conditions are to be expected. It was observed that the deformations of the sidewalls in the footwall drives are not isotropic and the majority of the damage occurs at the lower west wall and upper east wall shoulder depending upon the dip of foliation planes and stresses. Several ground control issues were observed in footwall drives at on -5L, +13L and -105L, see Figure 4.3. The ground control issues were generally associated with signs rock bolt taking loads (bending of plates), failure of rock bolt plates, cracking of shotcrete in the sidewalls and separation of foliation slabs in the form of loose rocks. Deformations in the sidewalls result in cracking of shotcrete, bagging of mesh and bulging of walls. Rehabilitation work was carried out at these locations to remove the broken material and re-support the walls using secondary ground support. It was also observed that at the intersections pillar corners were susceptible to slabbing failure, and often required additional surface support to manage the failure.

The mine has also experienced minor mine seismicity in the form of minor strain bursting. At

locations where contrast in rock mass strength properties occur during development, minor strain bursting, rock noise, and in a few instances rock projectiles were observed. This type of behaviour was often observed when GBSG/GBSS would occur close to stronger rock such as pegmatite or amphibolite bands. Additional surface support was utilized at these locations, and often the development cycle was increased to allow the strain energy to dissipate to manage the strain bursting conditions.

Figure 4.3: Observed rock mass damage at -105L footwall drive

Chimney type failures in the form of small cave-ins were observed during the development of ore access crosscuts at a few locations when mining through ore shear zone. The height of failure of more than 2 m has been observed at a few locations. The failure was result of unravelling of the rock mass in the roof of the excavations after the sheared portion of the ore zone was exposed. The mine utilizes fore polling technique to control the failure and develop

crosscuts in ore shear zones. In addition to fore polling, heavy surface support is also used to prevent any ground control problems in the ore shear zone during the development of ore access crosscuts.

4.1.5 Geotechnical Monitoring and data collection

Scanline mapping technique is a common method used at mine for rock mass characterization and collecting structural data. The mine uses Q-system proposed by Barton et al. (1974) to classify the quality of rock mass and ascertain the ground support requirements. Geotechnical monitoring is carried out by a combination of monitoring instruments such as vibrating wire stress cells, multi-point borehole extensometer (MPBX), tape extensometer and cavity monitoring systems (CMS). Stress cells are used to capture the changes in stresses during stoping. Mechanical MPBX are used to monitor the deformation of stopes wall in ore shear zone, and digital MPBX are used to monitor deformation of stope crowns during and after stope extraction. However, the MPBX installed in stope crowns are prone to stope blasting and are often damaged before any reliable results are produced.

Convergence monitoring of drives susceptible to squeezing ground conditions is carried out using tape extensometers and CMS scans. Two monitoring stations are installed on both sidewalls of a selected cross-section of excavations. The convergence between these two stations is measured periodically to capture the drive convergence. Periodical CMS scans of selected locations are carried out to investigate the displacement profile and quantify the amount of tunnel strain developed between two scan dates.

4.1.6 Ground support practices

RA-UG mine utilizes a combination of primary and secondary rock reinforcement and surface support elements to manage the squeezing ground conditions. For primary rock reinforcement, the mine uses fully grouted resin rebars, split sets are only restricted to mesh

pining, and rehabilitation works due to low capacity. High deformations in sidewall often lead to failure of rock bolt plates or sucking of plates into the rock. It was observed that the split sets would lock up and fail in shear when deformations occurred in sidewalls. For secondary rock reinforcement, the mine utilizes fully grouted cable bolts to provide more depth for reinforcement in wider excavations and intersections. In few instances fully, grouted cable bolts were installed in sidewalls of footwall drive to control the deformations due to squeezing. The mine utilizes fore polling to reinforce the sheared rock mass ahead of development in ore access crosscuts.

For surface support, the mine utilizes a combination of fibre reinforced shotcrete, welded mesh, and OSRO straps. All underground excavations are shotcreted following the exposure, and to provide enough short-term strength to install primary rock reinforcement. The shotcrete also helps in binding the small rock fragments between the bolts together and prevent them from falling. However, due to low strength, the shotcrete cracks early in the deformation process and needs to be scaled down to prevent any rockfall hazards. In addition to fibre reinforced shotcrete, galvanized welded wire mesh is used embedded between two shotcrete layers in excavations parallel to foliation where higher deformations are to be expected. For secondary surface support, OSRO straps are utilized to provide additional strength to the installed surface support. OSRO straps are used to support pillar corners and, in some cases, used with fully grouted cable bolts to control the sidewall deformations in footwall drives.

4.2 LaRonde mine

The LaRonde Penna Au-rich volcanogenic massive sulphide (VMS) deposit is one of the largest Au deposit currently mined in Canada. The deposit is part of Doyon-Bousquet-LaRonde mining camp located in the eastern part of the Blake River Group of the Abitibi

greenstone belt. The LaRonde deposit consists of massive to semi-massive sulphide lenses (Au-Zn-Ag-Cu-Pb) (Mercier-Langevin et al., 2007). The LaRonde underground mine is located near the village of Preissac in northern Quebec. The mine is operating since 1988 with over 600 employees for an average production of 7200 tonnes of per day. The mine uses a 2,240 m-deep, Penna shaft for hoisting ore (Mercier-Langevin, 2010). The LaRonde ore body is a world-class, Au-Ag-Cu-Zn-Pb massive sulphide lenses complex extending below 3110 m depth (Karampinos, 2016).

4.2.1 Geological setting

The ore reserves are found in four principal stratigraphic units (from north to south: zones 7, 19, 20, and 21) see Figure 4.4. Majority of mining activities at LaRonde are concentrated in zones 19 and 20 as they contain over 90% of the reserve. These zones are contiguous and depending on their grades, are mined separately. The combined thickness of these zones varies between 1 and 40 m. Zone 7 and 21 are narrow with a width varying between 1 to 5 m and are discontinuous sulphide lenses. Both zones dip 70 to 85° towards the south, and the four zones have a pitch of 70 to 80° towards the west (Mercier-Langevin, 2010).

Majority of the permanent mine excavations, such as the shaft are in basalt, and most of the development of the mine is located directly in the footwall which consists of very weak felsic tuff. The regional fabric in felsic tuff consists of tightly spaced foliations that dips approximately 70 to 85° with the strike parallel to the ore body. The presence of foliation creates weaker planes and makes the rock strongly anisotropic. Rock mass properties may further be deteriorated by localized bands of sericitic alterations. Generally, the closer to the ore-body, the tighter the foliation becomes and the more likely it is to be associated with sericitic alterations (Mercier-Langevin, 2010). The combination of tighter foliation and high in-situ stresses which are estimated to be more than 105 MPa at the elevation of 245 level,

excavations closer to the orebody such as haulage drifts typically exhibit varying degree of squeezing. As the spacing of the foliation planes and degree of sericitic alteration vary within the rock mass, its resulting behaviour can vary dramatically from one area of the mine to another (Mercier-Langevin, 2010).

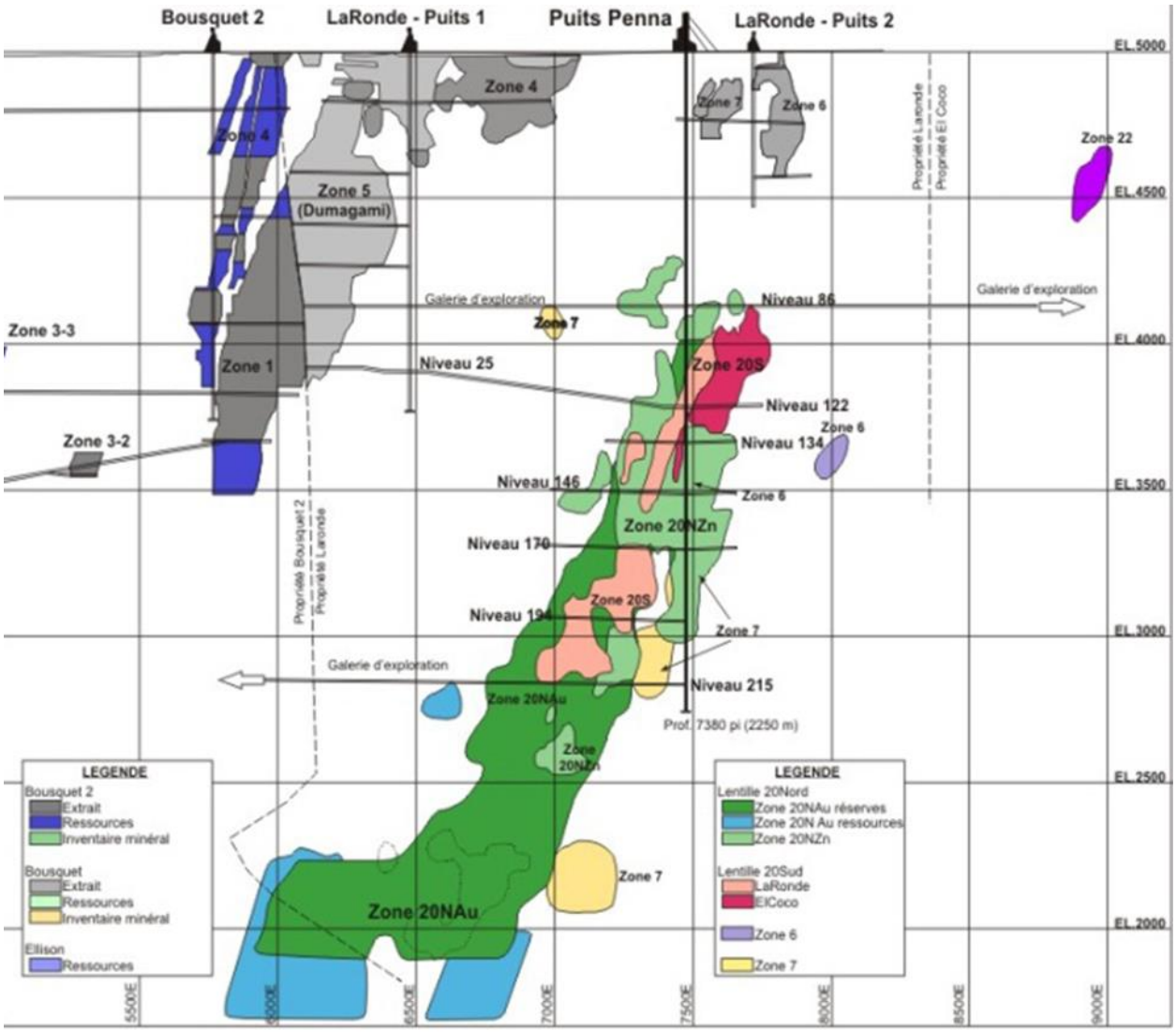

Figure 4.4: Longitudinal view of LaRond mine (Mercier-Langevin, 2010)

4.2.2 Mining method

LaRonde mine utilizes transverse open stoping with primary and secondary stopes to extract

the ore body. Stopes are typically 30 m high (floor to floor). Primary stopes are 13.5 m wide and secondary stopes are 16.5 m wide. The mine does not use any panelling, even in the thicker parts of the orebody and the stopes can be as thick as 40 m. The mine uses a chevron-type front to manage the stresses and redirects them away from mining activities. An idealized mining sequence of primary and secondary stopes is shown in Figure 4.5. The primary stopes are backfilled using paste fill or cemented rockfill, and secondary stopes are backfilled with dry rockfill. The mine also utilizes longitudinal retreat stoping in the narrow zones such as zone 7, some part of zone 21 and extremities of zone 20. Longitudinal stopes are backfilled with either paste fill or cemented rock fill.

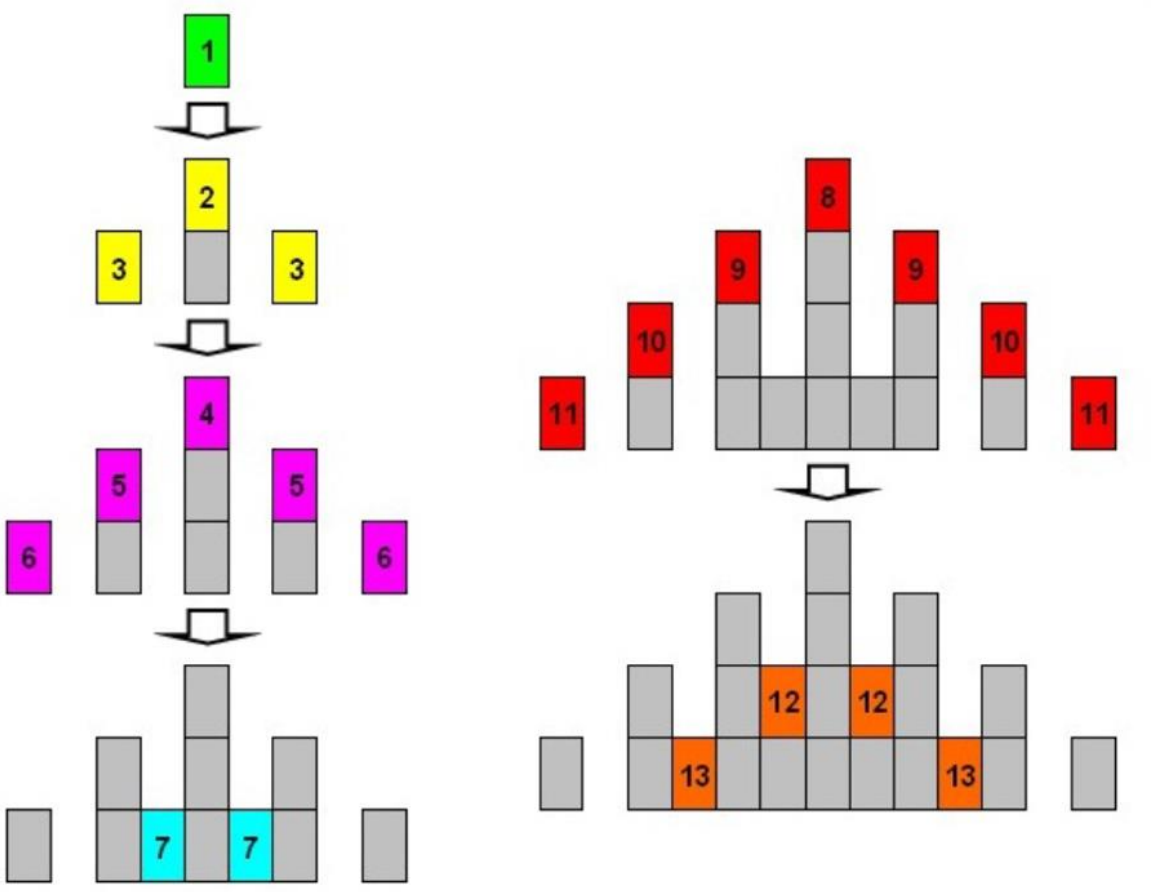

Figure 4.5: Ideal mining sequence at LaRonde mine (Mercier-Langevin, 2011)

4.2.3 In-situ stress conditions

According to Karampinos (2016), a series of stress measurements were performed in the past

to examine the in-situ stress fields at LaRonde mine. The in-situ measurements at levels 146, 150, 218 and 219 were carried out between 1999 and 2004. In 2006, additional stress measurements were carried out on level 215. The results from all measurements agree that the major and intermediate principal stress components i.e. $\sigma_1$and σ_2, respectively, are sub-horizontal and the minor principal stress component σ_3 is sub-vertical. Minor discrepancies have been reported on the orientation of the principal stress which could be due to the influence of mining induced stresses or yielding in the rock mass. The stress gradients used at the LaRonde mine are based on numerical modeling work, following the calibration of a 3DEC model against seismic activity recorded in the two pyramids at 1940 and 2150 m depth. Stress gradients used at LaRonde mine used to estimate in-situ stresses are provided in Table 4.2.

Table 4.2: Stress gradients at LaRonde mine, Mercier-Langevin and Turcotte (2007)

Stress component	**Equations**	**Plunge (°)**	**Trend (°)**	**Value at 227 Level (2270m depth) (MPa)**
σ_1	8.62 + 0.04z	0	000	99 MPa
σ_2	5.39 + 0.0262z	0	090	65 MPa
σ_3	0.0281z	90	000	64 MPa

4.2.4 Ground conditions

Due to the varying spacing of foliation planes and the degree of sericitic alterations within the rock mass, the LaRonde mine experiences a dramatically varying rock mass behaviour. The western part of the lower levels is characterized by tighter foliation and a higher degree of alteration, which can result in large-scale aseismic deformations in haulage drives. Closures of up to 1 m over a few weeks have been observed (Mercier-Langevin, 2010). Karampinos (2016) reported that varying rock mass quality results in varying ground response to mining activities. Seismicity and squeezing ground conditions may be present in different areas of

the same level and this has been observed below 215 level in the east part of the mine, where higher foliation spacing and lower degree of alterations resulted in more brittle behavior of the rock mass and relatively higher seismic activity (Mercier-Langevin and Hudyma, 2007)

Mercier-Langevin (2010) reports that the failure zone created by mining activities is quite extensive. In well-established mining horizon, the failure front created by the abutments can be traced as far as 30 m away from the actual mining front, and this correlates well with the field observation made during mining of primary and secondary stopes. The drilling in primary stopes becomes difficult, and the holes display various degrees of dog-earing, whereas drilling in secondary stopes is usually very easy and no sign of pressure is visible in the holes. One of the most significant challenges faced by the mine is the management of severe squeezing of haulage drives.

The haulage drives are subjected to heavy squeezing conditions. These drives run parallel to the foliation plane (east-west axis), with principal stress perpendicular to the walls of excavation, which makes them highly sensitive to wall buckling and overall squeezing. Signs of closure have been observed in every haulage drive below level 194. Wall convergence as high as 1 m and depth of failure as high as 6-7 m has been observed in several areas. Pronounce wall convergence reduces the clearance for some equipment and requires purging of the broken material and re-supporting of the drives. Often, it is difficult to control the amount of broken material, which leads to increase in the span of the excavations following the purging operations and it becomes necessary to install secondary back support such as cable bolts to stabilize the greater spans created.

4.2.5 Geotechnical monitoring and data collection

At LaRonde mine over 61 case studies were examined by Karampinos (2016), which covered over 26 drifts at 17 different level between 1790 m and 2690 m. Rock mass characterization

data included measurements of the orientation of foliation planes, i.e., dip and dip directions with respect to mining was collected. A qualitative assessment of the degree of squeezing for each case was carried out, observed damage, geological unit, development date, the effect of stress due to mining activity, ground support systems, additional ground support installed, history of rehabilitation and purging were documented, and scanline mapping was used for collecting geological information.

Convergence monitoring at LaRonde mine was carried out using cavity monitoring system (CMS) surveys along with laser measurement device and borehole extensometers. The cavity monitoring systems were used to capture the profile of the drift during various stages of the squeezing process. In cases where CMS survey was not possible, laser measuring device was used to measure the distance between two sidewalls at the height of 1.5 and 2.5m from the drift floor. The mine uses digital and mechanical extensometers to quantify the extent of the depth of failure in the drift sidewalls and back. Fully grouted multi-point borehole extensometer from Mine Design Technology and the D-EXTO from Yield Point with six anchor points were used. However, the extensometers were susceptible to shear and often failed after several tens of centimetres of deformations, depending on the ground conditions.

4.2.6 Ground support practices

Mercier-Langevin (2010) provided a review of mining practices at LaRonde mine. The ground support practices are summarized as follows. The mine utilizes a combination of primary and secondary reinforcement elements for managing the squeezing ground conditions. For primary reinforcements, the mine uses resin grouted rebars, friction bolts, Swellex, resin/cement grouted cable bolts and hybrid bolt. Resin grouted rebars are used in the excavations walls and back, friction bolts due to low capacity are only used in the excavations walls. Swellex bolts are used in rehabilitation works, these bolts have been

effective in the failed ground in which convergence has stopped, and shearing forces are unlikely to develop. Also, Swellex bolts are used in short-term development in ore and spilling applications. Resin grouted cable bolts provide long-term support in the first pass of installation. However, the resin is susceptible to infiltrate the cracks in the damaged ground and results in poor encapsulation and are only successfully used in basalt, which is less fractured. LaRonde mine developed the hybrid bolt to deal with the increasingly difficult ground conditions at depth. The hybrid bolt has outperformed all other types of reinforcement elements in squeezing ground conditions. Field observations suggest that the hybrid bolt has significant energy dissipation capacities in dynamic loading conditions.

For secondary reinforcement, LaRonde mine uses cement grouted cable bolts and modified cone bolts. Secondary reinforcements are used to provide additional reach for larger spans, greater capacity or better energy absorption during dynamic loading. To control wall deformations in haulage drives high capacity rigid support of 6.0 m long cement grouted cable bolts were used in conjugation with zero-gauge mesh straps. However, this support was not enough to control the movement and was too stiff to yield under load. It was observed that the cable plates either failed or were sucked into the walls. Based on observation partially de-bonded, 6.0 m cable bolts were used to introduce the yielding capacity into the support systems. Even though the de-bonded cable provided some allowance for closure, the magnitude of the deformations in the haulage drives was too high for the cables to accommodate and eventually these cables failed or sunk into the excavations wall. Modified cone bolts were also tried in squeezing ground. However, it was observed that within few weeks of installation the internal wall shearing was effectively pinching the bolts and locked the bolts in place resulting in similar behaviour to that of the rebars.

LaRonde mine uses galvanized welded wire mesh, zero-gauge mesh straps and fibre

reinforced shotcrete for providing surface support. The surface support at LaRonde is particularly important to the overall performance of support systems as it is critical in preventing unravelling of small rock fragments around reinforcement elements. LaRonde mine uses six-gauge, galvanized welded wire mesh screens. It was observed that the eight or nine-gauge screen was too fragile to resist the baggage load generated in haulage drives and chain link screen was too flexible that lead to excessive bulging between the bolts. Fibre reinforced shotcrete is widely used at the mine however due to its week tensile properties, its usefulness in the fractured ground is limited to agglomerating small pieces of fractured ground into larger easy to support panels and to provide enough confinement of highly fractured ground to install primary support.

4.3 Chapter summary

Rampura Agucha underground mine has experienced minor to moderate squeezing ground conditions at a depth of less than 500 m from the surface. As the mine goes deeper to exploit the deposit, the degree of squeezing is expected to increase. The mine experiences squeezing in excavations parallel and sub-parallel to the strike of foliation planes. Signs of squeezing in the form of shotcrete cracks, separation of foliated slabs from excavation walls have been observed at several locations. In squeezing ground, anisotropic failure mechanism is observed. The eastern wall of excavations shows buckling failure in the upper corner of the excavation and the western wall shows sliding due to shear forces in the lower portion. The squeezing conditions lead to the failure of resin rebars, the plates of the bolts cracked or failed under load during squeezing deformations. Cracking of shotcrete is an early indication of deformations. Mesh bagging and failure of pillar corners was observed at several locations.

The mine uses tape extensometer and CMS survey scans to quantify and monitor squeezing ground conditions. In addition to geotechnical instrumentation, the mine relies on

observational damage mapping of the excavations experiencing squeezing to provide a qualitative assessment of the degree of squeezing. Extensive records of the date of excavation, convergence over time, failure mode, the location of the failure and associated mining in the vicinity of the excavation are maintained. To manage the squeezing ground conditions the mine utilizes resin rebar bolt in conjugation with mesh embedded between two layers of shotcrete as primary ground support. In cases where deformation exceeds the capacity of primary ground support system, secondary support in the form of fully grouted cable bolts and OSRO straps are used to manage the deformations.

LaRonde mine has experienced dramatically varying rock mass behaviour including squeezing ground conditions and mine seismicity. Severe squeezing of excavations in foliated rock masses has been experienced with wall convergence as high as 1 m and depth of failure as high as 6-7 m. The squeezing ground conditions are monitored using a series of geotechnical monitoring instruments including cavity monitoring systems (CMS) surveys, mechanical and digital multi-point borehole extensometers. The mine has evaluated and experimented on various rock reinforcement and surface support elements and strategies to manage the squeezing ground conditions. Hybrid bolt was developed at LaRonde mine to manage the extremely difficult ground conditions at depth, and the bolt outperformed all other types of rock reinforcement elements in squeezing ground conditions.

Chapter 5

5 Numerical investigation of strength anisotropy and rock mass failure mechanism

This chapter of the thesis provides a detailed description of numerical simulations carried out to investigate the non-linear anisotropic response of foliated rocks. Chapter provides a description of the Ubiquitous-joint model used for the analysis. Modelling methodology, material properties, boundary and loading conditions and model results are presented. The chapter also provides discussions on the generated results. Numerical experimentations to simulate the laboratory uniaxial compression tests on foliated GBSG intact rock sample at RA-UG mine are presented, and model results are discussed. The chapter also provides details of numerical simulations carried out to investigate rock mass failure mechanisms at RA-UG and LaRonde mines. The conclusions and discussions on the failure mechanism at RA-UG and LaRonde mines are presented.

5.1 The Ubiquitous-Joint model

The Ubiquitous-Joint model corresponds to a Mohr-Coulomb material that exhibits strong strength anisotropy as a result of embedded weakness planes such as foliation planes. The weakness planes can be assigned varying orientation for each finite difference zone in the numerical models, see Figure 5.1. The criterion for the failure on the plane of weakness consists of a composite Mohr-Coulomb envelope with a tension cut-off. The numerical formulation of the constitutive model assumes the direction of weakness with no association to the spacing or length of the weakness plane. The position of the stress point on the Mohr-Coulomb envelope is controlled by a non-associated flow rule for shear failure and associated rule for tension failure. In this model, the general failure is first detected, and relevant plastic corrections are applied. The new stresses are then analyzed for the failure on the weak plane and updated accordingly (Itasca Consulting Group, 2017a). The mathematical formulation

and implementation procedure of the Mohr-Coulomb and weakness plane failure criteria used in the Ubiquitous-Joint model in FLAC3D are described below.

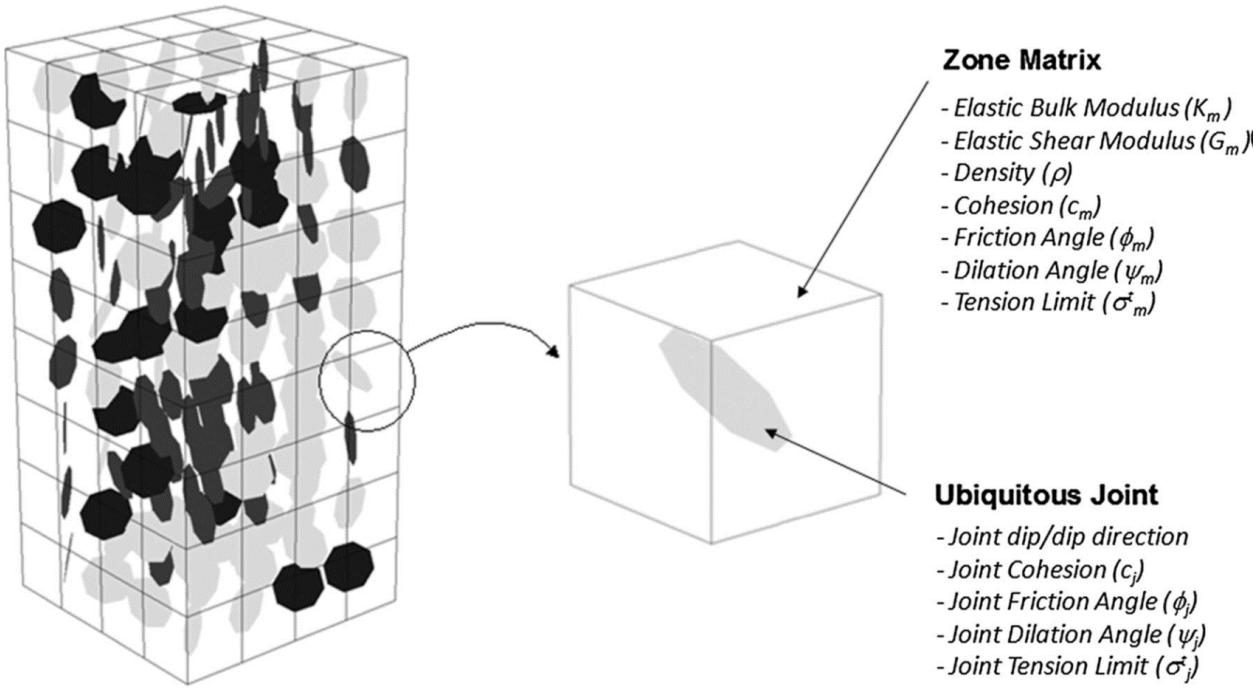

Figure 5.1: Properties of ubiquitous joint and zone-based matrix in FLAC3D, after Sainsbury et al. (2008)

5.1.1 Mohr-Coulomb criterion

The failure envelope for the Mohr-Coulomb model in FLAC3D corresponds to a Mohr-Coulomb criterion using a shear yield function with a tension cut-off which uses a tension yield function. The position of stress point on the envelope is controlled by a non-associated flow rule for shear failure and an associated rule for tension failure. The Mohr-Coulomb criterion in FLAC3D is expressed in terms of the principal stresses σ_1, σ_2 and σ_3 such that $\sigma_1 \leq \sigma_2 \leq \sigma_3$ and the criterion is represented in the σ_1, σ_3 plane as shown in Figure 5.2. The failure envelope $f(\sigma_1, \sigma_3) = 0$ is defined from point A to B in Figure 5.2 by the Mohr-Coulomb failure criterion of the form $f^s = 0$ and from point B to C by a tension failure criterion of the form $f^t = 0$. Note that the compressive stresses are negative.

$$f^s = -\sigma_1 + \sigma_3 N_\emptyset - 2c\sqrt{N_\emptyset} \tag{5.1}$$

$$f^t = \sigma_3 - \sigma^t \tag{5.2}$$

where $\emptyset$ is the friction angle, c is the cohesion and σ^t is the tensile strength of the zone matrix and $N_\emptyset$ is given by:

$$N_\emptyset = \frac{1 + \sin \emptyset}{1 - \sin \emptyset}$$

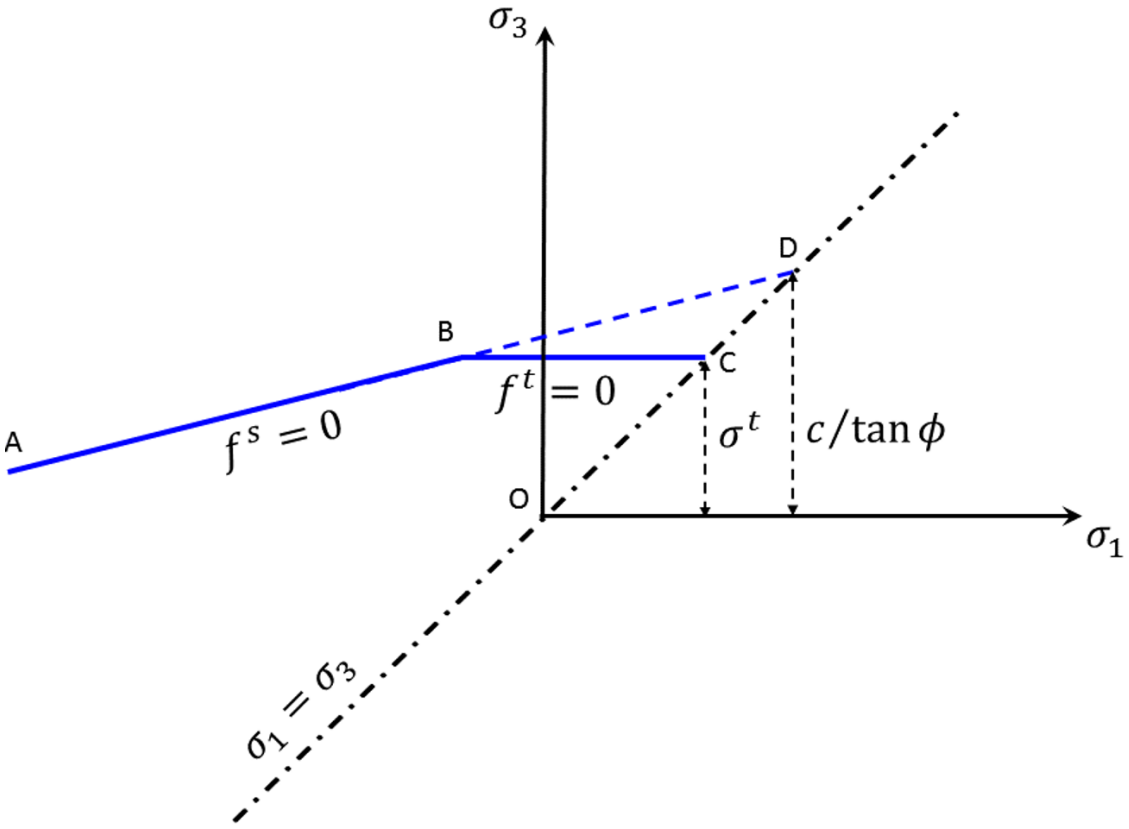

Figure 5.2: Mohr-Coulomb criterion in FLAC3D, after Itasca Consulting Group (2017a)

It should be noted that the tensile strength of the material representing the zone matrix cannot exceed the value of σ_3 corresponding to the intersection point of the straight lines $f^s = 0$ and $\sigma_1 = \sigma_3$ in the (σ_1, σ_3) plane as shown by point D in Figure 5.2. The maximum value of the tensile strength of the material is given by:

$$\sigma_{max}^{t} = \frac{c}{\tan \emptyset} \tag{5.3}$$

The plastic potential function for the Mohr-Coulomb criterion is described by utilizing two functions, g^s to define the shear plastic flow and g^t to define the tensile plastic flow. The function g^s uses a non-associated flow rule and the g^t function uses an associated flow rule. The two functions are given by the following forms.

$$g^s = -\sigma_1 + \sigma_3 N_\psi \tag{5.4}$$

$$g^t = \sigma_3 \tag{5.5}$$

where ψ is the dilation angle and N_ψ is given by the following form:

$$N_\psi = \frac{1 + \sin \psi}{1 - \sin \psi}$$

The flow rule for the Mohr-Coulomb model is provided with a unique definition by dividing the plastic region in the (σ_1, σ_3) plane into two domains using a diagonal line as shown in Figure 5.3. The line represented by the diagonal between the representation of $f^s = 0$ and $f^t = 0$ in the (σ_1, σ_3) plane divides the domain such that an elastic guess violating the composite yield function falls into either of the two domains i.e. domain 1 or domain 2. In the case where the stress point falls within the domain 1, shear failure is declared, and the stress point is placed on the curve $f^s = 0$ utilizing a flow rule derived from the plastic potential function g^s. In the case where the stress point falls within domain 2, tensile failure is declared, and the new stress point is placed on $f^t = 0$ utilizing a flow rule derived from potential function g^t.

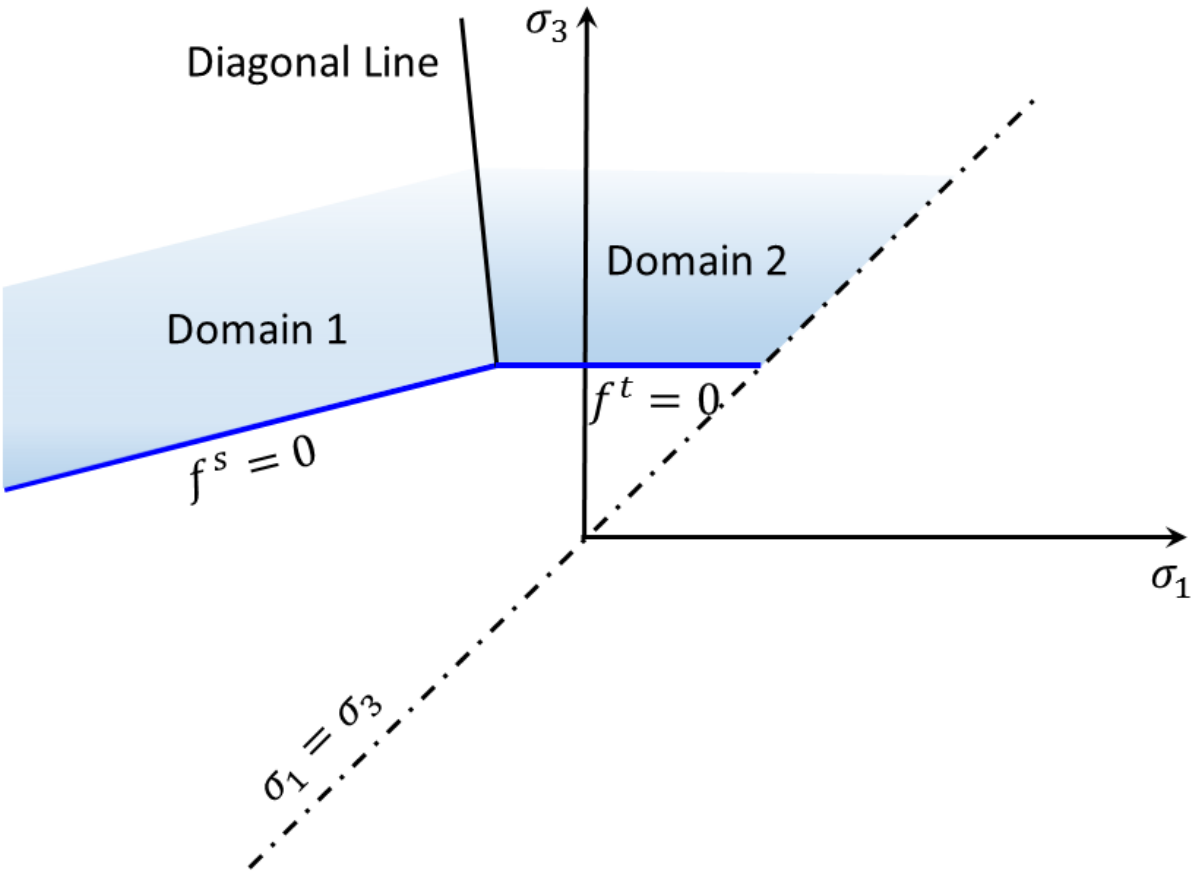

Figure 5.3: Domains used in the definition of the flow rule in Mohr-Coulomb model of FLAC3D, after Itasca Consulting Group (2017a).

The Mohr-Coulomb criterion is implemented in FLAC3D using the following procedure. First, an elastic guess is computed by adding the stress components and increments by applying the Hooke's law to the total strain increments. Following which, principal stresses and corresponding directions are calculated. If the stresses violate the composite yield criterion given by equation 4.1 and 4.2, then the point would either lie in domain 1 or domain 2. In the first case, shear failure is declared, and shear plastic correction is applied. In the second case, tensile failure is declared, and tensile plastic corrections are applied. Once the relevant plastic corrections are applied new principal stress components are then evaluated assuming that the principal directions have not been affected by the occurrence of the plastic corrections. If the stress points fall below the representation of composite failure envelope in

the (σ_1, σ_3) plane, no plastic flow takes place and the new principal stresses are calculated assuming elastic behavior.

5.1.2 Weakness plane criterion

In the Ubiquitous-Joint model, a general failure is first detected and relevant plastic corrections are then applied on the zone matrix using the Mohr-Coulomb model, as described in Sub-section 5.1.1. The new stresses are then analyzed for the failure on the weak plane and updated accordingly. The orientation of the weak-plane is provided by the Cartesian components of a unit normal to the plane in the global x-, y-, z-axes. A local right-handed system of reference axes (x´, y´, z´) is defined for the weakness plane with the z´-axis pointing in the direction of the unit normal, the x´-axis pointing downward in the dip direction, and the y´-axis is horizontal. Stress components in the local-axes are then computed by transforming the global stress components using direction cosines and stress rotation tensor, and the stresses in the local axes system are referred as σ_{ij}^{o}. The magnitude of tangential traction (τ) component on the weak plane is computed. The generalized stress vector used to describe weak-plane failure has four components $\sigma_{1'1'}, \sigma_{2'2'}, \sigma_{3'3'}$ and τ where subscript 1,2 and 3 correspond, respectively, to x´, y´, and, z´ of the local axes system of the weak plane.

The weak-plane failure criterion used in FLAC3D is a composite Mohr-Coulomb criterion with tension cut-off expressed in terms of stress normal to the weakness plane ($\sigma_{3'3'}$) and tangential traction (τ). Note that the compressive stresses are negative. The composite failure envelope for the weak plane is provided in Figure 5.4. The failure envelope $f(\sigma_{3'3'}, \tau) = 0$ is defined from point A to B in Figure 5.4 by the Mohr-Coulomb criterion of the form $f_j^s = 0$, using the following equation:

$$f_j^s = \tau + \sigma_{3'3'} \tan \emptyset_j - c_j \quad (5.6)$$

and from B to C by a tension failure criterion of form $f_j^t = 0$, using the following equation:

$$f_j^t = \sigma_{3'3'} - \sigma_j^t \quad (5.7)$$

where, $\emptyset_j$, c_j and σ_j^t are the friction, cohesion and tensile strength of the weak plane, respectively. In the case of a non-zero friction angle, the maximum value of the tensile strength of the weakness plane is given by point D in Figure 5.4 and is expressed as,

$$\sigma_{j\,max}^t = \frac{c_j}{\tan \emptyset_j} \quad (5.8)$$

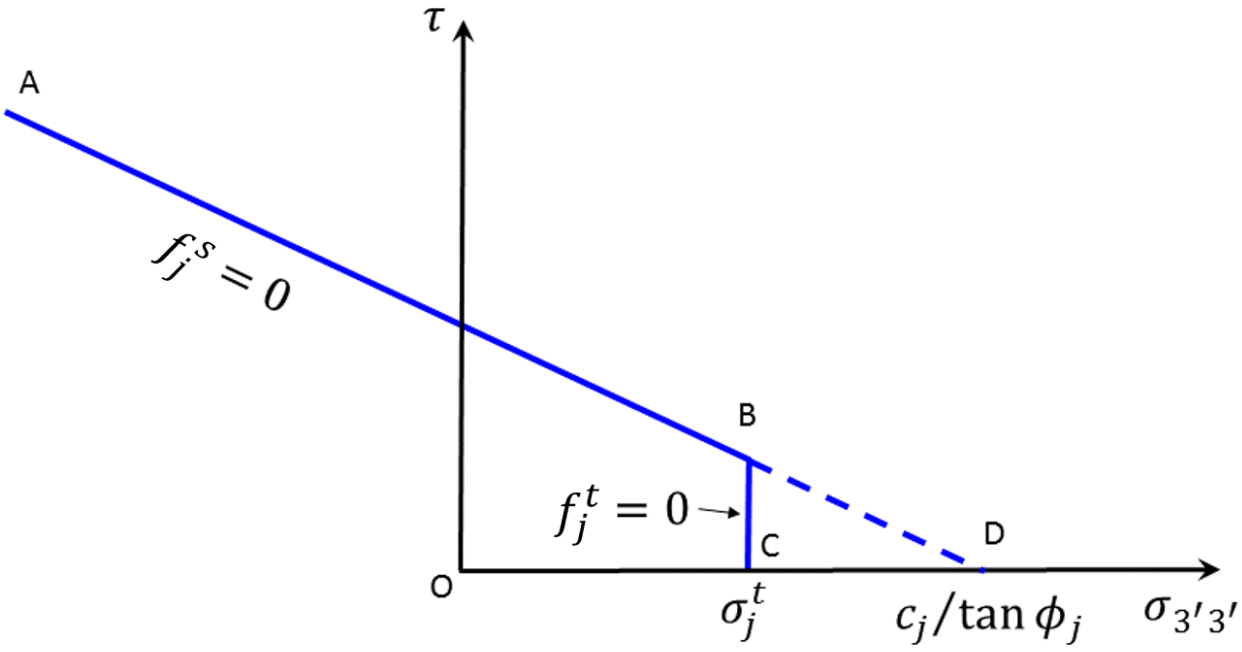

Figure 5.4: Weak plane failure criterion in FLAC3D, after Itasca Consulting Group (2017a).

The plastic potential function for the weak plane failure criterion is composed of two functions: g_j^s and f_j^t used to define shear and tensile flows, respectively. The functiong_j^s corresponds to a non-associated flow rule and is given by the following equation:

$$g_j^s = \tau + \sigma_{3'3'} \tan \psi_j \tag{5.9}$$

where, ψ_j is the dilation angle of the weak plane. The tensile potential function g_j^t corresponds to an associated flow rule and is given by the following equation:

$$g_j^t = \sigma_{3'3'} \tag{5.10}$$

To evaluate the failure on the weak plane, an elastic guess is made. If the elastic guess violates the composite yield function, it is represented by a point in the $(\sigma_{3'3'}, \tau)$-plane. The point will fall either in domain 1 or domain 2, partitioned by the diagonal line between the lines defined by $f_j^s = 0$ and $f_j^t = 0$ as shown in Figure 5.5. If the stress point falls in domain 1, shear failure is declared, and the stress point is placed on the line $f_j^s = 0$ using a flow rule derived using the plastic potential function g_j^s. In case the stress point falls in domain 2, a tensile failure is declared and the stress point is placed on the line $f_j^t = 0$ by using a flow rule derived from the plastic potential function g_j^t. For both types of failures, relevant plastic correction is applied accordingly to the stress components. In large strain models, the orientation of weakness planes is adjusted per zone to account for the rigid-body rotation and the rotations due to deformations.

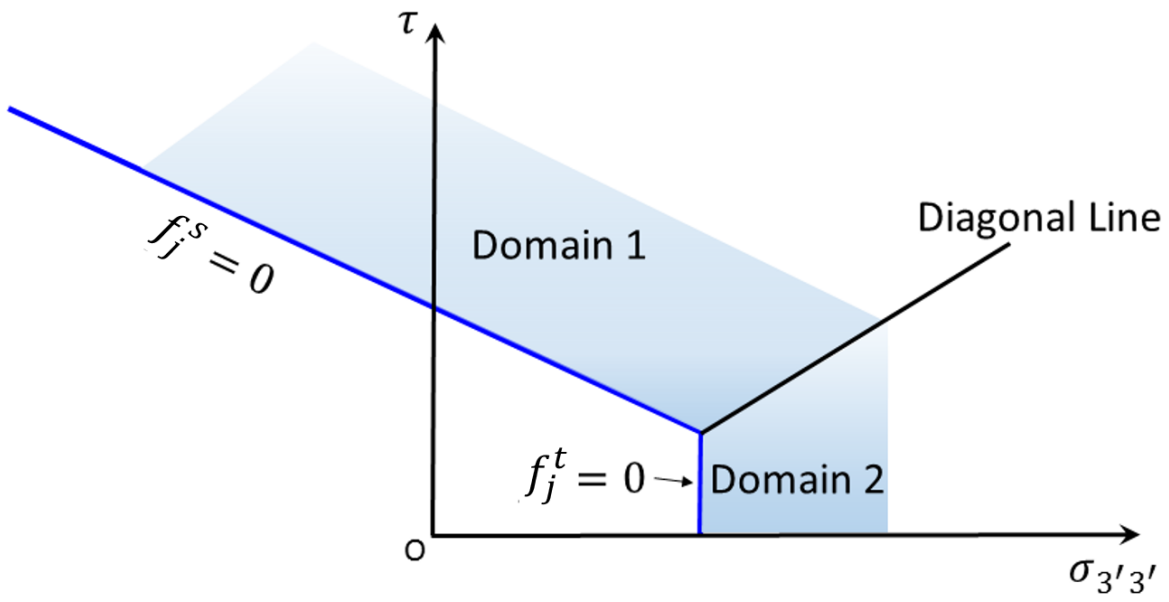

Figure 5.5: Domains used in the definition of the flow rule of the weak plane failure criterion in FLAC3D, after Itasca Consulting Group (2017a).

The Ubiquitous-Joint model is implemented in FLAC3D using the following procedure. The elastic guess for the step is first analyzed for a general failure in the zone matrix, and relevant plastic corrections are applied using the methodology described in Mohr-Coulomb model in sub-section 5.1.1. The resulting stress components are labelled as σ_{ij}^{o} and then the failure on the weak plane is examined. The global stress components are transformed to local axes system of the weak plane and, the tangential traction component is computed. The new elastic guess for the weak plane is made, if the new stresses $\sigma_{3'3'}^{o}$ and τ^{o} violates the composite yield criterion, the point either lies in domain 1 or domain 2 of Figure 5.5. Shear and tensile failures takes place for domain 1 and 2, respectively. Following the identification of the type of failure, relevant plastic corrections for the stresses are carried out. The tensor of stress corrections is expressed in the system of reference axes by transformation and added to $[\sigma_{ij}]^{o}$. If the stress point $(\sigma_{3'3'}^{o}, \tau^{o})$ is located below the representation of the composite failure criterion in the plane $(\sigma_{3'3'}, \tau)$, no plastic flow takes place for this step and the new

stresses are the same and given by σ_{ij}^{o}.

5.2 Strength anisotropy

Foliated rocks are associated with anisotropy of strength that varies with the direction of planes of anisotropy with respect to the loading direction. The strength anisotropy of intact rock sample is established by testing intact rock specimen at the varying orientation of inherent anisotropy relative to the direction of loading. Numerical experimentation to simulate the laboratory compression tests was carried out by utilizing the ubiquitous-joint model in FLAC3D 6.0 (Itasca Consulting Group Inc., 2017a) to investigate the strength anisotropy of GBSG (Garnet Biotite Sillimanite Gneiss) intact rock sample at RA-UG mine. The geometry of numerical simulations, mechanical properties of intact rock and foliations, loading conditions employed and modelling results are presented in the following sub-sections.

5.2.1 Model Methodology

The uniaxial compressive strength (UCS) of a foliated intact rock sample is a function of the intact rock material, joint properties and angle between the loading direction and the foliation plane (β). For numerical simulations of compression test on intact rock sample, the sample specifications were based on ISRM guidelines. Cylindrical sample with length to diameter ratio of 2.5 was used. The top and bottom walls of the cylinder were used as loading platens for the simulating compression as suggested by Wang et al. (2016).

The FLAC3D grid for the numerical simulations was generated using advanced mesh generation software Griddle 1.0 (Itasca Consulting Group, 2017b) in conjugation with 3D CAD software Rhinoceros 5.0 (Robert McNeel and Associates, 2017). Grid size for numerical simulations was selected following a series of grid convergence tests. The grid size (S) to sample length (L) ratio was varied by decreasing the grid size and displacements at five

different locations along the length of the sample was monitored. The locations of monitoring points are provided in Figure 5.6. The results of grid convergence tests are summarized in Table 5.1. For convergence criteria, it was assumed that the grid size is converged when the difference between displacements of two consecutive grid sizes was less than 10%. Based on results of grid convergence test, grid size to length (S/L) ratio of 0.02 was used for numerical simulations.

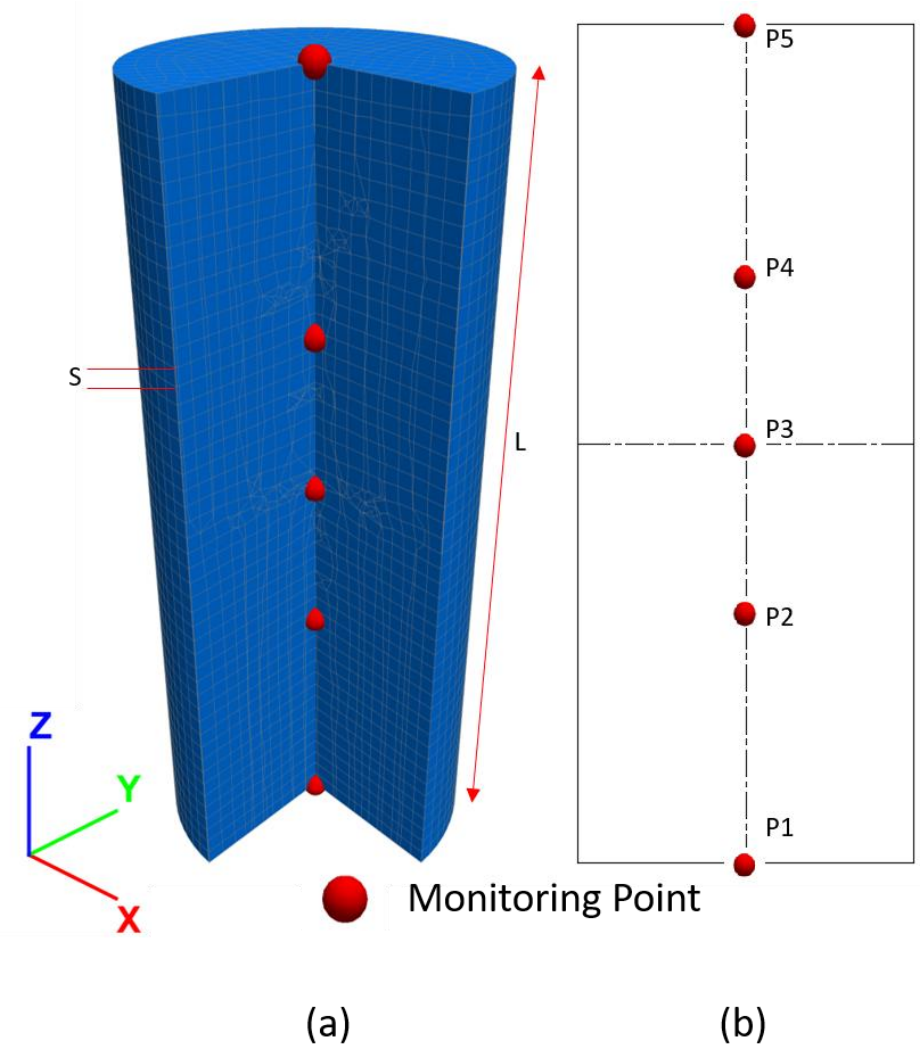

Figure 5.6: Monitoring points for grid convergence tests (a) FLAC3D grid (b) Schematic

Table 5.1: Cylindrical grid convergence test

S / L	P1	P2	P3	P4	P5

Ratio	Disp. (mm)	% Diff.	Disp. (mm)	% Diff.	Disp. (mm)	% Diff.	Disp. (mm)	% Diff.	Disp. (mm)	% Diff.
0.08	10.0	-	4.0	-	0.75	-	4.0	-	10.0	-
0.04	9.9	-0.1%	3.9	-0.2%	0.63	-16.1%	3.9	-0.3%	9.9	-0.1%
0.02	10.0	0.0%	4.0	0.0%	0.38	-40.2%	3.9	0.1%	10.0	0.0%
0.01	10.0	0.0%	3.9	-0.1%	0.35	-7.7%	3.9	0.0%	10.0	0.0%

The FLAC3D discretized grid and schematic showing foliation representation and loading direction during numerical simulations are provided in Figure 5.7. For loading, a uniform velocity was applied normal to the top and bottom walls to simulate compression of the cylindrical sample. Following the initiation of failure, the state of stress in the sample often becomes non-uniform in such numerical simulations and may lead to numerical instabilities during the simulations, therefore to better control the deformations, the normal velocities applied to the top and bottom ends of the cylinder were controlled using servo-control mechanism. For each simulation, the sample was strained to the value that would initiate failure for all values of β. The influence of β was studied from 0° - 90° in increments of 5°.

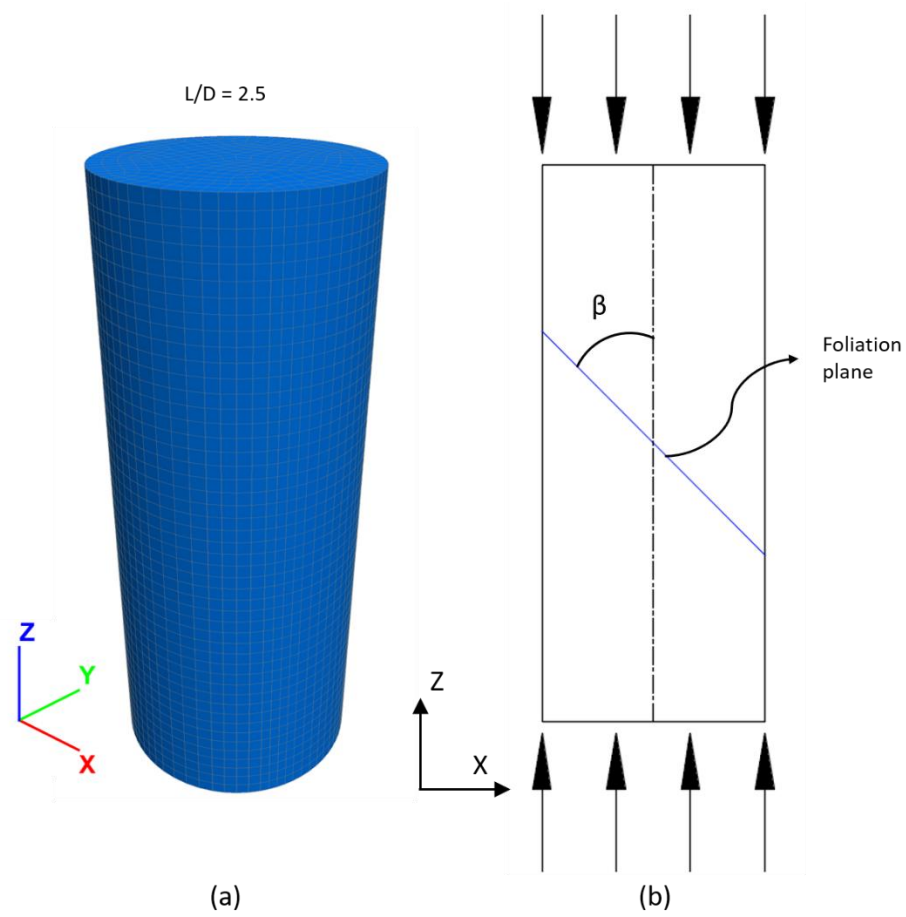

Figure 5.7: (a) FLAC3D grid (b) schematic showing loading direction, β and foliation

5.2.2 Material properties

Mishra et al. (2015) carried out geotechnical lab testing of drill core samples from RA UG mine. RocData 5.0 (Rocscience Inc., 2017) was utilized to determine the mechanical properties of intact rock (GBSG) and foliations for numerical simulations. The input parameters of foliation planes were determined from the geological mapping and core logging data from RA-UG mine. The base properties were calibrated using laboratory values of UCS. It was assumed that the rock and foliation are non-dilatant. The material and joint properties used in the numerical simulations are provided in Table 5.2.

Table 5.2: Material and joint properties for GBSG sample, derived from Mishra et al. (2015)

Material properties	**Unit**	**Value**

Young's modulus	GPa	12.0
Poisson's ratio	-	0.25
Cohesion	MPa	8.3
Friction	°	55.0
Dilation	°	0.0
Tensile strength	MPa	4.5
Joint cohesion	MPa	8.0
Joint friction	°	35.0
Joint dilation	°	0.0
Joint tensile strength	MPa	4.0

5.2.3 Modelling results and discussion

The variation of the UCS of the intact rock sample of foliated GBSG rock unit at RA-UG mine is illustrated in Figure 5.8. The strength variation of intact rock sample presents an approximate "U" shaped curve against the β angle. The UCS values produced by the numerical models are compared to the UCS values generated from laboratory testing results of the rock samples. The laboratory data presents some outliers, however considering the inherent complexities of the rock, the agreement in results is good. The maximum UCS of rock specimen obtained from numerical simulations was for β less than 10° or greater than 50°. The values of UCS varied for orientation of foliation for β between 10° - 50° and the minimum value was obtained for β between 25° - 30°. The anisotropy factor i.e. ratio of maximum to minimum values of UCS from numerical simulation was 1.87 and from experimental data was found to be 1.78. The intact rock can be classified as low anisotropy (Vakili et al., 2014).

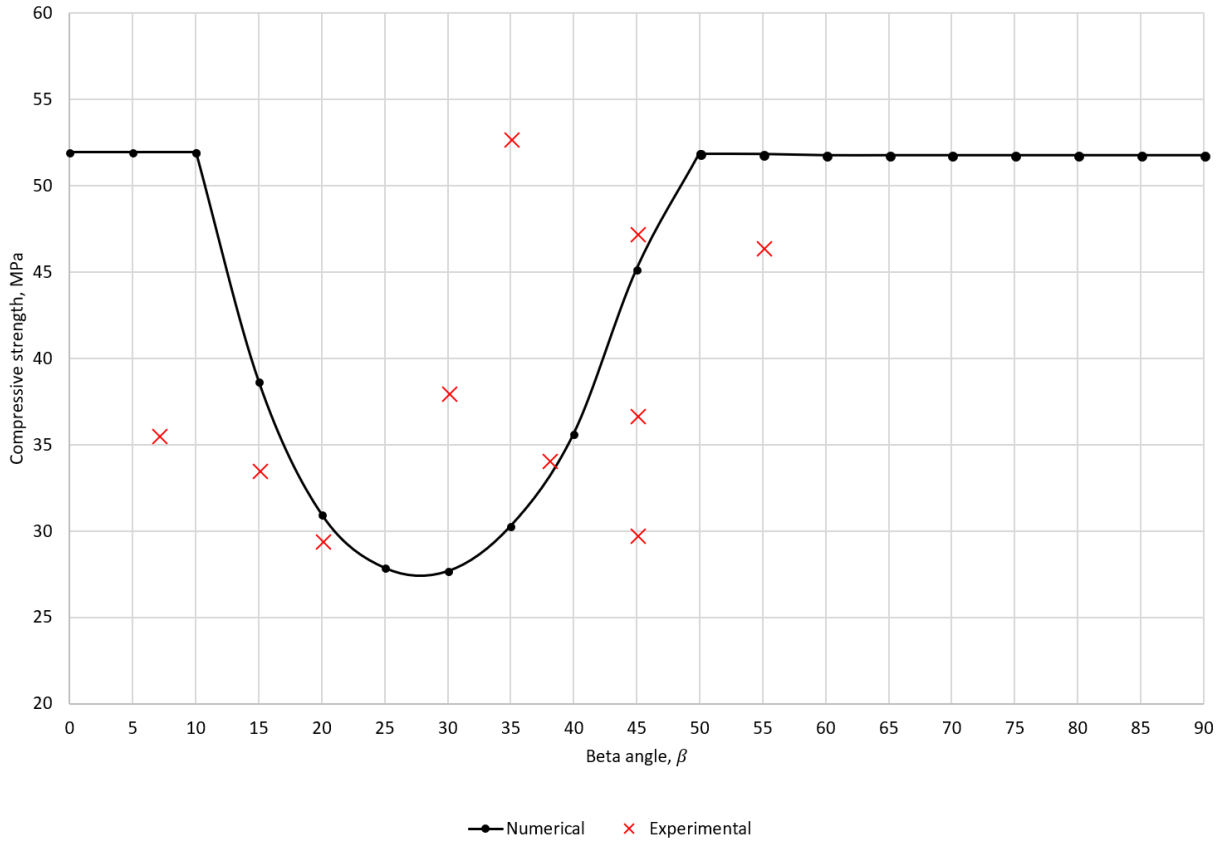

Figure 5.8: Variation of UCS of intact GBSG sample with respect to β

Szwedzicki (2007) provided a hypothesis on modes of failure of rock samples tested in uniaxial compressions and provided five distinct failure modes. Yao et al. (2017) carried out an experimental study on failure characteristics of schist under loading conditions and reported that the schist rock samples failed in coupling mode of shear and tension under uniaxial compression and failed in shear mode under conventional triaxial compression. Yao et al. (2017) classified failure modes of schist samples as shear, multiple fracturing and multiple extension.

Modelling results suggest that for β ranging from 10° to 50°, the foliation planes dominate the mechanical behaviour of the rock sample and under compressive loading, the failure occurs along the foliation planes resulting in lower values of UCS. Simple shear type failure mode was observed in these cases. Major shear plane developing along the direction of

foliation planes was observed, the plane commenced from top or bottom of the sample and progressed outwards. The failure modes observed in numerical simulations were similar to those observed during laboratory testing as provided in Figure 5.9.

Figure 5.9: Failure mechanism for $\beta = 30°$ (a) modelled strain (b) sample tested (Mishra et al. 2015) (c) post failure (Mishra et al. 2015)

For β less than 10° and greater than 50° the mechanical behaviour of the sample is governed by the intact rock, the failure in these simulations occurred in intact rock, resulting in relatively higher values of UCS. Multiple fracturing type failure mechanism was observed in the numerical simulations, Yao et al. (2017) reported that such failure mechanism is associated with disintegration of rock sample along a number of tensile or shearing cracks at various angles. Numerical simulation of the failure mechanism and observed failure during

laboratory testing is provided in Figure 5.10.

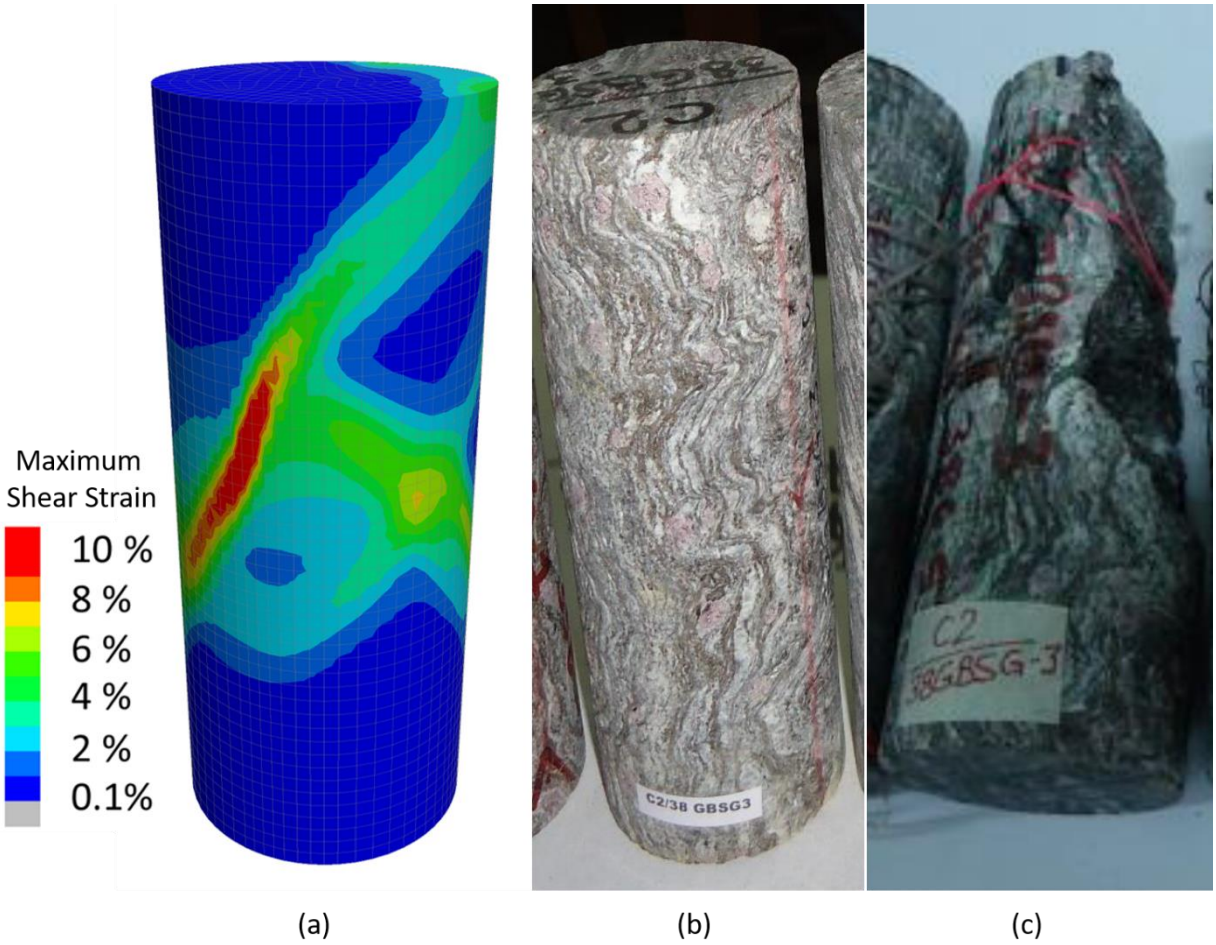

Figure 5.10: Failure mechanism (a) modelled strain for $\beta = 5°$ (b) sample tested in laboratory $\beta = 7°$ (Mishra et al. 2015) (c) post failure (Mishra et al. 2015)

5.3 Rock mass failure mechanism

Rock mass failure mechanisms in foliated rock masses are governed by foliations as they result in anisotropic deformations and stress redistributions around underground excavations. Understanding these failure mechanisms is the first step towards managing squeezing ground conditions. Identifying failure mechanisms can help in improving the understanding of driving forces associated with squeezing ground conditions. The nature of forces experienced by rock reinforcement and surface support elements can be estimated, and suitable ground support elements can be selected. Failure mechanisms at RA-UG and LaRonde mines were

investigated by employing the ubiquitous-joint model in FLAC3D 6.0 (Itasca Consulting Group, 2017a). Model description, material properties, boundary conditions and model results are provided in the following sub-sections.

5.3.1 Modelling approach

Karampinos (2016) utilized Distinct Element Method (DEM) in 3DEC (Itasca Consulting Group, 2013) to simulate the buckling failure mechanism observed at LaRonde mine. Mellies (2009) and Mercier-Langevin and Turcotte (2007) employed Finite Element Method (FEM) with explicit representation of foliations in Phase2 (Rocscience Inc., 2006) to investigate the rock mass failure mechanisms at LaRonde mine. Yadav et al. (2016) carried out a numerical investigation of rock mass failure mechanism and influence of depth on the level of squeezing at RA-UG mine utilizing Finite Difference Method (FDM) in FLAC3D 5.0 (Itasca Consulting Group, 2012).

The DEM and FEM methods used at LaRonde mine utilized an explicit representation of foliation in the form of joints for conducting numerical simulations. The DEM employed by Karampinos (2016) allowed for simulation of block rotation and relative block movement, however, 3D simulation of haulage drifts was not carried out due to computational restriction and time limitations. Due to such limitations, investigation of some 3D parameters such as the influence of varying interception angle between foliation and drift walls on the degree of squeezing could not be carried out. The ubiquitous-joint model in FLAC3D 6.0 (Itasca Consulting Group, 2017a) was employed to overcome these limitations as it allows to account for the presence of foliation planes to simulate the anisotropic response in 3D numerical simulations.

Failure mechanism was investigated at RA-UG mine, in excavations parallel to the strike of foliation planes such as footwall drive. The model geometry and grid size were selected

based on series of convergence tests carried out for determining external boundary and grid size. For convergence tests, displacements at twelve different points were monitored, and wall to wall closure (C1 – C3) and back to floor closure (C4 – C6) were calculated from the recorded displacements. The schematics showing the standard footwall drive geometry and monitoring points for convergence test are provided in Figure 5.11. For convergence criteria, it assumed that the parameters have converged if the closure (δ) between two consecutive variation of external boundary or grid size was less than 10%. Convergence test to determine the external boundary, was carried out by increasing the expansion factor (EF) and grid size convergence test was carried out by reducing the grid size to excavation width (GS/EW) ratio. In addition to the grid size and external boundary convergence tests, excavation length convergence tests were also conducted to study the influence of modelled length on the displacements. The results of convergence tests are summarized in Table 5.3.

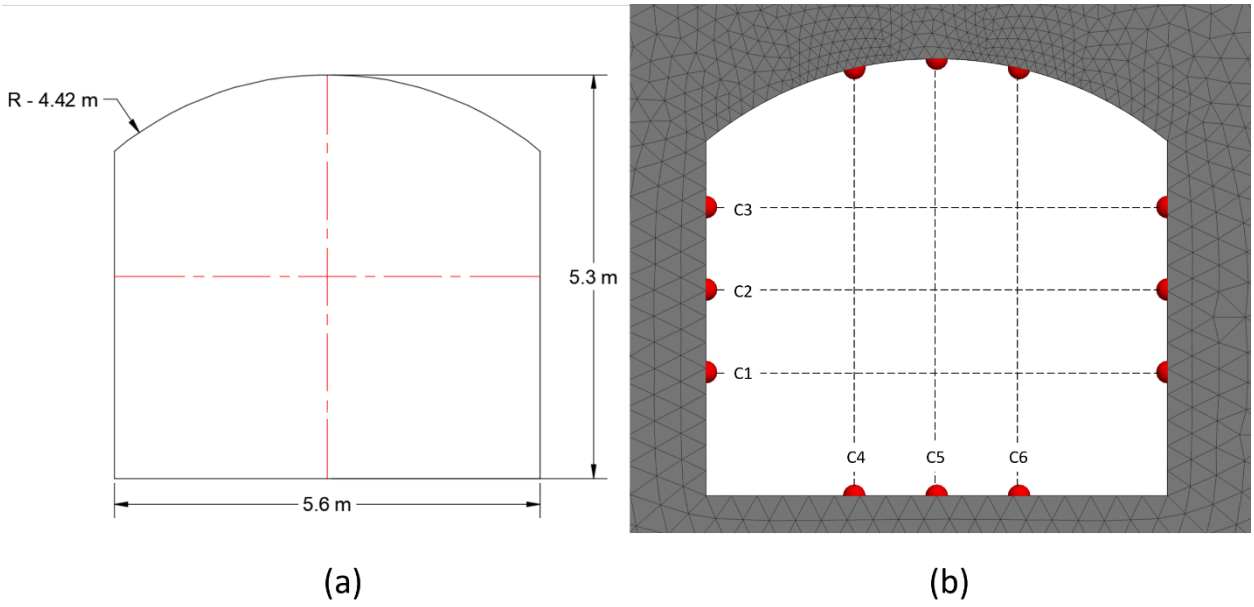

Figure 5.11: RA-UG mine footwall drive geometry for convergence models (a) schematic (b) monitoring points on the FLAC3D grid

Based on convergence tests, external boundary of 78 m and grid size to excavation width of 0.05 was used for the numerical model. Results of length convergence tests suggest that for

the modelled length, the displacements for all cases was within 10%. The discretized FLAC3D grid showing the simulated geometry and boundary conditions are provided in Figure 5.12. All velocities at the bottom face of the model were restricted, velocities perpendicular to the faces were restricted at side faces of the external boundary, normal stress was applied at the top face of the external boundary to simulate the vertical stress generated due to the overburden. The in-situ stresses shown in the Figure 5.12 corresponds to major (σ_1), intermediate (σ_2) and minor (σ_3) principal stresses. Large strain mode and gravity were used in the model. It was assumed that the foliation is parallel to the wall of footwall drive for its entire length and the drive was assumed to be at a depth of 382 m (+13L) below the surface. The dip of foliation planes was taken to be 70°, and 20 m of the drive length was simulated

Table 5.3: RA-UG numerical model boundary, mesh and drive length convergence test results

RA-UG Convergence Tests	Wall to wall convergence						Back to floor convergence					
	C1		C2		C3		C4		C5		C6	
	δ (mm)	% Diff.	δ (mm)	% Diff.	δ (mm)	% Diff.	δ (mm)	% Diff.	δ (mm)	% Diff.	δ (mm)	% Diff.
EXF	**External boundary convergence test**											
3.0	25.9	-	25.4	-	22.9	-	22.6	-	23.3	-	22.6	-
6.0	26.1	0.6%	25.0	-1.8%	21.4	-6.4%	22.8	0.9%	23.5	0.8%	22.6	0.3%
9.0	23.7	-8.9%	25.8	3.4%	22.5	4.9%	23.1	1.3%	23.9	1.4%	23.0	1.7%
GS/EW	**Grid size convergence test**											
0.1	22.9	-	24.6	-	21.9	-	22.7	-	23.5	-	22.5	-
0.05	25.9	13.3%	26.9	9.4%	22.5	2.8%	23.7	4.3%	24.2	3.1%	23.5	4.4%
0.025	28.1	8.4%	29.2	8.8%	24.2	7.7%	24.6	3.8%	25.0	3.6%	24.6	4.6%
Length (m)	**Drive length convergence test**											
10	23.2	-	24.3	-	21.4	-	22.7	-	23.3	-	22.5	-
20	21.1	-8.9%	22.3	-8.1%	20.0	-6.6%	22.2	-2.1%	23.0	-1.3%	22.1	-1.5%
40	22.5	6.5%	22.8	2.2%	21.4	7.0%	22.4	0.8%	23.2	0.5%	22.3	0.9%

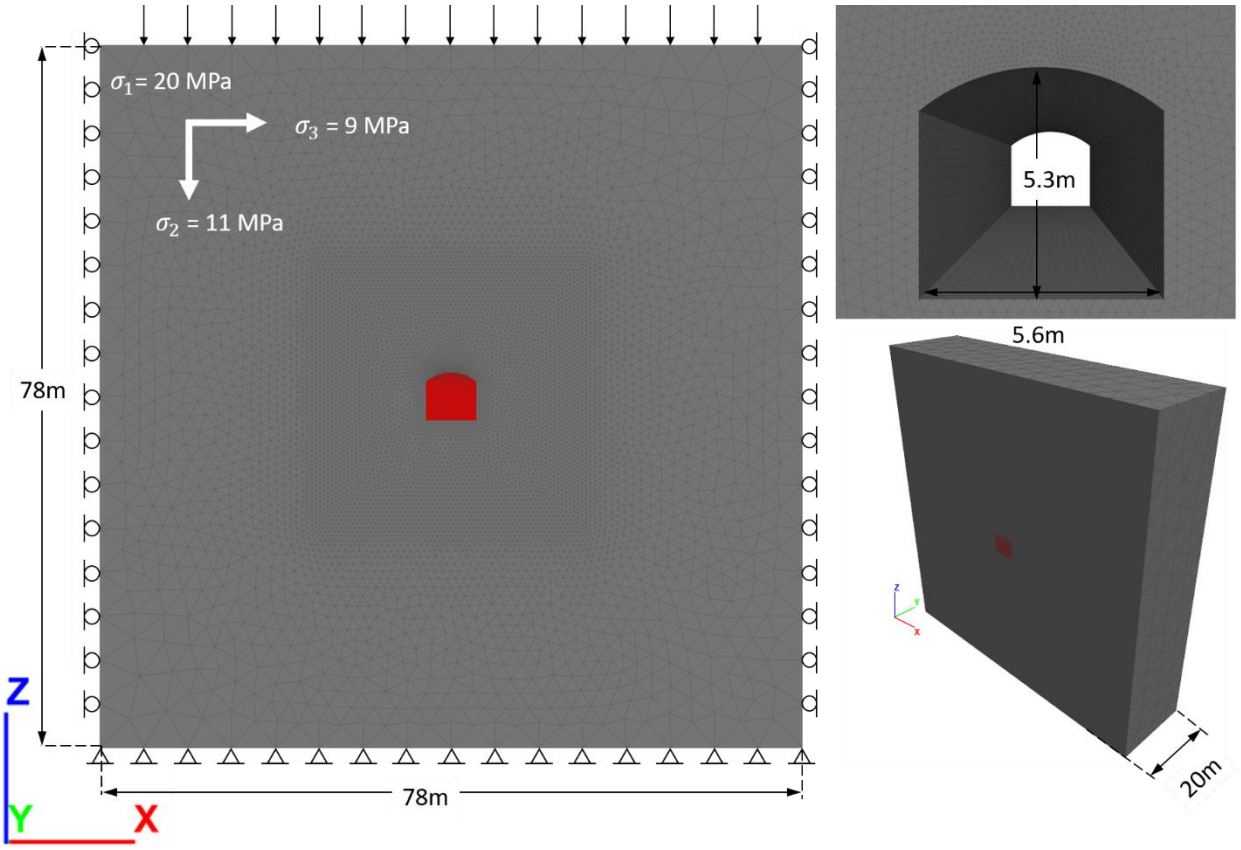

Figure 5.12: RA-UG mine FLAC3D grid and boundary conditions for failure mechanism model

The specifications of numerical models for LaRonde mine were based on the numerical simulations carried out by Karampinos (2016). Convergence test was carried out to ascertain the extent of external boundary and grid size to be used in the numerical model. Displacements at ten different points along the perimeter of haulage drift were monitored. Wall to wall closure (C1, C2) and back to floor closure (C3-C6) were calculated from the recorded displacements. The schematic showing standard haulage drift geometry (Mercier-Langevin and Turcotte, 2007) and monitoring points for convergence tests are provided in Figure 5.13. For convergence criteria, it was assumed that the parameters have converged if the closure (δ) between two consecutive variation of external boundary or grid size was less than 10%. Convergence test to determine the external boundary was carried out by increasing the expansion factor (EF) of the

external boundary and grid size convergence test was carried out by reducing the grid size to drift width (GS/DW) ratio. In addition to the grid size and external boundary convergence tests, excavation length convergence tests were also conducted to study the influence of modelled length on the displacements. The results of convergence tests are summarized in Table 5.4.

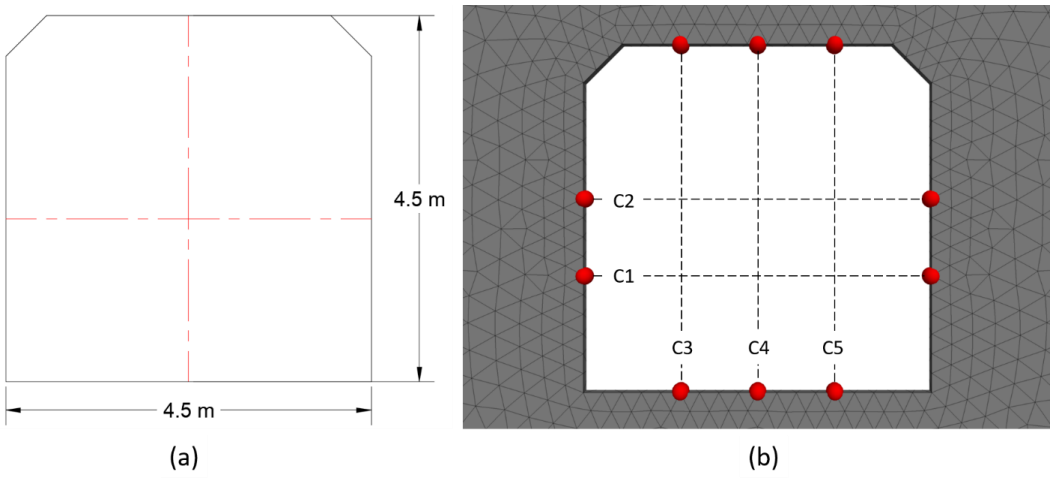

Figure 5.13: LaRonde mine haulage drift geometry for convergence model (a) schematic (b) Monitoring points on the FLAC3D grid

Karampinos (2016) used the external boundary of 60 m for numerical simulation of buckling failure mechanism at LaRonde mine. The convergence tests results are in good agreement with the parameters used by Karampinos (2016). External boundary of 65 m and grid size to drift width of 0.06 was used for the numerical model. Results of length convergence tests suggest that for the modelled length, the displacements for all cases was within 10%. The discretized FLAC3D grid showing the simulated geometry and boundary conditions are provided in Figure 5.14. Drift dimension of 5.0m wide and 4.5 m high was used in the numerical model for investigating failure mechanism based on dimensions of DEM model by Karampinos (2016). Velocities at the bottom face of the external boundary were restricted in all directions, for side faces velocities perpendicular to the face were restricted. Normal stress was applied to the top

face of the boundary to simulate vertical stress generated due to the overburden. The in-situ stresses shown in the Figure 5.14 corresponds to major (σ_1), intermediate (σ_2) and minor (σ_3) principal stresses. Large strain mode and gravity were used in the model. It was assumed that the foliation is parallel to the walls of haulage drift for its entire length and the drift is at a depth of 2,550 m below the surface. The dip of foliation was assumed to be 80°, and 20 m of the haulage drift length was simulated.

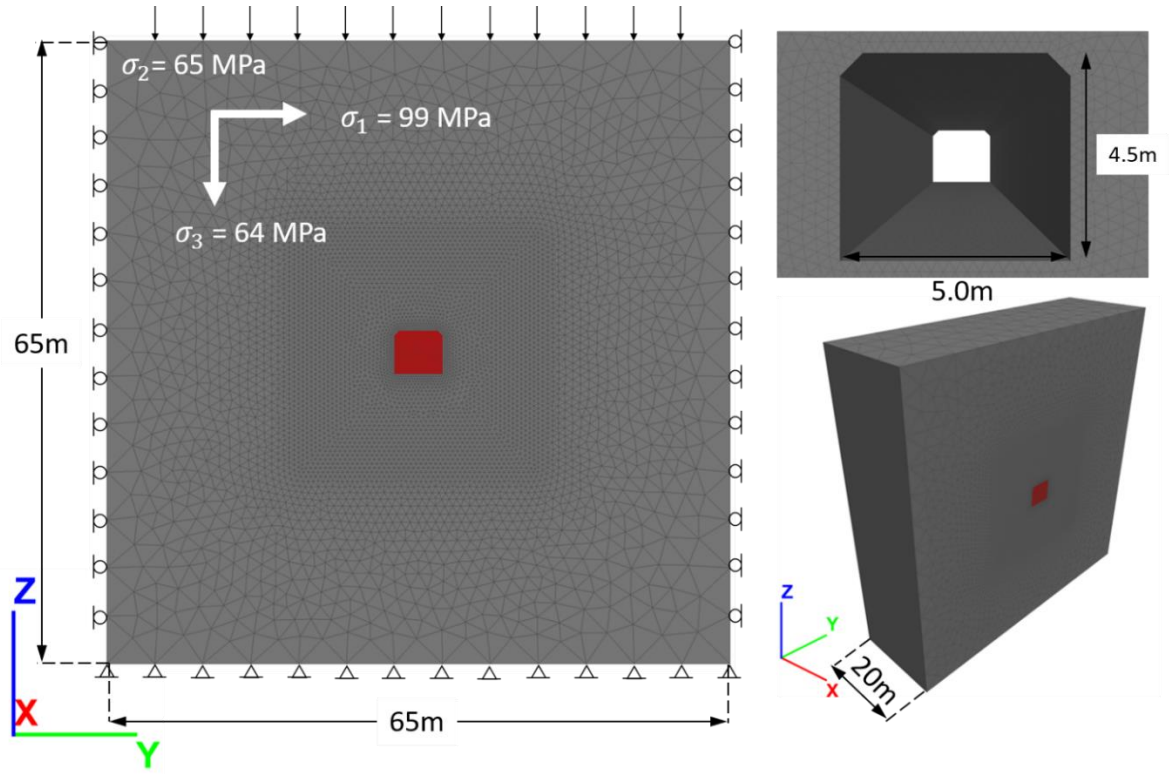

Figure 5.14: LaRonde mine FLAC3D grid and boundary conditions for failure mechanism model

FLAC3D is a static solver, and any sudden excavation may show more damage in the results and to prevent this, zone relaxation logic was used to simulate the extraction of the tunnels in both numerical models to slowly reduce the influence of the zone to be extracted over time and prevent any shock to the numerical system..

Table 5.4: LaRonde mine boundary, mesh and length convergence test results

LaRonde Convergence Tests	Wall to wall convergence				Back to floor convergence					
	C1		C2		C3		C4		C5	
	δ (m)	% Diff.	δ (m)	% Diff.	δ (m)	% Diff.	δ (m)	% Diff.	δ (m)	% Diff.
EXF	**External boundary convergence test**									
3.0	0.52	-	0.60	-	0.10	-	0.11	-	0.10	-
6.0	0.47	-9.6%	0.50	-16.6%	0.10	2%	0.11	2%	0.10	1%
9.0	0.50	8.0%	0.54	7.8%	0.10	0%	0.11	0%	0.10	-2%
GS/DW	**Grid size convergence test**									
0.1	0.54	-	0.57	-	0.10	-	0.11	-	0.10	-
0.05	0.55	2%	0.56	-3%	0.13	32%	0.14	31%	0.13	29%
0.025	0.51	-7.4%	0.53	-5%	0.14	5%	0.15	6%	0.14	7%
Length (m)	**Drift length convergence test**									
10	0.56	-	0.56	-	0.43	-	0.45	-	0.41	-
20	0.53	-6.9%	0.57	2.8%	0.43	1.3%	0.48	4.9%	0.43	5.3%
40	0.50	-4.6%	0.53	-7.9%	0.43	-1.3%	0.47	-1.8%	0.43	-0.6%

5.3.2 Material properties

The mechanical properties of RA-UG mine model were determined from the results of geotechnical lab testing data of drill core samples (Mishra et al., 2015) using Rocdata 5.0 (Rocscience Inc., 2017). The foliation properties were derived from geological mapping data of the rock mass and foliation planes from the mine. The material properties were calibrated to produce comparable displacements to those recorded underground.

For LaRonde mine the material properties reported by Karampinos (2016) were utilized. The material properties were further calibrated to produce to squeezing ground conditions and modelled displacements comparable to those reported by Karampinos (2016). The calibrated material properties used in numerical simulations of failure mechanism at RA-UG and LaRonde mine are provided in Table 5.5.

For both numerical models, it was assumed that the rock mass and foliations are non-dilatant, following the modelling methodology used by Karampinos (2016) to simulate the failure mechanism at LaRonde mine.

Table 5.5: Material properties for rock mass failure mechanism models

Material properties	**Unit**	**RA-UG**	**LaRonde**
Young's modulus	GPa	12.0	48.0
Poisson's ratio	-	0.25	0.16
Cohesion	MPa	2.0	4.5
Friction	°	40.0	22
Dilation	°	0.0	0.0
Tensile strength	MPa	0.2	0.15
Joint cohesion	MPa	0.2	0.0
Joint friction	°	23	20.0
Joint dilation	°	0.0	0.0
Joint tensile strength	MPa	0.0	0.0

5.3.3 Influence of foliation on failure mechanism

The ubiquitous joint model was successful in reproducing the failure mechanisms observed underground at RA-UG and LaRonde mines. Model results indicate that the squeezing ground conditions at RA-UG mine are associated with two distinct failure mechanisms. Displacement vectors suggest that on the western sidewall the deformations will occur along the foliation planes resulting in shearing and sliding between foliation planes and on the eastern sidewall deformations will occur perpendicular to the excavation sidewall and will result in a buckling type failure mechanism. The numerical model produced a wall to wall convergence of 70.8 mm between the two side walls measured at the height of 1.5 m from the drive floor, and this correlates well with the recorded displacement of 71.3 mm (1.27% strain) within 40 days of monitoring in the hanging wall drive between S120 and S150 crosscuts at a depth of ~380 m

(+13L) below surface. Model results also suggest that the rock mass damage in the two sidewalls of footwall drives are anisotropic and most of the damage and deformations in western sidewall should be expected to be within 2.5 m from the excavation floor. In eastern sidewall, the deformations should be expected to be within 2.5 m of the excavation shoulder. The model results are in agreement with the observations reported by Yadav et al. (2016). The modelled displacements, schematics of failure mechanism and underground examples of observed failures at RA-UG mine are provided in Figure 5.15.

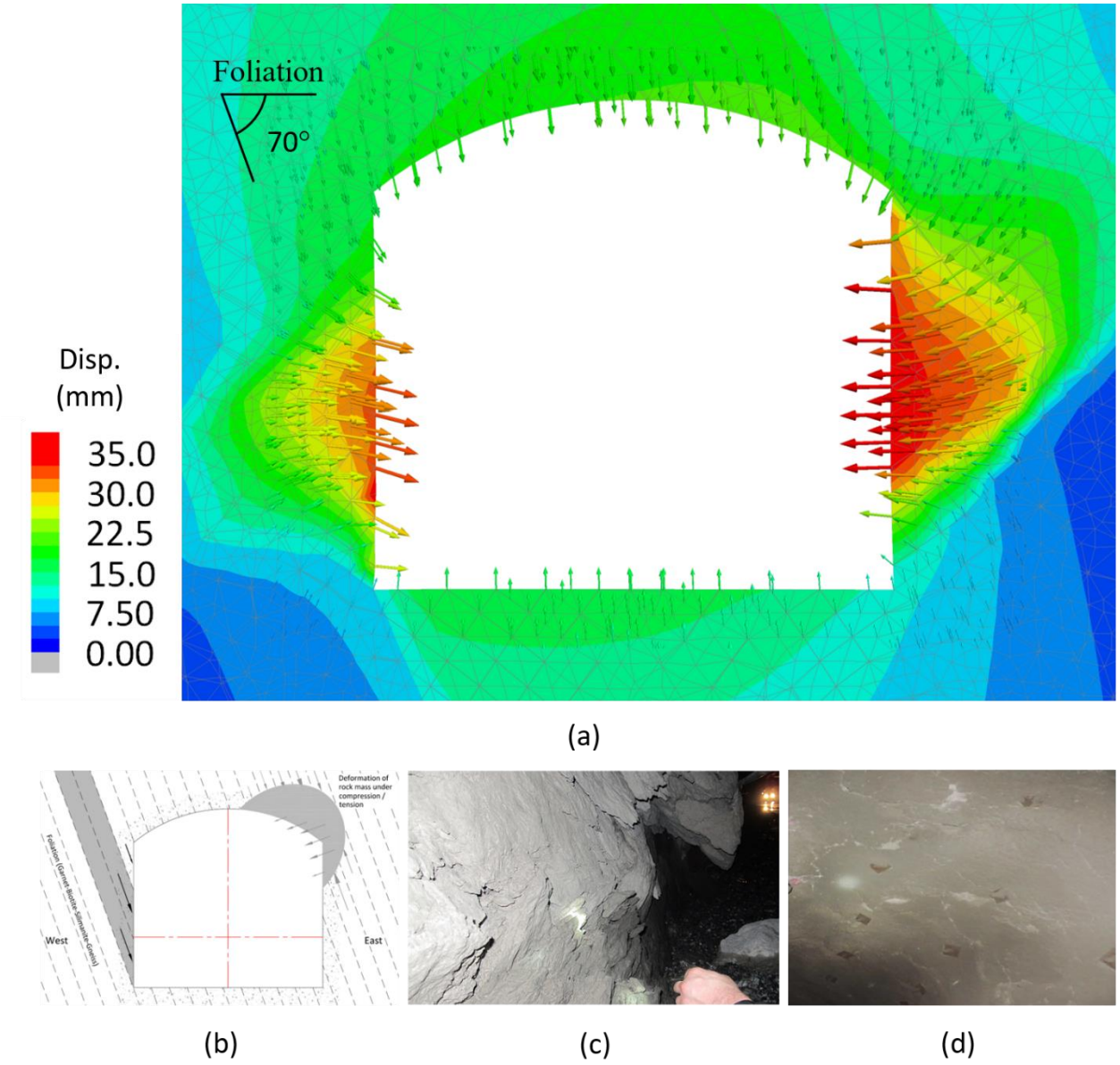

Figure 5.15: Squeezing conditions at RA-UG mine (a) modelled displacements (b) schematic (c) observed damage on the western wall (d) observed damage on eastern wall (Yadav et al., 2016)

For LaRonde mine, the displacements produced by numerical model correlates well with the observation reported by Karampinos (2016) of a haulage drift at 2550 m depth that experienced wall to wall convergence of 1.79 m in 306 days after development. The results are also in good agreement with the modelled displacement of 0.85 m (33% strain) in sidewalls of the 3DEC

model reported by Karampinos (2016). The displacement vectors indicate that for haulage drift at LaRonde mine under squeezing conditions, the deformations will occur perpendicular to the excavation sidewalls and would result in buckling failure mechanism in both sidewalls. However, the presence of foliation planes would result in anisotropic deformations as illustrated in Figure 5.16. Model results also suggest that some difference in the height of rock mass damage should be expected on the two walls. Mellies (2009) reported observations from Drift 227-43-E at LaRonde mine, where lower displacements were recorded in the footwall than in hanging wall, and the displacement profiles showed that large displacements were observed in the upper portion of the hanging wall and the lower portion of footwall side, as shown in Figure 5.16.

The RA-UG mine experiences a combination of two distinct failure mechanisms on each sidewall in squeezing ground conditions, i.e. sliding and shearing along foliation planes and buckling failure mechanisms, whereas the LaRonde mine experiences, buckling failure mechanisms on both sidewalls. This may be a result of the difference in the dip of foliation plane with respect to the excavation wall and orientation of principal stresses for the two mines. RA-UG mine has comparatively flatter dipping foliations than LaRonde mine, and the major principal stress at RA-UG is parallel to the strike of foliations as opposed to major principal stress being perpendicular to foliation planes at LaRonde mine, thus resulting in a difference in failure mechanisms at the two mines.

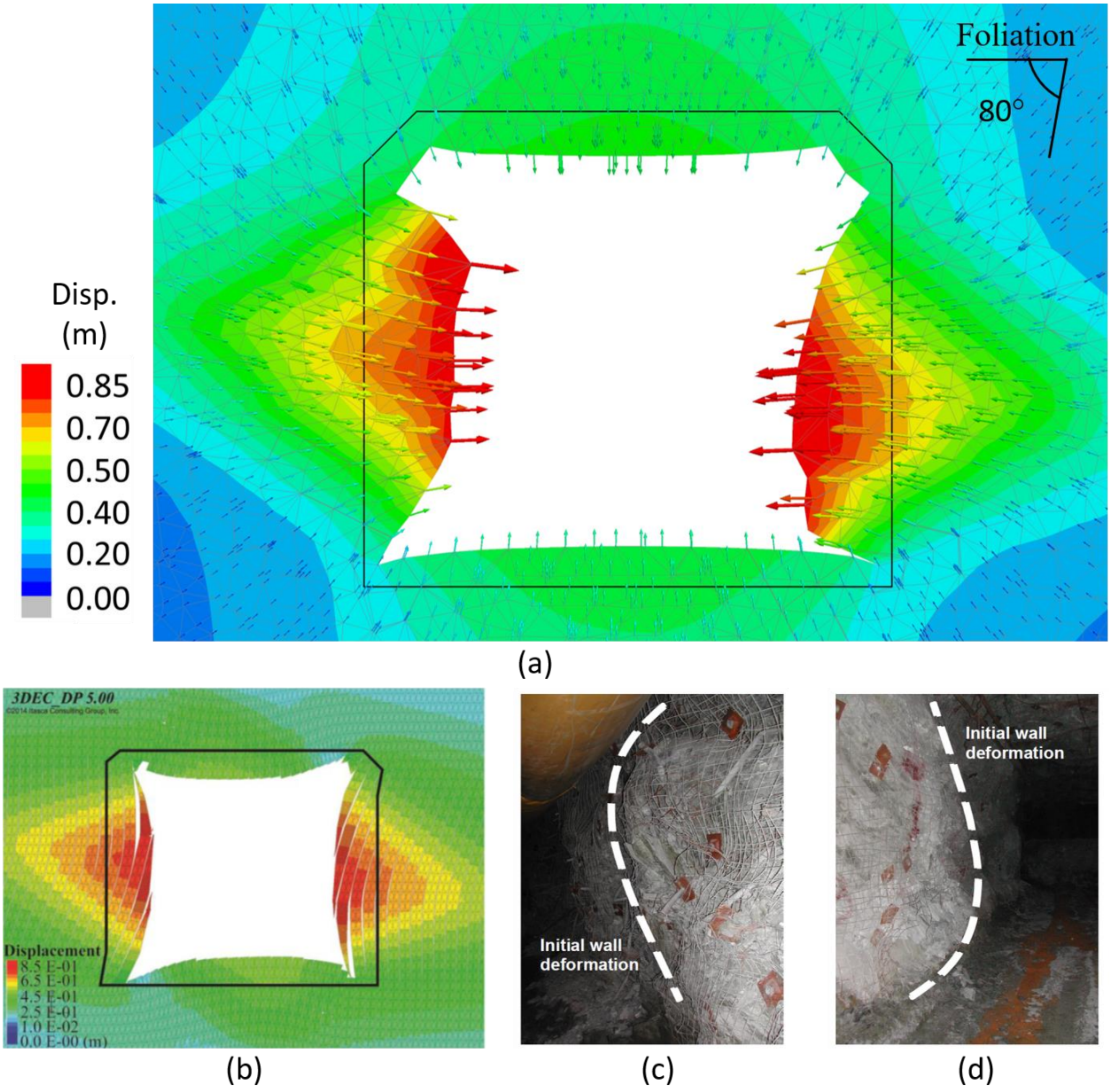

Figure 5.16: Squeezing conditions at LaRonde mine (a) Modelled displacement (b) displacement simulated by DEM (Karampinos, 2016) (c) observed displacement of Hanging wall (d) observed displacement of Footwall (Mellies, 2009)

5.4 Chapter summary

The Ubiquitous-Joint model in FLAC3D allows the simulation of the anisotropic behaviour of the foliated rock mass by considering a single orientation of the weak plane inside finite difference grid. The elastic guess is first checked for failure on the zone matrix and then on the weakness plane using a composite Mohr-Coulomb failure criterion with tension cut-off.

The strength anisotropy of intact foliated GBSG rock at RA-UG mine was simulated utilizing the ubiquitous-joint model in FLAC3D 6.0 (Itasca Consulting Group, 2017a). The model results when compared to laboratory testing results, were found to be in good agreement. The numerical models produce a 'U' shaped curve for variation of UCS values with respect to angle β. The ubiquitous-joint model was successful in reproducing the strength anisotropy observed during the laboratory testing of intact foliated rock. The numerical simulations produced anisotropy factor of 1.87. The mechanical behaviour of intact rock is dominated by foliation planes for β ranging from 10° to 50° and simple shear type failure mechanism along the foliation planes were observed in these simulations.

The rock mass failure mechanism was investigated for RA-UG and LaRonde mines in excavations parallel to the foliation planes utilizing the ubiquitous-joint model in FLAC3D 6.0. The modelled displacements and observed failure mechanisms were in good agreement with those reported by Yadav et al. (2016) for RA-UG mine and by Karampinos (2016) for LaRonde mine. The failure mechanism at RA-UG mine is a combination of shearing and sliding along foliation planes on the western sidewall where the foliation planes dip into the excavation and buckling type failure in the eastern wall. Excavations parallel to foliation at LaRonde mine experiences buckling type failure on both sidewalls.

Chapter 6

6 Influence of various parameters on the severity of squeezing

This chapter of the thesis provides details of numerical simulations carried out to investigate the influence of various parameters on the level of squeezing around underground excavations at RA-UG and LaRonde mines. The chapter also provides a description of the squeezing classification scheme used at both mines. Criteria adopted for interpreting the results of numerical simulations are discussed. Influence of varying interception angle between foliation and excavations walls was investigated. Numerical investigation into the influence of excavation shape and over-break around underground excavations on the degree of squeezing was carried out. To investigate the influence of mining-induced stresses due to other excavations on the degree of squeezing, numerical simulations of parallel excavations were carried out. The modelling details, material properties and boundary conditions for numerical models are presented. The chapter also provides the results and discussions of parameters investigated.

6.1 Classification of squeezing ground conditions

Steiner (1996) reported that there are several classification schemes that can be used for squeezing ground conditions. Terzaghi (1946) provided a behavioural description of the ground by assigning a pressure related to loading of the initial support. Aydan et al. (1993) and Jethwa et al. (1984) proposed to relate the strength of the intact rock to the overburden. Singh et al. (2007) correlated the overburden with Barton's rock mass quality (Q). Butler and Leonardi (2016) utilized Rock Condition Factor (RCF) to classify squeezing ground conditions at Mount Isa Mines.

For classification of squeezing ground conditions at LaRonde and Lapa mines, Karampinos

(2016) reported that the severity of squeezing ground conditions could be quantified by deformation recorded or damage observed. The magnitude of drift closure is often related to squeezing ground conditions and is reported as a wall to wall deformation, tunnel strain or closure strain. Vakili et al. (2012) provided another measure for quantifying the squeezing ground conditions by using area of damage (percentage of excavation profile affected) and depth of damage in addition to excavation closure strain.

Both RA-UG and LaRonde mines utilize closure strain based classification schemes to categorize the severity of the squeezing ground conditions. Karampinos (2016) reported that at LaRonde mine total wall to wall convergence (δ_{total}) is estimated from the difference between the two surveyed widths (s) and the lowest sidewall distance measured. Similarly, the back to floor convergence at LaRonde mine is derived using the lowest back to floor distance and drift height measured in the surveyed profile. Using the total wall to wall or back to floor convergence total strain (ε_{total}) percentage is calculated by using the following equation.

$$\varepsilon_{total} = \frac{\delta_{total}}{s} * 100 \tag{6.1}$$

Karampinos (2016) proposed a revised classification scheme for identifying squeezing in hard-rock mines as follows:

- No or low squeezing (0% < ε_{total} < 5%)
- Moderate squeezing (5% < ε_{total} < 10%)
- Pronounced squeezing (10% < ε_{total} < 35%)
- Extreme squeezing (ε_{total} > 35%)

These values are considerably higher than the published work in civil engineering summarized by Potvin and Hadjigeorgiou (2008). Karampinos (2016) postulated that this difference in the values of classification schemes might be a result of the higher tolerance of rock mass failure mechanism in a mining environment.

Based on experience in numerical modelling and underground observations, site consultants developed a damage classification scheme that can be used to relate the underground damage and rehabilitation history to the displacement monitoring data and numerical modelling output parameters at RA-UG mine. This classification scheme was used to relate the expected damage level to the excavation closure strain obtained from the FLAC3D results. The total wall to wall convergence at RA-UG mine is estimated from displacement monitoring data collected utilizing tape extensometers and from the surveyed profile. The total closure strain is calculated utilizing Equation 7.1. The damage classification scheme used at RA-UG mine is provided in Table 6.1. The table shows the expected closure strain, depth of failure (D_f) and area of damage (A_d) for various damage levels.

6.2 Interpretation of modelling results

Vakili et al. (2012) provided a guideline for non-linear numerical model interpretation based on the past modelling and field experience. The guidelines were based on back analysis of the failure mechanism of a raise bore shaft in a highly stresses and foliated rock mass. Zhang and Mitri (2008) described three evaluation criteria that were used as the basis for the interpretation of numerical model results. The criteria used to interpret the numerical model results in this study are provided in the following sub-sections.

Table 6.1: Damage classification scheme used at RA-UG mine, after (Vakili et al., 2012)

Damage Level	**General Description**	**Damage Description and Ground control**	D_f **(m)**	A_d **(%)**	**Minimum boundary strain**	
					GSI < 50	**GSI > 75**
S0	No visible damage	No stress induced damage visible. Easily controlled with minimal support (e.g. split set and mesh)	0.0	0%	<0.1%	<0.3%
S1	Minor damage	Superficial damage only, easily scaled back to good rock. Easily controlled with minimal support (e.g. split set and mesh)	0.5	<10%	0.1%	0.3%
S2	Moderate damage	Spalling clearly developed and more widespread in walls and backs. Minor rehabilitation required for high utilization excavations	0.8	10-50%	0.3%	0.6%
S3	Significant damage	Damage evident in all excavation surface. 'Bagging' in the mesh clearly developed, shearing on foliation/bedding clearly indicated and isolated split set failures. Significant rehabilitation efforts required to maintain safe access.	1.5	>50%	0.6%	2.0%
S4	Severe damage	Severe damage with up to 2m wall or back convergence and/or significant floor heave. Passable on foot, with extreme caution, but serviceability significantly reduced. Many bolts broken in shear, mesh severely bagged, some local rock falls. Limit of rehabilitation with conventional support.	2.5	>80%	2.0%	5.0%
S5	Extreme damage	Widespread support failure and large rock falls (>1000 tonnes) and in some cases complete or nearly complete drive closure. Access not advisable, beyond rehabilitation.	>2.5	100%	>2.0%	>5.0%

6.2.1 Displacement or convergence criteria

Zhang and Mitri (2008) carried out elasto-plastic stability analysis of mine haulage drift in the vicinity of mined stopes and utilized displacement convergence criteria to assess the geotechnical stability of the modelled drift. They reported that the displacement convergence criteria are generally site-specific as the criteria would depend not only on the rock mass stiffness but also on the intended use of the underground opening as well as the design.

For interpreting the results of the numerical simulations carried out to investigate the influence of various parameters on the level of squeezing at RA-UG and LaRonde mines, displacement convergence criteria were used. Displacement magnitude at selected sections along the length of simulated excavation was monitored for the numerical simulations. Total wall to wall and floor to back convergence values were calculated from the recorded displacements. Closure strain was estimated from the convergence values, and the final total closure strains were compared to the squeezing classification used at both mines. In addition to closure strains, contours for displacement magnitude were compared for assessing the influence of various parameters on the displacements around the simulated excavations.

6.2.2 Volumetric strain criteria

Vakili et al. (2014) provided a visual representation of the degree of rock disintegration at various levels of volumetric strain in non-linear numerical models. Watson et al. (2015) utilized volumetric strain criteria to investigate the potential depth of failure around shafts utilizing FLAC3D numerical simulations. The authors reported that the negative volumetric strain implies contraction in rock mass that would occur at high confinement levels and the positive value indicated rock mass dilation that would occur at in lower confinement levels such as near the

excavation boundary. The authors also reported that experience in numerical back analysis at several mining operations showed that a modelled volumetric strain of between 1-3% often generated similar over break/breakout volumes to those obtained from actual underground excavations. Representation of various volumetric strain with respect to the degree of disintegration and qualitative description as simulated in a fully discontinuum model through modelling of uniaxial loading of a rock sample is provided in Figure 6.1.Contours of volumetric strain were used to compare the level of damage around the underground opening in the numerical simulations for RA-UG and LaRonde mines. In addition to volumetric strain contours, iso-surface of selected values of volumetric strains were compared to assess the influence of various parameters.

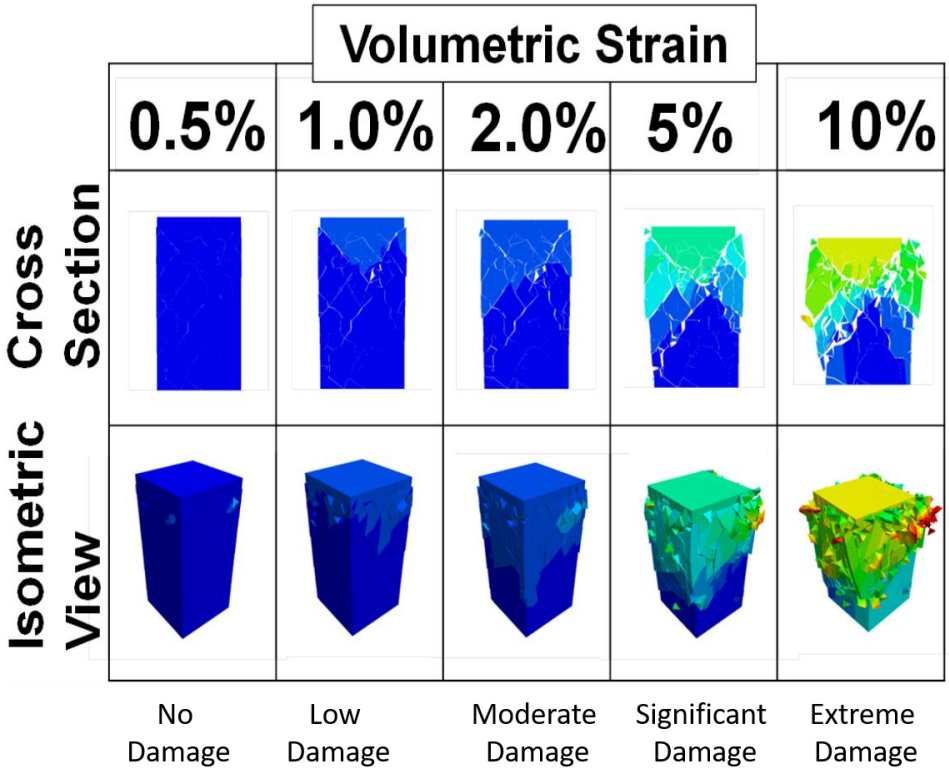

Figure 6.1: Visual representation of the degree of rock disintegration at various levels of volumetric strain, after (Vakili et al., 2012)

6.3 Influence of interception angle, ψ

The relative orientation of the foliation planes with excavation walls has an important influence on the mechanical behaviour of the foliated rock mass around underground excavations. It controls the potential failure mechanism and the longitudinal development of the displacements. Case histories have shown that the magnitude of displacements can differ almost by order of magnitude for the cases where the strike is parallel and perpendicular to the tunnel axis respectively. The reason is the usually low shear strength parallel to the foliation, which can lead to shearing or buckling failure modes. This makes understanding the influence of the relative foliation orientation on the mechanical behaviour of the ground extremely critical for excavation stability and ground support design (Schubert and Mendez, 2017).

This behaviour of foliated rocks can be quantified using the angle of interception (ψ). Mercier-Langevin and Hadjigeorgiou (2011) defined the interception angle as the angle between the normal to the foliation planes and the normal to the excavation wall of interest as shown in Figure 7.2. Hadjigeorgiou et al. (2013) reported that at the LaRonde mine it was recognized that there was a potential advantage of modifying the drift orientation with respect to in-situ foliation orientation. Driving haulage drives at a favourable angle to the foliation resulted in a significant reduction in the cost associated with reconditioning and associated production delays. Mercier-Langevin and Hadjigeorgiou (2011) reported that the field observation at LaRonde mine support the hypothesis that the angle of drift walls with respect to the orientation of the foliation has a significant influence on the level of squeezing. Similar behaviour was observed at RA-UG mine, where modifying the orientations of underground excavations resulted in a significant reduction in the rehabilitation requirements and associated ground support and rehabilitation costs.

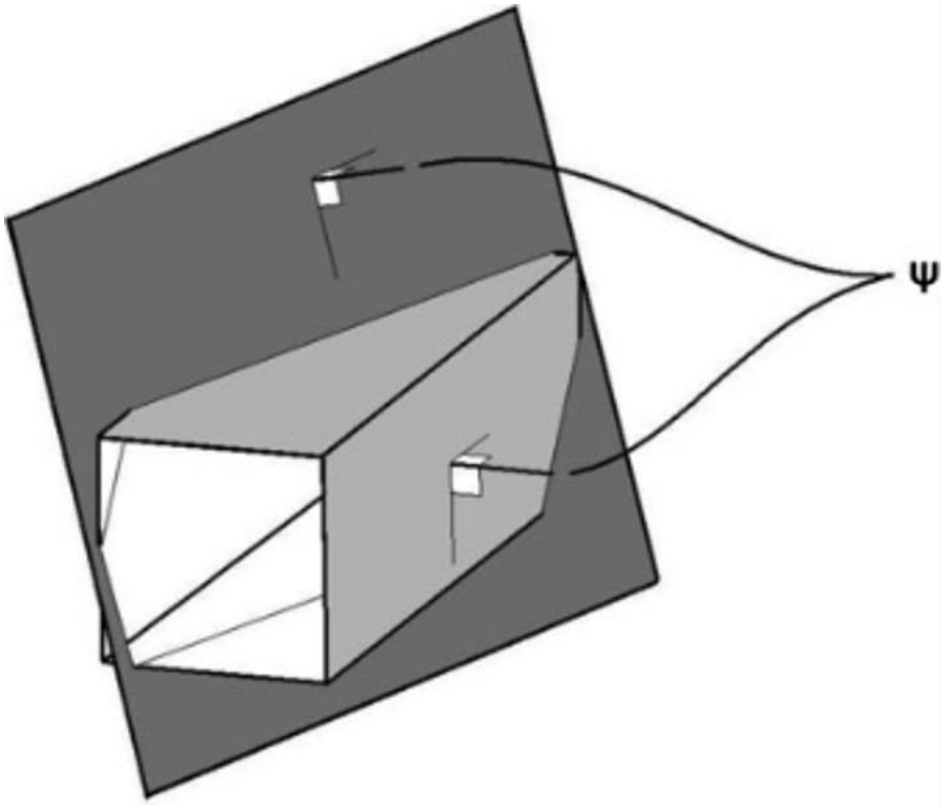

Figure 6.2: Definition of angle of interception (ψ), after (Mercier-Langevin and Hadjigeorgiou, 2011)

The influence of varying interception angle between excavation walls and foliation planes was investigated for RA-UG and LaRonde mines in footwall drive and haulage drift respectively by employing the ubiquitous joint model in FLAC3D. The external boundary, grid size and boundary conditions for numerical simulations were used from the failure mechanism models described in Section 6.2. A base case orientation of excavations and interception angle was selected for both mines, and the numerical simulations were carried out to study the severity of squeezing ground conditions for varying interception angles.

The base case of RA-UG mine was simulated for the footwall drive at -130L (depth ~ 525 m) between N30 and N90 crosscuts. Total wall to wall convergence of 60 mm (strain 1.1%) was

recorded at this location from April 2016 to November 2017. The numerical models were calibrated to reproduce the displacements observed underground. It was assumed that the rock mass and foliation are non-dilatant and the dip of foliation was assumed to be 70°. It was assumed that the strike of foliation is parallel to the length of the drive and 60 m for drive length was simulated. The interception angle was varied by rotating the drive, in increments of 15° from 0° to 90° resulting in an increase in the interception angle between the foliation and excavation walls from 20° to 90°. The interception angles below the base case, i.e. 20° were simulated by increasing the dip of foliation planes from 70° to 90° in 10° increments.

The base case model of LaRonde mine was simulated for haulage drift at a depth of 2270 m from the surface. Karampinos (2016) reported 13.0% wall to wall, and 10.8% back to floor strain at this location and the displacements in the numerical models for the base case were calibrated to reproduce the reported strain values. It was assumed that the dip of foliation is 80° and the interception angle was varied by rotating the haulage drift in 15° increments from 0° to 90° resulting in an increase in the interception angle between the foliation and excavation wall from 10° to 90°. A total drift length of 60 m was simulated. To simulate the interception angles less than the base case, i.e. 10°, the dip of foliation was increased from 80° to 90°, keeping the excavation walls parallel to the foliation strike. The rock mass and foliations were assumed to be non-dilatant. The calibrated properties used in the numerical simulations for both mine models are provided in Table 6.2.

Table 6.2: Calibrated material properties used in the interception angle models

Material properties	**Unit**	**RA-UG**	**LaRonde**
Young's modulus	GPa	12.0	48.0
Poisson's ratio	-	0.25	0.16
Cohesion	MPa	3.1	5.0
Friction	°	49.0	27.0
Dilation	°	0.0	0.0
Tensile strength	MPa	0.20	0.27
Joint cohesion	MPa	0.2	1.5
Joint friction	°	20.0	32.0
Joint dilation	°	0.0	0.0
Joint tensile strength	MPa	0.0	0.0

The trend of the wall to wall closure strain for varying interception angle for RA-UG mine simulations is provided in Figure 6.3. The trend suggests that the foliation planes have no influence on the closure strains for ψ greater than 45° and have significant influence for ψ less than 45°. A total drop of 64% in the wall to wall closure strain was observed when ψ was increased from 0° to 45°. The modelling results also indicate a slight increase in the closure strain when ψ was increased from 75° to 90°, this is a result of footwall drive walls becoming perpendicular to the major principal stress (σ_1) as the interception angle approaches 90°. The slope of the curve suggests a higher rate of decrease in the wall to wall closure strain for ψ = 0°-30°, a moderate rate of decrease for ψ = 30°-45° and no significant change for ψ = 45°-90°.

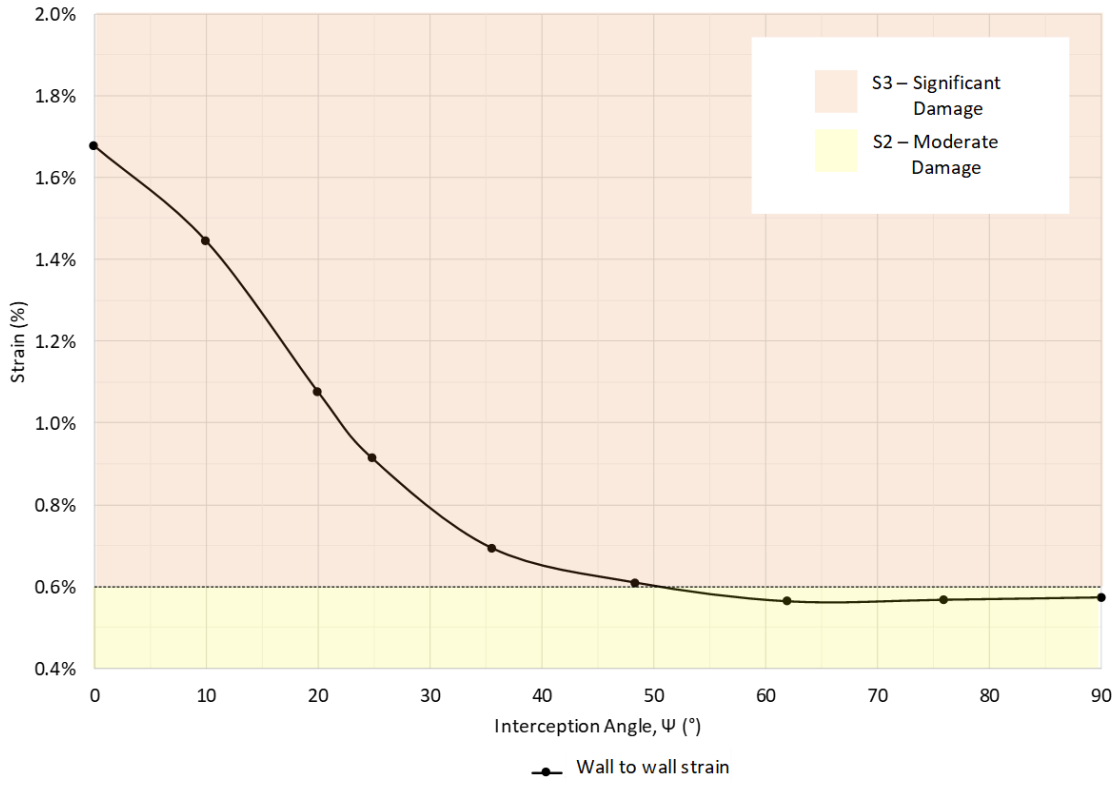

Figure 6.3: Influence of varying interception angle on the wall to wall closure strain at RA-UG mine

The contours of displacement, volumetric strain and iso-surface plots for 1.5 % volumetric strain are provided in Figure 6.4. The volumetric strain contours and iso-surface plots were used to compare the rock mass damage between the simulated values of interception angle, 1.5% volumetric strain represents low to moderate rock mass damage. The volumetric strain plots suggest moderate rock mass damage for ψ between 0° and 30°, low rock mass damage for ψ between 30° and 45°. No considerable rock mass damage was observed for ψ greater than 45°. Underground observations at RA-UG mine suggest moderate to significant rock mass damage in excavations parallel to the strike of foliation planes and no signs of squeezing was observed for excavations at ψ greater than 45°. The modelling results are in good agreement with the underground observations.

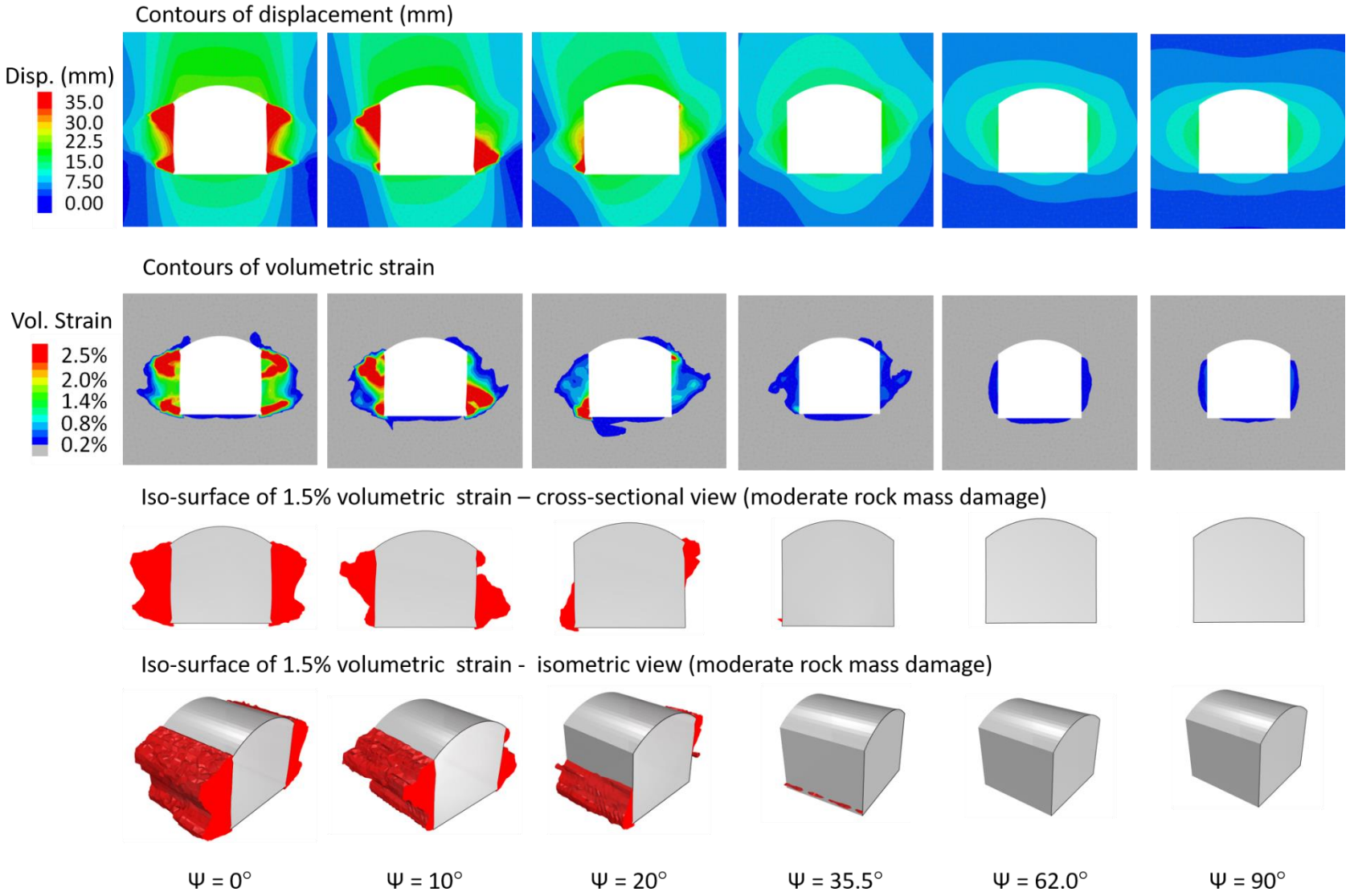

Figure 6.4: Modelled displacement and volumetric strain for varying interception angle at RA-UG mine

The results of numerical simulation for investigating the influence of varying interception angle at LaRonde mine are provided in Figure 6.5. The trend in closure strain with varying interception angle suggests that at LaRonde mine the foliation planes have a significant influence on the level of squeezing for ψ less than 45° and no significant influence for ψ greater than 45°. A total drop of 66% was observed in the wall to wall closure strain when ψ was increased from 0° to 45°. The trend also suggests a slight increase in closure strain when ψ was increased from 75° to 90°, this is because the drift walls become perpendicular to the intermediate principal stress (σ_2) as the interception angle approaches 90°. The slope of the curve suggests a high rate of decrease in the wall to wall closure strain for ψ between 0°-30°, moderate rate of decrease for ψ = 30°-45°, and no significant decrease in closure strain for interception angle greater than 45°.

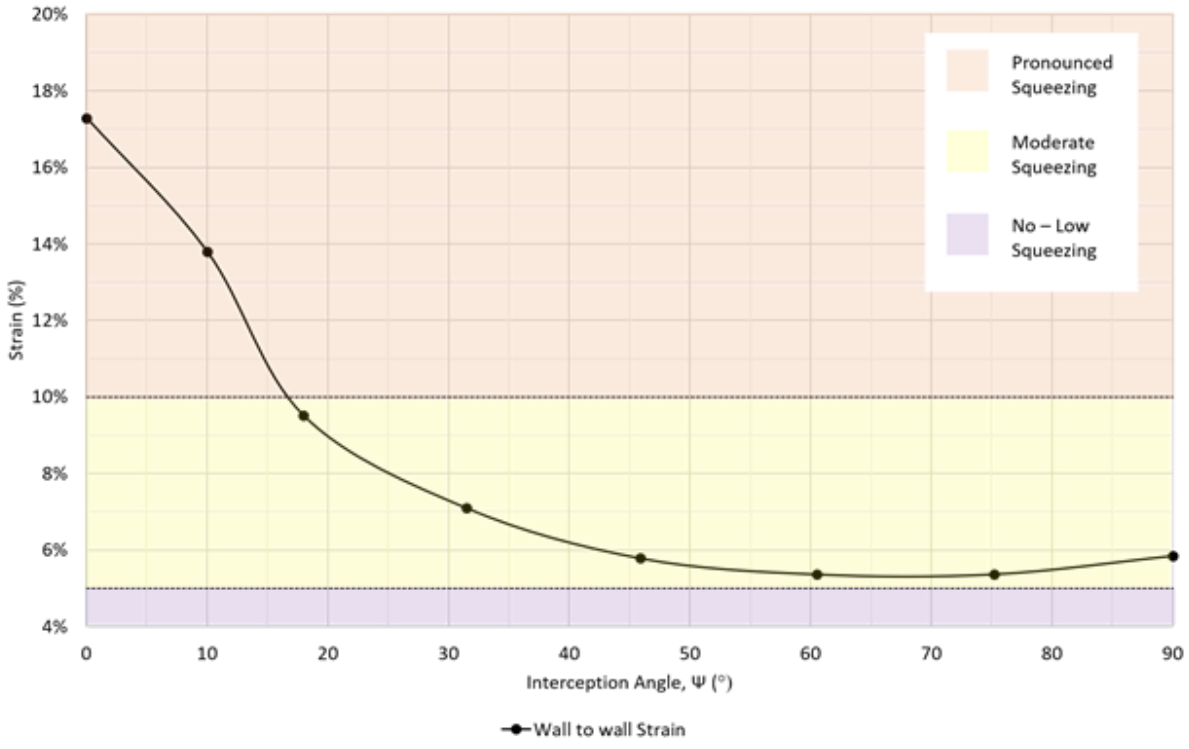

Figure 6.5: Influence of varying interception angle (ψ) on the wall to wall closure strain at LaRonde mine

The contours of displacement, volumetric strain and iso-surface plots showing 5.0% volumetric strain around haulage drift at LaRonde mine are provided in Figure 6.6. The volumetric contours and iso-surface plots were used to compare the rock mass damage between the simulated values of ψ and 5.0% volumetric strain represents significant rock mass damage. Modelling results indicate that the haulage drive experiences significant to extreme rock mass damage for ψ between 0°-30°, moderate rock mass damage for ψ between 30°-45° and no to low rock mass damage for ψ greater than 45°. The modelling results when compared to the field observations were found to be in agreement. Figure 6.7a provides the reported closure strain values recorded underground at LaRonde and Lapa mine, the recorded cases suggests that for interception angle less than 45° pronounced and extreme squeezing was encountered and for interception angle greater than 45° only low to moderate squeezing was encountered. Mercier-Langevin and Hadjigeorgiou (2011) reported field observations from haulage drift at 2,150 m depth from the surface, at this location there was little evidence of squeezing when the foliation planes were perpendicular to the drift orientation. Drift with ψ = 45° experienced minor to no squeezing and severe squeezing was observed in drifts parallel to the foliation planes (see Figure 6.7 b-d). Modeling results are also in good agreement with the trend of the closure strain with varying interception angle reported by Karampinos (2016) for LaRonde and Lapa mines. The closure strain data suggests that most of the moderate to extreme squeezing cases were recorded for ψ less than 45° and the majority of the pronounced and extreme squeezing cases were recorded for ψ between 0° and 30°.

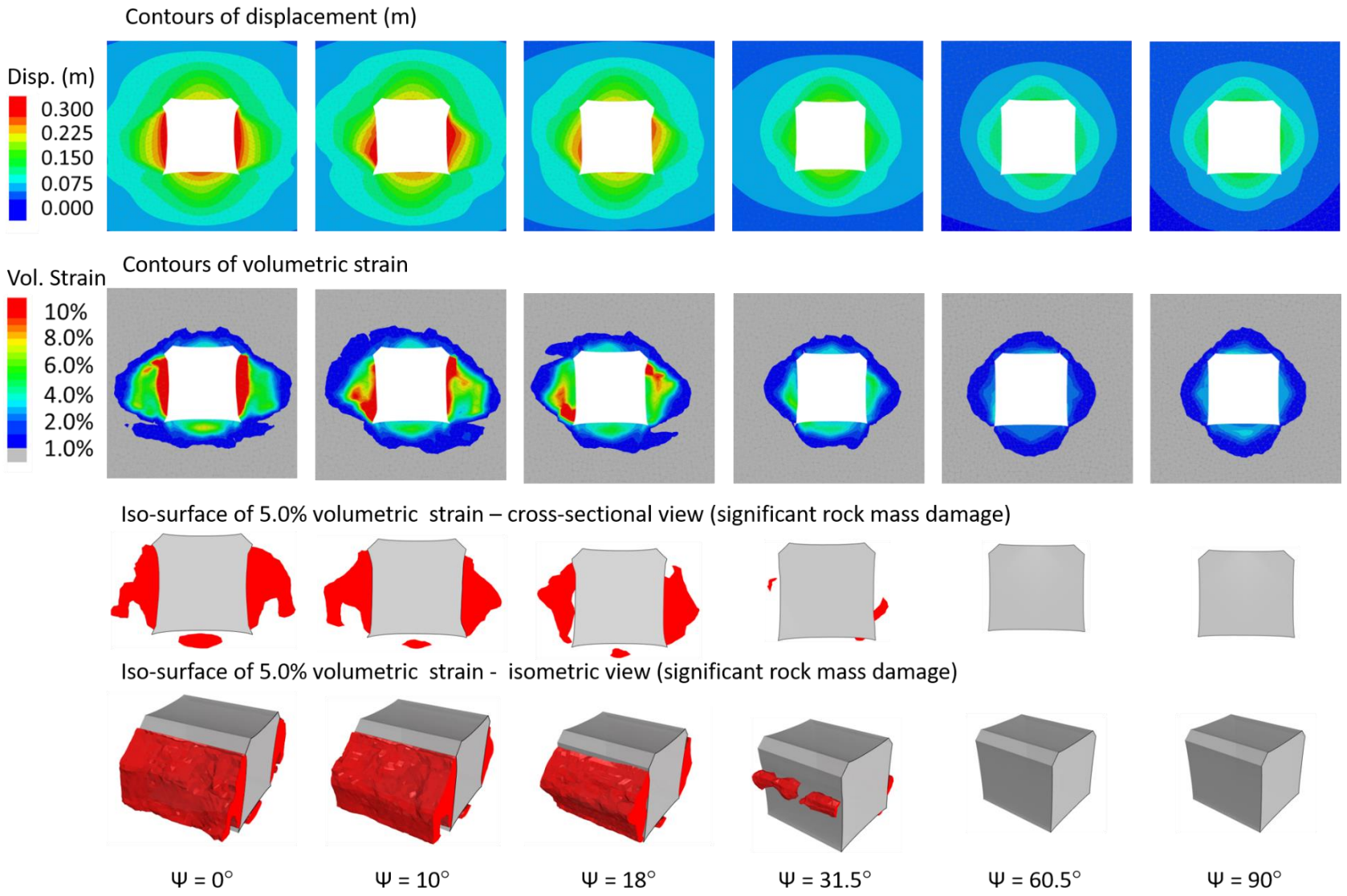

Figure 6.6: Modelled displacement and volumetric strain for varying interception angle at LaRonde mine

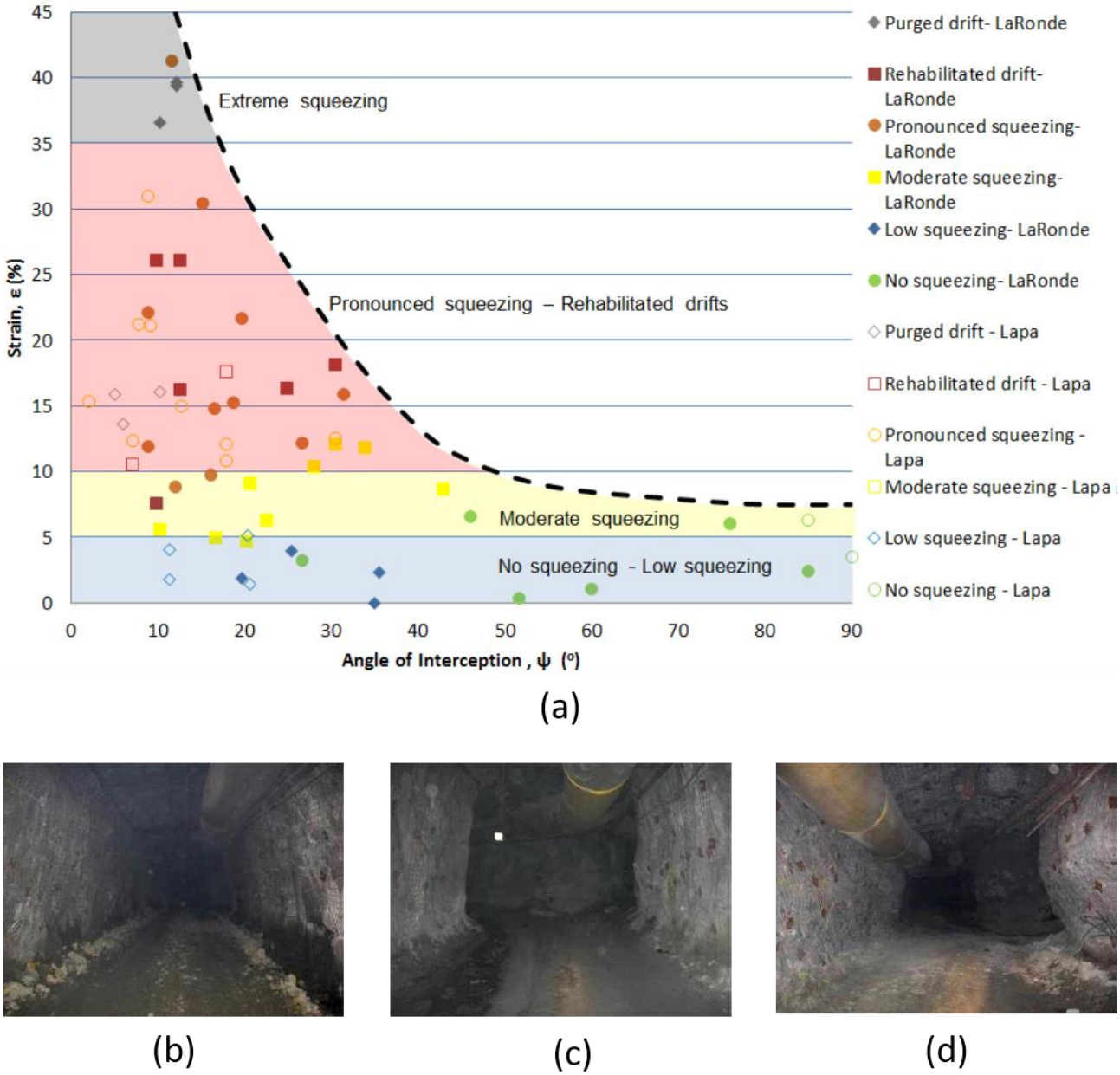

Figure 6.7: Underground observation of influence of interception angle on squeezing at LaRonde and Lapa mine (a) Influence of ψ on wall to wall closure strain, after Karampinos (2016), squeezing in (b) perpendicular (c) 45 degrees (d) parallel excavations at LaRonde mine, after (Mercier-Langevin and Hadjigeorgiou, 2011)

The numerical modelling results for the two cases are also in agreement with the numerical modelling results reported by Vakili et al. (2014). The authors investigated the behaviour of the

anisotropic rock mass around underground excavation utilizing improved unified constitutive model (IUCM) in FLAC3D and reported that the development subparallel to the anisotropy plane would experience higher closure strain and rock mass damage as compared to the developments perpendicular to the plane of anisotropy. The authors also indicated that the closure strain and orientation dependency could vary significantly with changes in stress conditions or degree of anisotropy. The modelling results reported by Vakili et al. (2014) are provided in Figure 6.8.

The modelling results from the two case studies, underground observation and closure strain data indicate that the relative orientation of foliation with excavation axis can significantly influence the severity of squeezing around underground excavations. The modelling results for both cases present similar trend in closure strain with the variation of interception angle and suggest that the foliation planes do not have any significant influence on rock mass behaviour for ψ greater than 45°. Results also indicate a comparetively higher influence of foliation on rock mass behvaiour for interception angles between 0° to 30° than for ψ between 30° to 45°. It should be noted that these values are based on numerical simulations of selected cases for both mines.

The influence of interception angle on the severity of squeezing can have serious repercussions on the ground support cost and rehabilitation requirements of the mine and understanding this behaviour can provide the essential information and tools to manage the squeezing ground conditions effectively.

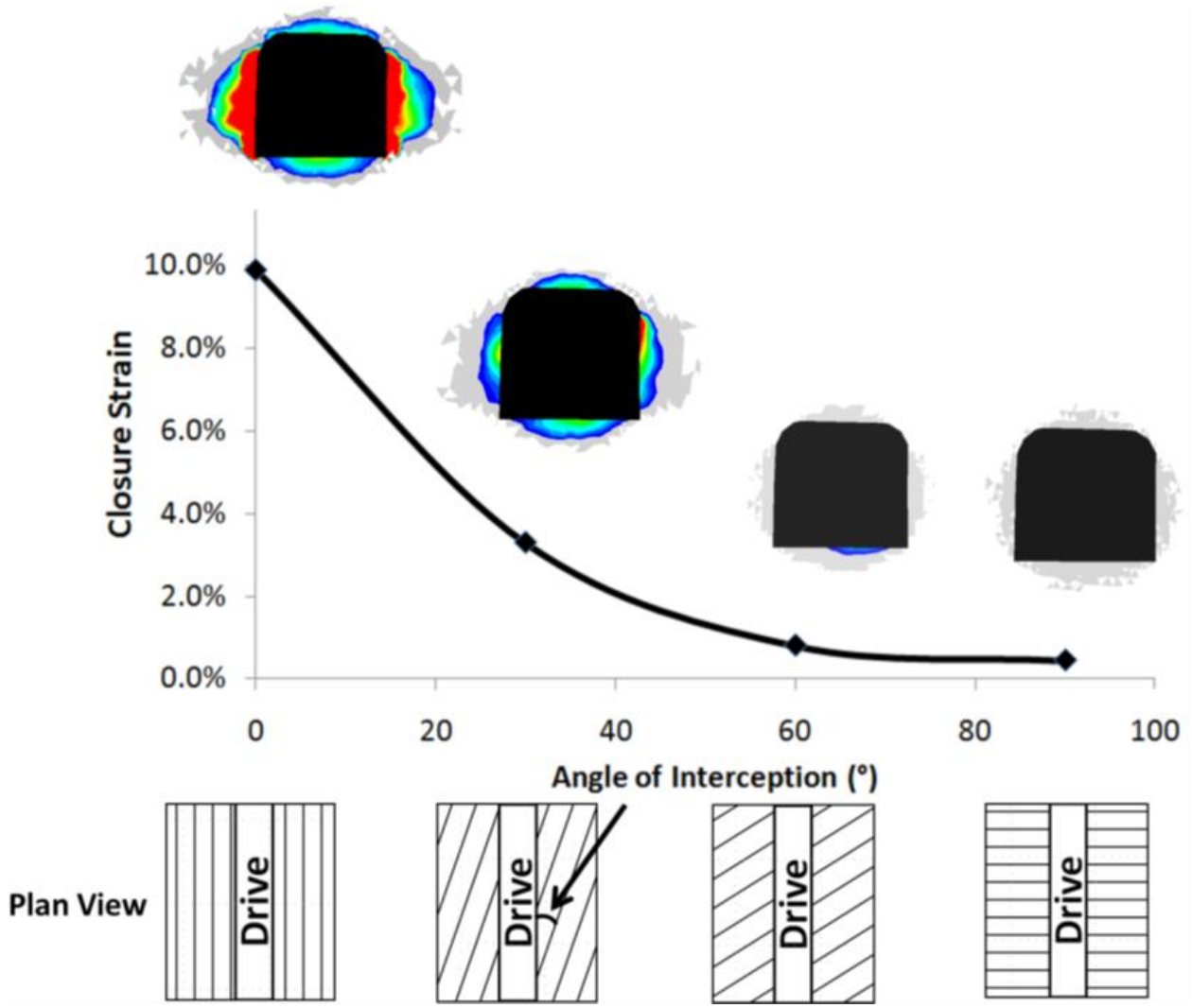

Figure 6.8: Influence of interception angle on closure strain, after Vakili et al. (2014)

6.4 Influence of excavation shape

Hoek and Brown (1980b) examined the influence of various excavation shapes on the redistribution of principal stresses around the underground opening to illustrate how the adverse stress conditions can be induced for certain excavation shapes and orientations. The effect of various excavation shapes on the stability of underground excavations has been investigated by several researchers. Zhang and Mitri (2008) carried out a parametric study to examine the influence of different excavation shapes used in various Canadian underground mines on the stability of mine haulage drifts. The authors reported that the three-centred arched roof offers the advantage of more uniform

stress redistribution and reduces the yielding in the back and floor of the drift. Peck et al. (2013) utilized the distinct element code UDEC to assess the performance of flat and arched-back roofs in shallow tunnels in a variety of geological settings. The effect of excavation shape on the displacements around underground excavations undergoing squeezing was examined for RA-UG and LaRonde mines. The simulated shapes are illustrated in Figure 6.9. The material properties, boundary conditions, grid size and loading conditions were adopted from the numerical models described in Section 7.3.

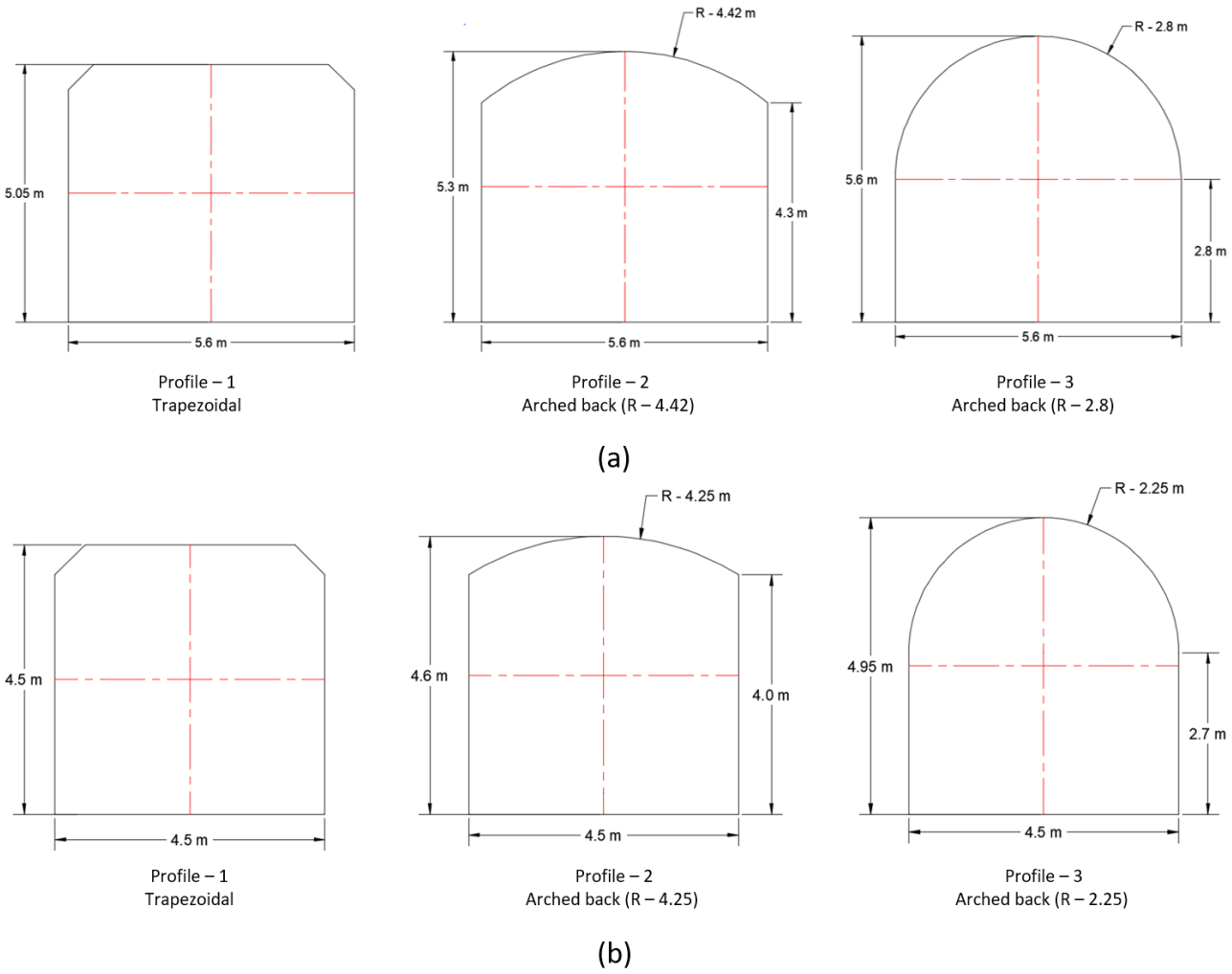

Figure 6.9: Excavation shapes modelled (a) RA-UG mine (b) LaRonde mine

Conventionally RA-UG mine utilizes arched-back profile with a large radius of curvature (see

Figure 6.9-a, Profile-2) for footwalls drives and LaRonde mine utilizes trapezoidal shape for haulage drifts (see Figure 6.9-b, Profile-1). Three excavations shapes – trapezoidal, arched back with a large radius of curvature and arched back with a small radius of curvature were examined for the two mines. In order to allow for comparative analysis between the simulated cases, the examined shapes for each mine were designed to have the same cross-sectional area of 28.0 m^2 for standard footwall drive at RA-UG mine and 20.0 m^2 for standard haulage drift at LaRonde. The displacement contours around footwall drives for RA-UG mine and haulage drift for LaRonde mine are provided in Figure 6.10.

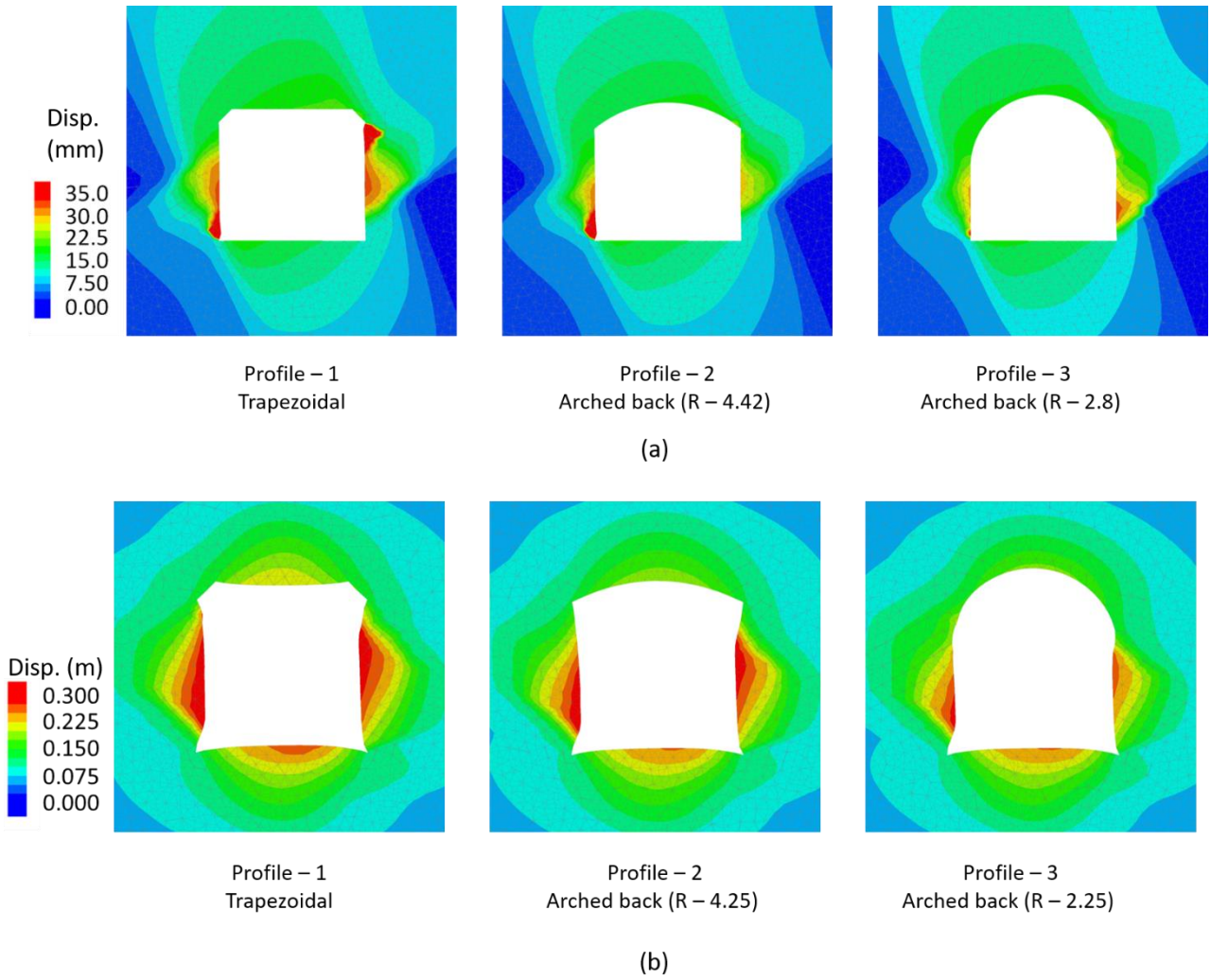

Figure 6.10: Modelled displacements for examined excavation shapes (a) RA-UG mine (b) LaRonde mine

The displacement contours around the footwall drive at RA-UG mine (Figure 6.10-a) suggest that the displacements in drive sidewalls are significantly influenced by excavation shape, and no major variation in displacements was observed in the drive back and floor for the simulated shapes. The displacement in the sidewall are considerably reduced in arched back profile with a smaller radius of curvature as compared to the standard footwall drive shape, and modelling results suggest a 9.0% decrease in the drive closure strain and the majority of the displacement in the sidewalls are restricted within 2.8 m from the drive floor for this profile. The trapezoidal shape results in higher

displacement in the sidewalls and modelling results suggest an 11% increase in the drive closure strain. This is because the arched back profile results in more uniform stress redistribution around underground excavations compared to a trapezoidal profile and thus reduces the displacements.

The displacement contours around haulage drift at LaRonde mine (Figure 6.10-b) suggests that the displacements in the drift sidewalls are significantly less in the arched back profiles as compared to the conventional trapezoidal profile of haulage drifts. The results also indicate a slight decrease in displacements in drift floor and back as the flat roof is arched. Total drops of 7.5% and 24% were observed in the wall to wall convergence strain when the shape was changed from conventional trapezoidal to 4.25 m radius arch and to 2.25 m radius arch respectively. The displacement contours also suggest that as the drift back is arched, the height of high displacement zone from the drift floor reduces and the high displacement zone for 2.25 m radius arch is within 2.7 m from the drive floor.

The modelling results from the two mines suggest that the displacements around underground excavation in squeezing ground conditions are considerably influenced by the excavation shape. Arched back shape with a smaller radius of curvature is the most favourable shape and can improve displacements associated with the squeezing conditions, however in practice often this shape cannot be adopted in mining environment considering the requirements for ventilation and equipment mobility. The results indicate that even a larger radius arching in the back can improve the deformations.

6.5 Influence of excavation over-break

Over-break around underground excavations depends on blasting techniques utilized and the local geology. Steiner (1996) reported that the excavations parallel to the foliation are susceptible to over-break due to buckling of the foliation. Numerical simulations were carried out to examine the

effect of excavation over-break on the displacements around excavation in squeezing ground conditions. In practice, over-break often results in a very uneven profile as shown in Figure 6.11-a and in order to simulate the over-break in the numerical models, equivalent linear over-break was used to provide a smooth profile in numerical models (see Figure 6.11-b). The influence of over-break was examined from 0% to 25% for footwall drive at RA-UG and haulage drift at LaRonde mine. The model properties, boundary conditions, grid size and loading conditions were adopted from the numerical models described in Section 7.3.

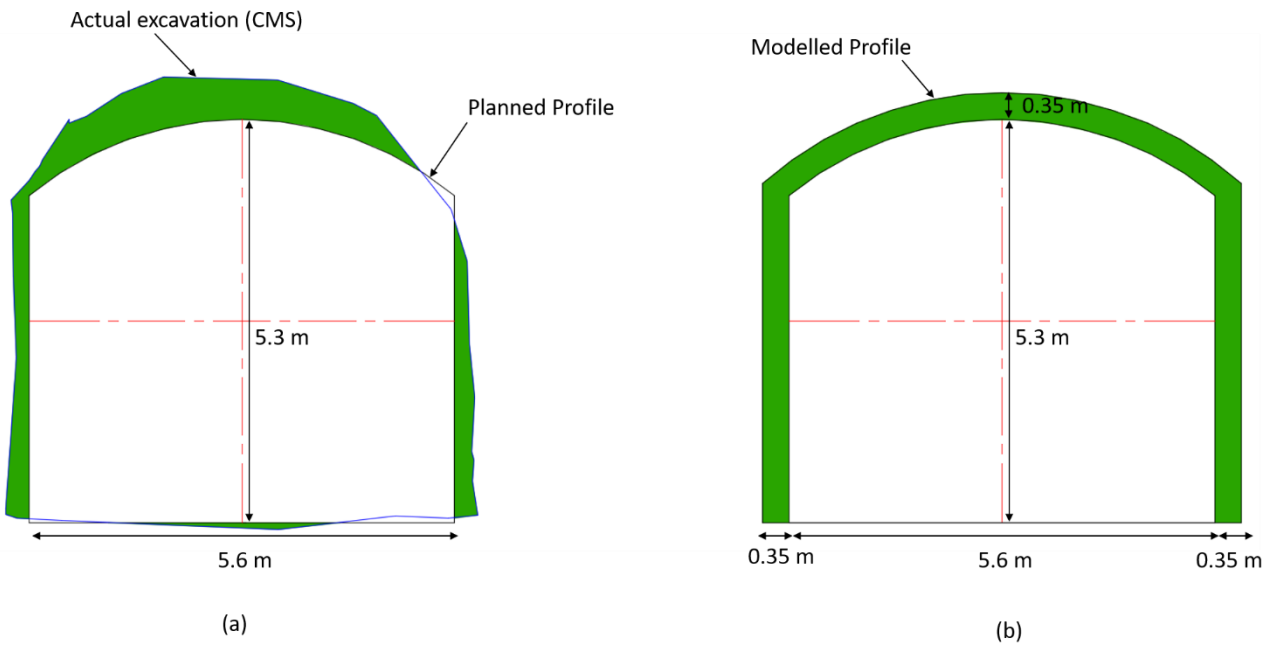

Figure 6.11: Equivalent linear over-break used in the numerical model showing 12% over-break at RA-UG mine (a) actual over-break (b) modelled over-break.

The results of numerical simulations carried out to examine the influence of over-break on displacements at RA-UG and LaRonde mines are provided in Figure 6.12. The displacement contours around footwall drive at RA-UG mine (Figure 6.12-a) shows that the displacements in the sidewalls increases as the percentage over-break increase and no significant increase in the displacements in the drive back and the floor is observed. The results indicate that the for an

increase in percentage over-break from 0%-25% the displacements in western wall increase by 39.1% and in the eastern wall by 13.5%. This suggests that the displacements in the western sidewall are more influenced by the over-break compared to the displacements in the eastern sidewall. This may be a result of two different failure mechanisms for the excavations walls at RA-UG mine. The modelling results show no significant increase in the drive closure strain for the simulated values of over-break.

The displacement contours around haulage drift at LaRonde mine suggest that the increase in percentage over-break would result in higher displacements around the drift. The results indicate that the displacements in walls would increase at a higher rate as compared to displacements in back and floor. No significant increase in the drift closure strain was observed for simulated values of over-break.

The modelling results from the two mines suggest that the excavation over-break does not result in significant increase in the closure strains. As the excavation dimensions increase due to the increase in the percentage over-break and the increase in resulting displacements is proportional, this would result in similar closure strain values. However, the over-break will result in higher displacements around the excavation and would increase the load on the surface support and rock reinforcement elements. This can reduce the life of ground support systems resulting in frequent rehabilitation and reduced serviceability of the excavations.

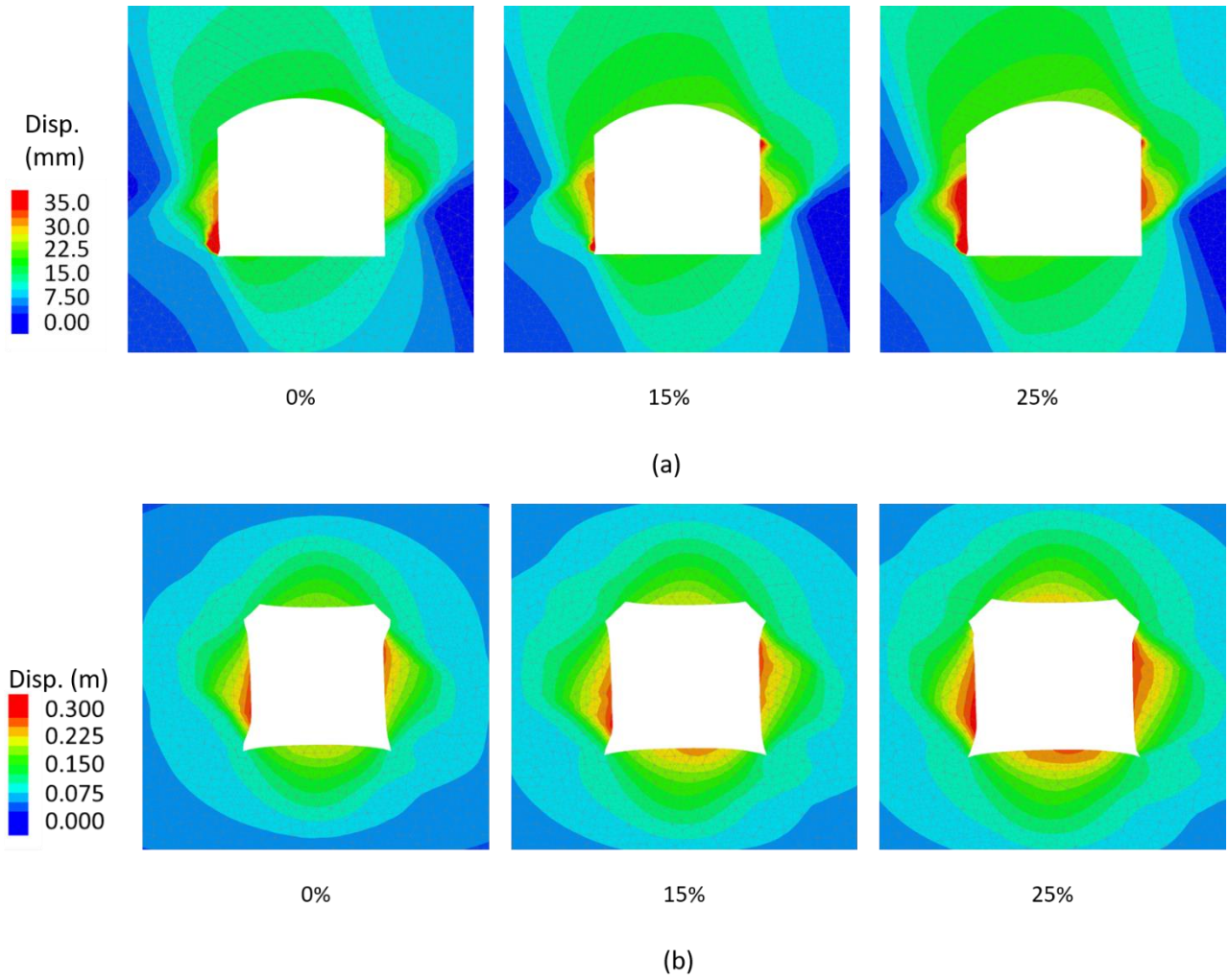

Figure 6.12: Modelled displacements for simulated over-break percentages (a) RA-UG mine (b) LaRonde mine

6.6 Effect of mining depth

Numerical modelling was carried out to examine the influence of increasing mining depth on the squeezing at RA-UG and LaRonde mines. The model geometry, boundary conditions, grid size and loading conditions were adopted from the numerical models described in Section 7.3. The results of numerical simulations are summarized in Figure 6.13. The results suggest that the total displacements around the excavations increase as the mining depth is increased and would thus result in higher closure strains. At RA-UG mine, the rate of increase in displacements with mining

depth in the eastern wall is comparatively higher than that in the western wall. This may be a result of flatter dipping foliation at RA-UG mine.

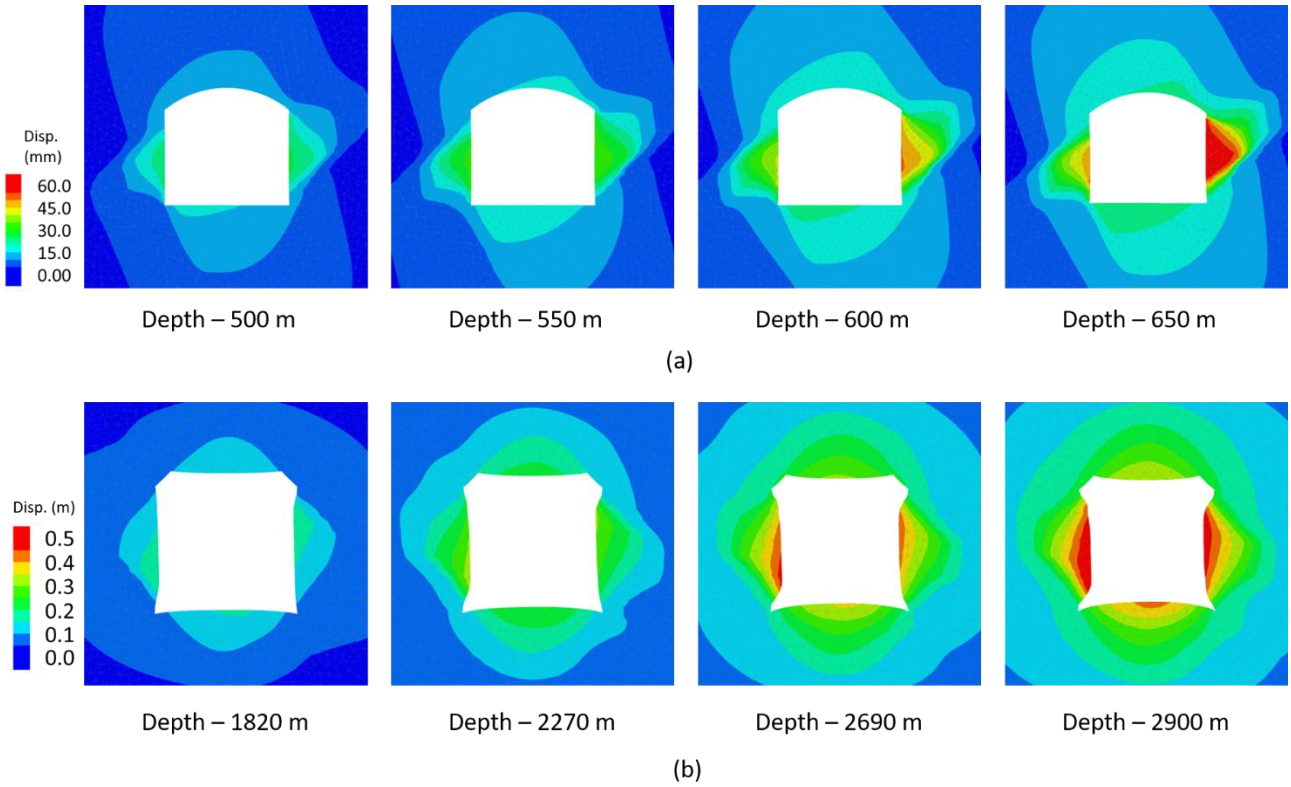

Figure 6.13: Modelled displacements for various mining depths (a) RA-UG mine (b) LaRonde mine

6.7 Influence of parallel excavations

The influence of wall to wall distance between excavations parallel to the foliation on the severity of squeezing was analyzed for RA-UG and LaRonde mines. A series of numerical simulations were carried out for varying wall to wall distance between the two excavations from 30 m to 5 m for LaRonde mine and 30 m to 10 m for RA-UG mine in 5 m intervals. The schematic showing an example of modelled geometry is provided in Figure 6.14. The model properties, boundary conditions, grid size and loading conditions were adopted from the numerical models described in Section 7.3.

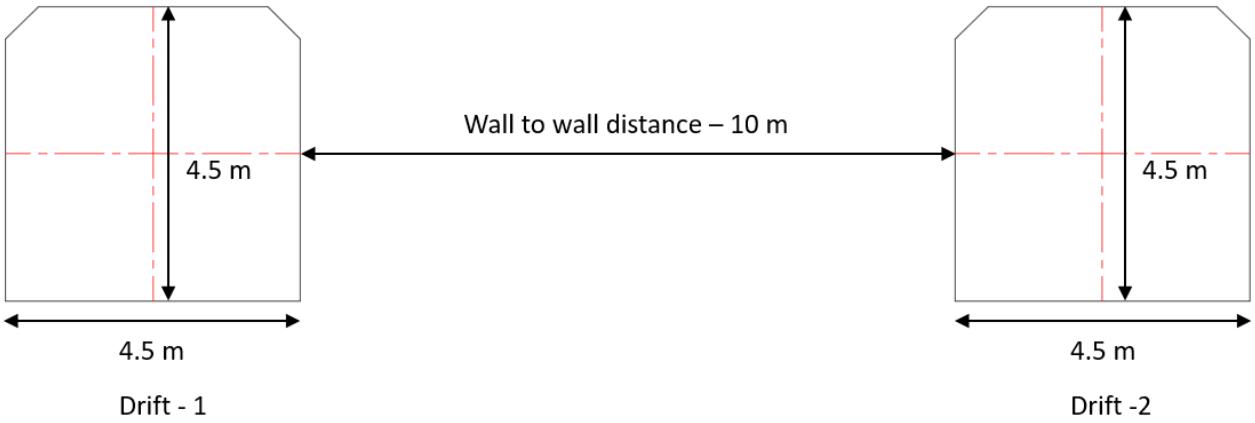

Figure 6.14: Schematic showing model geometry for 10 m wall to wall distance at LaRonde mine

The modelled displacements for the various wall to wall distances between footwall drives parallel to the foliation at RA-UG mine are provided in Figure 6.15. The modelling results suggest that the wall to wall distance between the drives have a significant influence on the degree of squeezing for distances less than 15 m and no influence on the displacements were observed for the simulated wall to wall distance of more than 15 m. The modelling results show a 60% increase in the closure strain as the wall to wall distance between the two drives at RA-UG was reduced from 15 m to 10 m. Results also suggest that majority of the increase in closure strain is due to significant increase in the displacements of walls of the forming pillar between the two drives and no major increase in the walls away from the forming pillar was observed.

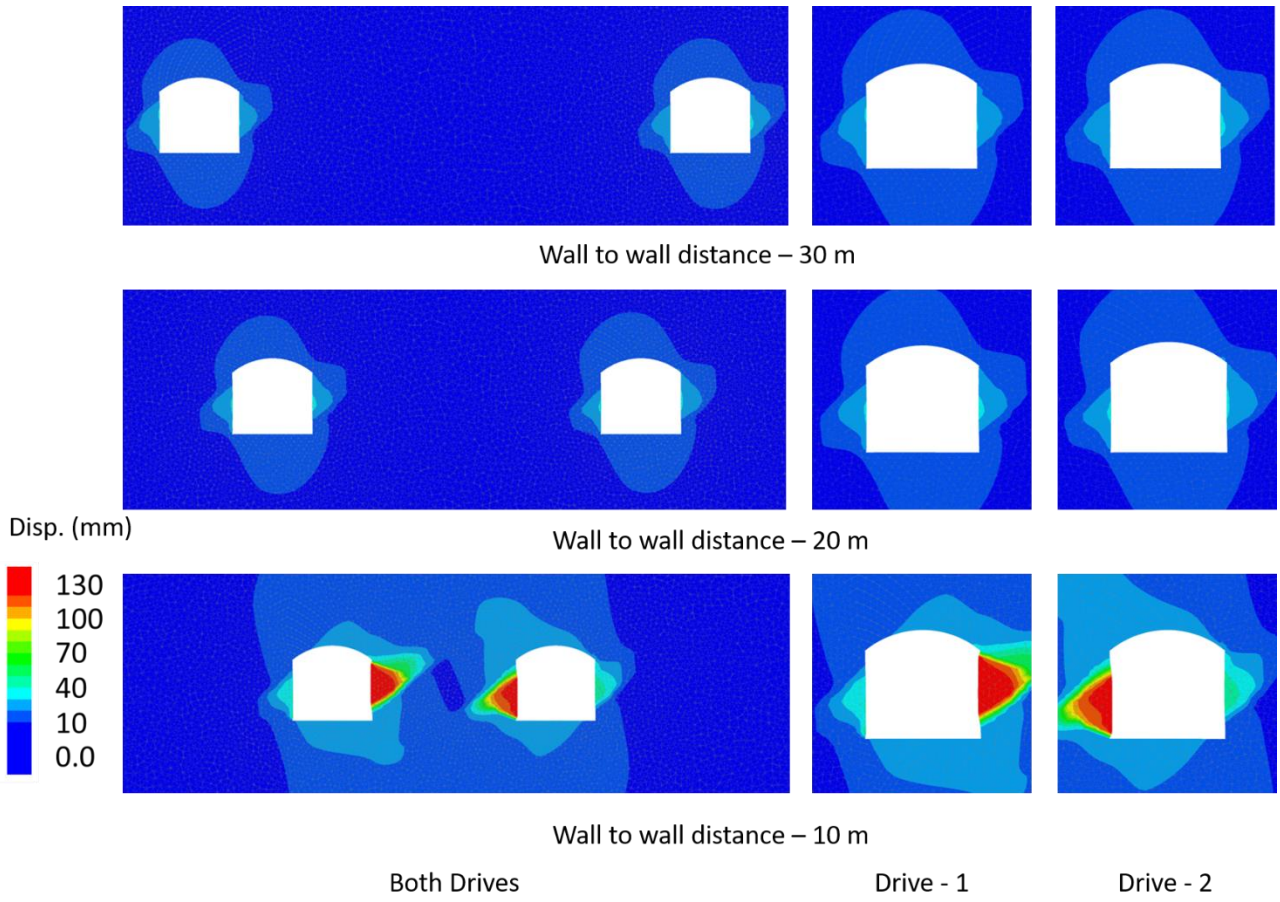

Figure 6.15: Modelled displacement for varying wall to wall distance between footwall drive at RA-UG mine

The drift closure strains for the simulated wall to wall distances at LaRonde mine are provided in Figure 6.16. The results suggest that the wall to wall distance between two parallel drifts has a significant influence on the total wall to wall closure of both drives for a distance less than 15 m and no significant difference in closure strains should be expected for a distance greater than 15 m. The displacement contours show that as the wall to wall distance between the two parallel haulage drifts is reduced the displacements in the wall forming the pillar increases. The excavation walls away from the forming pillar do not show any considerable increase in the displacements.

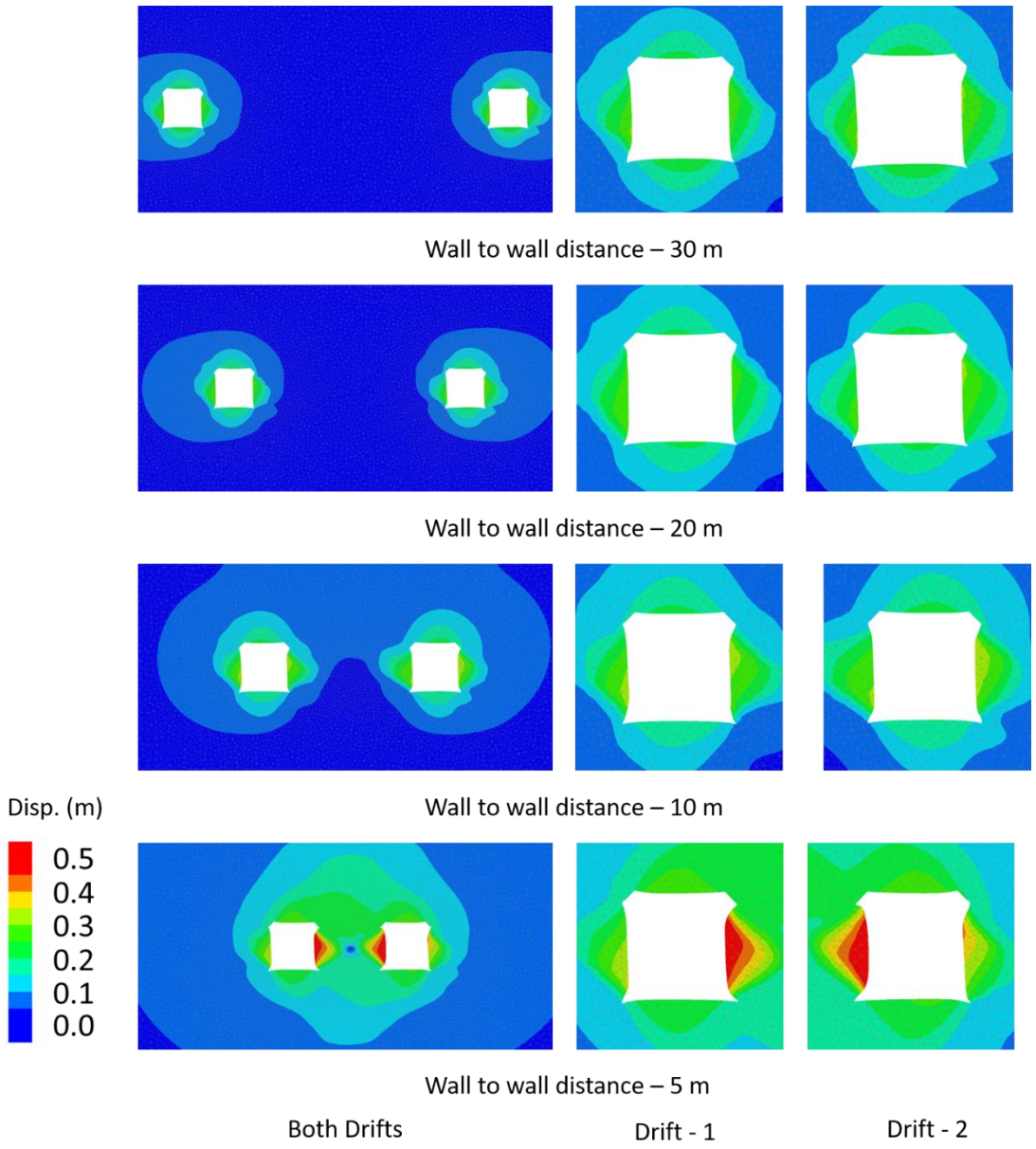

Figure 6.16: Modelled displacement for varying wall to wall distance between haulage drifts at LaRonde mine

6.8 Chapter summary

The squeezing ground condition in underground hard rock mines is governed by several geological, geotechnical, mine design and mine planning factors and parameters. A methodology to conduct a numerical investigation into some of the key parameters was presented in this chapter of the thesis. The modelling results suggest that the relative orientation of foliation with the excavation walls can

have a significant influence on the severity of squeezing ground conditions in foliated rock mass which is generally quantified by using interception angle (ψ). The results indicated that the foliation has significant influence for ψ less than 45° and no influence of the interception angle was observed on squeezing for values greater than 45°. The numerical modelling results are in good agreement with the underground observations from RA-UG mine and the case histories reported by Karampinos (2016) for LaRonde and Lapa mines. The influence of excavation shape and excavation over-break was also investigated for the two mines and the results suggests that the excavations shape can have a significant influence on the squeezing conditions and utilizing arched back profile with a smaller radius of curvature can improve these conditions. The influence of excavation over-break was examined for over-break between 0% to 25% and the modelling results show no significant increase in the total wall to wall closure strain for simulated values of excavation over-break. However, a considerable increase in the displacements of the excavation walls was observed.

The influence of pre-mining stresses and induced stresses on the severity of squeezing was examined. For investigating pre-mining stresses, the depth of excavations was varied. The results indicate that the increase in excavation depth can result in significant increase in closure strains. The influence of mining-induced stresses was examined by simulating two parallel excavations in foliated rock with the excavation length parallel to the foliation strike. The wall to wall distance between the two excavations was reduced, and the influence on displacements was studied. The results from the numerical simulation of two mines suggest that as the pillar between the two parallel excavations is reduced to less than 15 m, a significant increase in the displacements at pillar walls should be expected. The magnitude of displacements and the deformation profile of the pillar is influenced by the relative orientation of foliation with respect to the two pillar walls.

Chapter 7

7 Time-dependent behaviour of foliated rocks

This chapter of the thesis provides the details of the numerical simulations carried out to investigate the time-dependent response of foliated rock mass to mining. Chapter provides a description and implementation procedure of the Power-Ubiquitous joint model used to investigate the anisotropic time dependent behaviour. A series of numerical models were generated to investigate the evolution of the displacements around decline and haulage drift over time at RA-UG and LaRonde mines respectively. Discussions on the modelling results are provided. The chapter also provides the details of numerical simulations carried out to evaluate the influence of the various type of ground support reinforcement elements used at the two mines on the severity of squeezing ground conditions. The impact of time of installation of primary, secondary and tertiary reinforcements in squeezing ground at the two mines was evaluated, and discussions on modelling results are presented.

7.1 Time-dependent deformations in squeezing ground

As mentioned in Chapter 2, Barla (1995) defined squeezing as large, time-dependent deformations that occur around underground excavations. These deformations are essentially associated with creep caused by exceeding limiting shear stress and may terminate during construction or may continue over a longer period. Malan (2002) reported that the mining activities result in a redistribution of local stress surrounding the excavations and the subsequent re-adjustment of the rock mass towards new equilibrium does not occur instantaneously but gradually over time. This process often results in inelastic creep deformations. For excavation stability, it is important to determine the time-dependent response of rock mass to mining and the ground control procedures and ground support design needs to consider the development of deformations over time in

squeezing ground in underground hard rock mines.

Sterpi and Gioda (2009) reported that the squeezing ground conditions result in non-reversible deviatoric creep strains that develop over time at a constant and eventually increasing rate, namely secondary and tertiary creep stages. In an engineering context, the prediction of the squeezing potential of an excavation is based on in-situ stress measurements that usually focuses on the state of stress and rock mass strength. However, for more accurate predictions of the rock mass response to mining in the foliated rock mass, the visco-plastic behaviour of the rock mass needs to be taken into consideration as well. To adequately represent the visco-plastic behaviour of the rock mass, proper calibration of the mechanical parameters is required. Considering the difference in the behaviour of intact rock and that of a rock mass, ideally the calibration of the mechanical parameters would require performing tests directly on the rock mass in-situ, this, however, is rarely carried out for analyzing the time-dependent effects due to operational difficulties and thus the mechanical properties are often derived from the testing of intact rock samples and the modelling parameters are calibrated using geotechnical monitoring data from various geotechnical monitoring instrumentations.

Barla et al. (2012) reported that the various approaches have been proposed for tunnel design in squeezing ground conditions that aimed at predicting with reasonable accuracy the magnitude of the tunnel convergence associated with squeezing. In cases where the detailed response of the interaction between the rock mass and the geological structures needs to be assessed in short and long terms, numerical analysis can be an effective approach provided that excavation construction sequence is accurately modelled and a suitable mechanical constitutive relation is adopted to represent the rock mass behaviour. Three-dimensional numerical models and suitable elasto-visco-plastic constitutive laws should be considered such that the time dependence is explicitly accounted

for. In these models, the time-dependent irreversible strains are governed by specific conditions of the state of stress and the associated viscous and plastic mechanical parameters. Another approach to simulate the time-dependent response of rock mass to mining is to utilize strength or pressure reduction in elasto-plastic models, these models take into account the time dependence by degrading the stiffness and shear-strength properties of the rock mass during excavation process, this approach was used by Karampinos (2016) for simulating the deformations of haulage drift in squeezing ground at LaRonde mine. However, this approach appears to be limited for the analysis of cases of severe squeezing ground conditions, and the only advantage is the simpler identification of the design parameters (Barla et al., 2012).

Time-dependent deformations associated with squeezing ground conditions in civil engineering tunnels have been reported by several authors, and various analysis techniques and numerical modelling methodologies have been used over the years. Over the past decade, several authors have reported similar conditions and time dependency of squeezing ground conditions in underground hard rock mines. As the mining progresses to deeper horizons, more severe conditions will be encountered by the underground hard rock mines. Bosman et al. (2000) reported time-dependent deformations in squeezing ground at Hartebeestfontein mine in South Africa. The authors reported observations from a strike-oriented tunnel that intersected weak quartzite layers that were sandwiched between two competent quartzite bands. The observed squeezing mechanism at this location was dominated by creep along the bedding planes with a soft talcaceous infilling that behaved like clay when saturated with water. The tunnel deformation was found to be driven by two separate mechanisms, the quartzite strata exposed in the sidewall of the tunnel resulted in dilatational deformations into the excavation and the presence of bedding planes with low frictional resistance inhibited the generation of confining stresses and therefore allowing greater horizontal freedom and hence more time-dependent deformations. Butler and Leonardi (2016) reported

observations from Northern 3500 orebody at Mount Isa mine. The high-stress conditions and relative orientation of tunnel to in-situ foliation resulted in substantial squeezing ground conditions around underground excavations that resulted in drive convergence. The convergence, particularly in sidewalls, showed time-dependent degradation of rock mass conditions and the rock mass continued to experience stress damage, and this resulted in multiple rehabilitations of the excavation.

Karampinos (2016) reported observations of time-dependent deformations encountered in squeezing ground conditions at LaRonde and Lapa mines in Canada. Several case studies were drawn from a range of squeezing ground conditions at LaRonde and Lapa mines between the depths of 1790 m to 2690 m and 540 m to 950 m respectively. The investigation revealed that the deformations were scattered widely over time and the displacement rates reduced over time. The field data suggested that higher displacement and displacement rates were recorded in the drift sidewalls than in the drift back and floor. Underground measurements and CMS scans suggest that the deformations continue at a low rate over the working life of the drift and this indicates time-dependent mechanism at the mines. An example showing the development of deformations over time at Lapa mine was provided by Karampinos (2016). The squeezing ground conditions at the two mines are typically characterized by deformations due to changes in the stress conditions around the drift during the drift development, and this stage was associated with high initial deformation rates. Following this stage, the deformations were a result of stress changes around the drift due to nearby mining activities. This stage typically showed high deformation rates for a certain period, and then the deformation rates decreased.

7.2 Power Ubiquitous-Joint model

FLAC 3D version 6.0 provides four visco-elastic and five visco-plastic constitutive models for

simulating the time-dependent behaviour of the rock mass. The Power-Ubiquitous model is a visco-plastic constitutive model that utilizes the two-component Power model and the Ubiquitous-Joint model. The constitutive model allows to simulate the anisotropic behaviour of the rock mass and explicitly represent the time-dependence in the numerical models. The details of the formulation of the Power-Ubiquitous model and implementation procedure in FLAC3D is provided below.

The Power-Ubiquitous model simulates the visco-elasto-plastic mechanical behaviour of ubiquitous joint rock with creep occurring in the rock matrix. The model also accounts for the presence of weakness planes and therefore, the yielding may occur either in the rock matrix or along the weak plane or both depending on the state of stress, the orientation of weakness plane and the material properties of the rock matrix and weakness plane. The two-component Power law can be written as,

$$\dot{\epsilon}_{cr} = A\bar{\sigma}^{n} \tag{7.1}$$

where, $\dot{\epsilon}_{cr}$ is the creep rate, A and n are material properties termed as creep constant and creep exponent, respectively. $\bar{\sigma}$ is the von Mises stress and is given by $\bar{\sigma} = \sqrt{3J_2}$, where J_2 is the second invariant of the effective deviatoric-stress tensor. The volumetric behavior of the zone matrix is assumed to be elastic and it does not consider creep. The creep behavior in Power model is triggered by the deviatoric stress. FLAC3D provides the option to use two component power law to simulate multiple creep mechanism and is given by the following equation.

$$\dot{\epsilon}_{cr} = \dot{\epsilon}_1 + \dot{\epsilon}_2 \tag{7.2}$$

where,

$$\dot{\epsilon}_1 = \begin{cases} A_1\bar{\sigma}^{n_1} & \bar{\sigma} \geq \sigma_1^{ref} \\ 0 & \bar{\sigma} < \sigma_1^{ref} \end{cases} \tag{7.3}$$

$$\dot{\epsilon}_2 = \begin{cases} A_2\bar{\sigma}^{n_2} & \bar{\sigma} \le \sigma_2^{ref} \\ 0 & \bar{\sigma} > \sigma_2^{ref} \end{cases} \tag{7.4}$$

The two-component power model provides several options to simulate creep utilizing the two terms provided in Equations (4.13) and (4.14) The available options are provided below.

i. The default option (single component power law):

$\sigma_1^{ref} = \sigma_2^{ref}$

$\bar{\sigma}$ is always positive, making this option a one-component power law and the creep strain rate is provided by

$\dot{\epsilon}_{cr} = A_1\bar{\sigma}^{n_1} \qquad \bar{\sigma} \ge \sigma_1^{ref}$

ii. Both components active (two-component power law)

$\sigma_1^{ref} = 0 \; and \; \sigma_2^{ref} = large$. In this case, the creep strain is given by

$\dot{\epsilon}_{cr} = A_1\bar{\sigma}^{n_1} + A_2\bar{\sigma}^{n_2} \qquad \sigma_1^{ref} < \bar{\sigma} < \sigma_2^{ref}$

iii. Different law for different stress regimes

a. $\sigma_1^{ref} = \sigma_2^{ref} = \sigma^{ref} > 0$

$$\dot{\epsilon}_{cr} = \begin{cases} A_2\bar{\sigma}^{n_2} & \bar{\sigma} < \sigma^{ref} \\ A_1\bar{\sigma}^{n_1} & \bar{\sigma} > \sigma^{ref} \end{cases}$$

b. $\sigma_1^{ref} < \sigma_2^{ref}$

$$\dot{\epsilon}_{cr} = \begin{cases} A_2\bar{\sigma}^{n_2} & \bar{\sigma} \le \sigma_1^{ref} \\ A_1\bar{\sigma}^{n_1} + A_2\bar{\sigma}^{n_2} & \sigma_1^{ref} < \bar{\sigma} < \sigma_2^{ref} \\ A_1\bar{\sigma}^{n_1} & \bar{\sigma} \ge \sigma_2^{ref} \end{cases}$$

c. $\sigma_1^{ref} > \sigma_2^{ref}$, this option should not be used as it implies that the creep occurs in for $\bar{\sigma} < \sigma_2^{ref}$ and for $\bar{\sigma} > \sigma_1^{ref}$, but not for $\sigma_2^{ref} < \bar{\sigma} < \sigma_1^{ref}$

The power ubiquitous joint model is implemented in FLAC3D using the following procedure. In the model formulation, the visco-elasto-plastic deviatoric stress rate is calculated from the creep and plastic strain rate components. The creep strain rate is derived using the von Mises stress in accordance with the Power Law, and the plastic strain rate is defined using Mohr-Coulomb flow rule. The volumetric stress rate is elasto-plastic. The final stress tensor is provided by the sum of deviatoric and isotropic components. For the new stresses, the Mohr-Coulomb yield criterion is checked, and the relevant plastic corrections are applied following the methodology described in section 4.1.2.1. The stresses modified after applying the relevant plastic corrections from the Mohr-Coulomb yield criteria are then analyzed for failure on the weak plane utilizing the methodology described in section 4.1.2.2. The relevant plastic corrections from the failure on the weak plane are made on the local axis components and then resolved into the global axis components.

For the time-dependent analysis, Itasca Consulting Group (2017a) recommends that the initial creep time step is at least two to three orders of magnitude smaller than the critical time step and the maximum value of the creep time step should not exceed the critical time step during the creep simulations. The critical time step for power-type creep model is calculated using the following equation.

$$\Delta t_{max}^{cr} = \frac{\bar{\sigma}^{1-n}}{AG} \tag{7.5}$$

where, G is the shear modulus.

7.3 Numerical investigation of time-dependent deformations

Tran Manh et al. (2015) reported that most of the visco-plastic models utilized to describe the constitutive behaviour of squeezing ground conditions often assume isotropic deformations. The squeezing ground in underground hard rock mines is characterized by not only large time-dependence but also often by anisotropic deformations, such as in the case of the foliated rock mass. To investigate the time-dependent response of foliated rock mass to mining at RA-UG and LaRonde mines under squeezing ground conditions 3D numerical modelling in FLAC3D was adopted. To simulate the anisotropic deformation and explicitly represent the time dependence in the numerical models, the Power Ubiquitous-Joint model described in Chapter 4 was utilized. The details of the numerical models and discussion of the modelling results are provided in the following sub-sections.

7.3.1 Model description and material properties

The boundary conditions and grid sizes used in the numerical models for both RA-UG and LaRonde mines were based on the numerical models described in section 6.2.1. For RA-UG mine, to investigate the time-dependent deformation in squeezing ground conditions, North decline section at a depth of 370 m from the surface was selected. Standard decline dimension of 5.6 m width and 5.3 m height was used in the numerical models. The foliation dip at this location was 70°, and the foliation strike was approximately parallel to the drive walls. The decline was excavated in April 2014 and the convergence monitoring at this location started in March 2015. A total of 40 mm wall to wall convergence was recorded at this location between March 2015 and May 2016. For numerical simulations, the beginning of the monitoring period was assumed as time zero of the model simulation time. For the numerical model, it was assumed that the development is parallel to

the foliations for its entire length and 20 m of drive length was simulated.

For LaRonde mine, haulage drift (227-73-E) at a depth of 2270 m below the surface was selected for the numerical simulations. Mellies (2009) reported that this drift was mined in July 2007. The dip of the foliation at this location was 75°, and the foliation strike was approximately parallel to the drift walls. The initial ground support at this location was installed following the development of the drift. Failure of split sets and mesh bagging was observed at this location as a result of squeezing and additional support was installed to replace the broken split sets and mesh at this location between November and December 2007. Observations from March 2008 reported by Mellies (2009) suggest broken foliation at several locations along the length of the drift within 60 cm of the drift floor, the drift surface suffered major damage, and the installed mesh showed bagging behind the mesh in both sidewalls. About 20 m of the drift length was monitored by Mellies (2009), and measurements of drift dimensions were carried out to quantify the drift convergence and severity of squeezing at this location. For the numerical model, the drift dimension of 5.25 m wide and 4.25 m high was used based on base-case measurement. The foliation was assumed to be parallel to the excavation walls for its entire length and 20 m of the drift length was simulated in the numerical model. For both numerical models the mechanical properties and creep, parameters were calibrated to reproduce the progression of deformations over time recorded underground at the selected locations. Calibrated material properties and creep parameters used in the numerical model are provided in Table 7.1.

Table 7.1: Material properties and creep parameters used in numerical models for RA-UG and LaRonde mines

Material properties	**Unit**	**RA-UG**	**LaRonde**
Young's modulus	GPa	12	48
Poisson's ratio	-	0.25	0.16
Cohesion	MPa	2.8	6.0
Friction angle	°	48.0	30.0
Tensile strength	MPa	0.15	0.55
Joint cohesion	MPa	0.23	1.5
Joint friction angle	°	20.0	32.0
Power-law constant	$Mpa^{-3}s^{-1}$	7E-33	15E-33
Power-law exponent	-	3.0	3.0

7.3.2 Evolution of deformations over time in squeezing ground

The numerical model to investigate the time-dependent deformation in squeezing ground conditions at RA-UG mine was calibrated to reproduce the displacements recorded underground in North decline at a depth of 370 m from the surface. To calibrate the numerical model first, an elasto-plastic simulation was carried out by turning off the creep function of the Power-Ubiquitous model. The wall to wall convergence in the numerical model was calibrated to the final wall to wall convergence reported underground by varying the mechanical properties of finite difference grid and foliation. Following the initial calibration, the creep mechanism in the numerical model was activated and the time dependence of the wall to wall convergence was calibrated by varying the power-law constant and time step used for calculation in FLAC3D. The results of the numerical simulations showing the evolution of modelled wall to wall convergence vs actual recorded convergence underground over time are provided in Figure 7.1.

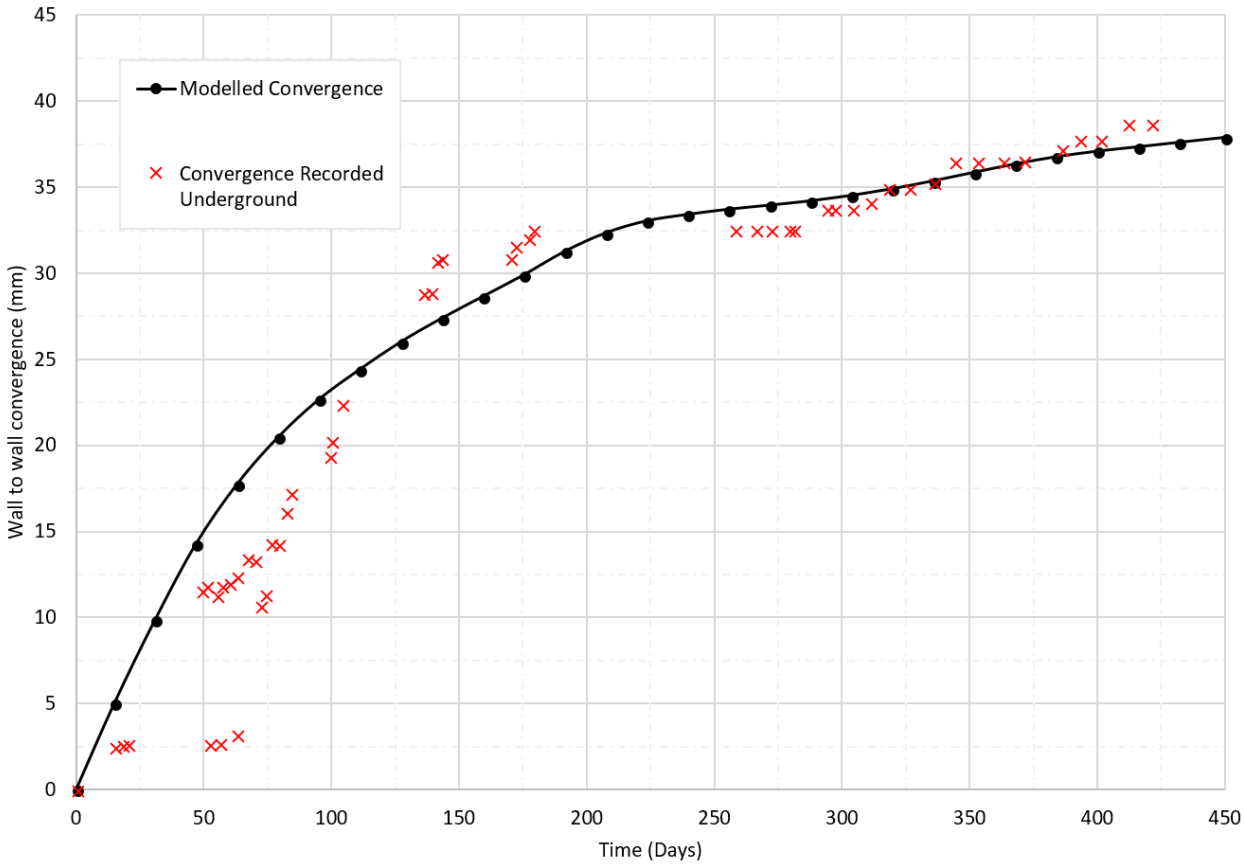

Figure 7.1: Wall to wall convergence over time at RA-UG mine, modelled vs actual

The trend of the wall to wall convergence over time at RA-UG mine suggests that the rate of displacement is not constant over time. The drive shows higher displacement rate early in the simulation time for about 200 days following which the displacement rate decreases and an almost constant displacement rate continues for the rest of the simulation time. The results indicate an initial displacement rate of 0.17 mm/day for about 200 days after which the displacement rate reduces to 0.02 mm/day. The contours showing the evolution of displacement and volumetric strain over time are provided in Figure 7.2. The displacement contours suggest that the displacements over time are anisotropic and the drive hanging wall experiences higher displacements earlier in the simulation time than the footwall. The high displacement region in the drive footwall is towards the floor and in the drive hanging wall is towards the drive shoulder. The contours also show that the

displacements in the drive sidewalls are considerably higher than those in the drive back and floor. The contours of volumetric strain provided in Figure 7.2 shows how the rock mass damage progresses over time. No to low rock mass damage (< 1% volumetric strain) was observed for the simulation time of up to 200 days. Minor signs of low to moderate rock mass damage (1-2.5% volumetric strain) were observed in the lower portion of the drive footwall and hanging wall shoulder towards the end of the simulation time.

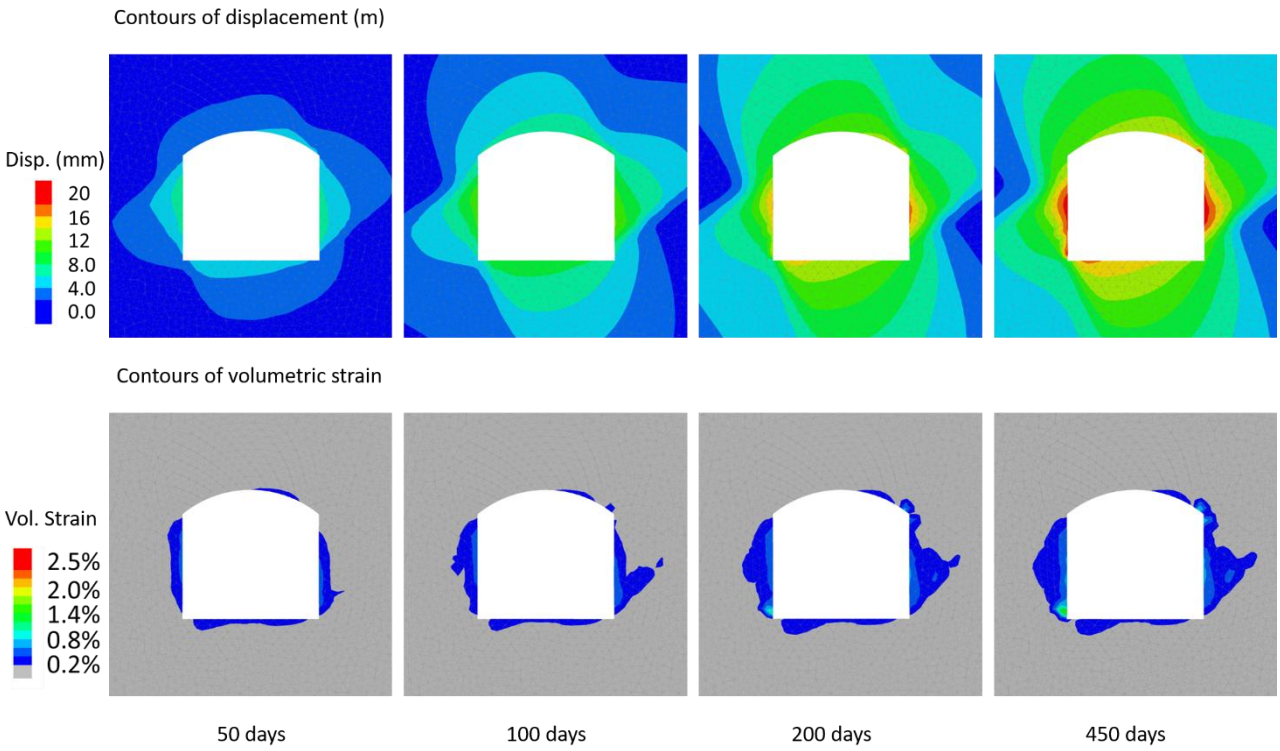

Figure 7.2: Contours showing modelled displacement and volumetric strain over time at RA-UG mine

The displacements over time for each wall of the drive are provided in Figure 7.3. The modelling results suggest no significant difference in final maximum displacements of the drive footwall and hanging wall. However, for the monitoring location at the same height from the drive floor, hanging wall displacements are 10% higher than the footwall displacements; this is because the relative orientation of the foliation with respect to the two sidewalls is different. In the footwall, the

foliation dips into the sidewall resulting in higher displacements towards the lower portion of the drive sidewall, and in the hanging wall, the foliation dips away from the wall resulting in higher displacements towards the drive shoulder. The results also show that the sidewall displacements are 23% higher than the floor and 36% higher than the back displacements, this is because the drive sidewalls are oriented parallel to the foliation which results in higher deformations. The displacements in the drive back are 11% less than the drive floor, this is a result of an arched back profile in the drive back and flat profile in the drive floor. This observation supports the premise that arched profile results in more uniform stress redistribution around the opening and results in a considerable decrease in the displacements. The results show that the long-term displacement rates of the drive sidewalls are about 43% higher than the drive back and floor.

Modelling results are in good agreement with the actual recorded convergence over time for North decline section at RA-UG mine. Underground observations at this location suggest moderate rock mass damage in May 2016. Broken foliations and separation of slabs from the drive sidewalls was observed. The rebars in the drive footwall showed bending of plates and several cracks in the shotcrete in the drive hanging wall shoulder, and lower footwall was observed.

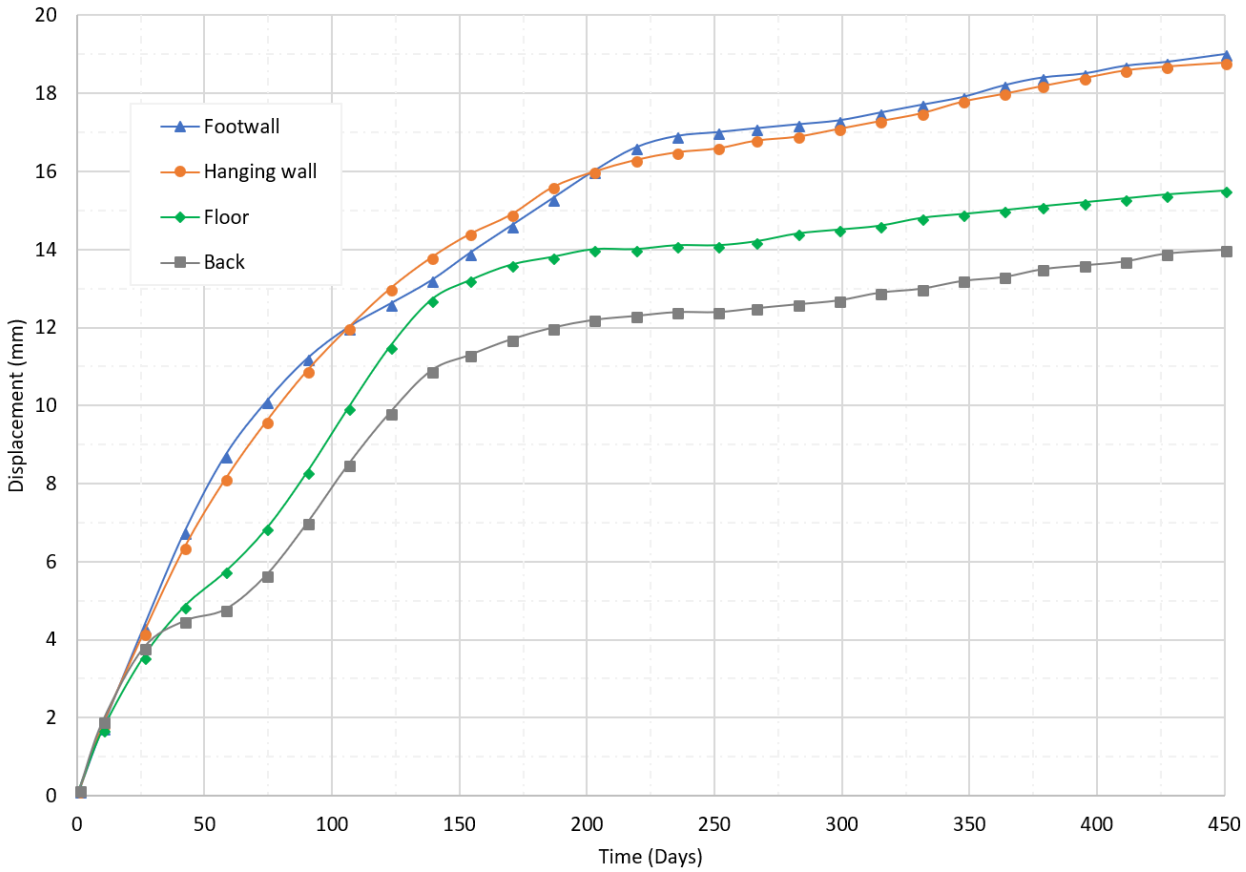

Figure 7.3: Modelled displacements over time for each drive wall at RA-UG mine

The numerical model for LaRonde mine was calibrated to reproduce the displacements recorded underground at drift 227-43-E between 22nd August 2007 and 30th November 2007 as reported by Mellies (2009). It was assumed that the drift development was completed for the monitored section by the end of July 2007, the convergence measurements at this location started on 22nd August 2007, this means that the convergence data for 22 days following the excavation was not available and the base reading was taken at least 22 days after the development and the first convergence measurement was carried out 38 days after the development. The displacements in the numerical models were calibrated to match the progression of deformation starting from the base measurements. A total of eight measurements were carried out at this location between August 22nd and October 25th, 2007. Modelling results showing the evolution of the modelled vs actual recorded

wall to wall convergence over time for the drift 227-43-E are provided in Figure 7.4.

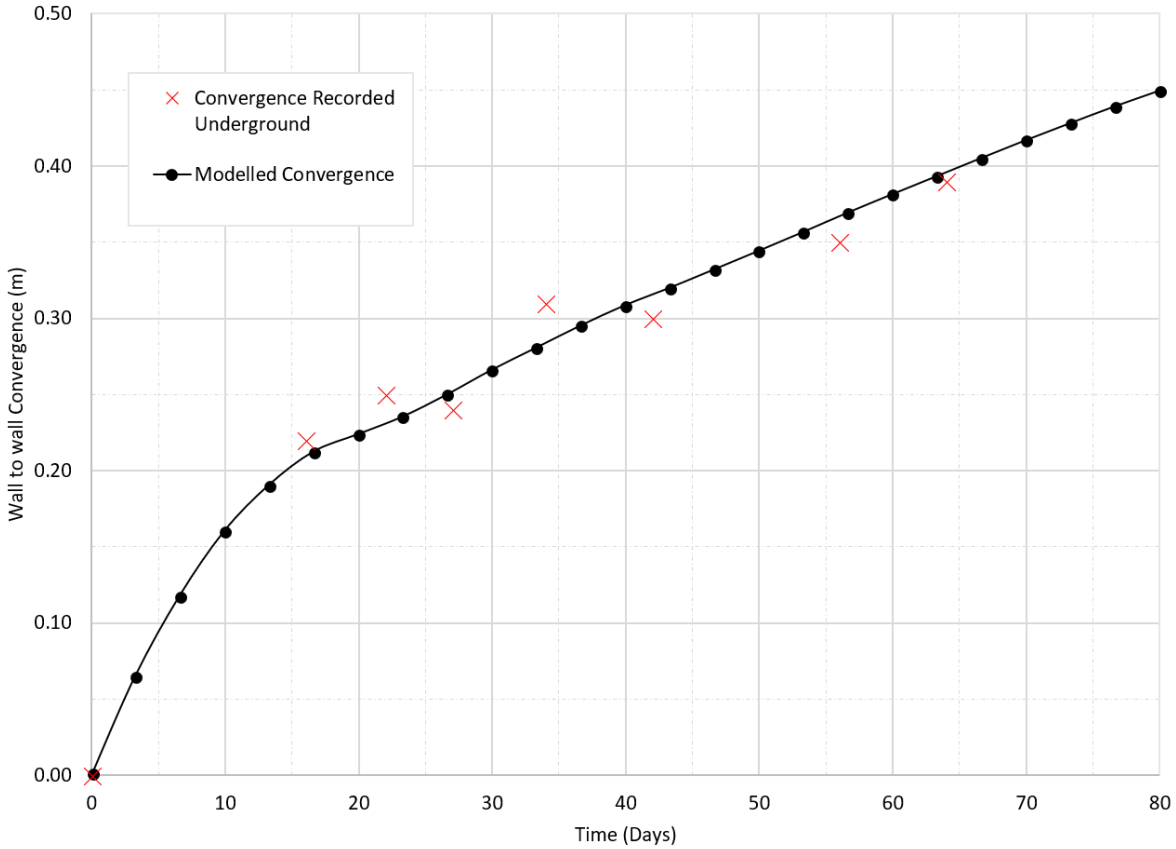

Figure 7.4: Wall to wall convergence over time at drift 227-43-E, modelled vs recorded.

The trend of the wall to wall convergence over time suggest that the displacement rates are not constant, higher displacement rates are observed following the development of the drift for some period, following which the rate of displacement decreases and a constant displacement rate continues over time. The results suggest initial displacement rate of $1.6x10^{-2}$ m/day for about 16 days of simulation time following which the displacement rate reduces to the $3.9x10^{-3}$ m/day for the remainder of the simulation time. The contour of displacement and volumetric strain over time are provided in Figure 7.5. The displacement contours suggest that the displacements are not isotropic, early in the simulation time, both walls show similar displacements, however with time the deformations in both walls vary, and the hanging wall shows higher displacements than the drift

footwall. This is because of the difference in the relative orientation of the foliation with respect to each wall. The results also indicate the displacement in the drift sidewalls is greater than those in drift back and floor. The volumetric strain contours provided in Figure 7.5 shows how the rock mass damage progresses over time for the simulated case. The results suggest low to moderate (1-2% volumetric strain) damage within 7 days of simulation time. The drift experiences moderate to significant damage (2-5% volumetric strain) within 60 days of simulation time. There is no major evidence of extreme rock mass damage (10% volumetric strain).

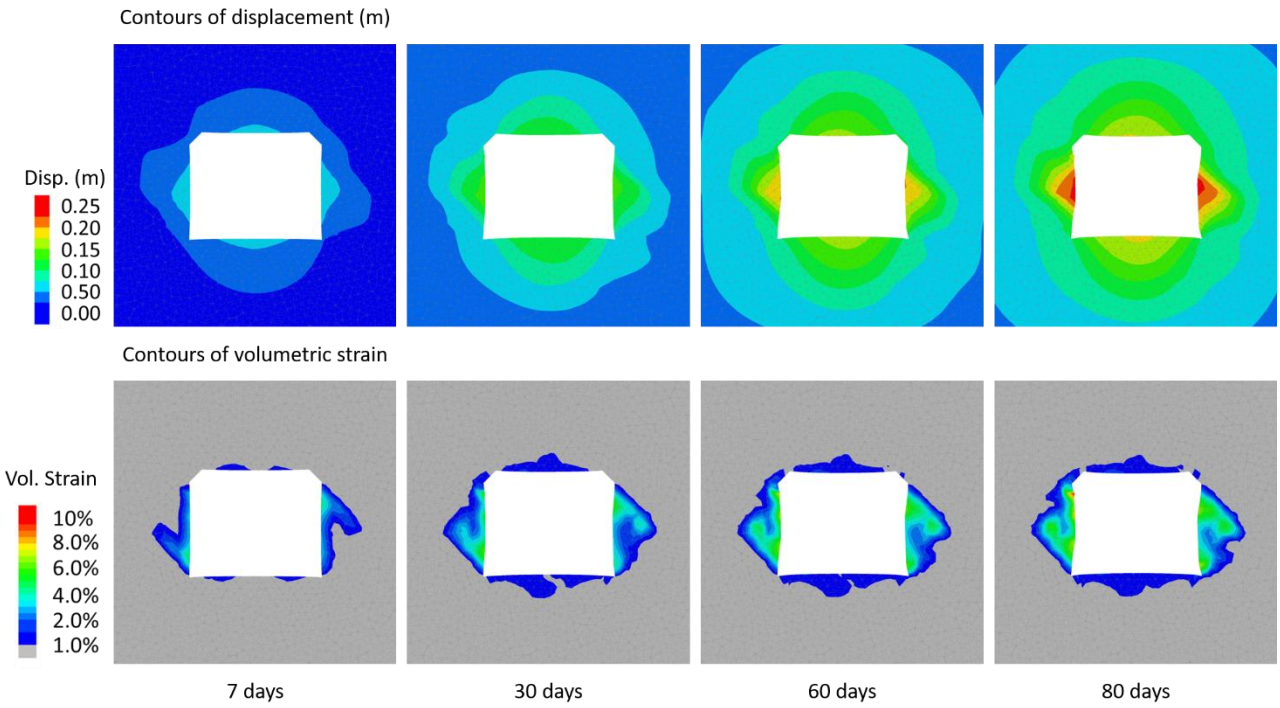

Figure 7.5: Contours showing modelled displacement and volumetric strain over time at LaRonde mine

The maximum displacement over time from the numerical model for each drift wall is provided in Figure 7.6. The results show that the displacements in the drift sidewalls are 23% higher than those of drift back and floor; this is a result of drift side walls being parallel to the foliation planes. The results also indicate that the hanging wall displacements are about 6.5% higher than the footwall

displacements, this is because the relative orientation of foliation with the two sidewalls is different. In the drift footwall, the foliation dips into the wall whereas in the hanging wall the foliation dips away from the drift sidewall, the hanging wall foliation would be subjected to an additional gravitational force resulting in higher displacements compared to the drift footwall. The results also suggest that the drift back experiences higher displacements than the drift floor by about 3.0%; this is simply because the drift backs experience gravitational loading. The results show that the long-term displacement rate in drift sidewalls is about 53% higher than those of drift back or floor.

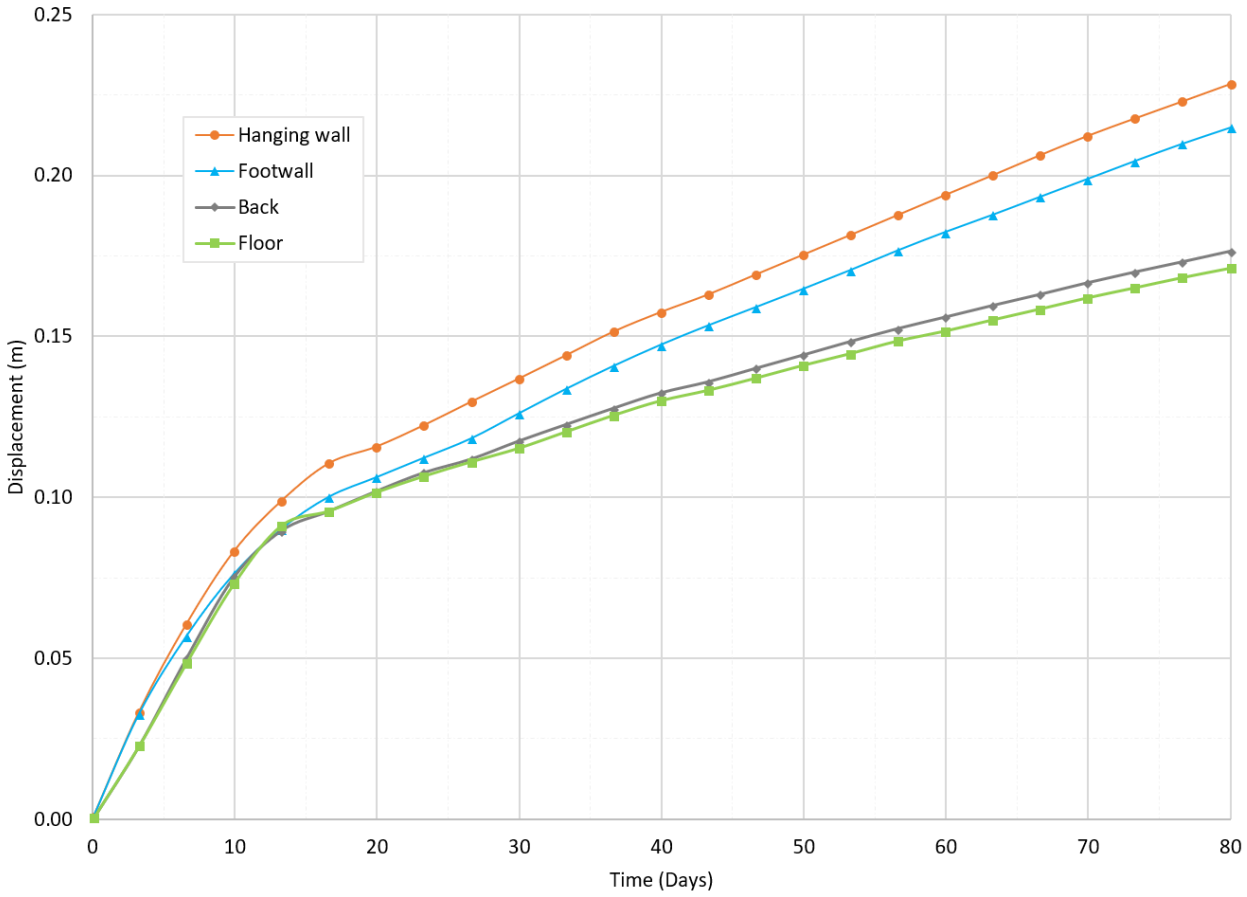

Figure 7.6: Modelled displacements over time for each drift wall at LaRonde mine

The modelling results for the given set of assumptions are in good agreement with the observations and convergence data recorded underground at drift 227-43-E by Mellies (2009). The evolution of

displacement over time in the numerical model correlates well with the progression of displacements from underground measurements. The results are also in good agreement with the observations reported by Karampinos (2016) for LaRonde mine. The author reported observations of deformations over time in squeezing ground conditions at LaRonde mine from several case studies between 1790 m to 2690 m depth. The field data from the reported case studies suggest that the displacement rates reduce over time and displacements continue at a low rate over the working life of the drift as reported by Karampinos (2016) for squeezing ground conditions at LaRonde and Lapa mines. Also, higher displacement and displacement rates were observed in drift sidewalls than the drift back and floor in most cases.

7.4 Review of structural elements in FLAC3D

Use of structural support to stabilize the rock mass is an important aspect of geo-mechanical analysis. FLAC3D 6.0 provides six structural elements that can be used to explicitly represent in the numerical models the various rock reinforcement and surface support element utilized in underground hard rock mines. These structural elements can either be independent of or coupled to the finite difference grid representing the solid continuum. The rock reinforcements used in the underground hard rock mines can be represented into the numerical models using the cable and pile structural elements. The basic formulation and description of these two structural elements are provided below.

Cable structural elements are straight finite elements made of two nodes and have six degrees of freedom with three translational and three rotational components. Each cable structural element is defined by its geometric, material and grout properties. A cable element is assumed to be a straight segment of the uniform cross-sectional area and material properties between the two nodal points. The cable element behaves as an elastic-perfectly plastic material that can yield in tension and

compression but cannot resist a bending moment. A cable may be grouted such that the force develops along its length in response to the relative motion between the cable and the finite difference grid. The grout behaves as an elastic-perfectly plastic material with its peak strength being dependent on the confining stress and shows no loss of strength after failure.

The axial behaviour of the cable structural element is assumed to be governed entirely by the reinforcing member, i.e. cable or rebar itself. The reinforcing member is usually composed of steel and it is assumed that the reinforcing element is slender and offers little bending resistance particularly in the case of cable bolts. The reinforcing element is treated as a one-dimensional structural member with the capacity to sustain uniaxial tension. The one-dimensional constitutive relation used to describe the axial behaviour of the reinforcing member of the cable structural element is provided by the following equation.

$$K = \frac{AE}{L} \tag{7.6}$$

where, K is the axial stiffness, A is the cross-sectional area, E is the Young's modulus of steel and L is the element length. To evaluate the axial forces that develop in the reinforcement, displacements are computed at nodal points along the axis. Out-of-balance nodal forces are computed from the axial and shear forces and, the axial displacements are calculated by integrating the nodal accelerations using the out-of-balance axial force and mass at each node. The cable structural element is represented numerically by a spring-slider system located at the nodal points along the axis of the cable as shown in Figure 7.7.

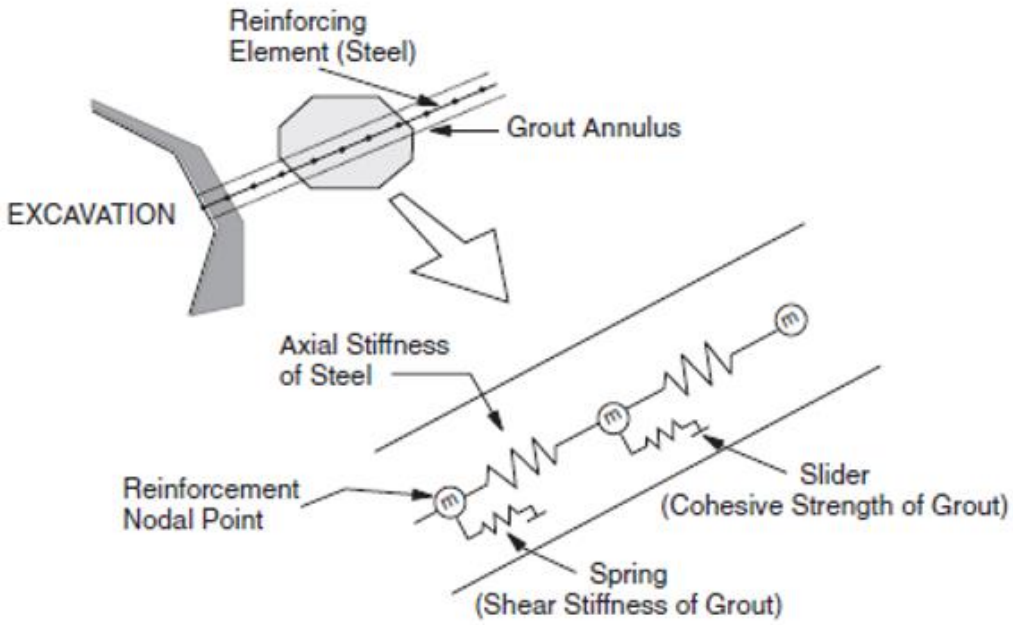

Figure 7.7: Mechanical representation of fully bonded cable reinforcement, after Itasca Consulting Group (2017a).

The shear behaviour of the cable-rock interface is cohesive and frictional in nature. The idealized cable structural element is provided in Figure 7.8a. The shear behaviour of the grout annulus during relative shear displacement between cable/grout and grout/rock interfaces is shown in Figure 7.8b, and the schematic of the effective confining stress is shown in Figure 7.8c. The mechanical behaviour of the grouted-cable system is depicted in terms of grout shear stiffness (k_g), grout cohesive strength (c_g), grout frictional angle ($\emptyset_g$), grout exposed perimeter (p_g) and effective confining stress (σ_m). The grout properties associated with each cable element are averaged at cable nodes.

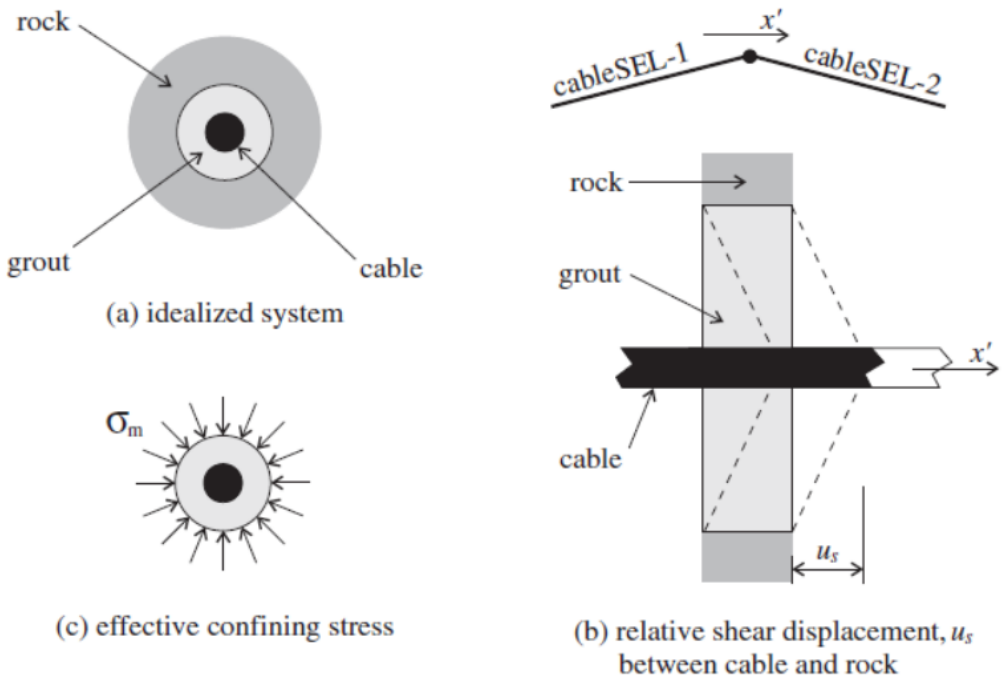

Figure 7.8: Idealized grouted cable reinforcement system, after Itasca Consulting Group (2017a).

The mechanical properties of the reinforcing element of the cable bolt such as cross-sectional area, modulus and yield strength are available from the manufacturers. The grout properties are difficult to estimate, and the following expressions are provided by Itasca Consulting Group (2017a) to estimate the shear stiffness and cohesive strength for the cable structural elements.

$$k_g = \frac{2\pi G}{\ln(1+\frac{2t}{D})} \tag{7.7}$$

$$c_g = \pi(D+2t)\,\tau_1 Q_B \tag{7.8}$$

where G is the shear modulus of the grout, D is the reinforcing dimeter, t is the annulus thickness, τ_1 is the peak shear strength of the grout and Q_B is the quality of the bond between the grout and rock ($Q_B = 1$ for perfect bonding). Usually, k_g can be determined directly from the laboratory pull-out tests and c_g and $\emptyset_g$ can be estimated from the results of pull-out tests conducted at varying

confining pressures. The mechanical behaviours of the cable and the grout material are provided in Figure 7.9. Failure of the reinforcing system does not always occur at the grout/rock interface and the failure may occur at the reinforcing/grout interfaces. Depending on the failure location the shear stresses are evaluated on the respective interface.

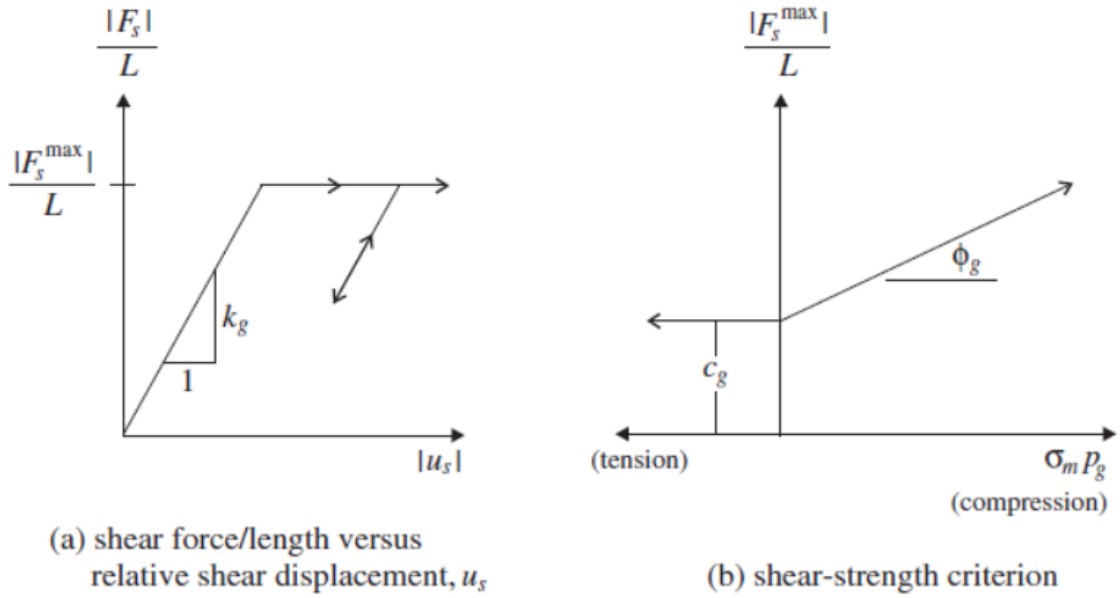

Figure 7.9: Grout material behaviour for cable elements, after Itasca Consulting Group (2017a).

Similar to the cable structural element, the pile structural element is defined by its geometrical, material and coupling-spring properties. A pile element is assumed to be a straight segment of uniform, bisymmetrical properties lying between two nodal points. The shear and normal behaviour of the pile-grid interface is cohesive and frictional in nature and the shear behaviour is modelled in a similar manner as a grouted-cable system described above. The normal behaviour of the pile-grid interface during relative normal displacement between the pile and the host medium is described numerically by the normal couplings. FLAC3D provides an extension of the pile element logic to simulate the behaviour of rock bolt reinforcements. The behaviour of these elements is similar to those of cable elements, except that they also include bending resistance. The rock bolt pile element can yield in the axial direction and rock bolt breakage can be simulated by providing a user-defined

tensile failure strain value.

7.4.1 Use of structural elements to simulate reinforcements

Several authors have reported utilizing structural elements in FLAC3D to simulate the rock reinforcements used in underground mines. Bahrani and Hadjigeorgiou (2017) utilized an explicit representation of rock reinforcements using cable and pile-rock bolt elements in the universal distinct element code (UDEC) to investigate the performance of local and global reinforcements. The numerical models were calibrated to reproduce the behaviour of a fully grouted rebar bolt tested under pure pull and pure shear loading conditions in a laboratory. Karampinos et al. (2016) explored the influence of reinforcements on the overall displacements in squeezing ground conditions at LaRonde mine by the explicit representation of various rock reinforcement elements in the three-dimensional discrete element model. The numerical simulations were calibrated based on field testing of the reinforcements and observations at the LaRonde mine. Thareja (2016) investigate the influence of varying ground support design parameters such as bolt spacing, length and type on the squeezing instability around underground excavations using the time-dependent model in 3DEC.

Bahrani and Hadjigeorgiou (2017) reported that the rock reinforcements could be simulated in the numerical models by using either material models or structural elements. Both approaches have been used by several authors to represent the behaviour of rock reinforcements under various loading conditions. However, the use of structural elements to represent the rock reinforcements in the numerical models is becoming more popular as the commercial three-dimensional numerical modelling codes such as FLAC3D, UDEC and 3DEC provide inbuilt structural elements to simulate the role of reinforcements in numerical models. The pile-rock bolt element can be used to better represent the behaviour of rock reinforcement elements such as rebar bolts, as it takes into

consideration the resistance against bending. The cable structural element can be used to simulate the behaviour of grouted cable bolts in underground hard rock mines because in an underground environment generally cable bolts are subjected to tensile loading only.

7.5 Numerical investigation of the influence of reinforcement on squeezing

Varden and Woods (2015) reported that the ground support schemes of several mines evolve over the life of mine. This is because as the extraction increases, the severity of ground control problems increases as well, and this often leads to a major reconsideration of ground support schemes and type of rock reinforcement and surface support elements used at the mine. This process can lead to additional expenses in the form of field trials of the various new types of rock bolts and surface support elements available in the market and can also cause significant production delays. Extensive trials and long monitoring periods may be required to assess the applicability of the new ground support elements to the mining conditions. Understanding the behaviour of rock mass through numerical modelling can help improve the understanding of the performance of the ground support systems and can provide valuable input in the ground support element selection and design strategies early in the mine life. This approach can also reduce the efforts and cost required for the field trials.

Hadjigeorgiou and Karampinos (2017) reported that there are several stress analysis packages that allow simulating the rock reinforcement and surface support elements in the numerical models; this, however, increases the complexities of the numerical models and results in longer computational time and also increases the efforts required for model calibration. A calibrated numerical model with the explicit representation of reinforcement and support elements can be used to explore various reinforcement strategies, and the numerical models can provide a useful means to investigate different options in the difficult ground such as squeezing. These numerical models can

also be used to investigate the performance of any new rock bolts.

Beck et al. (2010) presented a multi-scale, discontinuum approach to model large deformations in deep underground mines. The approach aimed to improve the reliability of simulating ground support capacity and demand and was used to demonstrate the performance of several heavy support systems used in difficult ground conditions such as squeezing ground. The authors tested the limitation and vulnerabilities of various ground support systems used in squeezing ground conditions utilizing numerical modelling. Thareja (2016) carried out numerical simulations of rock bolt utilizing time-dependent model in 3DEC (Itasca Consulting Group, 2013) and performed sensitivity analysis to study the effect of various rock support design parameters for varying excavation sizes and depths in squeezing ground conditions in Nevada gold mines. Karampinos (2016) utilized pressure reduction method in the pseudo-3D 3DEC model to simulate the time-dependent deformations in squeezing conditions and to investigate the effect of various reinforcement elements installed at different stages in the model on the displacements in squeezing ground at LaRonde mine.

The role of various rock reinforcement elements used at RA-UG and LaRonde mines was investigated by employing pile and cable structural elements and the Power-Ubiquitous joint model in FLAC3D. The details of the numerical models and discussion of the modelling results are provided in the following sub-sections. The role of surface support elements such as shotcrete, welded mesh, mesh straps and OSRO straps used at the two mines were not considered in the numerical simulations.

7.5.1 Role of reinforcement at LaRonde mine

The model geometry, boundary conditions, rock mass properties and creep parameters used for the numerical models to investigate the role of various ground support reinforcement elements at

LaRonde mine were based on the model described in Section 8.2.1. The reinforcements were simulated in the numerical models using pile and cable structural elements described in Chapter 4. Each structural element was divided into several segments with nodal points located at the end of each segment. Each node is linked to the finite difference zone for computing the shear forces between the zone and elements. The first node of each structural element was made stiffer and a rigid connection to the finite difference zone was created to replicate the effect of faceplates. As described in Chapter 5, in squeezing ground conditions LaRonde mine utilizes three-stage ground support system, i.e. primary, secondary and tertiary support. In squeezing ground conditions, i.e. for interception angle less than 45° at LaRonde mine, the primary reinforcements comprise of alternate rows of 1.9 m and 2.3 m long 22 mm diameter rebars in the drift back. The sidewall support in squeezing ground is extended up to 0.6 m from the drift floor and comprises of 2.0 m long 39 mm diameter friction rock stabilizers (FRS). The primary reinforcements are installed in conjugation with 4.1 mm galvanized welded wire mesh. The secondary support in these conditions comprises of hybrid bolts in the drift sidewalls and zero-gauge mesh straps. The hybrid bolts are installed at an offset height on the south wall to account for the deformations associated with the foliation. In the south wall, the hybrid bolts are installed starting at 0.6 m from the drift back and an in-plane spacing of 1.2 m. In the north wall, the hybrid bolts are installed starting at 0.6 m from the floor at an in-plane spacing of 1.2 m. The hybrid bolts are installed 12 m behind the development face. The tertiary reinforcement comprises of cable bolts installed in the drift back and sidewalls. Hybrid bolts were introduced at LaRonde and Lapa mine to manage squeezing ground conditions. The complete mechanism of hybrid bolts is still not fully understood and considerable efforts are being made to investigate various aspects of hybrid bolts. Due their complex mechanism and the fact that it uses both friction bolt and rebar to provide rock reinforcement, simulating these bolts in the numerical model presents challenges. In this work, simplification was made by assuming a single

reinforcement element. The tensile capacity and the bond strength were based on the pull testing results from LaRonde and Lapa mines. Generally, the drift is cable bolted prior to commencing secondary stoping or in some cases after purging the drift sidewalls. Shotcrete is mostly used for rehabilitation works (Hadjigeorgiou et al., 2013). The schematic of ground support systems used at LaRonde mine is provided in Figure 7.10.

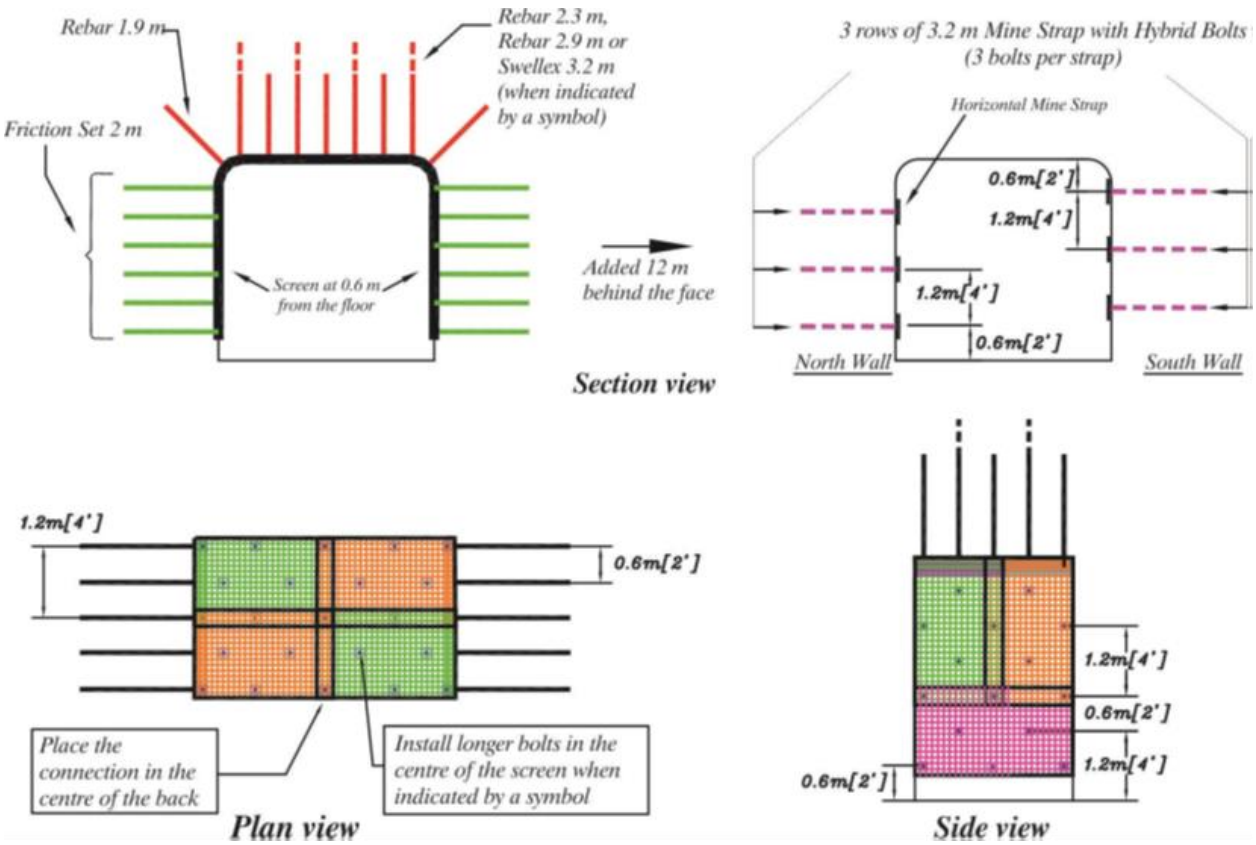

Figure 7.10: Ground support in squeezing ground at LaRonde mine, after Hadjigeorgiou et al. (2013).

The rebars, friction rock stabilizers and the hybrid bolts were simulated in the numerical models utilizing pile structural element. The cable bolts used at LaRonde mine for tertiary support were simulated in the numerical models using cable structural element in FLAC3D. The material properties of the structural elements used in the numerical simulations were based on the values reported by Karampinos (2016) from the field pull testing and calibrated 3DEC model and are

provided in Table 7.2. The model geometry, boundary conditions and the creep parameters used in the numerical models were the same as those described in Section 8.2.1 for LaRonde mine.

Table 7.2: Material properties for reinforcement elements used at LaRonde mine, after Karampinos (2016)

Material properties	**Unit**	**FRS**	**Rebars**	**Hybrid Bolts**	**Cable Bolts**
Young's modulus	GPa	200	200	200	200
Tensile yield strength	kN	127	185	367	275
Strain limit	%	12.0	35.0	12.0	3.5
Bond stiffness	kN/m/m	2.33E3	1.5E4	6.4E3	5.56E3
Bond cohesive strength	kN/m	35.0	550	80.0	400

The role of various reinforcement elements on the severity of squeezing ground conditions and displacements around the haulage drift at LaRonde mine was investigated by introducing the structural elements to simulate the primary, secondary and tertiary supports at various stages of the deformation process. First, a base case model (L0) was simulated, in this model no reinforcements were introduced. The base case simply looked at the total displacements when no support was installed. This model was generated to provide reference case for comparative analysis, as in practice the mine would install reinforcements following the development. Three cases were simulated for primary, secondary and tertiary reinforcements. In Case L1a, only primary reinforcements were introduced in the numerical model 8 hours after the excavation. In Case L1b, primary reinforcements were introduced 8 hours following the excavation, and the secondary reinforcements were introduced after 7 days of simulation time. In Case L1c, primary

reinforcements were introduced 8 hours following the excavation, secondary reinforcements were introduced after 7 days, and the tertiary reinforcements were introduced in the model after 30 days of simulation time, see Figure 7.11.

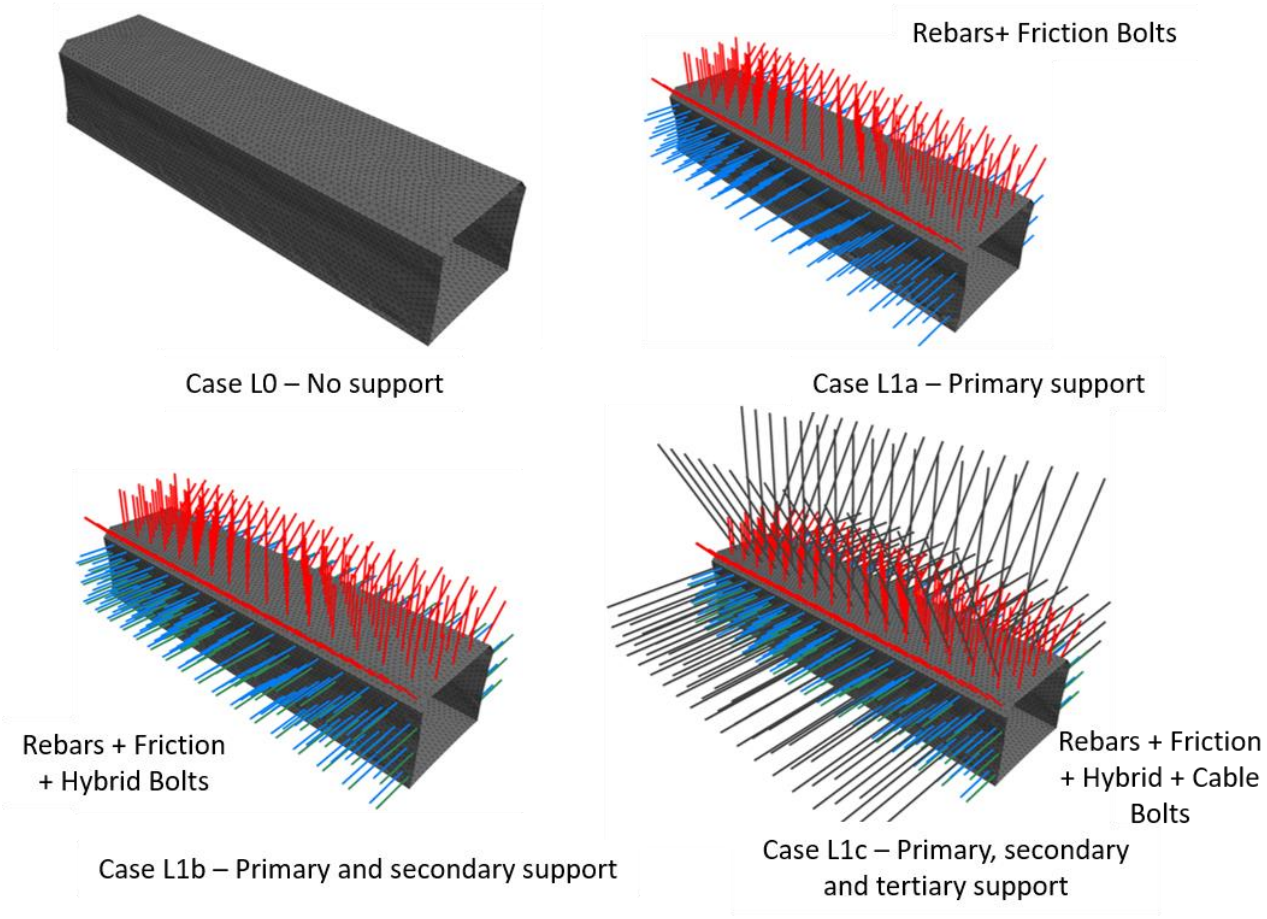

Figure 7.11: Various reinforcement cases simulated for LaRonde mine

In all four cases (L0, L1a, L1b, L1c), the models were run for a total simulation time of 80 days. The trends of the total wall to wall and back to floor convergence over time for simulated cases are provided in Figure 7.12, and the contours showing total displacements and axial force on the reinforcement elements for modelled cases are provided in Figure 7.13.

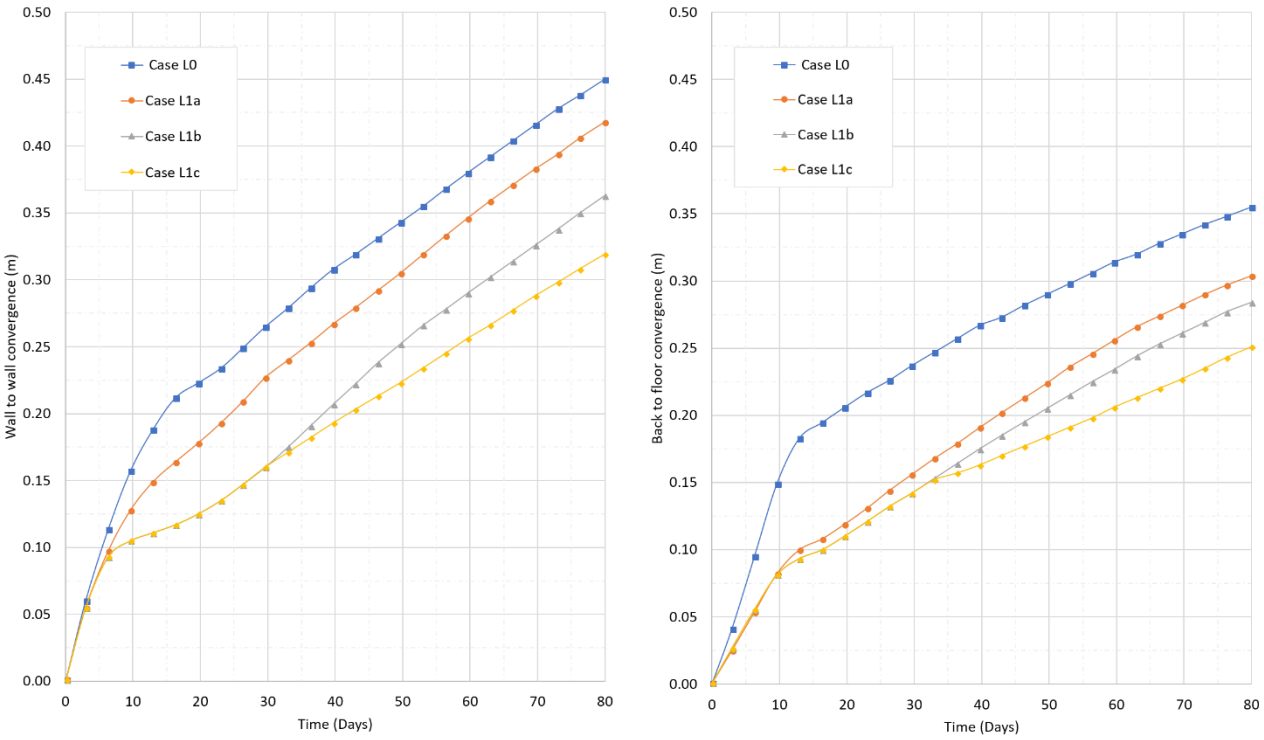

Figure 7.12: Modelled convergence for cases L0-L1c, (a) wall to wall convergence (b) back to floor convergence

Introduction of reinforcements in the numerical models show a significant reduction in the total displacements around the drift, see Figure 7.12. In Case L1a, where only primary reinforcements were introduced 8 hours after the excavation, a minor reduction of about 7% in the wall to wall convergence was observed, whereas, introducing rebars in the drift back resulted in 14% reduction in the total back to floor convergence. The results also show that rebars in the drift back have an immediate effect on the displacements and the FRS show effect on the displacements after some time in the simulation. This is because the rebars are stiffer reinforcement elements and they immediately restrict the displacements in the drift back; FRS, on the other hand, have lower stiffness and require some time to develop enough friction between the FRS and the rock mass to influence the displacements. In Case L1b, where the hybrid bolts were introduced in the drift sidewalls in the L1a model after one week of simulation time, 13% decrease in the wall to wall

convergence was observed. The introduction of hybrid bolts in the drift sidewalls also resulted in 6% decrease in back to floor convergence. This is because installing hybrid bolts in the drift sidewalls results in an increase in the confinement of the walls, which in turn increases the load-bearing capacity of the sidewalls resulting in a decrease in displacement of the drift back and floor. The results also indicate that the hybrid bolts have an immediate influence on the displacements as they are stiffer reinforcement elements as compared to FRS. In Case L1c, where the cable bolts were introduced after 30 days of simulation time in Case L1b model, a total of 12% decrease in the wall to wall convergence and 11% decrease in back to floor convergence was observed.

The contours of displacement and axial force in the reinforcements are provided in Figure 7.13. The contours of displacement show how the displacements around the haulage drift decrease as various reinforcements are introduced in the numerical simulations. The contours of axial force of the reinforcements show that the rebars in the excavation back are loaded to the full axial capacity of 185 kN; however, no failure of the bond was observed for the rebars. The FRS and hybrid bolts show a significant failure of the bond between the elements and the finite difference zone. The sidewall cable bolts are loaded to the full capacity of 275 kN and the cable bolts in the drift back were loaded to 170 kN, about 60% of the total axial capacity.

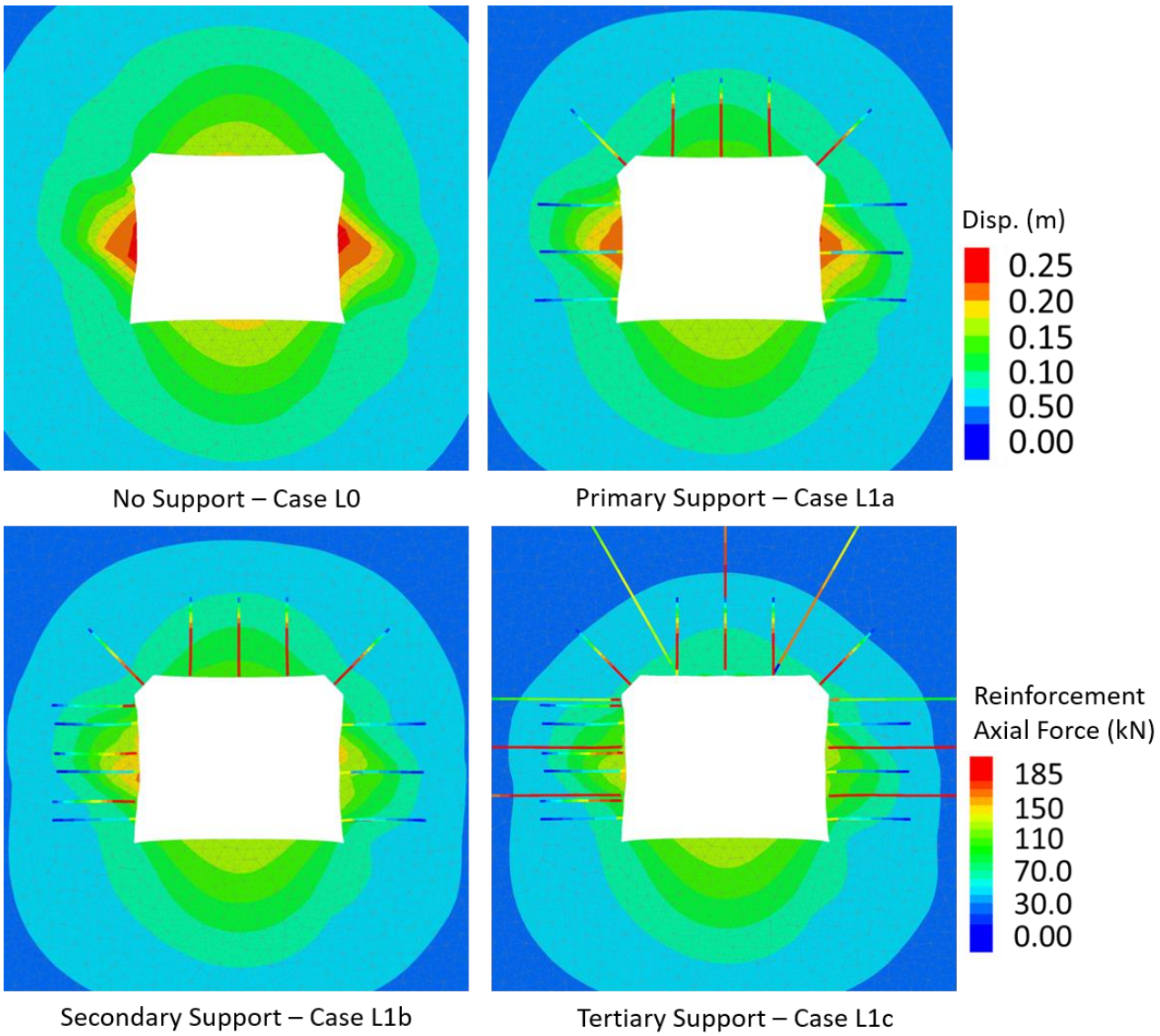

Figure 7.13: Modelled displacements and reinforcement axial force after 80 days of simulation time for simulated cases

The development of axial force over time for reinforcement elements is provided in Figure 7.14. Figure 7.14-a shows the axial force of rebars installed in the drift back for Cases L1a-L1c. The results suggest the in the simulated cases the rebars in the drift back are loaded to the full axial capacity of 185 kN. The trend of the development of axial force suggests that the force in the rebars and hybrid bolts increase over time. The trend of axial force in FRS suggests that the FRS is loaded to their axial capacity of 127 kN within few days of installation. However, the force reduces over

time as the bond between the FRS and finite difference zone starts to fail. The results also indicate that the hanging wall FRS experiences 18% higher force than the footwall FRS and the hanging wall hybrid bolts experience 21% higher axial force than the footwall hybrid bolts. This is to be expected as hanging wall displacements were higher than footwall displacements. In Case L1b, where primary support was introduced 8 hours after excavation, and secondary support was introduced 7 days after excavation, the results show that the introduction of hybrid bolts in the drift sidewalls results in an immediate drop in the axial force of FRS. This is because the hybrid bolts are stiffer reinforcement and majority of the load is taken by hybrid bolts. In Case L1c, where cable bolts were introduced in the L1b model 30 days after development, the results show that the final hybrid bolt loads are comparatively less than those in Case L1b, this is because cable bolts provide some confinement and share the load.

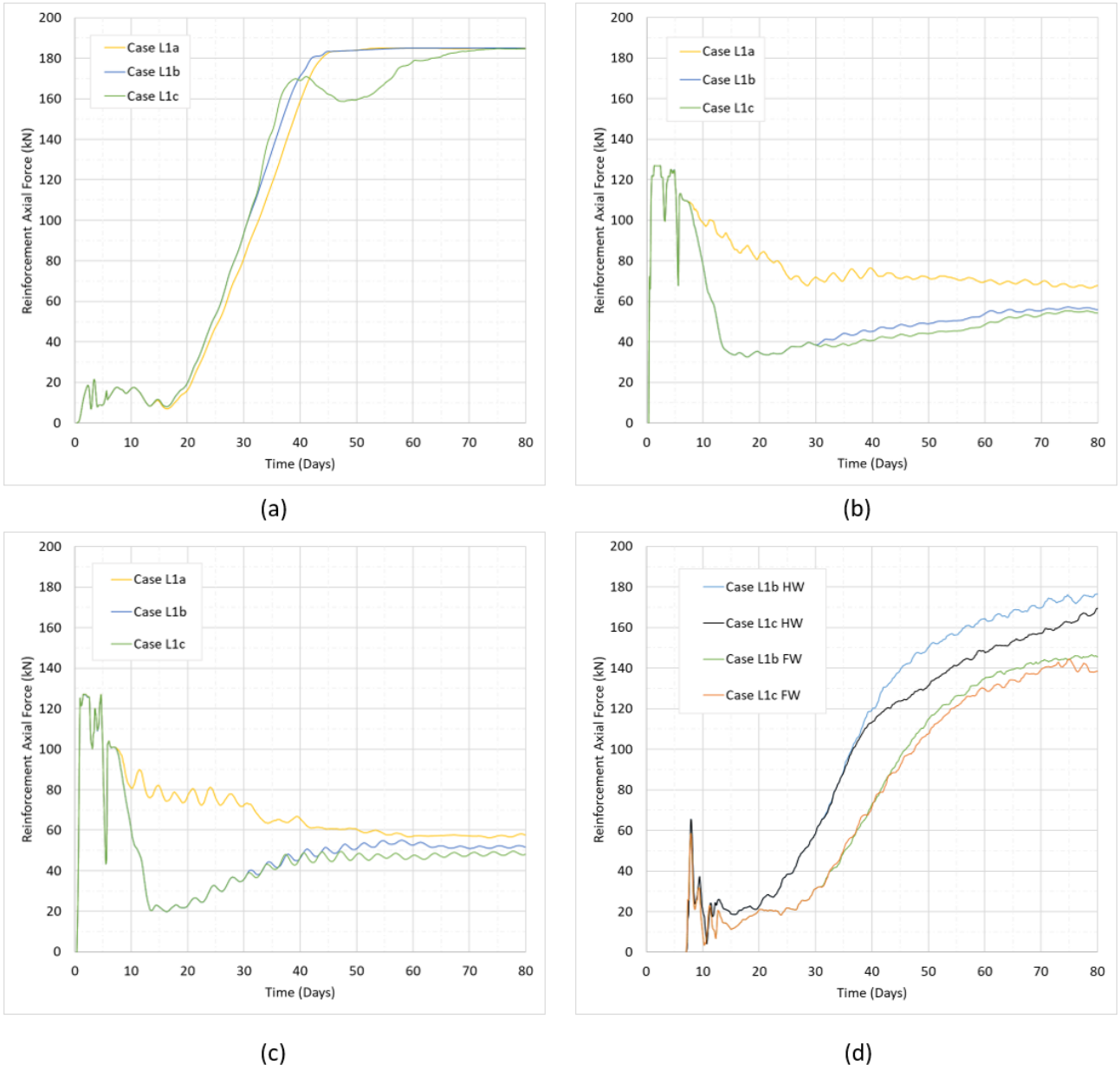

Figure 7.14: Reinforcement axial force for the modelled cases (a) back rebar (b) hanging wall FRS (c) footwall FRS (d) hybrid bolts

7.5.1.1 Effect of time of time of installation of supports

To investigate the effect of the delayed installation of reinforcement elements, a series of numerical simulations were carried out. In Cases L2a-L2d, only primary reinforcement was introduced in the model after 8, 24, 48 and 96 hours of the simulation time respectively. In Cases L3a-L3c, the

primary reinforcement was introduced in the model 8 hours into the simulation time and secondary reinforcements were introduced at 7, 14, 30 and 60 days of simulation time respectively. In Cases L4a-L4c, the primary and secondary reinforcements were introduced in the model at 8 hours and 7 days into the simulation time respectively, and the tertiary reinforcements were introduced at 30, 45 and 60 days of simulation time respectively. The total wall to wall and back to floor convergence for the simulated cases are provided in Figure 7.15. The results show that in Cases L2a-L2d, where the time of installation of primary reinforcements was delayed, no significant difference in the final convergence was observed, however, the trend showed comparatively higher convergence in the short-term when the installation was delayed for 96 hours. In Cases L3a-L3d, where the time of installation of hybrid bolts was delayed, results show that there is a significant increase in the short-term wall to wall convergence and there were no significant changes in the back to floor convergence. In Cases L4a-L4c, where the installation of the cable bolts was delayed results show that there is a considerable difference in both wall to wall and back to floor convergence. In Case L4c, where the cable bolts were introduced in the model after 60 days of simulation time, 9% increase in back to floor and 6% increase in wall to wall convergence, was observed.

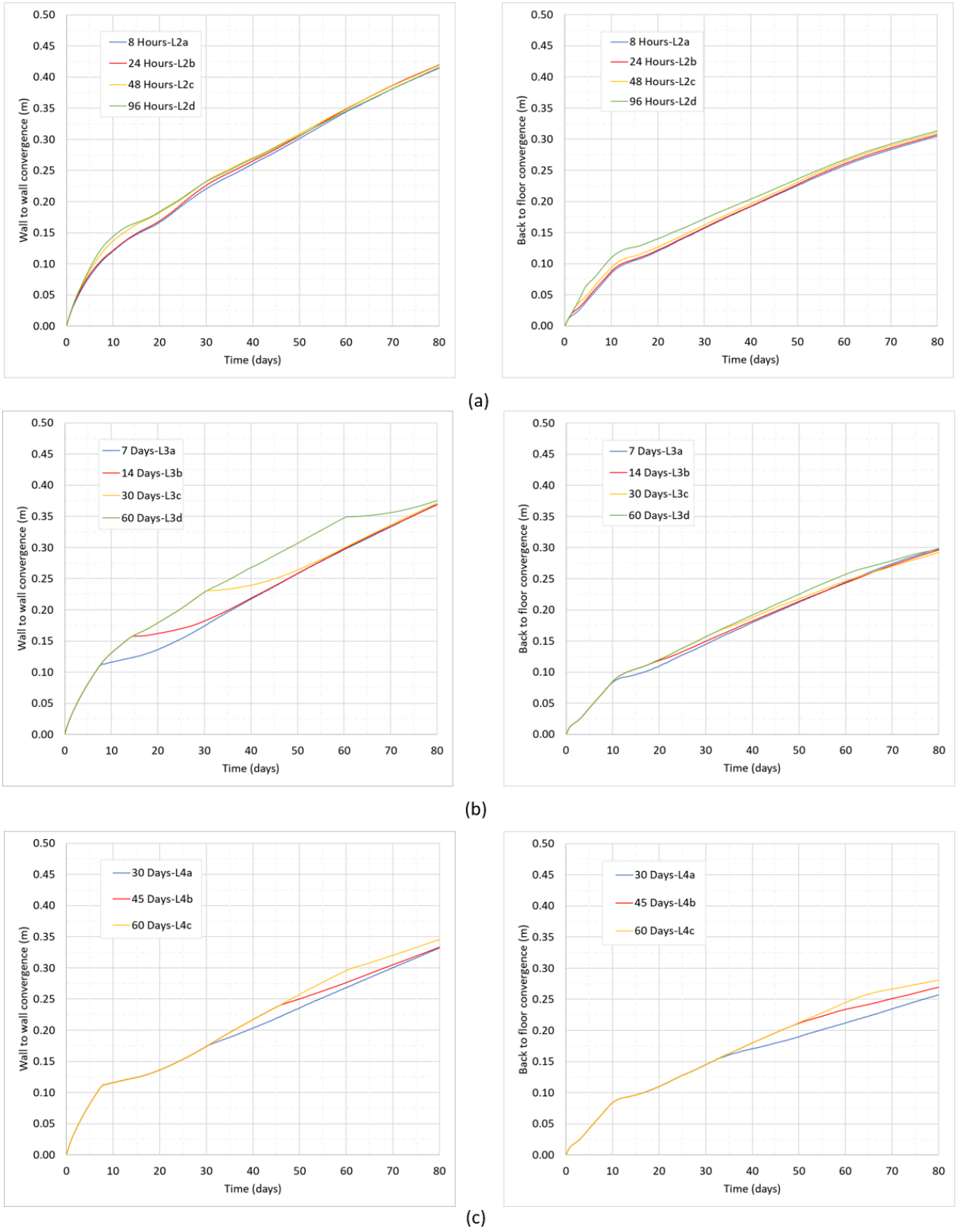

Figure 7.15: Wall to wall and back to floor convergence for Cases L2 – L4 (a) Case L2 (b) Case L3 (c) Case L4

7.5.2 Role of reinforcement at RA-UG mine

The model geometry, boundary conditions, rock mass properties and creep parameters used for the numerical models to investigate the role of reinforcements on the displacements around decline at RA-UG mine were based on the numerical model described in Section 8.2.1 The role of reinforcement was simulated by using pile and cable structural elements in FLAC3D to simulate rock bolts and cable bolts respectively. In squeezing ground conditions, RA-UG mine utilizes two-stage ground support system; primary and secondary. For primary reinforcement, the mine utilizes 2.4 m long, 25 mm diameter rebar installed in the drift back and walls with an in-plane spacing of 1.2 m and rings spaced at 1.2 m. The primary reinforcements are installed with mesh reinforced shotcrete of 100 mm thickness. The secondary reinforcements comprise of four cable bolts installed with an in-plane spacing of 1.2 m and rings spaced at 2.0 m in case of high deformations. No set guidelines are present as to when the secondary reinforcements are installed and often the decision to install secondary reinforcements is based on the severity of damage due to squeezing. The schematics showing primary and secondary reinforcements are provided in Figure 7.16. The axial capacities of the structural elements in the numerical models were assumed to be 200 kN for rebars and 275kN for cable bolts.

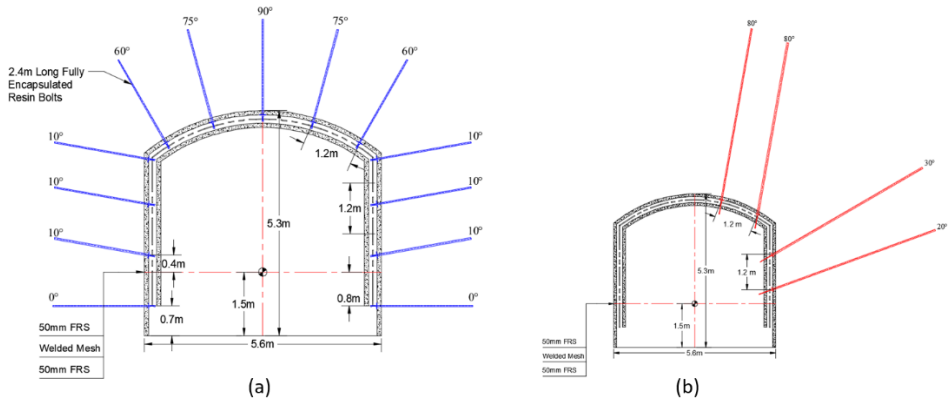

Figure 7.16: Schematic showing ground support in squeezing ground at RA-UG mine (a) primary rebars (b) secondary cable bolts

The spring stiffness and cohesion properties of the structural elements used in the numerical model were based on properties described in Section 8.3.1. The physical parameters such as cross-sectional area and tensile failure strength were based on 25 mm diameter rebar and 15.8 mm cable bolts. The effects of primary and secondary rock reinforcements were investigated by introducing the structural elements in the numerical models at various stages. First, a base case model (R0) was generated with no reinforcements, the base case model looked at the total displacements around the drive when no reinforcements were installed and was used for comparative analysis of the subsequent modelled cases. Two reinforcement model cases generated were R1a and R1b. In Case R1a, only primary reinforcements, i.e. rebars were introduced in the numerical model 8 hours after excavation. In Case R1b, primary reinforcements were introduced in the model 8 hours after excavation and secondary reinforcements, i.e. cable bolts were introduced after 100 days of simulation time, see Figure 7.17. In all three cases (R0, R1a and R1b), the model was run for a total simulation time of 450 days. The trend of the wall to wall and back to floor convergence for modelled cases are provided in Figure 7.18 and contours of displacement and reinforcement axial force are provided in Figure 7.19.

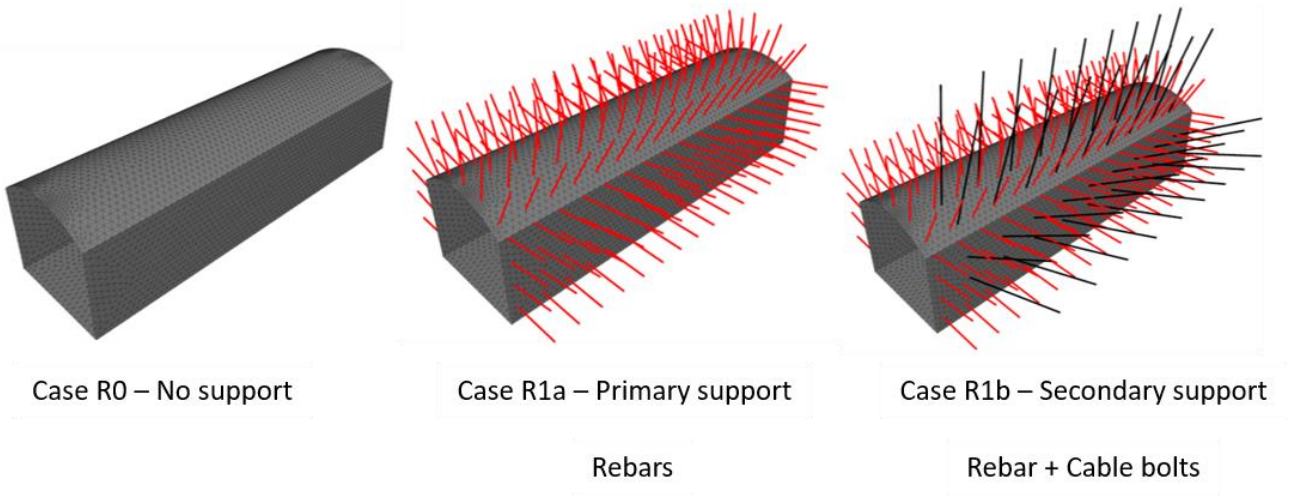

Figure 7.17: Various reinforcement cases simulated for RA-UG mine

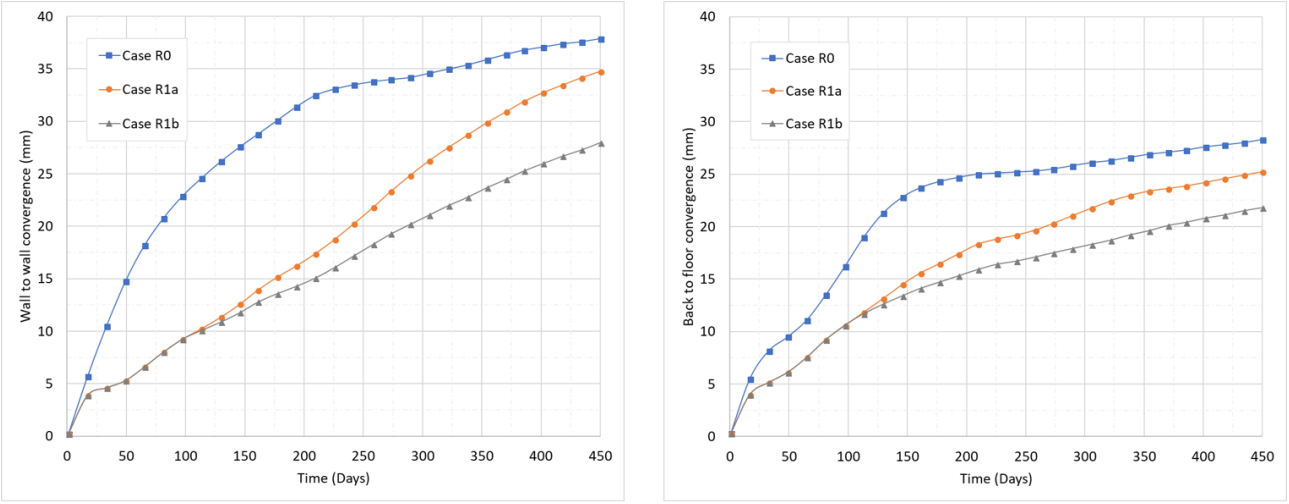

Figure 7.18: Modelled convergence over time for R0 - R1b cases at RA-UG mine (a) wall to wall (b) back to floor

The trend of convergence over time for Cases R0 – R1b suggests that reinforcements have a significant influence on the total displacements around the drive. The results show that in Case R1a, where primary reinforcements were introduced 8 hours after excavation, 8% decrease in wall to wall and 11% decrease in back to floor convergences were observed from the base case. In Case R1b, where cable bolts were introduced in the R1a case model after 100 days of simulation time 20% decrease in the wall to wall and 14% decrease in back to floor convergences from the R1a case were observed. The contours of displacements provided in Figure 7.19 shows how the displacements around the drive reduce with the introduction of primary and secondary reinforcements. The contours of reinforcement axial force suggest that the footwall rebars experience significantly higher load as compared to hanging wall rebars. The rebars in the drive back towards the footwall side experience a lower axial force as compared to rebars towards the hanging wall side and this is because in the drive hanging wall high deformation area is towards the drive shoulder, thus resulting in higher loads in the back rebars towards the hanging wall. The results also suggest that the cable bolts do no experience any significant load (<50kN). This may be

because the cable bolts are installed too early in the deformation stage. In practice, no cable bolts were installed at this location and the deformations were managed by the primary reinforcement only.

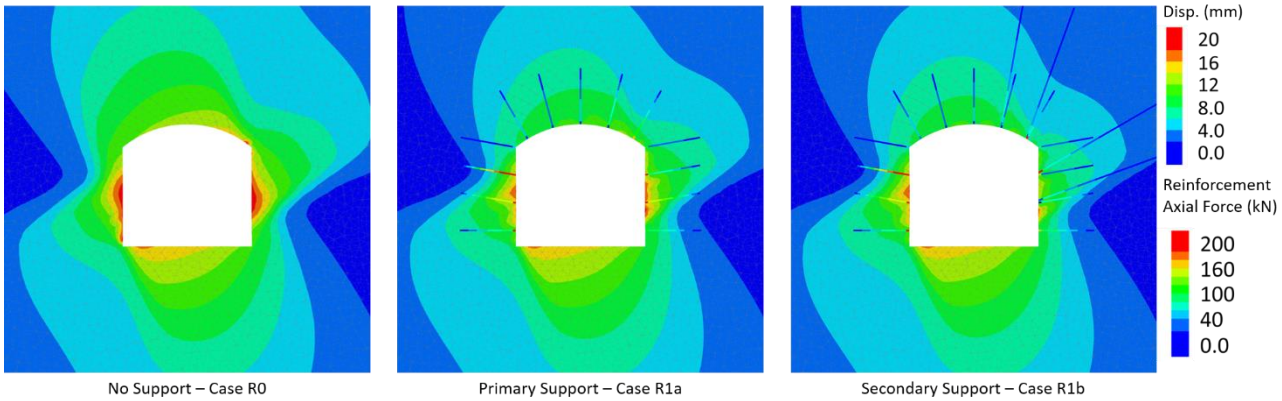

Figure 7.19: Modelled displacement and reinforcement axial force for Cases R0 - R1b at RA-UG mine

The trend of axial forces over time for the reinforcement elements are provided in Figure 7.20. The trend suggests that the axial forces in the rebars develop over time. The result shows that the highest axial force of 189 kN about 95% of the axial capacity, is experienced by a rebar in the footwall. The rebars in the drive back experience 45 % lower and hanging wall rebars experience 35% lower axial force as compared to footwall rebars. The results also suggest that when the secondary reinforcements are introduced in the model, the final axial forces of the back rebars go down by 38% and those of the hanging wall rebars go down by 60%. No significant effect on the axial force of the footwall rebars was observed. This is to be expected as there were no cable bolts installed towards the drive footwall.

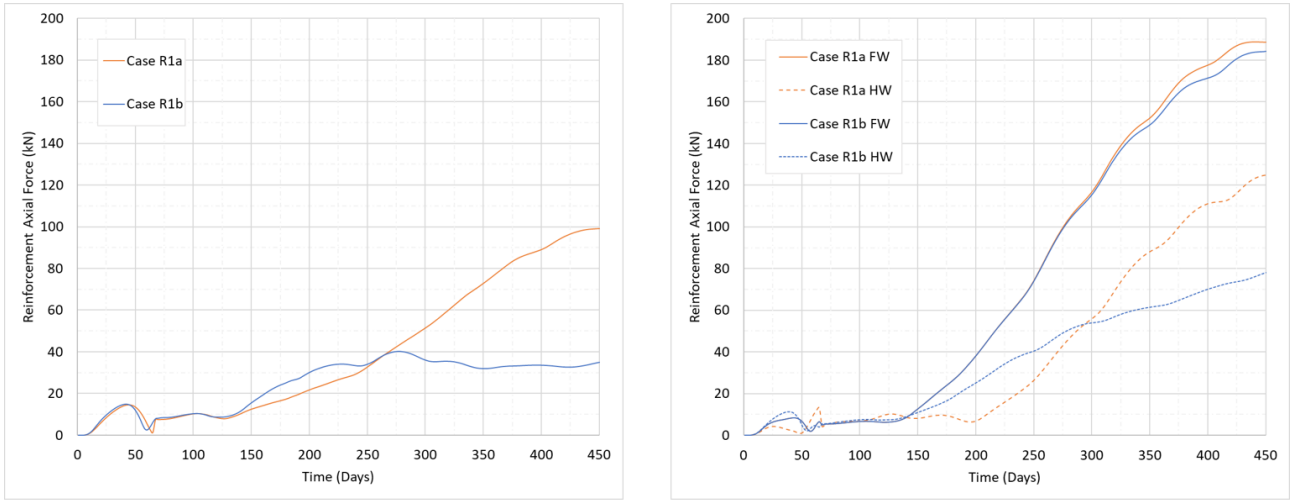

Figure 7.20: Reinforcement axial force over time at RA-UG mine (a) back rebar (b) sidewall rebars

7.5.2.1 Effect of time of installation of supports

The influence of delayed installation of primary and secondary reinforcements at RA-UG mine was investigated by introducing the reinforcements at various stages in the models. To study the effect of the delayed installation of primary reinforcements a series of numerical models were generated, i.e. Cases R2a-R2d and the time of installation of the primary reinforcements was varied and introduced in the model at 8, 24, 48 and 96 hours respectively. For secondary reinforcements, in Cases R3a-R3c, the time of installation of cable bolts was delayed, and the cable bolts were installed at 100, 200 and 300 days of simulation time respectively. In all simulated cases, the model was run for a total simulation time of 450 days. The trends of displacements for all modelled cases is provided in Figure 7.21. The results show that in Case R2 where only primary reinforcements were installed in the model and the time of installation was varied, no significant influence on the total convergences was observed. The results show that in Case R3, where the time of installation of secondary reinforcements was varied for the first two cases, R3a and R3b, no significant difference in the displacements was observed. However, when the cable bolts were installed after 300 days of simulation time (Case R3c), a 13% increase in wall to wall and 6% increase in back to floor

convergence was observed. This suggests that in cases where the secondary reinforcements are significantly delayed, displacements would result in more plastic deformations, and higher final displacements would be observed.

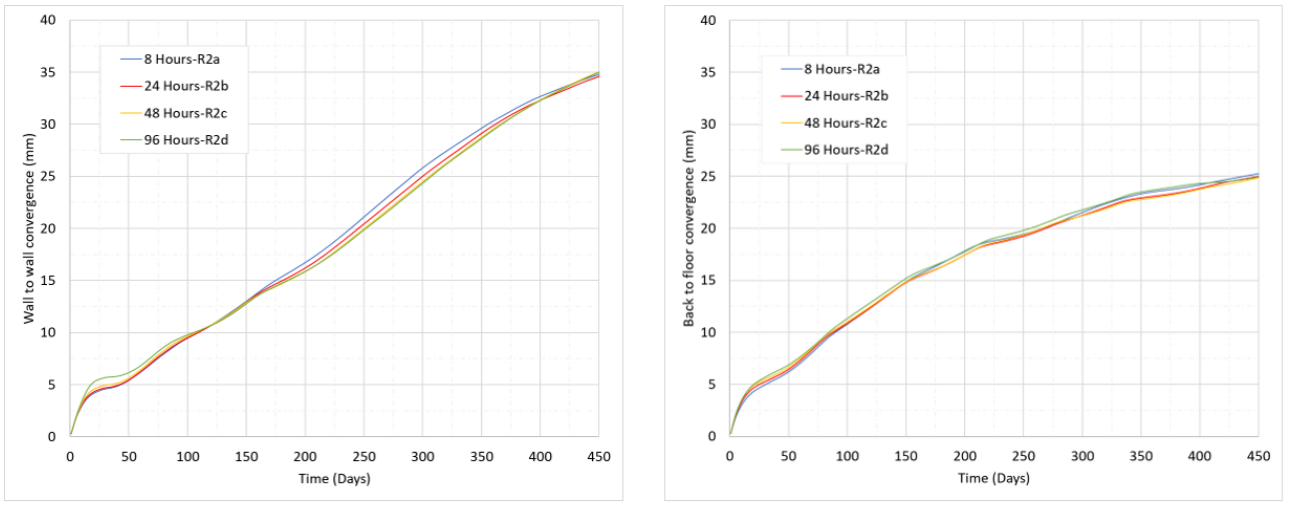

(a)

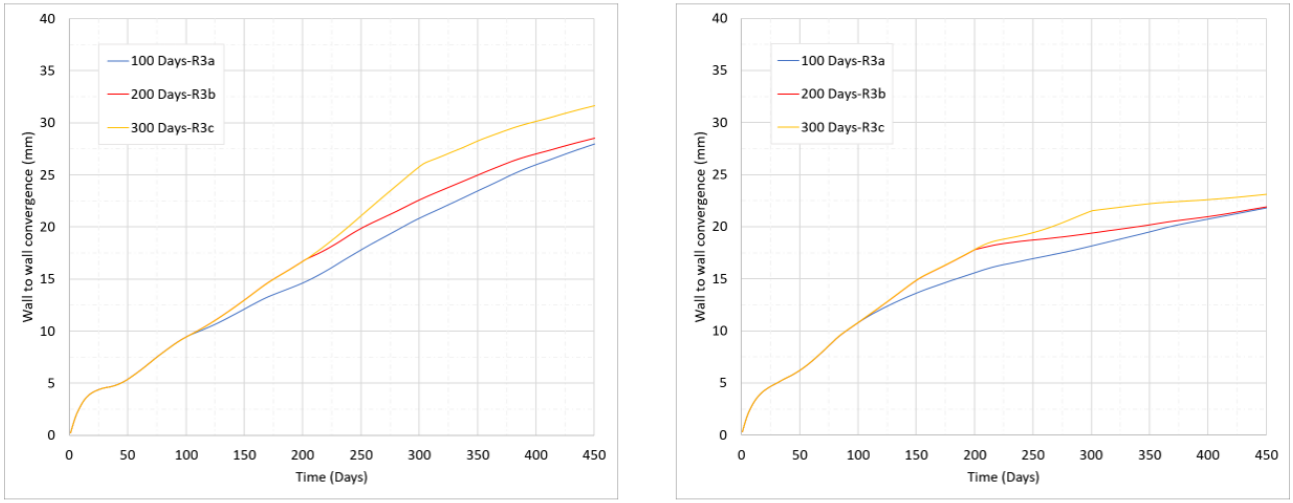

(b)

Figure 7.21: Effect of delayed installation of primary and secondary reinforcements (a) Case R2 (b) Case R3

7.6 Chapter Summary

Time-dependent behaviour of the foliated rock mass is one of the key characteristics of a squeezing ground. In the case where the time-dependent behaviour of the foliated rock mass needs to be

considered in the numerical simulation, FLAC3D provides the option to explicitly represent the time dependency in the numerical simulations by utilizing Power-Ubiquitous model.

This behaviour can result in large and anisotropic deformations which continue over the working life of the mining excavations. Understanding the time-dependent response is essential for ground support design and maintaining excavation stability. This chapter presented a methodology to investigate the time-dependent deformations in the foliated rock mass for the two case studies from LaRonde and RA-UG mines. The results from the modelling suggest that the displacement and displacement rate around underground excavation in foliated rock mass are not constant over time. The modelling results and underground convergence data for the simulated cases suggests the excavation experiences higher displacement rates immediately after development. This displacement rate reduces over time and after a certain time and a constant displacement rate continues. The results also show that the excavation sidewalls experience higher displacements and displacement rates as compared to excavation back and floor. This is because the walls are oriented parallel to the foliations.

The FLAC3D code also provides an option to use several structural elements to represent the role of rock reinforcements in the numerical models. The Pile – rock bolt structural element can be used to represent the reinforcement for which the resistance to bending needs to be taken into consideration, such as rock bolts, split sets and swellex. The cable structural element can be used for the reinforcement for which only the tensile behaviour needs to be considered such as the cable bolts.

The chapter provides a methodology to investigate the role of reinforcement at the two mines. The results show that reinforcements have a significant influence on the displacements around underground excavations at the two mines. At LaRonde mine, FRS in the sidewalls has a minor effect on the displacements and rebars in the drifts in the back show a significant decrease in the

displacements. Results also suggest that the hanging wall reinforcements experience higher axial forces as compared to footwall reinforcements. The effect of the delayed installation of reinforcements was also investigated for LaRonde mine, and the results show that the delayed installation of primary and secondary reinforcements results in no significant difference in the final displacements. However, there is a considerable increase in the short-term displacements around the drift when installation of the hybrid bolts was delayed. Delayed installation of tertiary reinforcements shows a minor increase in final displacements.

For RA-UG mine, the modelling results show that the footwall rebars experience higher axial forces as compared to the rebars in the drive back and hanging wall. Installation of cable bolts results in a considerable decrease in the displacements and axial reinforcement forces of the hanging wall rebars. In the case where installation of primary reinforcements was delayed in the RA-UG mine model, no significant increase in the displacements was observed. However, in the case where the installation of secondary reinforcements was delayed, a considerable increase in final displacements was observed.

Chapter 8

8 Conclusion

Squeezing ground conditions have become a significant challenge for various underground hard rock mines as the mining operations exploit the ore reserves at greater depths. Squeezing grounds in underground hard rock mines are often the result of the presence of geological features such as foliation planes. Foliated rock mass is prone to large anisotropic and time-dependent deformations when subjected to high-stress conditions and these deformations result in a significant rock mass damage around underground excavations and thus makes it difficult to keep the excavations operational. To better manage the ground control challenges associated with squeezing of foliated rock mass it is critical to understand the response of foliated rock mass to various mining conditions. This thesis provided a numerical modelling methodology using continuum modelling in FLAC3D to investigate the anisotropic and time-dependent response of foliated rock mass undergoing squeezing under various mining conditions.

The numerical models used to simulate the anisotropic behaviour of the foliated rock mass utilized ubiquitous joint model in FLAC3D to simulate the role of foliation planes in the numerical simulations. The ubiquitous joint model was successful in reproducing the observed rock mass failure mechanisms at LaRonde and RA-UG mines considered for the analysis. The model also captured the observed failure mechanism during compressive laboratory testing of the intact GBSG rock sample at RA-UG mine. The time-dependence in numerical models was simulated by using the power ubiquitous model in FLAC3D. The model was successful in reproducing the evolution of displacements around underground excavations at the two mines over time. Structural elements in FLAC3D were used to simulate the role of rock reinforcements in the numerical models and were successful in reproducing the behaviour observed in the field.

8.1 Contributions

The thesis is a contribution towards improving the understanding of the complex response of the foliated rock mass to various mining conditions. The numerical modelling methodology presented in this thesis can potentially be extended to investigate the complex time-dependent and anisotropic behaviour of various anisotropic rock masses. The methodology can be used to evaluate various rock reinforcement strategies and schemes and performance of any new rock reinforcement elements. The key contributions of this thesis are provided below.

8.1.1 Improved understanding of the influence of foliation on squeezing

It was demonstrated that numerical models utilizing ubiquitous-joint model in FLAC3D were successful in reproducing the observed failure mechanisms in the foliated rock mass at the two mines considered for the analysis. The modelling results show that the rock mass failure mechanism in the foliated rock mass is a function of the relative orientation of foliation planes and principal stresses. In the case where steeply dipping foliations are present with the major principal stress oriented perpendicular to the foliation strike, both sidewalls of the excavation show buckling type of failure mechanisms. In the case where the foliation dips at a relatively shallow angle and the major principal stress is oriented parallel to the foliated strike, the failure mechanism in the two excavation sidewalls varies and, in this case, the footwall shows a shearing and sliding failure and the excavation hanging wall shows buckling type of failure mechanism. The modelling results showed that the deformations in the excavation sidewalls are anisotropic and the squeezing of foliated rock mass results in high deformation areas towards the drive floor in the footwall and towards the drive shoulder in the hanging wall.

Numerical investigation of the influence of varying interception angle between the foliation planes

and excavation walls on the severity of squeezing ground conditions revealed that the foliation planes have a significant influence on the closure strain around underground excavations for interception angle less than 45° and no major influence of foliation planes should be expected for interception angle greater than 45°. The results also showed that for interception angle less than 45°, the foliation planes show considerably greater influence on the severity of squeezing for interception angle between 0° and 30° than for interception angle between 30° and 45°. It was demonstrated that the excavation shape and wall to wall distance between excavations parallel to the foliation also have a significant influence on the severity of squeezing ground conditions. The modelling results showed that the using an arched back profile for excavations susceptible to squeezing could result in a significant reduction on displacements around the excavations. The results also show that for parallel excavations with walls oriented parallel to the strike of foliation, a wall to wall distance of less than 15 m between the excavations will result in a significant increase in the severity of squeezing. These observations from modelling results can provide valuable input in mine design and planning process.

The observations from the numerical modelling results can provide valuable input in mine design process and ground support strategies for underground mining operations facing the challenges associated with squeezing ground conditions in the foliated rock mass. By identifying the rock mass failure mechanisms, a more informed decision on the use of various rock reinforcement elements can be made. For example, in cases where the excavations show buckling failure mechanism, split sets can potentially be used as primary support keeping in mind their low capacity. However, in cases where shearing and sliding failure mechanisms are expected, split sets would not function as they would be subjected to shearing forces resulting in premature failure due shearing and locking of the split sets near the excavation boundary. In such cases, reinforcement elements capable of withstanding shear movements should be utilized such as rebars. The information on interception

angle can potentially be used to plan the orientation of major mining infrastructures such as major mine accesses, substation, raise bore chambers and crusher chambers. It can also be utilized to classify the mine accesses and stoping developments into categories of squeezing and suitable ground support schemes can be used for each category as shown in Figure 8.1. This can help reduce the ground support and rehabilitation costs for the mining operations. Modelling results have shown that when developing two parallel drives with walls oriented parallel to the strike of foliation planes, the wall to wall distance between the drives should be kept more than 15 m to prevent aggravating the deformations. Also, the excavation shapes are often decided early in the mine design and based on the modelling results, arched back roof is more stable than trapezoidal shapes. These observations from the modelling results can provide useful mine design parameters for squeezing grounds.

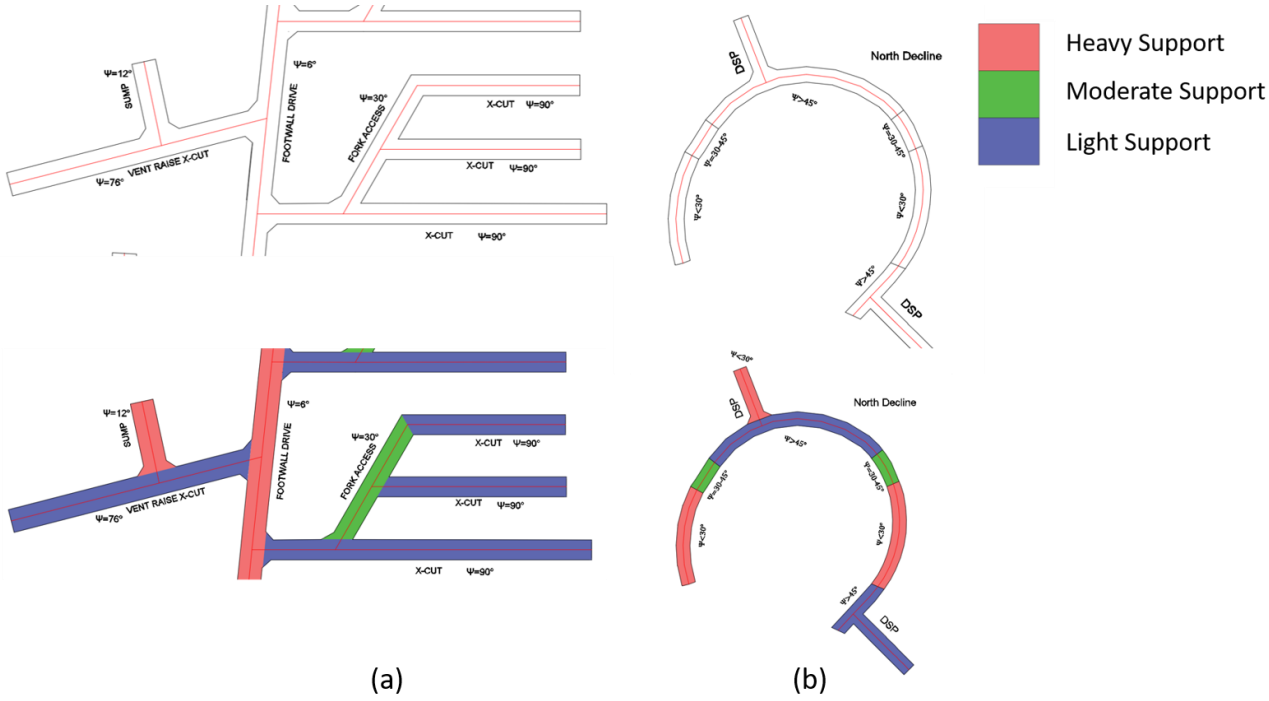

Figure 8.1: Example of potential ground support strategies based on varying interception angle (a) Level development layout (b) Decline development layout

8.1.2 Capturing time dependence and effect of rock reinforcements

The numerical models utilizing the power ubiquitous model were successful in reproducing the time-dependent response of the foliated rock mass to mining and the structural elements in FLAC3D were successful in simulating the influence of various rock reinforcement elements on displacements around underground excavations. The results of numerical models used to simulate the excavation convergence over time were in good agreement with the convergence values recorded underground at both mines. The modelling results showed that the displacement rates around underground excavations in foliated rock mass are not constant over time. Higher displacement rates are observed immediately after the development and the displacement rates reduce over time and continue at a constant rate over the working life of the excavations. Life of all mining excavations is not the same and it varies depending on the use of excavations. For example, level access declines and mining infrastructure are needed during the entire mine life. However, stope access crosscuts are temporary and only required for developing the stopes to be extracted. The results of time-dependent models can be used to better plan the development and support strategies for permanent and temporary mining excavations and it can also be used to form more informed rehabilitation strategy.

It was demonstrated that the role of various reinforcement elements could be successfully simulated in the numerical models utilizing cable and pile structural elements in FLAC3D. The modelling results showed that introduction of reinforcements in the numerical models showed significant reduction displacements around the excavations. The modelling results show that rebar and hybrid bolts being stiffer reinforcement elements show an immediate influence on displacements. FRS, however, do not show an immediate effect on displacements. Modelling results also show that the axial force on reinforcement of hanging wall and footwall varies for both mines. The calibrated

numerical models can be used to evaluate the various ground support schemes such as varying bolt spacing, length etc. The model can also be used to evaluate the performance of any new rock reinforcement elements and the influence of delayed or early installation of secondary and tertiary reinforcements.

8.2 Limitations of adopted methodology

The limitations of the numerical modelling methodology adopted in this thesis are provided below.

- The continuum modelling utilizing the ubiquitous-joint model cannot capture block separation, the opening of fracture and block detachments that may be possible in the distinct element method.
- The numerical models generated to investigate the role of rock reinforcements on the severity of squeezing did not consider the role of surface support such as shotcrete, mesh and straps.
- The numerical models cannot consider several geological features of foliation planes such as plane spacing, plane length etc.
- Continuum numerical models used to simulate the anisotropic and time-dependent behaviour of foliated rock mass required significant efforts in model calibration and need good quality data for model calibration.

8.3 Recommendations for future work

The numerical modelling approach used in this thesis can potentially be used to further investigate the behaviour of the foliated rock mass to mining. It is recommended that this methodology should be applied to other reported squeezing ground cases. This would allow for further validation of the methodology. Additional work can be carried out to investigate the effect of 3D parameters such as the influence of intersections and stope extraction on the severity of squeezing ground conditions,

this, however, would require larger scale models. The modelling methodology can also be extended to a bigger scale model that can be used to investigate the effect of various stoping sequences on the severity of squeezing of mining infrastructures and permanent developments.

The geological parameters of the foliation planes such as the spacing, length and condition, cannot be directly considered in the numerical models. Further work can be done to take into consideration the geological characteristics of foliation planes by varying the foliation properties. Influence of other joint sets can be investigated by introducing discrete fracture network (DFN) in continuum numerical models. The surface support elements were not considered in the numerical models. The role of ground support can be investigated further by using liner or shell structural elements to simulate various surface support elements used in squeezing ground conditions.

References

Amadei, B., 1996. Importance of anisotropy when estimating and measuring in situ stresses in rock. Int. J. Rock. Mech. Min. Sci. Geomech. Abstr. 33 (3), 293–325

Amadei, B., 1983. Rock anisotropy and the theory of stress measurements (Vol. 2). Springer Science & Business Media.

Amadei, B., 1979. Creep behaviour of rock joints. Doctoral dissertation, University of Toronto, Canada.

Armatys, M., 2012. Modification des classifications géomécaniques pour les massifs rocheux schisteux. Ecole Polytechnique, Montreal (Canada).

Aydan, Ö., Akagi, T. and Kawamoto, T., 1993. The squeezing potential of rocks around tunnels; theory and prediction. Rock Mechanics and Rock Engineering, 26(2), pp.137-163.

Bahrani, N. and Hadjigeorgiou, J., 2017. Explicit reinforcement models for fully-grouted rebar rock bolts. Journal of Rock Mechanics and Geotechnical Engineering, 9(2), pp.267-280.

Barla, G., 2001. Tunnelling under squeezing rock conditions. Euro summer-School in Tunnel Mechanics, Innsbruck, pp.169-268.

Barla, G., 1995. Squeezing rocks in tunnels. ISRM News Journal, 2(3), pp.44-49.

Barla, G., Debernardi, D. and Sterpi, D., 2012. Time-dependent modelling of tunnels in squeezing conditions. International Journal of Geomechanics, 12(6), pp.697-710.

Barton, N., Lien, R. and Lunde, J., 1974. Engineering classification of rock masses for the design of tunnel support. Rock mechanics, 6(4), pp.189-236.

Beck, D., Kassbohm, S. and Putzar, G., 2010. Multi-scale simulation of ground support designs for extreme tunnel closure. In Second International Symposium on Block and Sublevel Caving, Perth, Australia.

Beck, D.A. and Sandy, M.P., 2003. Mine sequencing for high recovery in Western Australian mines. AusIMM Bulletin, vol. May/June, no.3.

Bewick, R.P. and Kaiser, P.K., 2009, May. Influence of rock mass anisotropy on tunnel stability. In ROCKENG09, Proceedings of the 3rd CANUS Rock Mechanics Symposium, Toronto, Ont. Edited by Diederichs and Grasselli. Paper (No. 3995).

Bosman, J.D., Malan, D.F. and Drescher, K., 2000. Time-dependent tunnel deformation at Hartebeestfontein Mine. Journal South African Institute of Mining and Metallurgy, 100(6), pp.333-340.

Bowden, R.K. and Curran, J.H., 1984. Time-dependent behaviour of joints in Shale. In The 25th US Symposium on Rock Mechanics (USRMS). American Rock Mechanics Association.

Brown, E.T., Bray, J.W., Ladanyi, B. and Hoek, E., 1983. Characteristic line calculations for rock tunnels. J. Geotech. Eng. Div. Am. Soc. Civ. Eng, 109, pp.15-39.

Butler, J.L. and Leonardi, C.R., 2016. Improvement of squeezing ground prediction and monitoring capabilities for Mount Isa Mines Northern 3500 orebody. Mining Technology, 125(3), pp.142-155.

Colak, K. and Unlu, T., 2004. Effect of transverse anisotropy on the Hoek–Brown strength parameter 'mi'for intact rocks. International Journal of Rock Mechanics and Mining Sciences, 41(6), pp.1045-1052.

Cristescu, N. and Gioda, G. eds., 1994. Visco-plastic behaviour of geomaterials. Springer-Verlag.

Duveau, G., Shao, J.F. and Henry, J.P., 1998. Assessment of some failure criteria for strongly anisotropic geomaterials. Mechanics of Cohesive-frictional Materials: An International Journal on Experiments, Modelling and Computation of Materials and Structures, 3(1), pp.1-26.

Einstein, H.H., 1996. Tunnelling in difficult ground—swelling behaviour and identification of swelling rocks. Rock mechanics and rock engineering, 29(3), pp.113-124.

Fahimifar, A., Karami, M. and Fahimifar, A., 2015. Modifications to an elasto-visco-plastic constitutive model for prediction of creep deformation of rock samples. Soils and Foundations, 55(6), pp.1364-1371.

Fernandez, F., Watt, G. and Ooi, J., 2012. Strategic management for squeezing ground conditions at the Argyle Diamonds block cave project. Australian Journal of Civil Engineering, 10(2), pp.193-206.

Gioda, G. and Cividini, A., 1996. Numerical methods for the analysis of tunnel performance in squeezing rocks. Rock mechanics and rock engineering, 29(4), pp.171-193.

Goodman, R.E., 1989. Introduction to rock mechanics (Vol. 2). New York: Wiley.

Goodman, R.E., 1967. Research on Rock Bolt Reinforcement and Integral Lined Tunnels (No. OMAHA-TR-3). CORPS OF ENGINEERS OMAHA NE.

Griggs, D., 1939. Creep of rocks. The Journal of Geology, 47(3), pp.225-251.

Hadjigeorgiou, J. and Karampinos, E., 2017, March. Design tools for squeezing ground conditions in hard rock mines. In Proceedings of the Eighth International Conference on Deep and High Stress Mining (pp. 693-705). Australian Centre for Geomechanics.

Hadjigeorgiou, J., Karampinos, E., Turcotte, P. and Mercier-Langevin, F., 2013, May. Assessment of the influence of drift orientation on observed levels of squeezing in hard rock mines. In Proceedings of the Seventh International Symposium on Ground Support in Mining and Underground Construction (pp. 109-117). Australian Centre for Geomechanics.

Helbig, K., 1996. Foundations of anisotropy for exploration seismics. In International Journal of Rock Mechanics and Mining Sciences and Geomechanics Abstracts (Vol. 1, No. 33, pp. 19A-20A).

Hill, R., 1998. The mathematical theory of plasticity (Vol. 11). Oxford university press.

Hoek, E., 2001. Big tunnels in bad rock. Journal of Geotechnical and Geoenvironmental Engineering, 127(9), pp.726-740.

Hoek, E., 1983. Strength of jointed rock masses. Géotechnique 33, 187–223. https://doi.org/10.1680/geot.1983.33.3.187

Hoek, E. and Brown, E.T., 1980a. Empirical strength criterion for rock masses. Journal of Geotechnical and Geoenvironmental Engineering, 106(ASCE 15715).

Hoek, E., and Brown, E.T. 1980b. Underground excavations in rock. The Institution of Mining and Metallurgy, London.

Hoek, E. and Marinos, P., 2000. Predicting tunnel squeezing problems in weak heterogeneous rock masses. Tunnels and tunnelling international, 32(11), pp.45-51.

Itasca Consulting Group Inc. (1999). FLAC — Fast Lagrangian Analysis of Continua (Version 3.40). Minneapolis: Itasca.

Itasca Consulting Group Inc. (2012). FLAC3D — Fast Lagrangian Analysis of Continua (Version 5.0). Minneapolis: Itasca.

Itasca Consulting Group Inc. (2013). 3DEC — Three-Dimensional Distinct Element Code (Version 5.0). Minneapolis: Itasca.

Itasca Consulting Group Inc. (2017a). FLAC3D — Fast Lagrangian Analysis of Continua (Version 6.0). Minneapolis: Itasca.

Itasca Consulting Group Inc. (2017b). Griddle – Advanced Grid Generation Software for Engineers (Version 1.0). Minneapolis: Itasca.

Jaeger, J.C., 1971. Friction of rocks and stability of rock slopes. Geotechnique, 21(2), pp.97-134.

Jaeger, J.C., 1960. Shear failure of anistropic rocks. Geological Magazine, 97(1), pp.65-72.

Jaeger, J.C., Cook, N.G. and Zimmerman, R., 2007. Fundamentals of rock mechanics. John Wiley & Sons.

Jethwa, J.L., Singh, B. and Singh, B., 1984. 28 Estimation of ultimate rock pressure for tunnel linings under squeezing rock conditions—a new approach. In Design and Performance of Underground Excavations: ISRM Symposium—Cambridge, UK, 3–6 September 1984 (pp. 231-238). Thomas Telford Publishing.

Karampinos, E., 2016. Management of Squeezing Ground Conditions in Hard Rock Mines. Doctoral dissertation, University of Toronto, Canada.

Karampinos, E., Hadjigeorgiou, J. and Turcotte, P., 2016. Discrete element modelling of the influence of reinforcement in structurally controlled squeezing mechanisms in a hard rock mine. Rock Mechanics and Rock Engineering, 49(12), pp.4869-4892.

Karampinos, E., Hadjigeorgiou, J., Hazzard, J. and Turcotte, P., 2015a. Discrete element modelling of the buckling phenomenon in deep hard rock mines. International Journal of Rock Mechanics and Mining Sciences, 80, pp.346-356.

Karampinos, E., Hadjigeorgiou, J., Turcotte, P. and Mercier-Langevin, F., 2015b. Large-scale deformation in underground hard-rock mines. Journal of the Southern African Institute of Mining and Metallurgy, 115(7), pp.645-652.

Kazakidis, V.N., 2002. Confinement effects and energy balance analyses for buckling failure under eccentric loading conditions. Rock mechanics and rock engineering, 35(2), pp.115-126.

Kazakidis VN, Diederichs MS. Understanding jointed rock mass behaviour using a ubiquitous joint approach. Int J Rock Mech Min Sci. 1993;30:163–172.

Kong, J., Yuan, J. and Pan, X., 2009. Secondary Development of FLAC3D and Application of Naylor KG Constitutive Model. In Computational Structural Engineering (pp. 1267-1273). Springer, Dordrecht.

Kovári, K., 1998. Tunneling in Squeezing Rock (Tunnelbau in druckhaftem Gebirge). Tunnel, 5, pp.12-31.

Lama, R.D. and Vutukuri, V.S., 1978. Handbook on mechanical properties of rocks-testing techniques and results-volume iii (Vol. 3, No. 2).

Li, G., Hong, L., Harumi, K. and Yoshiaki, M., 2003. Application of ubiquitous joint model in numerical modelling of hilltop mines in JAPAN. Chinese J. Rock Mech. Eng 22(6), pp.951-956.

Malan, D.F., 2002. Manuel Rocha medal recipient simulating the time-dependent behaviour of excavations in hard rock. Rock Mechanics and Rock Engineering, 35(4), pp.225-254.

Malan, D.F. and F.R.P. Basson, 1998. Ultra-deep mining: the increased potential for squeezing conditions. Journal of the Southern African Institute of Mining and Metallurgy, 98(7), pp.353-363.

Marlow, P. and Mikula, P.A., 2013, May. Shotcrete ribs and cemented rock fill ground control methods for stoping in weak squeezing rock at Wattle Dam Gold Mine. In Proceedings of the Seventh International Symposium on Ground Support in Mining and Underground Construction (pp. 133-147). Australian Centre for Geomechanics.

Mellies, G., 2009. Two case studies of excavations in fractured rock. Master dissertation, Université Laval. Canada.

Mercier-Langevin, F., 2011. LaRonde Extension–mine design at three kilometres. Mining Technology, 120(2), pp.95-104.

Mercier-Langevin, F., 2010. Review of mining practices at depth at Agnico-Eagle's LaRonde mine. CIM Journal, Vol. 1, No. 3.

Mercier-Langevin, F. and Hadjigeorgiou, J., 2011. Towards a better understanding of squeezing potential in hard rock mines. Mining Technology, 120(1), pp.36-44.

Mercier-Langevin, F. and Hudyma, M., 2007. The development and implementation of a comprehensive seismic risk management plan at Agnico-Eagle's LaRonde Mine. Deep Mining, pp.221-240.

Mercier-Langevin, F. and Turcotte, P., 2007, January. Evolution of Ground Support Practices at Agnico-Eagle's LaRonde Division-Innovative Solutions to High-stress Yielding Ground. In 1st Canada-US Rock Mechanics Symposium. American Rock Mechanics Association.

Mercier-Langevin, F. and Wilson, D. 2013. Lapa mine - ground control practices in extreme squeezing ground. Proceedings of the Seventh International Symposium on Ground Support in Mining and Underground Construction, Perth, Australia, 13-15 May 2013. Brady, B. and Potvin, Y. (eds). Australian Centre for Geomechanics, Perth. pp. 119-132

Mercier-Langevin, P., Dubé, B., Hannington, M.D., Davis, D.W., Lafrance, B. and Gosselin, G., 2007. The LaRonde Penna Au-rich volcanogenic massive sulfide deposit, Abitibi greenstone belt, Quebec: Part I. Geology and geochronology. Economic Geology, 102(4), pp.585-609.

Mesy, 2011. Hydraulic Injection Tests, Rampura Agucha Mine Project, Hindustan Zinc Limited. Mesy India Pvt. Ltd., Lucknow, India.

Milnes, A.G., Hudson, J., Wikström, L. and Aaltonen, I., 2006. Foliation: geological background, rock mechanics significance, and preliminary investigations at Olkiluoto (No. POSIVA-WR--06-03). Posiva Oy.

Mishra, A.K., Panigrahi, D.C., Behera, P.K., Sinha, R.K., Munshi, B., 2015. Geotechnical Lab Testing of Drill Core Samples from RA UG Mine, Internal Report HZL. Indian School of Mines, Dhanbad, India.

Noorian B. M., and Jing, L., 2014. Anisotropy of strength and deformability of fractured rocks. Journal of Rock Mechanics and Geotechnical Engineering 6, 156–164.

O'Rourke, T.D., 1984. Guidelines for tunnel lining design. ASCE. New York.

Paraskevopoulou, C., 2016. Time-dependency of rocks and implications associated with tunnelling. Doctoral dissertation, Queen's University, Canada.

Paraskevopoulou, C. and Diederichs, M., 2018. Analysis of time-dependent deformation in tunnels using the Convergence-Confinement Method. Tunnelling and Underground Space Technology, 71, pp.62-80.

Pariseau, W.G., 1968, January. Plasticity theory for anisotropic rocks and soil. In The 10th US Symposium on Rock Mechanics (USRMS). American Rock Mechanics Association.

Passchier, C.W. and Trouw, R.A., 2005. Microtectonics (Vol. 1). Springer Science & Business Media.

Paul, B., 1961. A modification of the Coulomb-Mohr theory of fracture. Journal of Applied Mechanics, 28(2), pp.259-268.

Peck, R.B., 1969. Advantages and limitations of the observational method in applied soil mechanics. Geotechnique, 19(2), pp.171-187.

Peck, W.A., Sainsbury, D.P., Lee, M.F., 2013. The importance of geology and roof shape on the stability of shallow caverns. Australian Geomechanics Journal 48, 1–14.

Pellet, F.L., 2016. Chapter 24: Rock creep mechanics, in: CRC Press / Balkema – Taylor & Francis Group, Leiden (Ed.), Rock Mechanics and Engineering: Vol. 1 Principles. pp. 745–770.

Plana D., López C., Cornelles J., Muñoz P. () Numerical Analysis of a Tunnel in an Anisotropy Rock Mass. Envalira Tunnel (Principality of Andorra). In: Hack R., Azzam R., Charlier R. (eds) Engineering Geology for Infrastructure Planning in Europe. Lecture Notes in Earth Sciences, vol 104. Springer, Berlin, Heidelberg

Potvin, Y. and Hadjigeorgiou, J., 2008. Ground support strategies to control large deformations in mining excavations. Journal of the Southern African Institute of Mining and Metallurgy, 108(7), pp.397-404.

Potvin, Y. and Slade, N., 2007. Controlling extreme ground deformation; Learning from four Australian case studies. Challenges in Deep and High Stress Mining, pp.355-361.

Roache, B., 2016. Mining in extreme squeezing conditions at the Henty mine. In Proceedings of Eighth International Symposium on Ground Control in Mining and Underground Construction. Lulea University, Sweden.

Robert McNeel and Associates. (2017). Rhinoceros – 3D CAD Software (Version 5.0). Seattle, WA, USA: McNeel

Rocscience Inc. (2006). Phase2 - Finite Element Analysis for Excavations and Slopes (Version 6.0). Toronto, Canada: Rocscience.

Rocscience Inc. (2008). Phase2 - Finite Element Analysis for Excavations and Slopes (Version 7.0). Toronto, Canada: Rocscience.

Rocscience Inc. (2017). RocData - Rock, Soil and Discontinuity strength analysis (Version 5.0). Toronto, Canada: Rocscience.

Russo, G., Repetto, L., Piraud, J. and Laviguerie, R., 2009. Back-analysis of the extreme squeezing conditions in the exploratory adit to the Lyon-Turin base tunnel. Rock Engineering in Difficult Conditions, Toronto, ON, Canada, pp.9-14.

Sainsbury, B., Pierce, M. and Mas Ivars, D., 2008. Analysis of caving behavior using a synthetic rock mass (SRM)–ubiquitous-joint rock mass (UJRM) modelling technique. in the Proceedings of the 1st Southern Hemisphere International Rock Mechanics Symposium (SHIRMS).

Sandy, M.P., Gibson, W. and Gaudreau, D., 2007. Canadian and Australian ground support practices in high deformation environments. Challenges in deep and high stress mining. Australian Centre for Geomechanics, Perth, pp.297-311.

Saroglou, H. and Tsiambaos, G., 2008. A modified Hoek–Brown failure criterion for anisotropic intact rock. International Journal of Rock Mechanics and Mining Sciences, 45(2), pp.223-234.

Schoenberg, M. and Sayers, C.M., 1995. Seismic anisotropy of fractured rock. Geophysics, 60(1), pp.204-211.

Schubert, W. and Mendez, J.M.D., 2017. Influence of Foliation Orientation on Tunnel Behavior. Procedia engineering, 191, pp.880-885.

Shi, X., Yang, X., Meng, Y. and Li, G., 2016. Modified Hoek–Brown failure criterion for anisotropic rocks. Environmental Earth Sciences, 75(11), p.995.

Singh, B., Jethwa, J.L., Dube, A.K. and Singh, B., 1992. Correlation between observed support pressure and rock mass quality. Tunnelling and Underground Space Technology, 7(1), pp.59-74.

Singh, M., Singh, B. and Choudhari, J., 2007. Critical strain and squeezing of rock mass in tunnels. Tunnelling and underground space technology, 22(3), pp.343-350.

Steiner, W., 1996. Tunnelling in squeezing rocks: case histories. Rock Mechanics and Rock Engineering, 29(4), pp.211-246.

Sterpi, D. and Gioda, G., 2009. Visco-plastic behaviour around advancing tunnels in squeezing rock. Rock Mechanics and Rock Engineering, 42(2), pp.319-339.

Struthers, M.A., Turner, M.H., McNabb, K. and Jenkins, P.A., 2000. Rock mechanics design and practice for squeezing ground and high stress conditions at Perseverance Mine. MassMin2000, Australasian Institute of Mining and Metallurgy, Brisbane.

Terzaghi, K., 1946. Rock defects and loads on tunnel supports. Proctor R.V., White T.L. (Eds.), Rock Tunnelling with Steel Supports, 1, Commercial Shearing and Stamping Company, Rotterdam (1946), pp. 17-99

Thareja, R., 2016. Numerical Modeling Methodology for Weak Rock Masses in Nevada Gold Mines. Doctoral dissertation, University of Nevada, Reno, USA.

Tran Manh, H., Sulem, J., Subrin, D. and Billaux, D., 2015. Anisotropic time-dependent modelling of tunnel excavation in squeezing ground. Rock Mechanics and Rock Engineering, 48(6), pp.2301-2317.

Ulusay, R. ed., 2015. The ISRM suggested methods for rock characterization, testing and monitoring: 2007-2014. Springer.

Vakili, A., Albrecht, J. and Sandy, M., 2014. Rock strength anisotropy and its importance in underground geotechnical design. Proceedings AusRock, pp.167-180.

Vakili, A., Sandy, M. and Albrecht, J., 2012, June. Interpretation of nonlinear numerical models in geomechanics–a case study in the application of numerical modelling for raise bored shaft design in a highly stressed and foliated rock mass. In Proceedings sixth International Conference and Exhibition on Mass Mining, Massmin, pp. 10-14.

Varden, R.P. and Woods, M.J., 2015, November. Design approach for squeezing ground. In Proceedings of the International Seminar on Design Methods in Underground Mining, pp. 489-504. Australian Centre for Geomechanics.

Vyazmensky, A., Yadav, P., 2015. Ground Control Management Plan Rampura Agucha Underground Project. Bhilwara, Rajasthan, India.

Wang, T.T. and Huang, T.H., 2011. Numerical simulation on anisotropic squeezing phenomenon of New Guanyin Tunnel. Journal of Geo-engineering, 6(3), pp.125-133.

Wang, T., Xu, D., Elsworth, D., Zhou, W., 2016. Distinct element modelling of strength variation in jointed rock masses under uniaxial compression. Geomechanics and Geophysics for Geo-Energy and Geo-Resources 2, 11–24.

Wanne, T., 2002. Rock strength and deformation dependence on schistosity. Simulation of rock with PFC3D. Report, 5.

Watson, J. M., Vakili, A., and Jakubowski, M. 2015 "Rock strength anisotropy in high stress conditions: a case study for application to shaft stability assessments." Studia Geotechnica et Mechanica 37, 115-125.

Woolley, C.E. and Andrews, P., 2015, November. Short-term solutions to squeezing ground at Agnew Gold Mine, Western Australia. In Proceedings of the International Seminar on Design Methods in Underground Mining, pp. 199-214. Australian Centre for Geomechanics.

Wu, H.M., Shu, Y.M. and Zhu, J.G., 2011. Implementation and verification of interface constitutive model in FLAC3D. Water Science and Engineering, 4(3), pp.305-316.

Wu, Q., Kou, Z. and Wan, S., 2012, August. Numerical Simulation for the Effect of Joint Inclination to the Stability of Stratified Rock Slope. In Proceedings of the 2012 International Conference on Computer Application and System Modelling. Atlantis Press.

Yadav, P., Panda, A., Sonam, M., Banerjee, B., Parihar, S., Paneri, D.C., 2016. Influence of foliation on excavation stability at Rampura Agucha underground mine, in: Venkatesh, H.S., Venkateswarlu, V. (Eds.), Proceedings of the Conference on Recent Advances in Rock Engineering (Rare 2016). Atlantis Press, Paris, pp. 158–163.

Zhang, Y. and Mitri, H.S., 2008. Elastoplastic stability analysis of mine haulage drift in the vicinity of mined stopes. International Journal of Rock Mechanics and Mining Sciences, 45(4), pp.574-593.

Zhang, Y., Xu, W.Y., Shao, J.F., Zhao, H.B. and Wang, W., 2015. Experimental investigation of creep behavior of clastic rock in Xiangjiaba Hydropower Project. Water Science and Engineering, 8(1), pp.55-62.

Curriculum Vitae

Name:	Pranay Yadav
Post-secondary Education and Degrees:	Laurentian University Sudbury, Ontario, Canada 2016-2018 MASc Natural Resource Engineering Indian School of Mines Dhanbad, Jharkhand, India 2009-2013 Bachelor of Technology, Mining Engineering
Honours and Awards:	Gord and Pat Slade Scholarship 2018 Itasca Education Partnership 2017-2018 Province of Ontario Graduate Scholarship 2017-2018 Dean Entrance Scholarship 2016
Related Work Experience:	Teaching Assistant Laurentian University 2017-2018 Ground Control Engineer Hindustan Zinc Limited 2013-2016
Publications:	Yadav et al. 2016, Influence of foliation on excavation stability at Rampura Agucha Underground mine. Proceedings of the conference on Recent Advances in Rock Engineering. Bengaluru, India. 158-163 Yadav et al. 2015, Ground control management plan – Rampura Agucha Underground mine. Proceedings of 2nd national conference of Mining Equipment: New Technologies, Challenges and Application. Dhanbad, India. 336-343
Contact Information	Email: pranay.ism09@gmail.com